



HAL
open science

Elaboration of novel hybrid ZnO and ZnAl₂O₄ as support for copper based catalysts for the hydrogenolysis of glycerol to 1,2-propanediol

Lama Omar

► **To cite this version:**

Lama Omar. Elaboration of novel hybrid ZnO and ZnAl₂O₄ as support for copper based catalysts for the hydrogenolysis of glycerol to 1,2-propanediol. Catalysis. Université de Lyon, 2019. English. NNT : 2019LYSE1265 . tel-03092282

HAL Id: tel-03092282

<https://theses.hal.science/tel-03092282>

Submitted on 2 Jan 2021

HAL is a multi-disciplinary open access archive for the deposit and dissemination of scientific research documents, whether they are published or not. The documents may come from teaching and research institutions in France or abroad, or from public or private research centers.

L'archive ouverte pluridisciplinaire **HAL**, est destinée au dépôt et à la diffusion de documents scientifiques de niveau recherche, publiés ou non, émanant des établissements d'enseignement et de recherche français ou étrangers, des laboratoires publics ou privés.

N°d'ordre NNT : xxx



THESE de DOCTORAT DE L'UNIVERSITE DE LYON

opérée au sein de
l'Université Claude Bernard Lyon 1

Ecole Doctorale ED 206
Chimie, Procédés, Environnement

Spécialité de doctorat : Chimie
Discipline : Chimie

Soutenue publiquement le 12/12/2019, par :
Lama OMAR

**Elaboration of novel hybrid ZnO and
ZnAl₂O₄ as support for copper based
catalysts for the hydrogenolysis of
glycerol to 1,2-propanediol**

Devant le jury composé de :

Mme Catherine Especel, Professeur, Université de Poitiers
M. Michel Langlet, Directeur de recherche, CNRS
M. Pascal Fongarland, Professeur, Université Lyon 1
M. Hubert Mutin, Directeur de recherche, CNRS
M. Stéphane Daniele, Professeur, Université Lyon 1
Mme Noémie Perrret, Chargé de recherche, CNRS

Rapporteur
Rapporteur
Examineur
Examineur
Directeur de thèse
Co-directrice de thèse

Université Claude Bernard – LYON 1

Président de l'Université	M. Frédéric FLEURY
Président du Conseil Académique	M. Hamda BEN HADID
Vice-Président du Conseil d'Administration	M. Didier REVEL
Vice-Président du Conseil des Etudes et de la Vie Universitaire	M. Philippe CHEVALLIER
Vice-Président de la Commission de Recherche	M. Jean-François MORNEX
Directeur Général des Services	M. Damien VERHAEGHE

COMPOSANTES SANTE

Faculté de Médecine Lyon-Est – Claude Bernard	Doyen : M. Gilles RODE
Faculté de Médecine et Maïeutique Lyon Sud Charles. Mérieux	Doyenne : Mme Carole BURILLON
UFR d'Odontologie	Doyenne : Mme Dominique SEUX
Institut des Sciences Pharmaceutiques et Biologiques	Directrice : Mme Christine VINCIGUERRA
Institut des Sciences et Techniques de la Réadaptation	Directeur : M. Xavier PERROT
Département de Formation et Centre de Recherche en Biologie Humaine	Directrice : Mme Anne-Marie SCHOTT

COMPOSANTES & DEPARTEMENTS DE SCIENCES & TECHNOLOGIE

UFR Biosciences	Directrice : Mme Kathrin GIESELER
Département Génie Electrique et des Procédés (GEP)	Directrice : Mme Rosaria FERRIGNO
Département Informatique	Directeur : M. Behzad SHARIAT
Département Mécanique	Directeur M. Marc BUFFAT
UFR - Faculté des Sciences	Administrateur provisoire : M. Bruno ANDRIOLETTI
UFR (STAPS)	Directeur : M. Yannick VANPOULLE
Observatoire de Lyon	Directrice : Mme Isabelle DANIEL
Ecole Polytechnique Universitaire Lyon 1	Directeur : Emmanuel PERRIN
Ecole Supérieure de Chimie, Physique, Electronique (CPE Lyon)	Directeur : Gérard PIGNAULT
Institut Universitaire de Technologie de Lyon 1	Directeur : M. Christophe VITON
Institut de Science Financière et d'Assurances	Directeur : M. Nicolas LEBOISNE
ESPE	Administrateur Provisoire : M. Pierre CHAREYRON

Abstract:

This work focuses on the synthesis of novel hybrid ZnO and ZnAl₂O₄ NPs by sol-gel method as support for the copper based catalysts and the evaluation of their catalytic performance in the hydrogenolysis of glycerol into 1,2-propanediol in aqueous phase using batch reactor.

The copper-based catalysts were prepared by deposition precipitation with urea (DPU method) and the commercial ZnO was used as benchmark to study the effect of the elaborated supports. The effect of the synthesis method was studied and a one pot method, similar to coprecipitation, was applied for the elaboration of these catalysts. The effects of the synthesis parameters were studied and the catalysts elaborated were robust and competitive in terms of conversion (96%) and selectivity (83%) comparing to the catalysts reported in the literature. Moreover, hybrid ZnO and ZnAl₂O₄ presented high specific surface area (in the range of 100 and 100 - 220 m².g⁻¹), only few being reported in the literature with the sol-gel method, with nanoparticles self-assembled in 3D spherical shapes resistant to high calcination temperatures as shown by TEM.

Keywords: Zinc oxide; zinc aluminium oxide; Cu/ZnAlO_x; hydrogenolysis; sol-gel; DPU; 1,2-PDO.

Résumé :

Ce travail de thèse porte sur le développement de nanomatériaux hybrides de ZnO et de ZnAl₂O₄ utilisés comme supports de catalyseurs à base de Cu^o pour l'hydrogénolyse du glycérol en 1,2-propanediol dans un réacteur batch et en phase liquide.

Plusieurs voies de synthèses ont été optimisées dont la méthode de dépôt précipitation en présence d'urée (DPU) et du ZnO commercial a été utilisé comme référence pour évaluer les caractéristiques des supports élaborés. Une méthode de dépôt innovante dite « one-pot », qui consiste à élaborer le support et le catalyseur dans le même réacteur, a été mise au point pour pallier des difficultés de reproductibilité par la méthode DPU. Cette voie de synthèse a permis d'élaborer des catalyseurs robustes et très compétitifs en terme de sélectivité (83%) et de conversion (96%) par rapport aux catalyseurs trouvés dans la littérature. Les supports et les catalyseurs élaborés ainsi présentent des caractéristiques physico-chimiques importantes

surtout au niveau de leurs grandes surfaces spécifiques (de l'ordre de 100 - 220 m².g⁻¹), peu courantes dans la littérature, permettant une dispersion importante des sites catalytiques.

Mots-clés : Oxyde de zinc, oxyde de zinc aluminium; Cu/ZnAlO_x; hydrogénolyse; sol-gel; DPU; 1,2-PDO.

Acknowledgments

This thesis was carried out at the Institute of Research on Catalysis and the Environment of Lyon (IRCELYON, France) within the CDFA (Chimie durable: du fondamental à l'application) group. I would like to thank Catherine PINEL, Director of IRCELYON, to have allowed me to perform this work in this laboratory and to DAW association - Lebanon who paid my scholarship.

I am very grateful to my thesis directors, Stéphane Daniele and Noémie Perret. Their advices, knowledge, experience in materials synthesis and catalysis, passion for research, were the key elements in the success of this project. They allowed me to enrich myself professionally and personally. For that and for the rest, thanks.

My thesis could not have happened without the participation and technical support of Thibaut Cornier and Stéphane Mangematin, technical engineers in the CDFA team. They accompanied me with courage whenever needed for installations or reparations. I would also like to thank the scientific services of IRCELYON for the characterization techniques: Pascale Mascunan and Nicolas Bonnet (ICP-OES), Yoann Aizac and Françoise Bosselet (P-XRD) and Laurence Burel (TEM).

My thoughts also go to all members of the CDFA team since my internship:

The PhD students: Khaled, Diane, Justyna, Hanaa, Ashraf, Wenzhang, Ayman, Wissam, Quoc An, Soraya, Kamila, Bhagyesh, Alexandre, Natalia, Aleksandra, Lucie, Miguel, Dolores, Amar, Antonio, Shefali, Oleksandra...

And the researchers: I would like to start thanking Shashank Mishra for all his support, scientific and personal. He was always available to answer my questions or even to just give me some advices with a very warm smile.

I would like to mention the role of the scientific discussions we have had during the frequent team meetings. And for that, I thank Laurent Djakovitch, Alexander Sorokin, Michèle Besson, Catherine Pinel and Nadine Essayem for sharing their scientific knowledge.

On the personal side, I have spent my last three years with irreplaceable people. During my internship, Diane and Justyna arrived more or less at the same time. We became very close in a very short period, and we had the craziest nights ever.

Two months after starting my PhD, Sweta Gahlot arrived and joined my office to start her M2 internship. It took her a bit of time to understand my over sociability but she finished by considering me her best friend in Lyon. We were always next to each other in bad and good moments in science or in life.

A few months later, I met Alejandra Bueno who was in my lab but not on my team. We signed up for the same course and we spent three days together that were enough to assure a lifetime friendship. Later she introduced me to Ana Rita Morgado Prates (I love saying her whole name) who was in her team and we started our flowership story.

The best lunch breaks were with my Lebanese girls (Zahraa Shahin, Marwa abo Hamdan and Ranin Atwi), we had always a food competition and funny stories to tell. They will always be my favorite Lebanese people met abroad.

Maintenant je dois écrire en français pour leur faire plaisir ! Donc oui du coup je parle des vieux avec qui j'avais les meilleurs pauses cafés. Sébastien Albert le responsable du magasin (là où on faisait nos courses du labo, on a la chance oui), est mon guru de la langue et culture française. J'ai appris avec lui du verlan, on parlait politique mais on se bagarrait donc on changeait du sujet mais surtout c'est un agriculteur n°1, il m'offrait avec beaucoup d'amour ce qu'il récoltait en Ardèche pendant les week-end.

Les autres vieux : Michel Dupanloup et Moustafa Ben Hadj, les responsables de l'atelier (oui un autre privilège). A chaque fois que je passais faire un prélèvement pour mes tests catalytiques, ils me reçoivent avec un sourire et une tasse de café pour parler de tout et rien (Michel disait parfois des blagues que je ne comprenais pas mais je rigolais quand même).

Pour clôturer je dois remercier Laurent Piccolo, je préfère l'appeler Lolo mais bon ça reste un document officiel ! Notre amitié a commencé pour des raisons scientifiques et s'est partie en live ! (L'expression préférée de Diane). Je pouvais lui raconter mes histoires les plus bizarres et il va toujours m'écouter avec beaucoup de patience et de compréhension. J'ai essayé de le trainer à mes cours de yoga mais ce n'était pas évident !

Pour finir je vais remercier tous les gens qui sont venus à ma soutenance, mes amis du labo des autres équipes : Thomas, Santiago, Eugénie, Alyssa, Corentin, Rémy, Christophe ...

Hors du labo : Ecaterina, Sabine, Farah, Melissa, Youssry, Islam, Thierry ...

A mes parents qui m'ont toujours soutenu dans ma vie, je vous dis que je ne serai jamais la même personne si vous n'étiez pas dans ma vie. A ma sœur qui est aussi mon mentor, je te remercie pour tous les moments qu'on a passés ensemble en France, c'était une des périodes les plus instructives dans ma vie personnelle et familiale. Tu es un exemple de femme que j'aimerais bien le suivre, t'avoir dans ma vie avec tes enfants (Adam et Yara) et ton mari c'est une vraie récompense que je tiens à cœur.

Pour finir je remercie ma coloc avec qui j'ai passé les derniers mois de thèse et qui n'étaient pas faciles ! Clarisson gracias por todo y por existir, te quiero mucho.

Lama Omar



List of Abbreviations

EtOH : Ethanol

MeOH : Methanol

1,2-PDO : 1,2-propanediol

1,3-PDO : 1,3-propanediol

A.T. : After test

au : Arbitrary unit

B.T. : Before test

com : Commercial

[Cu²⁺] : Concentration of Cu²⁺

DEZ, ZnEt₂ : Diethyl zinc

DPU : Deposition Precipitation with Urea

EDX : Energy dispersive X-Ray

EG : Ethylene glycol

exp : Experimental

FT-IR : Fourier-Transform Infrared Spectroscopy

GC : Gas chromatography

GLY : Glycerol

ICP : Inductively Coupled Plasma

Mw : Molecular weight

NPs : Nanoparticles

PAAH : Polyacrylic acid

RT : Room temperature

S.S.A. : Specific surface area

SEM: Scanning Electron Microscopy

T° : Temperature

TEM : Transmission Electron Microscopy

TG : Thermogravimetric

TMA, AlMe₃ : Trimethyl aluminium

vs : Versus

wt% : Weight percentage

XRD : X-ray diffraction

List of Glossaries

$\text{Cu/ZnO}_{\text{com}}$: Copper supported on commercial ZnO prepared by DPU

Cu-ZnO : Catalyst prepared by one pot method in presence of PAA2

$\text{Cu/Zn}_x\text{Al}_y\text{O-PAA2-z}$ and $\text{Cu/Zn}_x\text{Al}_y\text{O-z}$: Copper supported on hybrid ZnAl oxides and ZnAl oxides

$\text{Cu-Zn}_x\text{Al}_y\text{O}_z$: Catalyst prepared by one pot method in presence of PAA2

CZA-XUHP : Catalyst prepared by a modified “one pot method” (CZA : $\text{Cu-ZnO-ZnAl}_2\text{O}_4$, X : theoretical weight percentage of copper, U : use of urea, H : heated and P : use of PAA2)

$\text{XCu/ZnO-PAAX}_{y-z}$: Copper supported on hybrid ZnO prepared by DPU (X : theoretical copper weight percentage, y : temperature of synthesis of support and z : number of experiment)

ZnO-PAAX : Hybrid ZnO elaborated by sol-gel method, X= molecular weight of polyacrylic acid

ZnAl_2O_4 : Zinc aluminium oxide

$\text{Zn}_x\text{Al}_y\text{O-PAA2}_z$: Hybrid ZnAl oxides prepared by sol-gel method in presence of PAA2 (x,y : molar content of zinc and aluminium and z : calcination temperature after synthesis)

$\text{Zn}_x\text{Al}_y\text{O-z}$: ZnAl oxides prepared by sol-gel method without PAA2 (x,y : molar content of zinc and aluminium and z : calcination temperature after synthesis)

Table of content

Introduction.....	1
References.....	4
Chapter I State of the art.....	5
I. ZnO	7
I.1. ZnO properties	8
I.1.1. Crystal structure.....	8
I.1.2. Chemical, electronic and optical properties.....	9
I.2. Methods of ZnO synthesis.....	11
I.2.1. Metallurgical process.....	11
I.2.2. Chemical process.....	12
I.2.2.1. Mechano-chemical process.....	13
I.2.2.2. Hydro(solvo)-thermal method.....	14
I.2.2.3. Controlled precipitation.....	15
I.2.2.4. Sol-gel method.....	15
I.2.2.5. Miscellaneous methods.....	20
I.3. Applications of ZnO.....	20
I.3.1. ZnO as additive in rubber industry.....	21
I.3.2. ZnO as antibacterial agent for food industry and medical applications.....	22
I.3.3. ZnO in electronic and technological applications.....	22
I.3.4. ZnO as photocatalyst.....	22
I.3.5. ZnO as support for heterogeneous catalysts.....	24
I.3.5.1. ZnO for CO oxidation.....	24
I.3.5.2. ZnO for methanol synthesis.....	25
I.3.5.3. ZnO for methanol steam reforming.....	25
I.3.5.4. ZnO for biomass transformation.....	26
II. Heterogeneous catalysts: preparation methods.....	27
II.1. Impregnation.....	28
II.2. Deposition-Precipitation (DP)	29
II.2.1. Deposition-Precipitation with urea (DPU)	32
II.3. Co-precipitation method.....	34
II.3.1. Alternative anions.....	36
II.4. Other preparation methods of Cu-ZnO.....	38
III. Glycerol as source for propanediols production.....	42
III.1. Different mechanisms for the hydrogenolysis of glycerol into propanediol.....	44
III.1.1. Dehydration of glycerol into 1,2-PDO and 1,3-PDO.....	44
III.1.2. Dehydrogenation of glycerol to 1,2-PDO.....	45
III.2. List of copper catalysts for glycerol hydrogenolysis.....	47
III.2.1. Cu-Cr catalysts.....	48
III.2.2. Cu/ZnO catalysts.....	50
III.2.3. Cu/MgO catalysts.....	56
III.2.4. Other Cu-based catalysts.....	56
IV. Objectives of the thesis.....	58
V. References.....	60
CHAPTER II Experimental part.....	72
I. Synthesis of ZnO by hydrolysis of ZnEt ₂ in a solution of PAAH at 0.63%.....	75
I.1. Effect of the molecular weight of PAAH.....	75
I.2. Study of the influence of the washing set up after synthesis.....	76

I.3.	Study of the influence of the concentration of PAAH.....	77
I.4.	Synthesis of ZnO/PAAH at different temperature.....	77
I.5.	Calcination after synthesis.....	78
II.	Synthesis of ZnO-ZnAl ₂ O ₄ by hydrolysis of ZnET ₂ and AlMe ₃	78
III.	Synthesis of supported Cu catalysts by deposition precipitation.....	80
III.1.	Deposition precipitation of Cu on commercial ZnO.....	80
III.1.1.	Synthesis of Cu/ZnO commercial with different concentration of Cu ²⁺ and wt% Cu°.....	81
III.2.	Synthesis of Cu/ZnO with the synthesized ZnO.....	82
III.2.1.	Deposition precipitation with ZnO/PAAX:.....	82
III.2.2.	Deposition precipitation with the calcined ZnO:	83
III.2.3.	Deposition precipitation of Cu with ZnO-ZnAl ₂ O ₄	84
IV.	Synthesis of Cu/ZnO-ZnAl ₂ O ₄ by one pot.....	84
IV.1.	Synthesis of Cu-ZnO and Cu/ZnO-ZnAl ₂ O ₄ in one pot-one step:	84
IV.2.	Synthesis of Cu/ZnO and Cu/ZnO-ZnAl ₂ O ₄ in one pot-two steps:	86
IV.3.	Synthesis of Cu/ZnO-ZnAl ₂ O ₄ in one pot-two steps without adding urea:	87
V.	Hydrogenolysis of glycerol in a batch reactor under H ₂ pressure.....	88
VI.	Characterization techniques.....	89
VI.1.	Powder X-Ray Diffraction (XRD)	89
VI.2.	Adsorption/desorption of nitrogen: specific surface area BET.....	90
VI.3.	Elemental analysis by ICP-OES.....	92
VI.4.	Transmission Electronic Microscopy (TEM)	92
VI.4.1.	Energy Dispersive X-Ray Spectroscopy (EDX) measurement.....	94
VI.5.	Thermogravimetric analysis (TGA)	94
VI.6.	Chromatographic analysis	95

CHAPTER III ZnO-PAAX: Study of the synthesis parameters.....98

I.	Effect of the synthesis parameters on ZnO-PAAX.....	99
I.1.	Effect of the molecular weight of PAAH.....	99
I.2.	Effect of the washing process after hydrolysis.....	110
I.2.1.	ZnO-PAA2 system.....	111
I.2.2.	ZnO-PAA5 system.....	114
I.3.	Effect of PAA2 concentration during synthesis.....	116
I.4.	Effect of the synthesis temperature.....	121
I.4.1.	Effect of the synthesis temperature on ZnO-PAA2.....	121
I.4.2.	Effect of the synthesis temperature on ZnO-PAA5.....	123
I.5.	Effect of calcination temperature after synthesis.....	128
I.5.1.	Effect of calcination temperature on ZnO-PAA2.....	128
I.5.2.	Effect of calcination temperature on ZnO-PAA5.....	133
II.	Conclusion.....	136
II.	References.....	137

CHAPTER IV Development of Cu/ZnO catalysts : support effect138

I.	Commercial ZnO as support.....	139
I.1.	Effect of CuO weight percentage.....	145
I.2.	Effect of Cu ²⁺ concentration.....	150
II.	ZnO-PAAX (X = 2, 5, 100) as supports.....	154
II.1.	ZnO-PAA2 non calcined.....	154
II.1.1.	Effect of the synthesis parameters (support and copper wt%).....	154
II.1.2.	Effect of the weight of the catalyst.....	159
II.1.3.	Recyclability of Cu/ZnO-PAA2.....	162
II.2.	ZnO-PAA2 calcined.....	164

II.3.	ZnO-PAA5 as support.....	167
II.3.1.	Non Calcined ZnO-PAA5.....	167
II.3.1.	Calcined ZnO-PAA5.....	169
II.4.	ZnO-PAA100 as support.....	169
III.	Cu-ZnO by a “one pot” method.....	170
III.1.	Cu-ZnO synthesis by a “one pot - one step” approach.....	171
III.2.	Cu-ZnO synthesis by a “one pot - two steps” approach.....	173
IV.	Conclusions.....	177
IV.	References.....	178

CHAPTER V Cu-Zn-Al : Effect of Al on the hydrogenolysis.....179

I.	Synthesis of Zn _x Al _y O-PAA2: Study of the molar ratio of metals.....	180
I.1.	Zn:Al (2:1) molar ratio in presence of PAA2 (Zn ₂ Al ₁ O-PAA2z)	181
I.2.	Zn:Al (1:2) molar ratio in presence of PAA2 (Zn ₁ Al ₂ O-PAA2z)	185
I.3.	Zn:Al (2:1) molar ratio without PAA2 (Zn ₂ Al ₁ O-z)	190
I.4.	Zn-Al (1:2) molar ratio without PAA2 (Zn ₁ Al ₂ O-z)	192
II.	Synthesis of Cu/ZnAl by DPU: study of the Zn-Al effect.....	196
II.1.	Deposition of 20 wt% of copper on Zn ₂ Al ₁ O-PAA2 and Zn ₂ Al ₁ O materials by DPU.....	197
II.2.	20 wt% of copper on Zn ₁ Al ₂ O-PAA2 and Zn ₁ Al ₂ O materials by DPU.....	200
III.	Synthesis of Cu-Zn _x Al _y O _z by a “one pot method”: Study of the synthesis parameters.....	205
III.1.	Synthesis of Cu-Zn _x Al _y O _z by a “one pot - one step” route.....	205
III.2.	Synthesis of Cu-Zn _x Al _y O _z by a “one pot -two steps” route.....	207
III.3.	Catalytic results over Cu-Zn _x Al _y O _z prepared by “one pot” routes.....	211
III.4.	Effect of synthesis parameters on Cu-Zn _x Al _y O _z by “one pot-two steps” route.....	213
IV.	Conclusions.....	220
IV.	References.....	222

General Conclusion.....223

Perspectives.....226

Appendixes.....228-236

Introduction

The depletion of fossil fuel reservoirs, together with the indispensable shift of the feedstock towards a biorefinery approach, necessitates the use of renewable resources on a large scale for the production of chemicals and fuel. Thus, the development of efficient and environmentally friendly technologies has become an imperative. The limitation of this concept is the high cost of the production of biofuel. In order to valorize this production, the co-products should be recovered and valorized. In the case of the production of biofuel via the transesterification of vegetable oils, glycerol is produced in large quantity (10 molecules of glycerol for 1 molecule of biodiesel) estimated to reach 42 billion liters in 2020 ¹.

Glycerol is one of the most versatile and valuable chemical substances known, with more than thousands of uses and applications ². Its physical and chemical properties make it a versatile organic compound. Food products, cosmetics, toiletries, and drugs are just a few of the products in which glycerol is employed either as a constituent of the processing or as a major reactant.

Glycerol can be converted by catalytic hydrogenolysis into ethylene and propylene glycols (1,2-propanediol and 1,3-propanediol), which are important chemical platform for various applications ³. Hydrogenolysis reactions, which results in the cleavage of C-C and C-O bonds, offer promising possibilities for future biorefinery processes. This reaction is currently intensively discussed in the context of the transformation of glycerol to ethylene and propylene glycols, but it also has great potential in regard to the conversion of biomass-derived polyols, such as sugars or sugar alcohols (sorbitol, xylitol, erythritol...). As multiple C-O and C-C bonds cleavage can occur, along with other side-reactions, selectivity in hydrogenolysis reactions remain a major challenge.

In the literature different systems have been studied for the conversion of glycerol depending on the desired product. **The hydrogenolysis** reaction can be done using water as solvent, in a batch reactor under hydrogen pressure and with the addition of noble metal catalysts. Rh ⁴, Ru ⁵ and Pt ⁶ show high yield of conversion and variable selectivity toward 1,2-propanediol (1,2-PDO) and 1,3-propanediol (1,3-PDO). Noble-free systems have the advantage of limiting the C-C bond cleavage, in favor of C-O bond cleavage ^{7,8}.

In our case we focused on the hydrogenolysis of glycerol into **1,2-propanediol (1,2-PDO)**, due to the large application of this molecule. 1,2-PDO is used as chemical feedstock for the production of unsaturated polyester resins. Related to this application, 1,2-PDO reacts with propylene oxide to give oligomers and polymers that are used to produce polyurethanes. 1,2-PDO is used in water based acrylic architectural paints to extend drying time due to its slower evaporation rate compared to water⁹. It is also used as a humectant, solvent and preservative in food and for tobacco products. In addition, it is one of the major ingredients, along with glycerol, of the e-liquid and cartridges used in electronic cigarettes where it is aerosolized in the atomizer. Last but not least, it is used in model railway and model boat applications to simulate steam or smoke¹⁰. Besides, it can be used in various consumable items such as coffee-based drinks, liquid sweeteners, ice cream, whipped dairy products and soda and as a solvent in many pharmaceuticals, including oral, injectable and topical formulations, such as for diazepam and lorazepam which are insoluble in water¹¹.

In literature noble-metal free systems have attracted attention for the transformation of glycerol into 1,2-PDO in the last decades, due to their low cost and abundance. **Cu-based nanoparticles (NPs)** have generated a great interest in recent years, especially in the field of catalysis. The possible modification of the chemical and physical properties of these nanoparticles using different synthetic strategies and conditions and/or via post-synthetic chemical treatments has been largely responsible for the rapid growth of interest in these nanomaterials and their applications in catalysis¹². Copper is a non-noble metal, known for its selectivity for the **cleavage of the C-O** bond and its low price compared to noble metals. Additionally, Cu's high boiling point makes it compatible with high temperature and pressure chemical reactions. Such properties are important for the development of reactive, selective and stable catalytic systems¹³.

Zinc oxide is a semiconductor which is used in extensive domains of industrial applications such as catalysis, antibacterial coating, UV sunscreen formulations... These applications require high specific surface area (nanometric materials) and the development of reproducible, efficient and easy-scalable industrial production processes¹⁴.

Our novel patented industry-capable (in terms of legislation concerns) and cost effective chemical solution approach (PCT WO 2016/038317 A1)¹⁵ from ZnEt₂ and polyacrylic acid (PAAH) led to mesospheric self-assembly hybrid ZnO-PAAH nanomaterials that can be used as original nanostructured and very high surface area ZnO support (> 100 m².g⁻¹).

Therefore, the main objective of our project was to study the interest our new hybrid ZnO-PAAH supports in the elaborations Cu/ZnO- or Cu/ZnAlO_x based noble free catalysts that could be used for the hydrogenolysis of glycerol.

In the first chapter, a review on the literature was done starting from the properties of zinc oxide as a material, to its different preparation methods and uses. In a second time, the hydrogenolysis of glycerol over varied catalysts, with a focus on Cu/ZnO catalysts, was reviewed to have a general idea on what had already been done and how it would be possible to enhance the catalytic properties of the catalyst.

The second chapter is dedicated to the experimental part where we describe briefly the synthesis methods for ZnO and the Cu catalysts, the characterization tools and the catalytic setup.

In the third chapter, the synthesis of ZnO-PAAH supports is detailed. Study of different parameters of synthesis, that can influence the properties of the ZnO-PAAH material such as the molecular weight (MW) of the modifying agent PAAX [X = 2 (MW = 2 000 g.mol⁻¹) or 5 (MW = 5 000 g.mol⁻¹), the synthesis temperature (between 0 and 40 °C), the effect of washing (EtOH, H₂O, various volumes and mixture) and the temperature of calcination (between 300 and 400 °C) are addressed. The aim of this chapter was to demonstrate how to get ZnO-PAAH or ZnO with **high specific surface area** and **well-defined morphology** in order to use them as support for copper catalysts.

The fourth chapter presents the catalytic results with various Cu/ZnO catalysts. These latter are synthesized on commercial ZnO by deposition precipitation with urea (**DPU**) **method** in order to optimize the parameters of Cu deposition. In a second time, ZnO-PAAX materials (described in chapter 3) are used as support for copper deposits. Finally, catalysts are synthesized by a “one pot method” in order to gain time and develop more reproducible catalysts. All the catalysts are tested for the hydrogenolysis of glycerol into 1,2-PDO.

In the fifth chapter, the effect of **aluminium addition** in the support is studied. Elaboration of a series of ZnAlO-PAAH supports and further **Cu/ZnAlO_x catalysts** are carried out changing different synthetic parameters (quantity of urea, nature of PAAH, calcination of the support ...). After morphological and structural characterizations, Cu/ZnAlO_x catalysts are tested for the hydrogenolysis of glycerol into 1,2-PDO. Elaboration of a highly active and robust Cu/ZnAlO_x catalysis achieved through a novel “one pot-two steps” route.

References

1. Nanda, M. R., Yuan, Z., Qin, W., Poirier, M. A. & Chunbao, X. Purification of crude glycerol using acidification: effects of acid types and product characterization. *Austin J. Chem. Eng.* **1**, 1–7 (2014).
2. Mota, C. J. A., Peres Pinto, B. & de Lima, A. L. Glycerol utilization from "Glycerol, A versatile renewable feedstock for the chemical industry". *Springer International Publishing, Cham*, (2017).
3. Pagliaro, M., Ciriminna, R., Kimura, H., Rossi, M. & Della Pina, C. From glycerol to value-added products. *Angew. Chem. Int. Ed.* **46**, 4434–4440 (2007).
4. Auneau, F., Michel, C., Delbecq, F., Pinel, C. & Sautet, P. Unravelling the mechanism of glycerol hydrogenolysis over rhodium catalyst through combined experimental-theoretical investigations. *Chem. - Eur. J.* **17**, 14288–14299 (2011).
5. Vasiliadou, E. S., Heracleous, E., Vasalos, I. A. & Lemonidou, A. A. Ru-based catalysts for glycerol hydrogenolysis—effect of support and metal precursor. *Appl. Catal. B Environ.* **92**, 90–99 (2009).
6. Dasari, M. A., Kiatsimkul, P.-P., Sutterlin, W. R. & Suppes, G. J. Low-pressure hydrogenolysis of glycerol to propylene glycol. *Appl. Catal. Gen.* **281**, 225–231 (2005).
7. Montassier, C., Giraud, D., Barbier, J. & Boitiaux, J. . Transformation de polyols par catalyse heterogene en phase liquide sur les metaux. *BullSocChim Fr* **2**, 148–155 (1989).
8. Mai, C.T.Q, Ng, F.T.T & Rempel, G.L. Recent advances on the conversion of glycerol to acrolein, 1,3-propanediol, propanol and propylene using acidic heterogeneous catalysts from "Catalysis". Edited by Spivey, J. and Han, Y-F. *Royal Society of Chemistry, Croydon*, **30**, 2018.
9. Samudrala, S. P. Glycerol Transformation to value-added 1, 3-propanediol production: a paradigm for a sustainable biorefinery process from "Glycerine production and transformation, an innovative platform for sustainable biorefinery and energy" *IntechOpen*, (2019).
10. Saxena, R. K., Anand, P., Saran, S., Isar, J. & Agarwal, L. Microbial production and applications of 1,2-propanediol. *Indian J. Microbiol.* **50**, 2–11 (2010).
11. EFSA Panel on Food Additives and Nutrient Sources added to Food (ANS) *et al.* Re-evaluation of propane-1,2-diol (E 1520) as a food additive. *EFSA J.* **16**, (2018).
12. Munnik, P., de Jongh, P. E. & de Jong, K. P. Recent Developments in the Synthesis of Supported Catalysts. *Chem. Rev.* **115**, 6687–6718 (2015).
13. Gawande, M. B. *et al.* Cu and Cu-Based Nanoparticles: Synthesis and Applications in Catalysis. *Chem. Rev.* **116**, 3722–3811 (2016).
14. Kołodziejczak-Radzimska, A. & Jesionowski, T. Zinc Oxide—From Synthesis to Application: A Review. *Materials* **7**, 2833–2881 (2014).
15. Daniele, S., Cornier, T. & Valette, A. Composition aqueuse de particules de ZnO suspendues. *Brev. FR20141458575* (2014).

Chapter I

State of the Art

Table of contents

Chapter I.....	5
I. ZnO.....	7
I.1. ZnO properties.....	8
I.1.1. Crystal structures.....	8
I.1.2. Chemical, electronic and optical properties.....	9
I.2. Methods of ZnO synthesis.....	11
I.2.1. Metallurgical process.....	11
I.2.2. Chemical process.....	12
I.2.2.1. Mechanico-chemical process.....	13
I.2.2.2. Hydro(solvo)-thermal method.....	14
I.2.2.3. Controlled precipitation.....	15
I.2.2.4. Sol-gel method.....	15
I.2.2.5. Miscellaneous methods.....	20
I.3. Applications of ZnO.....	20
I.3.1. ZnO as additive in rubber industry.....	21
I.3.2. ZnO as antibacterial agent for food industry and medical applications ..	22
I.3.3. ZnO in electronic and technological applications.....	22
I.3.4. ZnO as photocatalyst.....	22
I.3.5. ZnO as support for heterogeneous catalysts.....	24
I.3.5.1. ZnO for CO oxidation.....	24
I.3.5.2. ZnO for methanol synthesis.....	25
I.3.5.3. ZnO for methanol steam reforming.....	25
I.3.5.4. ZnO for biomass transformation.....	26
II. Heterogeneous catalysts: preparation methods.....	27

II.1. Impregnation	28
II.2. Deposition-Precipitation (DP)	29
II.2.1. Deposition-Precipitation with urea (DPU)	32
II.3. Co-precipitation method	34
II.3.1. Alternative anions.....	36
II.4. Other preparation methods of Cu-ZnO.....	38
III. Glycerol as source for propanediols production.....	42
III.1. Different mechanisms for the hydrogenolysis of glycerol into propanediol... 44	
III.1.1. Dehydration of glycerol into 1,2-PDO and 1,3-PDO	44
III.1.2. Dehydrogenation of glycerol to 1,2-PDO	45
III.2. List of copper catalysts for glycerol hydrogenolysis.....	47
III.2.1. Cu-Cr catalysts	48
III.2.2. Cu/ZnO catalysts	50
III.2.3. Cu/MgO catalysts.....	56
III.2.4. Other Cu-based catalysts.....	56
IV. Objectives of the thesis	58
V. References.....	60

I. ZnO

Zinc oxide is known to be a material combining interesting chemical and physical properties. It is an oxide with high chemical stability, high electrochemical coupling coefficient, high photostability and broad range of radiation absorption ^{1,2}. Zinc oxide is classified as a semiconductor in Groups IIb-VIa (12-16) in materials science, whose covalency lies at the boundary between ionic and covalent semiconductors. It is an interesting candidate in laser technologies and optoelectronics applications due to its wide band gap ($E_g \sim 3.37$ eV), large exciton binding energy (60 meV), high mechanical stability at room temperature and strong thermal stability at high temperatures ^{3,4}.

In addition, it can be used as a converter, sensor, energy generator and photocatalyst in hydrogen production due to its piezoelectric properties ^{5,6}. Its low toxicity, biodegradability and biocompatibility makes it an interesting material for biomedicine and pro-ecological systems. It can also be used in the ceramic industry due to its hardness and rigidity ⁷⁻⁹. Due to its nanometric structures variety, it can be used in many applications in nanotechnology (as additives in cosmetics ¹⁰, tyre industry ¹¹ ...).

Zinc oxide can be elaborated as one-dimensional (1D), two-dimensional (2D) or three-dimensional (3D) structures:

- **1D structures represent the largest structural group, including nanorods ¹², needles ¹³, rings ¹⁴, wires ¹⁵, tubes ¹⁶**
- **2D structures such as nanoplate/nanosheet and nanopellets ¹⁷,**
- **3D structures of ZnO include flower, snowflakes, dandelion, coniferous urchin-like, etc. ¹⁸.**

Some examples of the various morphologies are included in Figure 1-1.

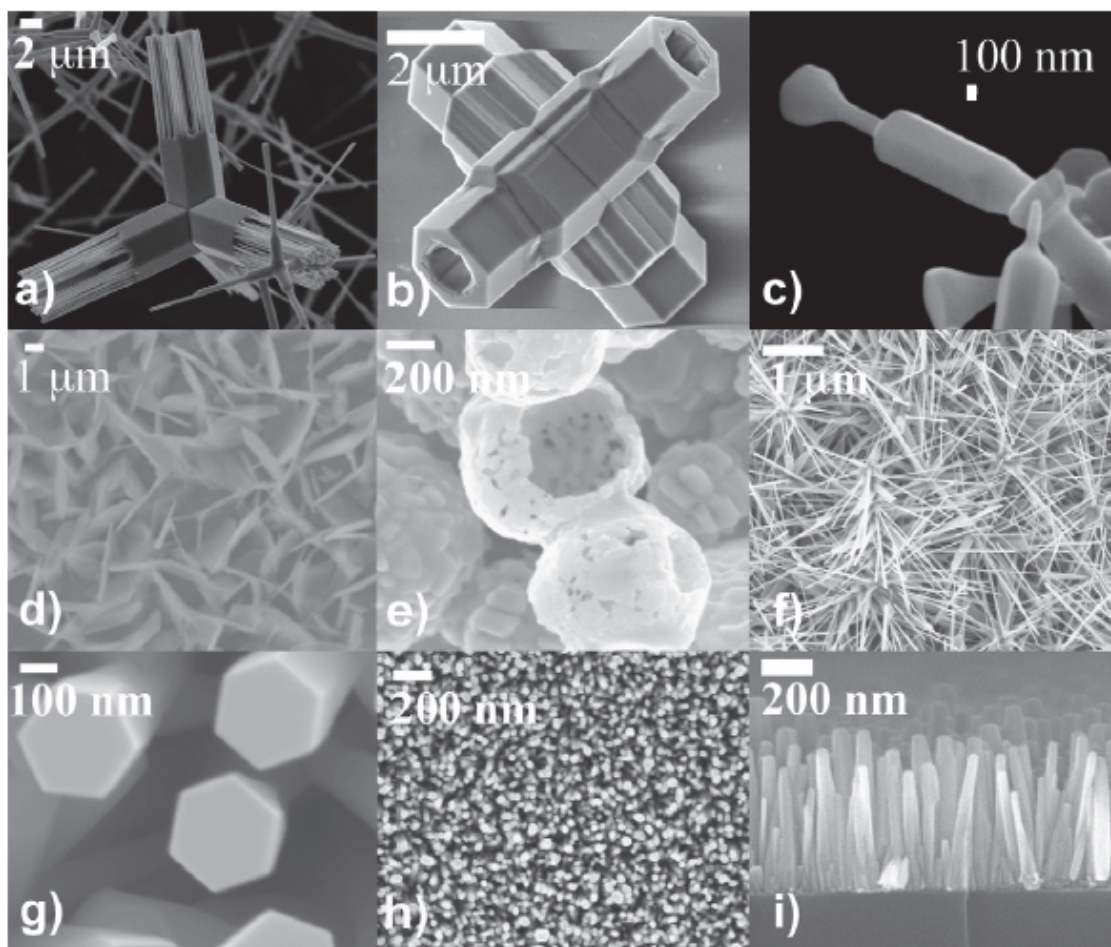


Figure 1-1: SEM images of some examples of various morphologies of ZnO nanostructures: (a), (b) tetrapod structures; (c) variable diameter structures; (d) nanosheets; (e) nanoshells; (f) multipods; (g), (h), and (i) nanorods.¹⁹

1.1. ZnO properties

1.1.1. Crystal structures

ZnO as an element of IIb-VIa group, crystallizes in two structures either cubic or hexagonal. In both structures, each Zn atom is surrounded by four O at the corners of a tetrahedron, and vice versa. This tetrahedral coordination is typical of the sp^3 covalent bonding, but at the same time, ZnO has a strong ionic character. The difference in electronegativity between the oxygen atom and the zinc atom places ZnO at the boundary between covalent polar semiconductor and ionic semiconductor. The crystal structures known for ZnO are cubic rocksalt (B1), cubic zinc blende (B3) and hexagonal wurtzite (B4) as shown in Figure 1-2. This specificity is related to the mixed nature of the bonds within the crystal.

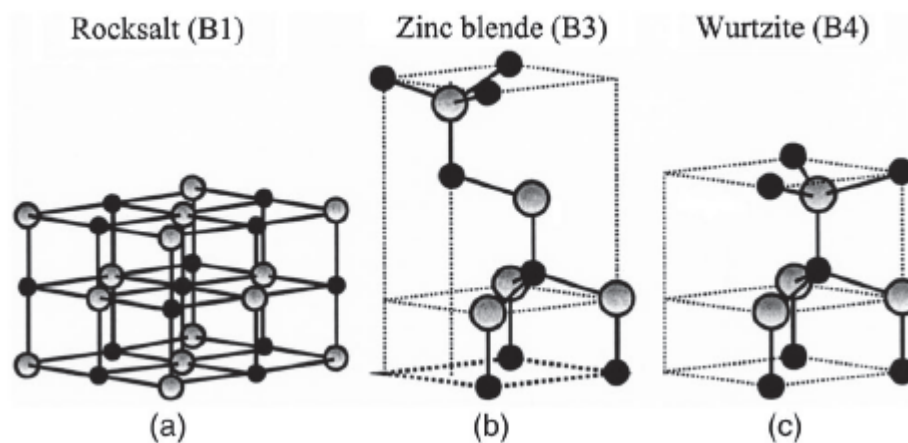


Figure 1-2: ZnO crystal structures: (a) cubic Rocksalt (B1), (b) cubic Zinc blende (B3) and (c) hexagonal Wurtzite (B4). (Black circles: O atoms, grey circles: Zn atoms) ²⁰

High pressures are needed to obtain the rocksalt structure (NaCl), growth on cubic substrates stabilize the zinc blende structure while the wurtzite form is widely preferred under normal temperature and pressure conditions. This latter is formed by the stacking of negatively charged oxygen atom planes and positively charged zinc atom planes. More precisely, it is composed of two interpenetrated sub-networks of the compact hexagonal type, which are displaced relative to each other along the c-axis with a translation coefficient (u) of 0.375 in an ideal structure. Zinc oxide crystallizes in the space group P63mc with lattice parameters $a = 3.250 \text{ \AA}$ and $c = 5.207 \text{ \AA}$.

1.1.2. Chemical, electronic and optical properties

Zinc oxide is almost insoluble in pure water (in the order of one millionth in mass proportion or $0.42 \times 10^{-3} \text{ g}$ per 100 g of pure water) and does not absorb carbon dioxide from the air. Nevertheless, it is an amphoteric oxide which is soluble in acid (Zn^{2+} form) and basic [$\text{Zn}(\text{OH})_4^{2-}$ zincate anions] solutions.

Zinc oxide is a 3.3 eV band gap semiconductor that therefore does not absorb visible light, and explains its transparency. White powder at room temperature, oxygen deficiencies can form in this material at high temperature, which explains why zinc oxide turns yellow when heated. This effect is called thermochromy. ZnO is one of the most popular piezoelectric materials due to its hexagonal crystal structure which does not have a center of symmetry. Zinc oxide defects, which can be impurities, crystallinity defects, extended defects or adsorbed molecules, will have a significant impact on the electronic properties of this compound. ZnO

is also known as n-type conductive material. In order to have good applications in optoelectronics, ZnO is generally doped with ²¹⁻²⁴:

- **N-type doping from group III like Ga, Al, In as Zn substitution and group VII as O substitution**
- **P-type doping, from group V and group I, harder to reproduce.**

Transition metals as Co, Fe, Ni and Mn have also been widely studied as dopant for ZnO materials ^{25,26}.

In order to determine the quality of as prepared ZnO nanostructures, studying the optical response of such nanomaterial can be crucial. One important technique to characterize these NPs is Low Temperature Photo Luminescence (PL). By studying carefully, the presence of different peaks corresponding to free exciton, biexcitons or green emission one can easily determine the quality of ZnO nanoparticles/structures. At very low temperature, around 10 K, the presence of free exciton peaks along with green emission has been shown an efficient way to analyze the quality of ZnO nanostructures²¹. Sometimes the presence of biexcitons peaks in the low temperature PL could also tell about the sample quality. So a careful analysis of all the peaks in the PL spectra is very much necessary.

Another important technique is Room Temperature Photo Luminescence (RTPL), which is very useful to identify the presence of defects in the sample. Since the intensity of defects emission is dependent on the temperature in a way that, higher the temperature is, more defects vibrations there are. This results in the origin of one or more peaks in the visible region of ZnO PL spectra in addition to the characteristic UV emission peaks. Although the exact origin of different peaks in visible region is not very clear, reports proposed origin of these to be attributed to zinc valency ²⁷, oxygen vacancy²⁸, zinc or oxygen interstitials ²⁹, hydroxyl groups³⁰, and many other surface impurities and defects.

Even if the ratio of UV to visible emission intensity could be used as a tool to verify the quality of the sample, this ratio is dependent on the excitation intensity and so is not a sufficient proof of good quality³¹. Most of the time the quality of the material is highly dependent on the synthesis method used.

1.2. Methods of ZnO synthesis

Two main processes are used to synthesis ZnO: metallurgical and chemical processes.

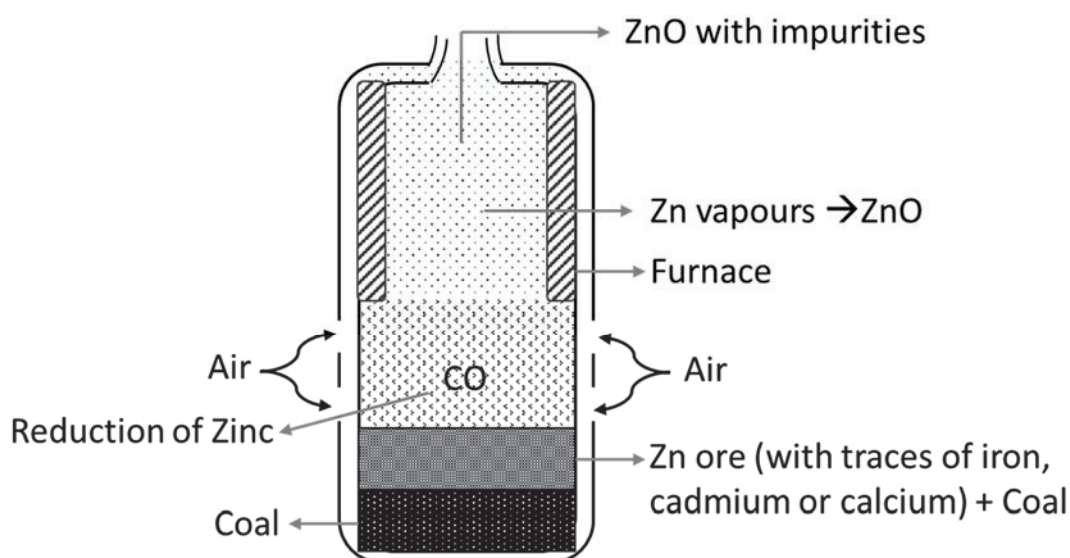
1.2.1. Metallurgical process

Zinc oxide can be obtained by metallurgical processes by roasting zinc ore.

Two types of zinc oxide can be obtained by this process ³² :

- **Type A obtained by direct process known as American process**
- **Type B obtained by indirect process known as French process**

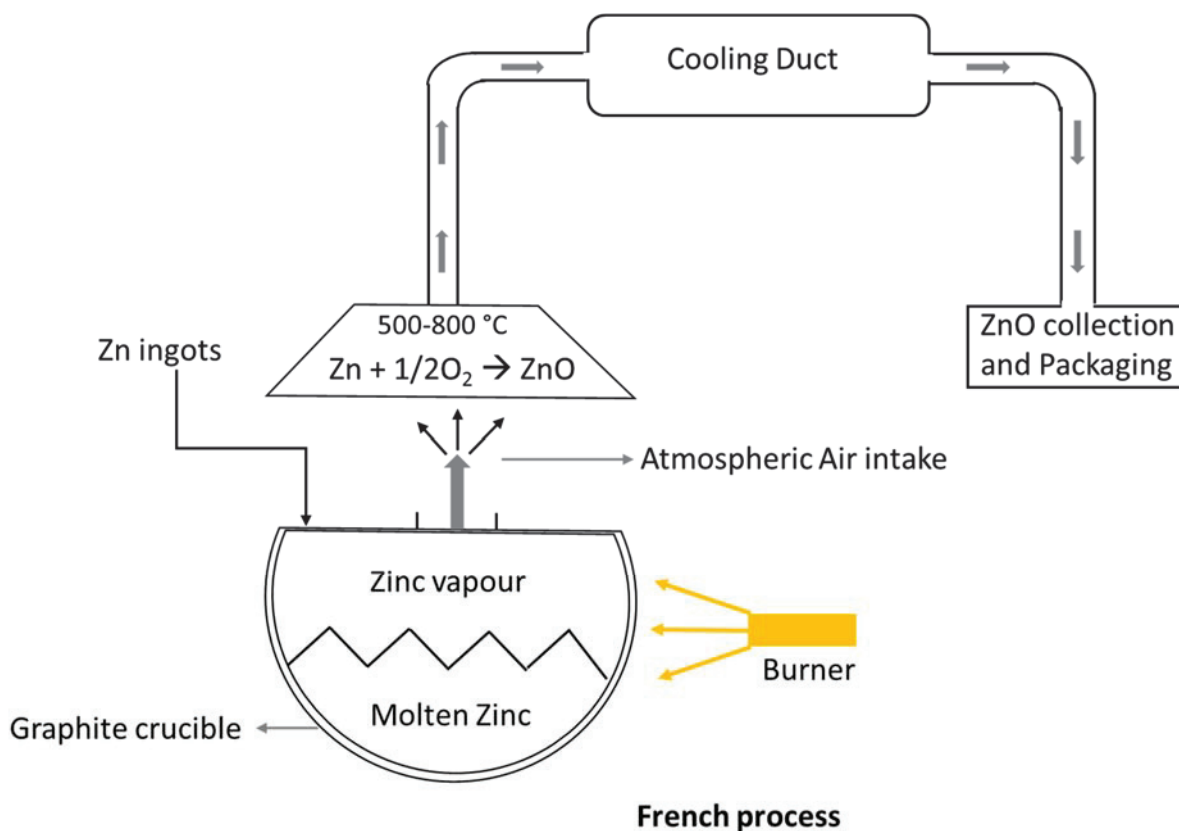
The American process, developed by Samuel Wetherill, takes place in a single production cycle. Zinc ore is reduced by coal heating in the first step, and zinc vapor is then oxidized in the same reactor in the second step. The process takes place in a furnace, in which the first layer consists of a coal bed and the second layer is in the form of zinc ore mixed with coal above the first. Carbon monoxide, resulting from blowing air to the reactor, is responsible for the reduction of zinc. Heating occurs to oxidize the reduced zinc into zinc oxide. As the raw material is impure (traces of iron, cadmium or calcium may be found in the zinc ore), the resulting zinc oxide (type A) contains impurities in the form of compounds of other metals. The particles are mainly needle-shaped, sometimes spheroidal and the color is not permanently white due to impurities. The process is illustrated in the scheme 1-1.



American process

Scheme 1-1: American process for elaborating ZnO from zinc ore

The French process, developed by LeClaire, consists of melting metallic zinc in a furnace until it evaporates, after heating to 1000 °C. Unlike the American process, the French process takes place in separated locations: vertical furnaces, vertical load, refining column, vaporizer and rotary combustion chamber ³³. The production of ZnO occurs by the immediate reaction of zinc vapor with oxygen in the air. A simplified scheme of the process is illustrated in scheme 1-2.



Scheme 1-2: French process for elaborating ZnO from zinc ore

Finally, with the two processes, the particles of zinc oxide are transported through a cooling duct and collected in a bag filtration station. The particles are mainly spheroidal in shape and range in size from 0.1 to a few micrometers assembled into agglomerates ³⁴ . However, type B has a higher degree of purity than type A since the starting material is purely metallic zinc.

1.2.2. Chemical process

Due to the interesting properties of zinc oxide, many researchers have worked on the

development of different synthesis methods to elaborate this material. Different chemical processes are used for the production of ZnO; the following paragraphs describe the most common ones.

1.2.2.1. Mechanico-chemical process

The process involves high-energy dry grinding, where the reaction is initiated through ball-powder impacts in a ball mill at low temperature.

Anhydrous zinc chloride and carbonate sodium are the usual starting materials for this process^{35,36}. However other precursors can be used, such as oxalic acid (C₂H₂O₄.2H₂O) instead of carbonate sodium³⁷. A solvent in solid form (usually NaCl) is added to the system to separate the formed nanoparticles.

ZnCO₃ formed after the first step is then calcined at a temperature of 400 °C to 800 °C. The process can be divided into two reactions:



The milling time and the calcination temperature can affect the particle size; some examples are presented in the following table (Table 1-1).

Table 1-1: Effect of milling time and calcination temperature on the ZnO particle size

Precursor	Milling time (hour)	Calcination temperature (°C)	Particle Size (nm)	References
Na₂CO₃	2	600	25	38
	6	600	21	
	10	600	21	
	6	400	18	
	6	600	21	
	6	800	36	
Na₂CO₃	1	400	26	36
Na₂CO₃	9	300	27	35
	9	450	56	
C₂H₂O₄.2H₂O	4	450	40	37

The paper of Ao et al.³⁸ reports an in-depth study on the effect of the milling time and the calcination temperature. At 600 °C, the increase in the milling time leads to a decrease in the

crystallite size attributed to the existence of a critical effect during mechanical milling. After 6 hours the crystallite size remain stable till 10 hours. On the other side, fixing the milling time to 6 hours and increasing the calcination temperature lead to an enormous increase in the crystallite size to 36 nm at 800 °C. Unfortunately, the article do not show the effect of the milling time and temperature on the specific surface area of the material. However in the article of Tsuzuki et al.,³¹ authors obtain spherical particles of 27 nm size leading to a medium surface area of ZnO = 47 m².g⁻¹ prepared by using the precursors cited above (ZnCl₂ and Na₂CO₃). Actually, as the surface area is related to the particle size, in this technique the experimental conditions control the specific surface area of the material but it is usually low to medium (below 60 m².g⁻¹).

One disadvantage of this method is the difficulty to attain a uniform grinding of the powder. Moreover, the reduction of the grains to the desired size requires higher energy and longer milling time resulting in an increase in the amount of impurities in the sample. Advantages of this method are the production on a large scale and at low costs of nanoparticles of small size, with low tendency to agglomerate, as well as the high homogeneity of the crystal structure and morphology.

1.2.2.2. Hydro(solvo)-thermal method

The hydro(solvo)-thermal method consists in adding the reactants to the solvent which can be water or other organic solvent (alcohols, DMF, acetone...) in an autoclave and to start the synthesis under high pressure and temperature. It is called hydrothermal when the solvent is water and solvothermal if a nonaqueous solvent is used.

The method guarantees a narrow particle size distribution of small crystalline particles, high purity and good chemical homogeneity through homogeneous nucleation during the process. This is achieved by controlling the desired parameters such as reaction time and temperature, pH of the solution, use of additives and the type of solvent in case of solvothermal method³⁹. In addition, the particles are obtained with all these properties without additional calcination⁴⁰. Compared to the co-precipitation method, hydrothermal technique leads to particles with a higher crystallinity and various (interesting) morphologies.

Some studies focus on the advantages and drawbacks of this method^{21,41-44}. First, it is an inexpensive method where all the precursors are generally cheap and the main cost comes

from the heating. In case of using water as a solvent it is considered as eco-friendly because no waste would be dangerous. In term of chemistry, it allows the synthesis of single crystals and the direct precipitation of thin films coatings onto the surfaces of substrates. This synthetic pathway is widely used to obtain ZnO nanowire carpets onto 2D support ⁴⁵. Nevertheless, it does not have the ability to handle the nucleation growth of the particles and since it is in a closed autoclave, the medium cannot be visible. It is also hard to manipulate it quickly so for example if a cooling down is necessary during the synthesis it will take time.

1.2.2.3. Controlled precipitation

Controlled precipitation of ZnO is achieved by reacting zinc salt (acetate, chloride, sulphate...) with basic reactants that release OH⁻ groups. The nature and the quantity of the basic reactant (sodium borohydride, hydrazine hydrate, urea, potassium hydroxide...) ⁴⁶, the pH ⁴⁷, the temperature ⁴⁸, the solvent ⁴⁹ and the precipitation time ⁵⁰ affect the particle size. After precipitation, the material is recovered and a thermal treatment followed by grinding is necessary to obtain pure ZnO.

The growth of ZnO particles can also be controlled by adding surfactants or ligands to the reactants as they affect coagulation and particles flocculation ⁵¹. The controlled precipitation method with additives involves usually the chelation of the metal cations of the precursor, in an aqueous environment, to control its reactivity. The large use of this method is due to the good reproducibility of the resulting material.

1.2.2.4. Sol-gel method

The sol-gel method is one of the most applied methods for the elaboration of metal oxide nanoparticles and mixed oxide composites in various rheologies (sol, gel or precipitate).

A sol is a stable dispersion of colloidal (or nanometric) particles in a solvent. Nanoparticles can interact through van der Waals forces or hydrogen bonds. A gel is a three-dimensional continuous network that contains a liquid phase. There are two types of gel: colloidal or polymeric. In a colloidal gel, the solid network consists of agglomeration of colloidal particles, these gels can be reversible to give back a sol. In a polymer gel, the particles are aggregated through strong interactions and these gels are irreversible. Depending on the type of drying, xerogels are obtained by removing the liquid from the medium under atmospheric or aerogel

by supercritical conditions.

Figure 1-3 shows various morphologies of (nano)materials that can be reached by sol-gel method: such as film from a colloidal sol (Figure 1-3 a), or powder from a colloidal sol transformed into a gel (Figure 1-3 b).

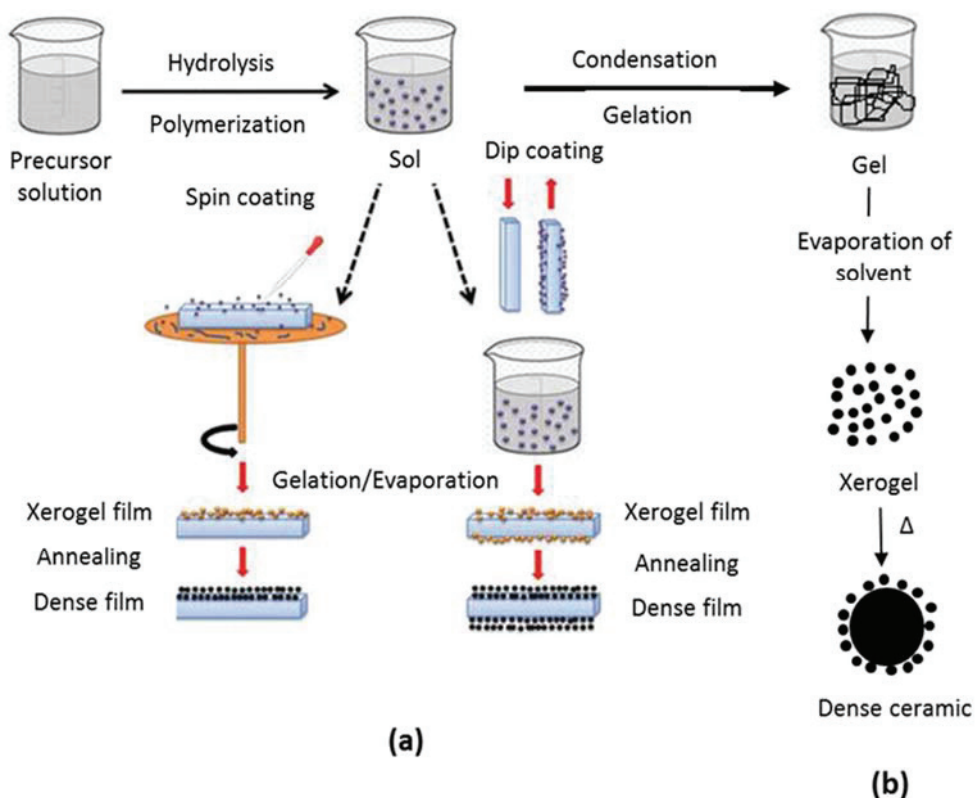
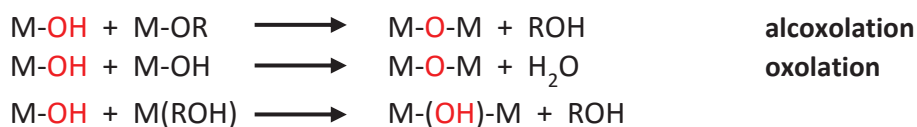


Figure 1-3: Examples of synthesis by the sol-gel method: (a) films from a colloidal sol; (b) powder from a colloidal sol via a gel. ⁵²

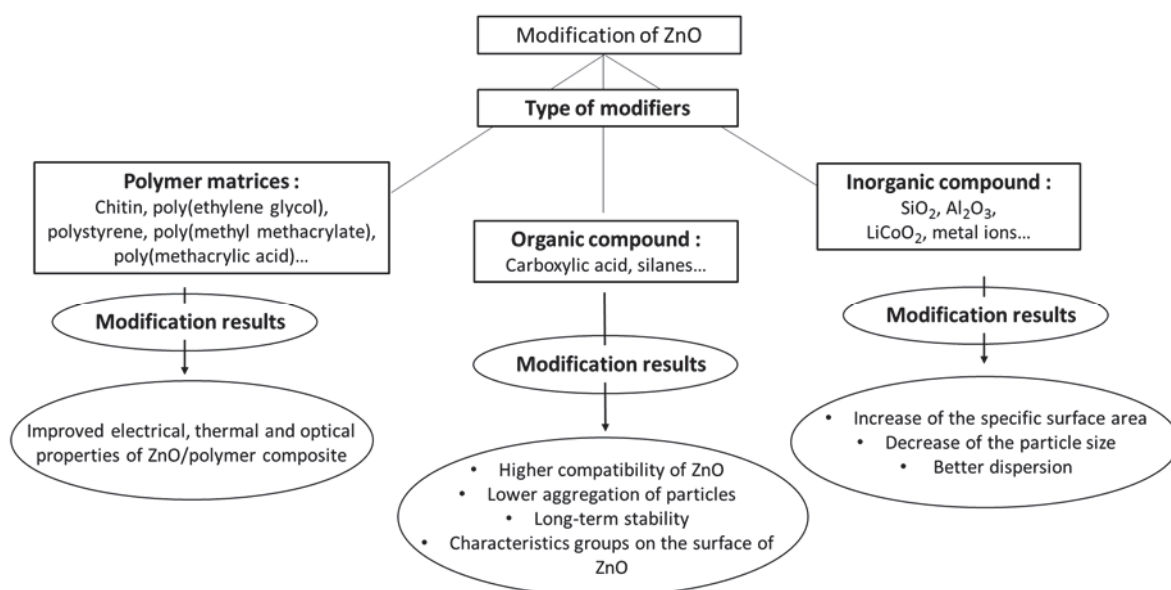
Sol-gel process is also known for its large ability on controlling and modifying the surface and the textural properties of the elaborated (nano)materials. The process can be described as formation of an oxide network through hydrolysis-polycondensation reactions of a molecular precursor (usually metal alkoxides and alkoxysilanes) in an organic solvent. The general formula of metal alkoxides is $[M(OR)_n]_m$ where M is the metal or non-metal element, R an alkyl or aryl group and m the nuclearity such as $Ti(O^iPr)_4$, $[Zr(OEt)_4]_4$, $Si(OEt)_4$... In the first step, the precursor is hydrolyzed into hydroxide species which undergo polycondensation step leading to the elaboration of an oxide /hydroxide network.

Hydrolysis reaction:**Polycondensation reactions:**

The sol-gel process is considered to be kinetically controlled and process parameters such as the nature of the metal and its oxidation state, the nuclearity (m) of the complex, the amount of water, the temperature and others will strongly influence the characteristics of the final material. In the case of transition metals, the hydrolysis kinetics of the sol-gel process is extremely fast which generally leads to amorphous materials that require annealing. Process control requires working on precursor engineering to slow hydrolysis in this case. In the case of silicon, on the other hand, the phenomenon must be accelerated by the addition of a catalyst such as HCl, NaOH, NH₄F...

The process is considered simple, inexpensive, reproducible and relatively easy to implement under soft synthetic conditions. In addition, the sol-gel method allows the surface of zinc oxide to be modified with selected organic compounds by adding a surfactant [polymers like poly(methyl methacrylate), polyacrylic acid, Pluronic 123...], esters, glycerol, or even biosurfactants (sophorolipids, Emulsan...) during the synthesis. On the other hand, it allows morphological and structural controls and creation of porous material by the control of the drying and aging step leading to an increase in the specific surface area of ZnO compared to the other methods. The main drawback of sol-gel is that most of the precursors are generally expensive and sensitive to air which can limit the scaling up. Sol-gel process is also known to be time consuming especially if the ageing and drying steps have to be controlled. Finally, some structural modifications can happen at the densification stage (shrinking phenomenon) creating some undesired defects.

ZnO nanoparticles obtained by the sol-gel method are involved in many fields of application because the process gives the possibility to modify the surface or texture of ZnO by adding different additives in situ or by post-modification.⁵³ The scheme below lists a certain type of modification depending on the final application of the material (Scheme 1-3).



Scheme 1-3: Modification of ZnO (Type of modifiers and applications)

However, the chemistry of zinc alkoxides is very limited because most compounds are insoluble; being polymeric and/or inert. Only $[\text{Zn}(\text{OiPr})_2]_m$ (CAS No. 13282-39-8) is commercialized but insoluble in most common organic solvents. For this reason, the sol-gel route to ZnO uses zinc alkyls $[\text{ZnR}_2]$ ($\text{R} = \text{Et}, \text{iPr}, \text{cyclohexyl}$) as a precursor of choice, which in the case of ZnEt_2 is a commodity product (especially for ZnO deposits in the gas phase such as CVD, ALD...) ^{54,55}.

Syntheses of ZnO from zinc alkyl precursors were previously illustrated by the works of groups of Klabunde et al. ⁵⁶ and Chaudret et al. ⁵⁷ This latter one has studied different synthesis parameters reacting bisalkyl zinc precursor $[\text{Zn}(\text{c-C}_6\text{H}_{11})_2]$ in different types of solvents and ligands. Leaving a solution of dicyclohexylzinc (II) in THF at room temperature in open air led to agglomerated and crystalline zincite ZnO particles with undefined shapes and different sizes. Therefore, when the synthesis was done under argon and in presence of ligands as long chain amines, different morphologies of ZnO depending on the synthesis conditions were obtained as shown in Figure 1-4. The ligands used in the synthesis were: dodecylamine (DDA), hexadecylamine (HAD) and octylamine (OA) and the three types of solvents were THF, toluene and heptane.

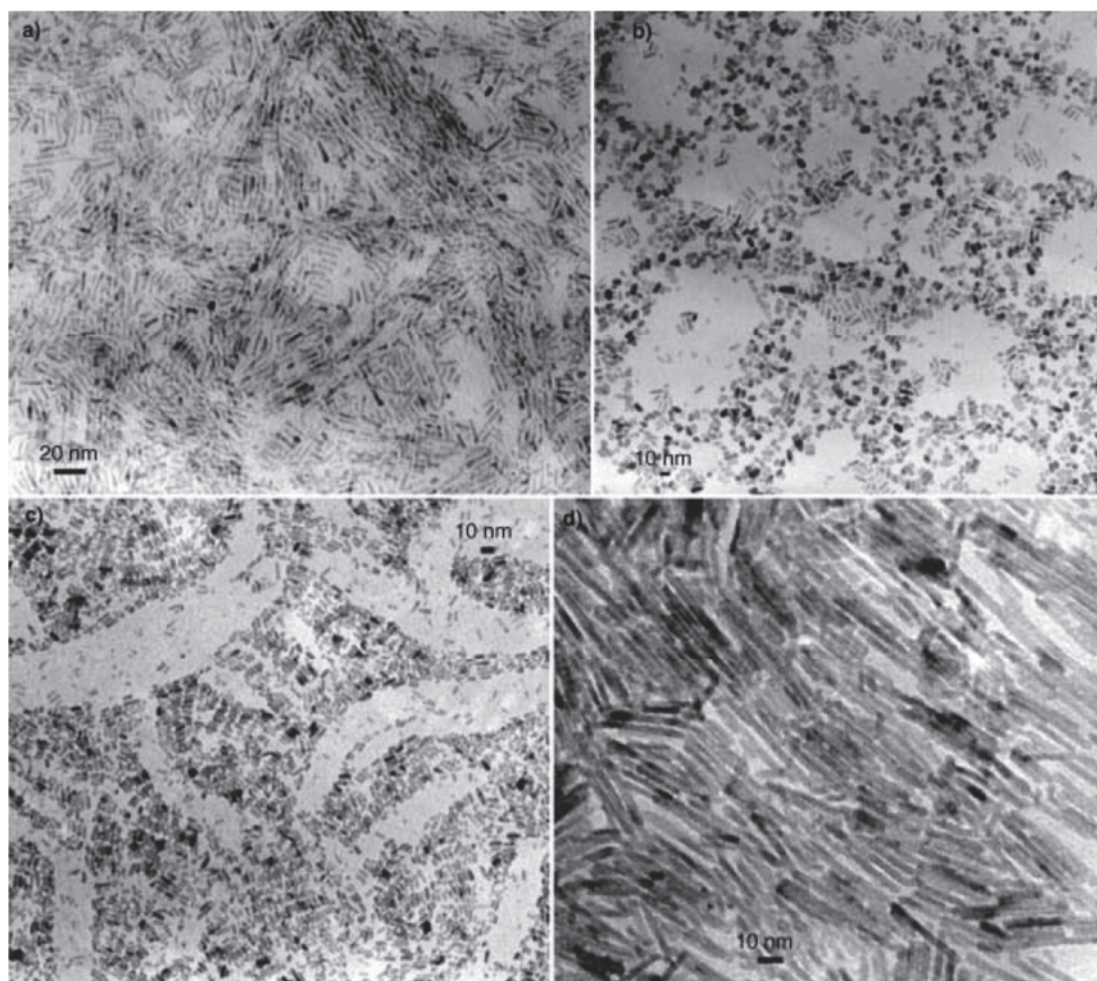


Figure 1-4: TEM micrographs of various ZnO nanorods, which were prepared using 1 equiv HDA (a), DDA (b), or OA (c) ligands in the absence of solvent; d) long ZnO nanorods obtained in the presence of 2 equiv OA as ligand, in the absence of solvent⁵⁷

All the syntheses were done at RT. Increasing the temperature till 45 °C under the same synthesis parameters (HDA ligand, 0.042 mol.L⁻¹ in presence of THF for 17 hours) resulted in the elaboration of nanodisks instead of nanorods with smaller size particle size of 4.8 nm diameter versus 8.1 x 2.6 nm (length x width), respectively. The presence of solvent helped having nanodisks in addition to nanorods while removing the solvent resulted in nanorods of inhomogeneous particles. The smallest nanodisks of 2.4 nm diameter were obtained in presence of HDA and heptane at RT. This study showed the importance of controlling the synthesis parameters and the relation between the type of the stabilizing agent and the morphology and the size of the final material.

Recently, we have studied the effect of polymeric modifying agent, such as polyacrylic acid

(PAAH), for the synthesis of ZnO from ZnEt₂ ⁵⁸. Sol-gel method was applied at RT, the ZnEt₂ precursor being added directly and under stirring into aqueous solution of PAAH at different concentrations. TEM images showed hybrid mesospherical ZnO-PAAH agglomerates elaborated in presence of PAAH (2 000 and 5 000 g.mol⁻¹) at 0.63 wt%. The particle size of the agglomerated particles was between 150-200 nm and 50-100 nm, respectively. Increasing the chain length to 100 000 and 240 000 g.mol⁻¹ resulted in different morphologies as platelets and undefined aggregates for the two systems. Very recently, Daniele et al. reported the doping of ZnO-PAAH with different metals (Ni, Co, Al, Cu...) and at three different concentrations (0.1, 1 and 5%) using the same approach ⁵⁹. The results showed that the increase in dopant concentration led to quenching of visible luminescence for ZnO nanoparticles. Nevertheless, at low doping concentration, this phenomenon could be avoided.

1.2.2.5. Miscellaneous methods

Other approaches to get different shapes of ZnO via chemical processes are possible but will not be detailed in this manuscript because outside the scope of this work, it is:

- Growing ZnO crystals from a gas phase described by Grasza et al. ⁶⁰
- Thin layer of ZnO by pulsed layer deposition (PLD) synthesized by Wei et al. ⁶¹
- Ultrapure particles of ZnO obtained by Zhao et al. via an aerosol pyrolysis ⁶²
- Connected rods of ZnO using a sonochemical process and microwave heating applied by Hu et al. ⁶³
- Ellipsoids and flakes of ZnO obtained by precipitation in an emulsion system described by Jesionowski et al. ⁶⁴

1.3. Applications of ZnO

ZnO is a very interesting material, applied in different fields as we will address in the following sections. From 2020, ZnO world production is estimated to be 10⁵ tons per year. For 2013, the producing countries and the fields of application are given in Figure 1-5 ⁶⁵:

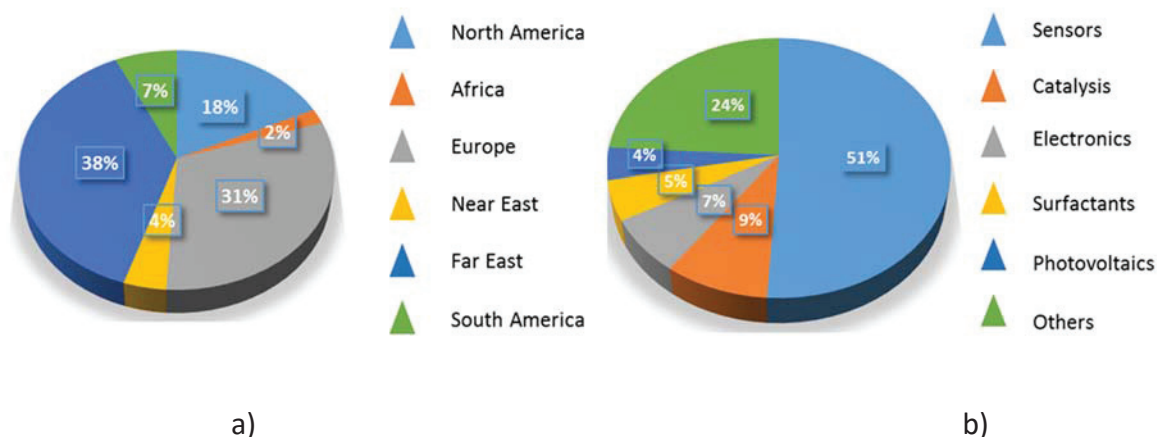


Figure 1-5: ZnO a) productive countries and b) applications fields. Redrawn from reference 65

1.3.1. ZnO as additive in rubber industry

ZnO is used as an additive in the manufacture of cross-linked rubber products ⁶⁶. In fact, the thermal conductivity of typical pure silicone rubber is low. In order to improve it, thermal conductivity fillers such as metal powders, metal oxides and inorganic particles can be added. ZnO can improve the thermal conductivity of silicone rubber while maintaining its high electrical resistance. However, ZnO tends to aggregate and to form larger particle size in the polymer matrix. In addition, ZnO is commonly used as a cross-linking agent for carboxylated elastomers. It can also be used to produce vulcanizates with high tensile strength. Unfortunately, zinc oxide crosslinked carboxylic elastomers have poor bending properties and high compression set.

In order to solve these problems, ZnO particles can be modified by adding different compounds to fit the upcoming criteria:

- Improve the interaction between ZnO nanoparticles and the polymer to have a better dispersion
- Produce vulcanizates with better mechanical properties and higher crosslink density
- Increase the interphase between elastomer carboxylic groups and ZnO nanoparticles mainly in form of snowflakes

The disadvantage of using ZnO in the rubber industry is its impact on the environment after the end of the product's life as zinc element has a toxic effect on aquatic organisms when releases in excess into the water ⁶⁷.

1.3.2. ZnO as antibacterial agent for food industry and medical applications

ZnO nanoparticles have been developed as a successful candidate in the food industry^{27,68}. Some of the main advantages of ZnO NPs are their capacity to inhibit bacterial growth when added on food packaging. The use of ZnO as an antibacterial agent against foodborne pathogens in food industry has required interdisciplinary research linking physicists, biologists, chemists, and medicine.

ZnO is also used for medical applications, as an oral medication for epilepsy and diarrhea⁶⁹. It can be used in dermatological substances against itching and inflammation due to its properties that accelerate wound healing. It can have a peeling effect when applied in higher concentration. ZnO is used in various types of food supplements, nutritional products, nail fortifiers and as component of dental pastes⁶⁸.

1.3.3. ZnO in electronic and technological applications

The wide band gap of ZnO and the high binding energy at room temperature make ZnO a perfect candidate for photoelectronic and electronic equipments. Due to its luminescent properties, ZnO is used in field emission display (FED) equipment such as TV and laptops⁷⁰. With regard to its conductivity and visible ray permeability, it is possible to obtain the production of light-permeable electrodes in solar batteries. Nevertheless, it is a promising material for UV emitting device and has potential for use as a transparent electrode in photovoltaic⁷¹. It is also found in gas sensors, lighting protectors, electrical equipment for protection against network overvoltages and production of varistors¹⁹.

1.3.4. ZnO as photocatalyst

ZnO is used as photocatalyst by being irradiated by light with an energy higher than its bandgap energy (3.3 eV). The mechanism is explained by the absorption of the light energy that triggers the charge separation and excites electrons from the valence band (VB) to the conduction band (CB). Holes are left in the VB⁷². The photogenerated e^-/h^+ carriers then move to the surface of the ZnO photocatalysts. Generally, the electrons play the role of reducing agents by transforming the O_2 molecules into O_2^- super oxide radical and the holes play the role of oxidative agents by transforming the reactant into his oxidative. A recombination phenomenon between e^- and h^+ can occur before attending the surface of ZnO and cause the

deactivation of the photocatalyst. The Figure 1-6 illustrates the photodegradation mechanism of pollutants by using ZnO ⁷³.

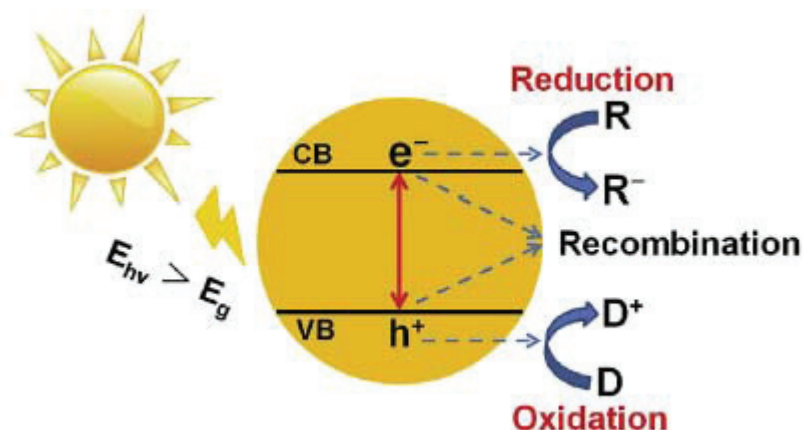


Figure 1-6: Basic mechanism of ZnO photocatalysis. E_{hv} is the irradiated photon energy, E_g is the energy gap, VB is the valence band, CB is the conduction band, R is the electron acceptor and D is the electron donor ⁷³.

The main drawback of ZnO photocatalysts is their limited effectiveness in the use of sunlight, as they are only active under UV irradiation and do not absorb visible light because of their wide band gap ⁷⁴. To overcome this drawback, researchers have developed several methods, such as doping of transition metals (Fe ⁷⁵, Co ⁷⁶, Ni ⁷⁷), or rare earth metals (Ce ⁷⁸, Dy ⁷⁹...) and alkali metals (Na ⁸⁰, Mg ⁸¹) and nonmetal atoms, coupling with other semiconductors or carbonaceous materials and deposition of noble metals ^{20,82,83}. In fact, doping metal or nonmetal atoms can modify the photoelectric properties of ZnO to extend its spectral response to the visible light region as it can effectively reduce the band gap of semiconductors ⁸⁴. Doped metal or nonmetal atoms change the coordination environment of the Zn atom and tune the electronic structure of the ZnO by adding localized electronic energy levels in the band gap (Figure 1-7). Photogenerated charge carriers are then trapped and photocatalytic activities are consequently increased in visible range ^{85,86}.

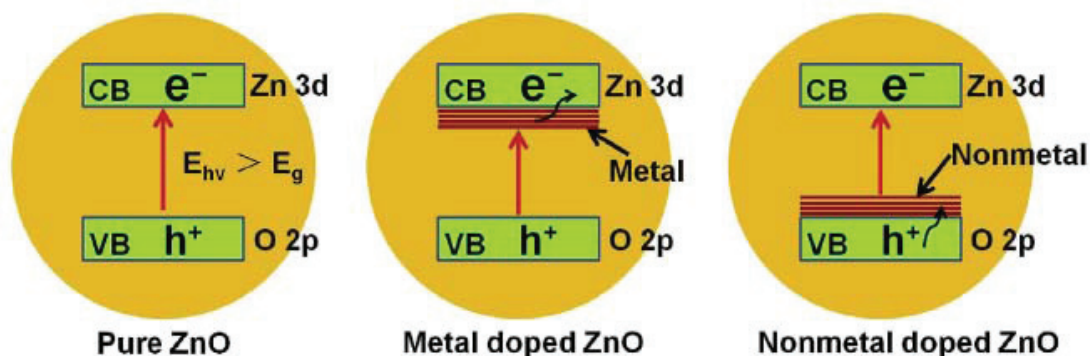


Figure 1-7: Schematic of the comparison of the band structures of pure, metal-doped ZnO, and nonmetal-doped ZnO ⁷³.

1.3.5. ZnO as support for heterogeneous catalysts

In addition to the use of ZnO as photocatalyst in different reactions as in water splitting and waste water treatment, ZnO is used in catalytic reactions as a support due to his wide morphology and its interesting properties. We will list some reactions and discuss more in detail the role of ZnO in the transformation of biomass.

1.3.5.1. ZnO for CO oxidation

The most used catalyst in this reaction with ZnO as support is Au as active metal. Many studies showed the impact of the morphology of ZnO on this reaction.

Carabineiro et al. ⁸⁷ studied three different ZnO for this reaction. They compared between two commercial ZnO (one purchased from Evonik and the second one from Strem Chemicals referred as ZnO_{EV} and ZnO_{SC}, respectively). They prepared their own ZnO by chemical vapour deposition (CVD). 1 wt% of gold was supported on the three supports to compare them and explore which sample will show a strong metal-support interaction. They found that the ZnO prepared with CVD (ZnO_{CVD}) is the one showing the highest activity for CO oxidation with 2 mol_{CO}/g_{Au}⁻¹.h⁻¹. When they compared the morphology of the three samples, they found that Au on ZnO_{CVD} is in the form of nanocrystals epitaxially oriented on the ZnO rods leading to a strong metal-support interaction and resulting in an increase in the catalytic activity. Au supported on ZnO_{EV} and ZnO_{SC} did not have a define morphology resulting in lower interaction between gold and ZnO NPs leading to a decrease in the activity of the catalyst compared to the Au/ZnO_{CVD}.

1.3.5.2. ZnO for methanol synthesis

For methanol synthesis by the hydrogenation of CO₂, the most active system is Cu/ZnO/Al₂O₃. As for CO oxidation, many studies focused on the effect of the morphology of ZnO on the activity of the catalyst. For example, Liao et al.⁸⁸ prepared copper catalysts supported on ZnO nanorods or ZnO nanoplates and Al₂O₃. The difference in morphology between the two ZnO led to difference in the interaction between copper particles and ZnO. Under different catalytic conditions (CO₂:H₂ molar ratio and temperature of reaction), the catalysts prepared with ZnO nanoplates had a higher selectivity toward methanol (around 70 % for all the reaction) than the copper supported on ZnO nanorods resulting in a selectivity of 40 %. The difference came from the higher concentration in oxygen vacancies with the ZnO nanoplates. Actually, in the case of the nanoplates a strong interaction between the (002) facet of ZnO and Cu existed due to the transfer of the electrons of ZnO to the Cu Fermi level.

Cu/ZnO (filament-like) and Cu/ZnO (rod-like) were studied by Lei et al.⁸⁹. Once again the higher interaction between ZnO and Cu due to the higher exposure of (002) ZnO facet resulted in higher activity of the Cu/ZnO (filament-like) with 16 % of CO₂ conversion and 78 % of selectivity toward methanol compared to 8% of conversion and 62 % of selectivity toward methanol with Cu/ZnO (rod-like) catalysts.

1.3.5.3. ZnO for methanol steam reforming

As for methanol synthesis, Cu/ZnO catalysts were extensively studied for the methanol steam reforming reaction. In the following example⁹⁰, the authors showed the importance of the high specific surface area of ZnO on the catalytic activity. They designed a core-shell nanostructured catalyst by elaborating nanorod of ZnO enclosed in Cu nanoparticles shell and compared the activity of their catalysts to a commercial one. The designed catalyst showed 93 % methanol conversion versus 88 % conversion with the commercial one but the main difference comes after the recyclability test where the conversion with the designed catalyst decreased only to 82 % while it decreased till 55 % with the commercial one. The authors explained the higher activity and resistance toward the catalytic reaction conditions of their system by the higher specific surface area compared to the commercial catalyst resulting in a better dispersion of copper particles on the ZnO support and facilitating the contact between methanol and the catalyst.

1.3.5.4. ZnO for biomass transformation

Since the conversion of biomass is attracting much attention, the researches related to this subject were extended to new innovative systems. Nevertheless, ZnO was always a good candidate for these reaction due to its interesting properties (surface modification, amphoteric character...). In the following sections, few articles about biomass transformations using ZnO as support are described:

a. Cu-ZnO for the hydrogenolysis of sorbitol into polyols

In the paper of Gallezot et al ⁹¹, authors investigated the role of CuO-ZnO (33 : 65) catalyst purchased from United catalysts Inc. in the hydrogenolysis of sorbitol derived from starch. They obtained an almost total conversion (98 %) of sorbitol under 130 bar of H₂ with 35 % selectivity to deoxyhexitol (hexane 1,2-diol, hexane 1,6-diol, hexane 1,2,3-triol ...) at 240 °C. At 180 °C under the same H₂ pressure, conversion decreased to 92 % but selectivity increased till 63 % toward deoxyhexitol. An important point to mention from this study was the leaching of zinc ions in the solution after catalysis due to the acidity of the reaction medium. Working in basic conditions reduced the amount of Zn²⁺ in solution from 30 to 13 ppm at 180 °C.

b. Ni/ZnO for the conversion of cellulose into 1,2-alkanediols

Wang et al. compared the effect of different oxide supports (ZnO, MgO, SiO₂, TiO₂, ZrO₂) and activated carbon with Ni-based catalysts for the conversion of cellulose ⁹². Among all these supports, ZnO showed the highest conversion due to his amphoteric character leading in accelerating the dehydration reaction (the 1st reaction in the mechanism). The authors showed that increasing the amount of nickel to 20 wt% achieved a total conversion till 30 wt% of Ni, which decreased when the amount of nickel was further increased. The authors explained this decrease in activity by the decrease of the specific surface area of the catalyst at higher loading of nickel (from 22 m².g⁻¹ to 16 m².g⁻¹).

c. Additional examples

One of the most interesting reactions in biomass conversion is the production of bio-diesel by transesterification of oils and fats. In the paper of Liu et al. ⁹³, authors produced biodiesel by transesterification of soybean oil in the presence of dispersed ZnO catalyst in methanol. The paper showed the effect of the pH of the solution on the nucleation growth of the ZnO particles and how it had an effect on the properties of ZnO and later on its catalytic activity.

In the paper of Morales et al.⁹⁴, authors studied the transformation of ethanol into aldehydes with ZnO nanoparticles. They found that (i) the ZnO with the highest specific surface area resulted in higher conversion and (ii) the catalyst with highest acidic sites resulted in higher selectivity toward ethylene. Many other examples exist in the literature for the use of ZnO as support in heterogeneous catalysts specially in hydrogenation reactions such as: hydrogenation of fructose to mannitol⁹⁵, hydrogenation of furfural to 2-methylfuran and furan⁹⁶, hydrogenation of butyric acid into butanol⁹⁷.

In conclusion, ZnO is a valuable support for the deposition of active metals in the form of nanoparticles for many applications. The quest now is to know how to deposit the catalyst in order to obtain high performance in glycerol hydrogenolysis.

II. Heterogeneous catalysts: preparation methods

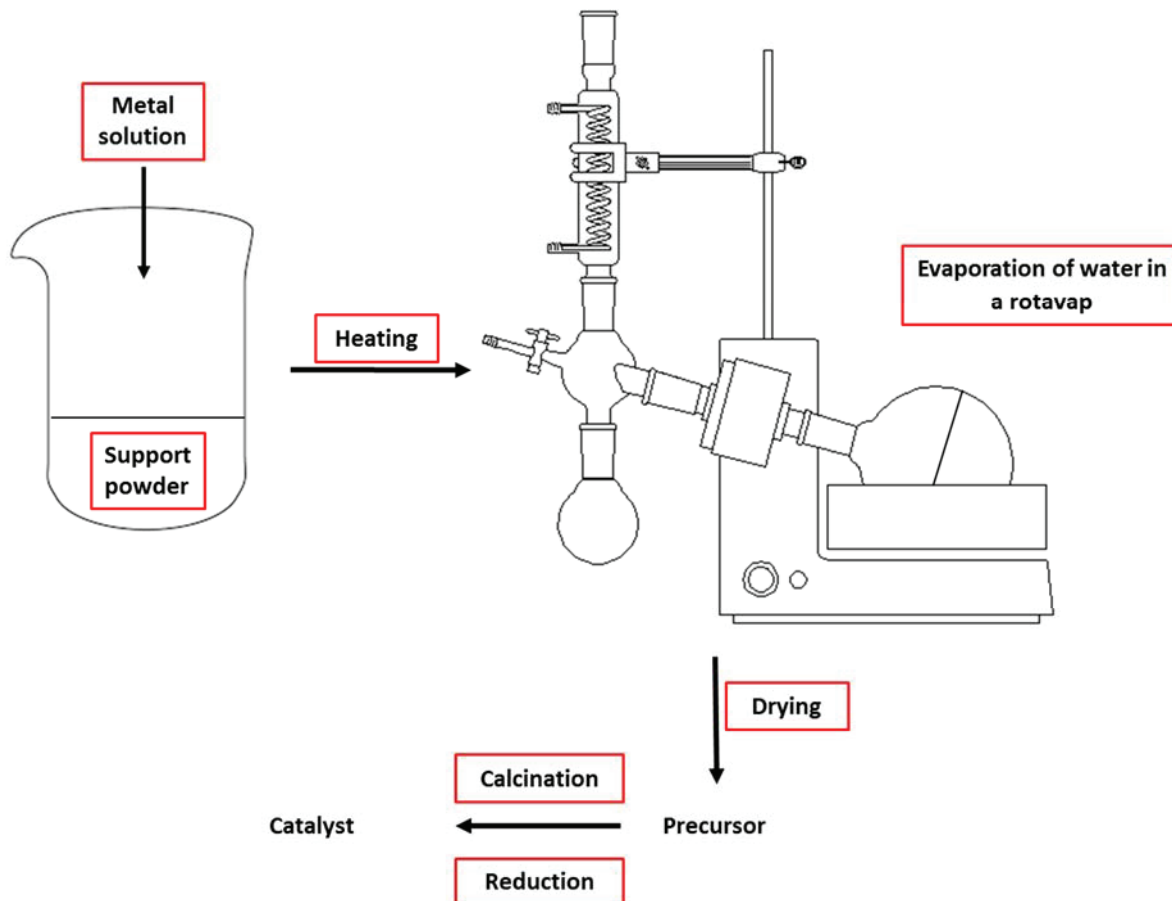
Heterogeneous catalysis, which consists of carrying out a reaction in the gas or liquid phase on a solid catalyst, is at the heart of modern energy and chemical industries. Most chemical processes are performed using functional nanomaterials as catalysts⁹⁸.

Moreover, heterogeneous catalysts encounter challenges during preparation. Having appropriate physico-chemical properties specific to the desired application is challenging. To have these properties, the catalyst must have active metal particles, a high dispersion of these particles on the support, a high resistance to avoid leaching problems and a high interaction with the support. At the same time, the support must have good distribution and high porosity, thermal stability to withstand harsh reaction parameters, acidity or basicity appropriate to the catalytic reaction. All these properties can lead to an increase in the activity, selectivity and stability of the support, and then of the catalyst. At the same time, as mentioned in LePage's book⁹⁹, this catalyst should be manufactured on an industrial scale without losing its properties and activity.

In order to produce the most efficient catalyst, many preparation methods have been developed. The following section describes the most common methods for synthesizing copper based catalysts. When possible, the examples will focus on Cu/ZnO and the effect of the preparation method on the specific surface area of the catalyst and the stability of copper particles during the catalytic reactions. We will see how the surface area of ZnO plays a major role in the dispersion of Cu particles and their size and how is it possible to control these

parameters. Most of the research conducted to elaborate copper-based catalysts were made for methanol synthesis^{100–102}.

II.1. Impregnation



Scheme 1-4: Simplified scheme for the preparation of catalysts by impregnation method

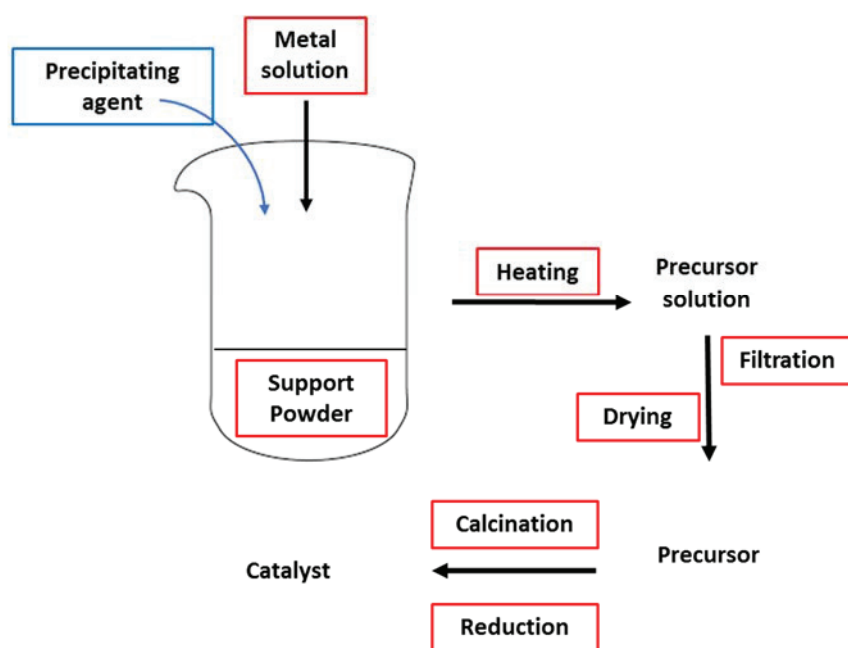
Impregnation is one of the easiest methods of preparing heterogeneous catalysts. It consists of dissolving a metal salt in water and adding a certain volume of this aqueous solution to the powder support followed by heating and stirring. If the volume of the aqueous solution of the metal precursor is greater than the pore volume of the support, the impregnation is called wet impregnation. At the end of the first step, the water is removed by a rotary evaporator. If the volume of the aqueous solution of the metal precursor is equal to the pore volume of the support, the method is called dry impregnation and the sample is just dried after the first step. In both cases, the sample has to undergo heat treatment (calcination and/or reduction) to transform the precursor into active metal particles. Scheme 1-4 presents an overlook of the preparation of a catalyst by impregnation method. One of the advantages of this method is

the large choice of supports that can be used, and the ease and low cost of preparation. It can be however hard to achieve high loading of active metals.

In the Wang's paper cited above ⁹², Ni/ZnO was prepared by incipient wetness impregnation using nickel nitrate $[\text{Ni}(\text{NO}_3)_2 \cdot 6\text{H}_2\text{O}]$ as precursor. The catalyst elaborated after being capped 12 hours at room temperature, calcined at 400 °C and reduced at 500 °C for 5 hours showed a very low specific surface area of 12 $\text{m}^2 \cdot \text{g}^{-1}$ and high crystallite size of Ni around 23 nm. The performance in terms of conversion were lower than compared to the same system prepared by co-precipitation.

Most of the studies elaborating metal-based catalyst (copper in particular) using ZnO as support, combine it with Al_2O_3 in order to increase the specific surface area of the catalyst. Tanaka et al. ¹⁰³ prepared Cu/ZnO/ Al_2O_3 by impregnating $\gamma\text{-Al}_2\text{O}_3$ support with an aqueous solution of copper and zinc nitrates. After calcination at 500 °C for 3 hours, the catalyst reached an average specific surface area of 115 $\text{m}^2 \cdot \text{g}^{-1}$. A high specific surface area is not always enough when the impregnation method is applied because the metal particles are usually inhomogeneous, in terms of size and morphology, due to the random nucleation growth that occurs during the drying step.

II.2. Deposition-Precipitation (DP)



Scheme 1-5: Simplified scheme for the preparation of catalysts by Deposition-Precipitation (DP) method

The elaboration of non-noble metal catalysts (nickel and copper) with high metal loadings using deposition-precipitation (DP) as a synthesis method, was developed by Geus et al.^{104,105}. The method involved the precipitation of a metal hydroxide on the surface of a support. In practice, an aqueous solution of the metal precursor and an alkaline precipitating agent [e.g. NaOH, NH₄OH, CO(NH₂)₂] were added to a suspension of the support powder. The method consisted in converting a highly soluble inorganic metal salts into another less soluble compound which precipitated on the support. The conversion of the metal precursor into low soluble compound was achieved by raising the pH of the solution. Figure 1-8 shows the principle of the method. In a first step, the metal precursor was converted into his low soluble compound which was above the saturation curve appointed as S and in a second step it precipitated in the area where the concentration was higher than the supersolubility (supersaturation) curve appointed as SS. In order to precipitate the metal precursor on the surface of the substrate and not in the solution, an interaction was mandatory. Therefore, the SS curve was shifted to the lower concentration in the presence of the support and it was called SS_{support}. The general mechanism of the DP method is illustrated in scheme 1-5.

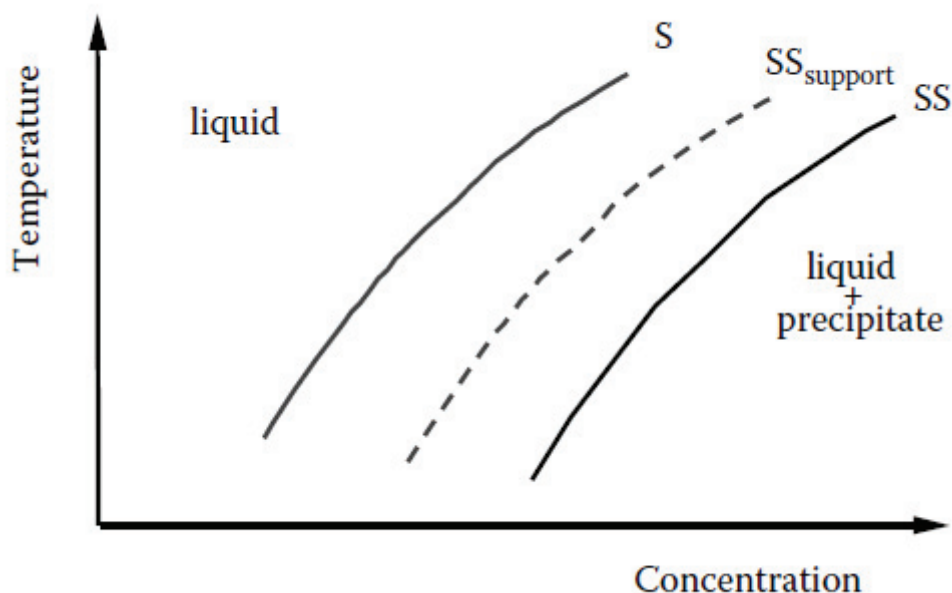


Figure 1-8: Diagram for precipitation of metal precursor. S= solubility curve, SS_{support}= supersolubility curve of the metal precursor in presence of the support and SS= supersolubility curve in liquid⁹⁸.

In order to have homogeneous dispersion of nucleates onto the support, the precipitating agent must be added gradually, otherwise the concentration above the SS curve increased drastically leading to a fast nucleation phenomenon of the precipitate in the solution. The nucleation barrier could be decreased by enhancing the interaction of the precursor with the support and this could be done if the nucleation at the surface of the support was occurring when the concentration was between S and SS. In the following section we will see some examples of catalysts prepared by deposition precipitation. The general experimental method consists in adding the carrier to the solution of the metal precursor under stirring; the precipitating agent is then added. The temperature and time of heating depend on the precipitating agent and the precursors. Most of the time, the longer the deposition time, the better the dispersion of the metal on the support.

As with the impregnation method, the sample after the synthesis is then washed, dried and subjected to a heat treatment (reduction) to be active. Several groups have used this preparation method for non-noble metals ^{105–107}, and later it was developed for the production of catalysts containing noble metals, in particular gold ¹⁰⁸. The main advantage of the deposition precipitation method is the possibility of depositing a large quantity of metal via a controlled deposition. Thanks to the good interaction between the support and the precursor, the metal is highly dispersed, which gives a very active phase after heat treatment.

The first use of Cu catalysts prepared by deposition precipitation for the hydrogenolysis of glycerol was reported by Xia et al in 2012 ¹⁰⁹. Two different catalysts of Cu/SiO₂ were prepared, the first by homogeneous deposition-precipitation and the second by heterogeneous deposition-precipitation. In the first case, aqueous solutions of ammonia-aqua copper complex ($[\text{Cu}(\text{NH}_3)_4(\text{H}_2\text{O})_n]\text{SO}_4$ with a pH 11) and silica (SiO₂ 40 wt%) were mixed under stirring at room temperature for 3 hours. The mixture was then heated to 80 °C and kept at that temperature for 20 hours to slowly remove the ammonia. The resulting gel was then filtered, washed in hot distilled water, dried at 120 °C overnight, and later calcined at 450 °C under air for 3 h. For the second catalyst, a suspension of dried SiO₂ gel was poured into an aqueous solution of Cu(NO₃)₂ and stirred for 3 hours at room temperature. Then, an aqueous NaOH solution (up to pH = 10) was added to quickly precipitate Cu(OH)₂ species on SiO₂. The temperature was then raised to 80 °C for 4 hours. The solution was washed at neutral pH and dried at 120 °C overnight and air-calcined at 450 °C for 3 hours. Table 1-2 shows the effect of

both preparation methods on material properties and catalyst activities.

Table 1-2: Texture of the calcined Cu/SiO₂ samples and results for the glycerol conversion

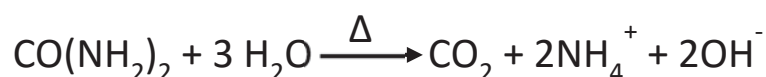
Catalyst Properties	Homogeneous deposition precipitation	Heterogeneous deposition precipitation
CuO ^a (wt%)	30.5	31.0
BET surface area (m ² .g ⁻¹)	366	334
Pore volume ^b (cm ³ .g ⁻¹)	0.72	0.85
Cu-dispersion ^c (%)	24.6	16.2
Cu particle size ^c (nm)	4.1	6.2
Conversion (%)	22.1	35.0
Selectivity for 1,2-PDO (%)	98.0	93.7

^a Measured by XRF, ^b BET Method, ^c Calculated from dissociative N₂O adsorption ¹⁰⁹.

As expected, the homogeneous deposition-precipitation method had resulted in higher copper dispersion and hence smaller copper particle size. Nevertheless, the catalytic properties of the catalyst prepared by heterogeneous-deposition precipitation showed a better conversion. It is unfortunate that the authors did not compare the characteristics of the catalysts after the reaction. However, they observed that the catalyst prepared by homogeneous deposition-precipitation was not stable and that after the catalysis, the metal particles were sintered into large aggregates.

II.2.1. Deposition-Precipitation with urea (DPU)

An interesting deposition precipitation method is by using urea as precipitating agent, noted as DPU method. When urea is added to the medium, the pH is increasing gradually after heating the medium because the decomposition temperature of urea is around 60 °C following the reaction:



Thus, compared to the traditional DP method, DPU allow to separate the addition of the base and the moment when the base starts to act, urea is known as a delay base. An important parameter to consider for the DPU method is the PZC (zero charge point) of the support. Even if the deposition of the metal begins before reaching the PZC of the substrate, the maturation step begins when the pH increases and reaches a plateau higher than the PZC of the substrate.

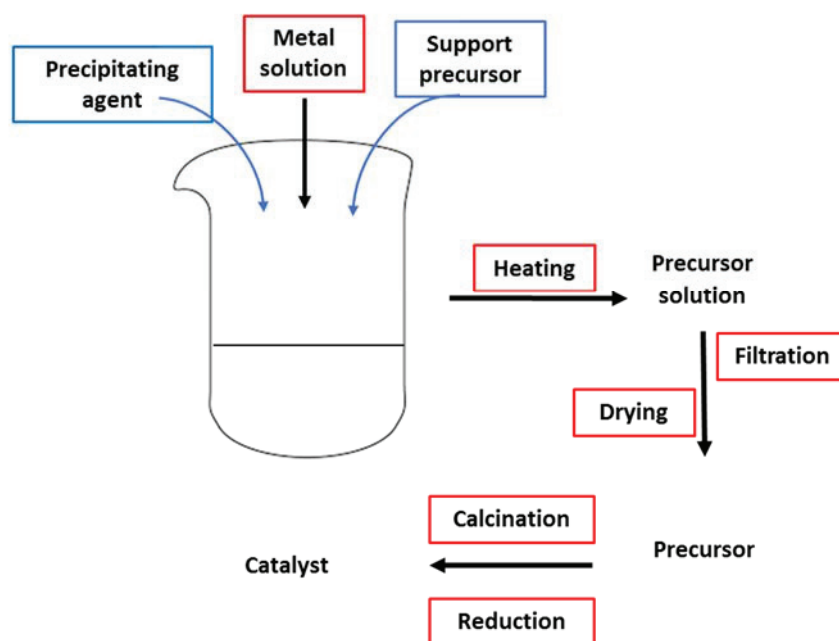
This phenomenon leads to a decrease in the particle size of the active metal as the maturation time increases.

The DPU method was notably developed by C. Louis *et al.* on Ni and Cu catalysts^{110,111}. Two of their studies, on Cu/ZnO¹¹² and Cu/TiO₂¹¹³ are discussed. These examples allow to compare the effect of the support on the properties of the final catalyst.

In the first report, 1% by weight of Cu/ZnO was synthesized by dissolving copper nitrate in an aqueous solution ($\text{Conc}_{\text{Cu}^{2+}} = 2.4 \times 10^{-3} \text{ M}$) and adding it to 3 g of commercial ZnO (Kadox-911, BET = 8 m².g⁻¹) in a glass reactor.¹¹² The mixture was heated at 80 °C and 0.96 g of urea was added to the solution and kept under heating and stirring for 20 h. The solution was centrifuged and the solid was washed several times with water and dried for 24 hours at room temperature under vacuum. After synthesis, the solid was calcined at 400 °C under oxygen for 2 h and reduced under hydrogen at 350 °C for 2 hours. The thermal treatment had a big impact on the catalyst and they consider that for the first time a Cu₃Zn alloy was formed in Cu/ZnO sample. In addition to the thermal effect, the study compared the effect of the preparation method on the behavior of the catalyst. For that reason, in parallel for Cu/ZnO prepared by DPU, Cu-ZnO was prepared by incipient wetness impregnation. It was found that by DPU method Cu⁰ nanoparticles of 4 nm were obtained compared to 22 nm by the impregnation method.

In the second report, different catalysts were prepared by changing the concentration of the copper precursor.¹¹³ The same preparation method: 0.8 wt% and 1.55 wt% of Cu/TiO₂ were prepared by mixing 1 g of TiO₂ (P25 Evonik – BET = 50 m².g⁻¹) in suspension in 100 mL of water and a copper nitrate solution. The mixture was heated at 80 °C for 20 hours after adding 5 g of urea. The drying procedure of the sample was the same: centrifugation followed by washing and drying. The sample was directly reduced under H₂ at 350 °C for 2 hours, without calcination. After studying the effect of the heating treatment on the catalysts, the pre-calcination step was shown to affect the size distribution of the metal but only when the precursor is different than copper nitrate. For that reason, in this study, authors abandoned the calcination step. This paper focused on studying the mechanism of DPU and the effect of Cu loading, time reaction and pH on the catalyst. Due to the high surface area of TiO₂, Cu⁰ particles with a size smaller than 1 nm were obtained. A high specific surface area therefore seems a prerequisite for obtaining very small nanoparticles and therefore a high dispersion.

11.3. Co-precipitation method



Scheme 1-6: Simplified scheme for the preparation of catalysts by co-precipitation method

The co-precipitation method is quite similar to the deposition-precipitation one; the difference being that the support is formed at the same time as the deposit. The method consists of adding solutions of both precursors at the same time to ensure nucleation and growth of the metal on the support and adding a precipitating agent as for deposition-precipitation. These compounds have low solubility and precipitate, a separation step is performed to recover the precipitate and heat treatments are used to activate the material. Solutions of metal precursors are often highly soluble (chlorides, sulfides and nitrates) and are likely to combine with basic reagents in the form of hydroxides and alkali carbonates to form metal hydroxides and metal carbonates. The conditions of synthesis such as the temperature, the stirring time, the nature of precursors, the washing, the drying and the method of mixing affect highly the structure of the catalyst and its surface. The high supersaturation levels, the changes in the solid phase during the process, the chemical changes during the aging of the precipitates and the low stability of supersaturated solutions make the study of the mechanism of this method difficult. In summary, the process consists on mixing precursors solutions, the formation of the primary particles by nucleation and crystal growth and the aggregation of these particles. Later the filtration, or any kind of separation, is done to remove

the excess of solutions followed by thermal treatment to activate the catalyst. Scheme 1-6 gives an overview of the preparation of the catalyst by the co-precipitation method.

Anyway, this method has many advantages, and the main one is that it guarantees small particle sizes even with a high metal loading (up to 80 % sometimes). This high content of metal on the support cannot be achieved by another preparation method. In one hand, the process is fast and it involves simple steps contributing in an easy control of the particle size and the composition of the catalyst. On the other hand, it gives high output and recovery and there are different ways to modify the surface of the particles leading to a high surface area. Unfortunately, this method results in large quantities of salt solutions after the filtration of the product. Another drawback is that the catalyst will be in powder form while for some catalytic reactions it is better to have it in a defined shape as tablet or extrudate.

In the review of Schlögl et al.¹¹⁴, copper and zinc nitrates are combined and alkali carbonates have been used as precipitating agent to produce Cu/ZnO. They showed that the atomic distribution of the different species within the solid solution was strongly related to the crystalline nature of the metal precursor. In addition, the choice of a pure and crystalline phase of the precursors made it possible to control the synthesis of the catalyst and thus to increase the reproducibility of the synthesis.

In this context, the objective was to find a composition that optimized the dilution of active species in a refractory matrix species. As a general rule, a 1:1 ratio should be advanced to reach high inter-dispersion. But in this example [zincian malachite: $(\text{Cu,Zn})_2(\text{OH})_2\text{CO}_3$], the 1:1 ratio is not compatible with the miscibility range of the target precursor phase. Authors also noted that the meso-structure of the precursor compound must be taken into account. Platelets, needles structures led to a large specific surface area accessible by creating porous aggregates. Ultimately, the heat treatment was carried out in a very specific way (the flow rate and heating temperature must be strongly controlled) and with particular attention. The low calcination and reduction temperatures saved the large interface between the matrix and the final phase.

Figure 1-9 shows the different steps before obtaining the active catalyst:

- First a step a) of meso-structuring is in progress. In this step, thin needles of zincian malachite are obtained by crystallization of the homogeneous precipitate of Cu, Zn

obtained by co-precipitation ageing at constant pH in the initial solution.

- The nano-structuring step b) is very important because it is the determining step in the porosity of the final catalyst. The resulting needles are calcined to decompose into a mixture of CuO and ZnO.
- The reduction step c) leads to the elaboration of the active catalyst Cu/ZnO with a microstructure revealing high Cu dispersion and porosity.

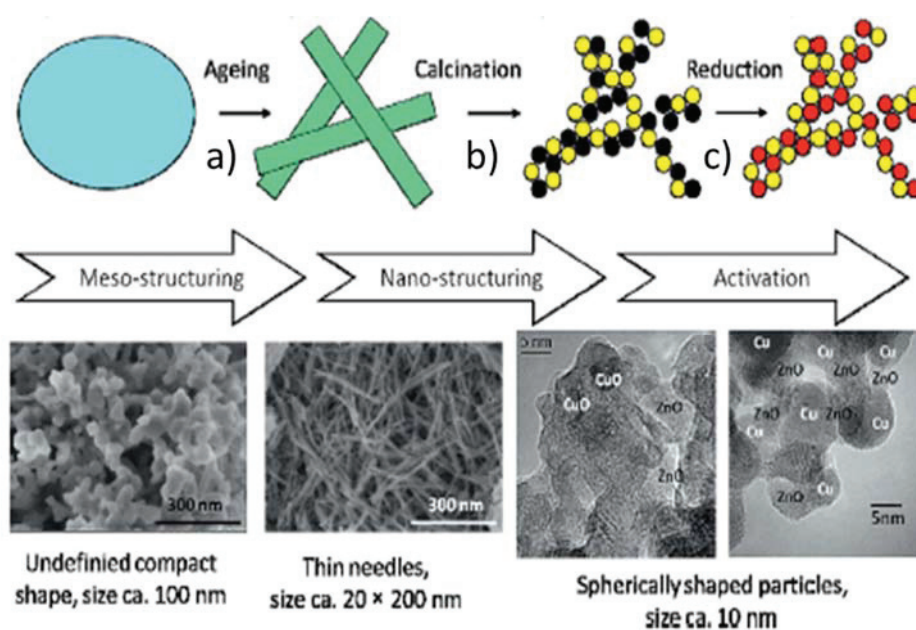


Figure 1-9: Preparation scheme of Cu/ZnO catalyst and TEM images of the different stages of preparation ¹¹⁴.

II.3.1. Alternative anions

In order to improve the contact between Cu and ZnO, an upgrade of the classical co-precipitation method was done and the method is known as alternative anions. In this method, citrate is used instead of carbonate. The method was developed by Courty et al. and was then used by different groups for the preparation of Cu/ZnO/Al₂O₃ ¹¹⁵.

It consists of mixing Cu(NO₃)₂·xH₂O, Zn(NO₃)₂·6H₂O, Al(NO₃)₃·9H₂O with an appropriate amount of citric acid. The solution is heated to 85 °C for 2 hours to obtain a homogeneous mixture. Solvent evaporation is carried out in a rotary evaporator under pressure (700 Pa) and at the same temperature overnight. After drying at 110 °C for 4 hours, a calcination step is carried out in flowing air and the final catalyst is obtained. In this study, the effect of the

calcination temperature on the specific surface area of Cu was investigated. The results are summarized in the Table 1-3.

Table 1-3: Effect of the calcination temperature and the compositions of the catalysts on the Cu surface determined by N₂O chemisorption copied from ¹¹⁶

Catalyst	Composition CuO/ZnO/Al ₂ O ₃ (wt%)	Temperature of calcination (°C)	Cu S.S.A. (m ² ·g ⁻¹)	S.S.A./BET catalyst (m ² ·g ⁻¹)
CuZnAl	65/28/07	400	6.6	n.d.
CuZnAl	65/28/07	350	11	n.d.
CuZnAl	65/28/07	320	7.6	n.d.
CuZnAl	65/28/07	Four step calcination up to 350	10	n.d.
CuZnAl	65/28/07	Four step calcination up to 320	13	44.4
CuZn	70/30/0	Four step calcination up to 320	5.0	15.0
CuAl	70/0/30	Four step calcination up to 320	7.0	48.2
CuZnAl prepared by co- precipitation	65/28/07	320	24	53.7

n.d. = Not determined.

The effect of the calcination temperature on the activity of the catalyst for methanol synthesis showed that the first three catalysts in Table 1-3 had a lower activity than the others which were calcined in four steps. The result was explained by the increase of Cu particles sizes obtained after the one-step calcination. The increase was due to the exothermic decomposition of the precursor which resulted in a significant increase in CuO size and sintering of the Cu particles. With the same calcination steps, catalysts with a higher Cu specific surface area showed higher activity. The catalysts prepared by this method were compared to another one prepared by standard co-precipitation. The catalyst prepared by the co-precipitation method has the largest Cu specific surface area after calcination at 320 °C but did not show the best activity. The last three entries of the table show that the addition of Al resulted in an increase in the BET surface area of the catalyst prepared by alternative anion method but it was not as high as that of the co-precipitated catalyst.

In conclusion, while the Cu dispersion is an important criterion for catalyst activity, the preparation method and the interaction between the catalyst components are also crucial parameters for controlling the activity.

11.4. Other preparation methods of Cu-ZnO

Another type of precursors was used by Epple and his coworkers for the preparation of Cu-ZnO catalysts¹¹⁷. Two types of preparation were used: the batch precipitation and the continuous overflow methods (Figure 1-10).

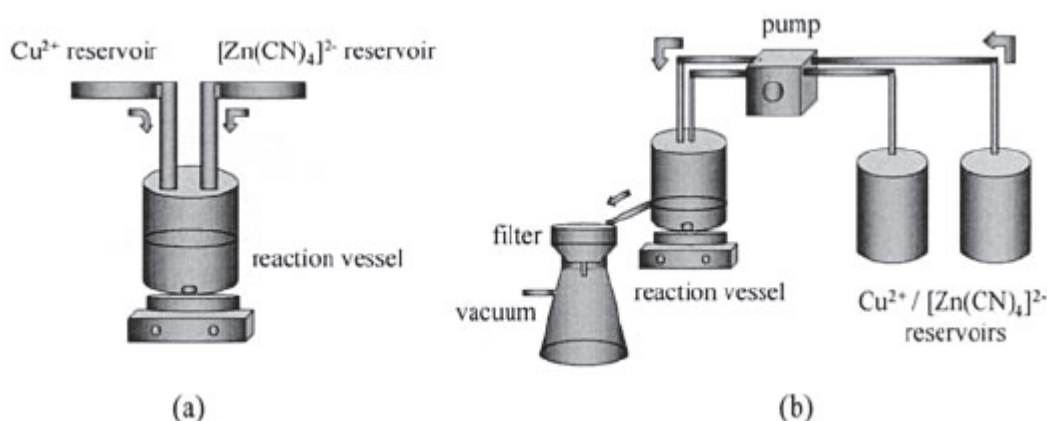


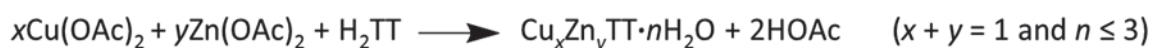
Figure 1-10: Setup of the batch precipitation method (a) and the continuous overflow method (b).¹¹⁷

In the batch precipitation method, [Zn(CN)₄]²⁻ was prepared by mixing aqueous solutions of zinc sulfate and potassium cyanide. Copper(II) sulfate was then added under stirring and copper zinc cyanide was obtained as precipitate. In the continuous overflow precipitation method, the aqueous solutions of K₂[Zn(CN)₄] and CuSO₄ were pumped at different flow rates into a stirred precipitation vessel at room temperature. The overflowing suspension was immediately filtered. The precipitate was air-dried overnight at room temperature.

In both preparation methods, the mixed coordination compound Zn[Cu(CN)₃] were heated at high temperature (300 °C to 500 °C) to give a 1:1 mixture of CuO and ZnO which was then reduced to Cu/ZnO under a mixture of H₂/N₂ (5/95) at 350 °C.¹¹⁷ The specific surface area obtained by this method was not reported but the particles size of copper was 3 nm and the catalyst particles were spherical which meant that the specific surface area should be high.

The same group worked on a different precursor: the mixed Cu/Zn L-tartrates¹¹⁸ which

contained both metals in a single solid phase and decomposed at moderate temperature (50 °C) because inorganic counter ions such as alkali metals or carbonate were avoided. The BET surface area increased with increasing ZnO content (from 2 m².g⁻¹ without ZnO to 45 m².g⁻¹ at 90 % molar of ZnO). The preparation method made it possible to obtain Metal L-tartrates (MTTs) with different Cu/Zn ratios. It consisted in precipitating the aqueous solution of copper acetate and zinc acetate with L-tartaric acid (H₂TT) according to this equation:



Sol-gel methods were also used by this group for the preparation of Cu/ZnO¹¹⁹. This paragraph lists two different ways to use metal nitrates as precursors [Cu(NO₃)₂.3H₂O, Zn(NO₃)₂.6H₂O and Al(NO₃)₃.9H₂O]:

First, a combination of sol-gel synthesis and photochemical oxidation was applied to obtain a mixture of CuO/ZnO nanocrystals. Sol-gel consisted of the precipitation of precursors in methanol by adding hydroxide in the presence of silane. Photochemical oxidation was responsible for the removal of organic substituents from the silane and contributed to the elaboration of an amorphous SiO₂ layer leading to a significant increase in the specific surface area of the catalyst (from 15 to 120 m².g⁻¹).

The second sol-gel method was done by using propylene oxide as gelation initiator to elaborate xerogels and aerogels of ZnO/Al₂O₃, CuO/Al₂O₃, and CuO/ZnO/Al₂O₃. For the aerogel preparation, the solvent was extracted with supercritical CO₂. Using the same synthesis parameters, aerogels had a higher specific surface area and a higher Cu specific surface area than the corresponding xerogels. These catalysts were used for methanol synthesis and aerogels catalysts showed a higher activity. By comparing catalysts with and without ZnO, the presence of ZnO revealed an increase in the catalytic activities of xerogel and aerogel due to stronger support-metal interaction.

Table 1-4: BET surface area, pore volume and catalytic activity of Cu/Zn/Al calcined xerogels and aerogels ¹¹⁹

Sample	Cu content (wt%)	Nature	BET S.S.A. catalyst (m ² .g ⁻¹)	Cu / S.S.A. (m ² .g ⁻¹)	Catalytic activity in methanol synthesis (%)
CuO/Al ₂ O ₃	50.9	Xerogel	34	3.7	2.0
CuO/Al ₂ O ₃	52.7	Aerogel	222	5.2	4.0
CuO/ZnO/Al ₂ O ₃	39.3	Xerogel	57	2.6	4.9
CuO/ZnO/Al ₂ O ₃	34.2	Aerogel	175	6.0	22

Organometallic complexes can be prepared by mixing equimolar quantities of copper bis stearate and diethyl zinc in toluene at room temperature. This preparation method was carried out by Williams et al ¹²⁰ for the synthesis of methanol as shown in the Scheme 1-7. Many changes in the solution color appeared during synthesis, proving the exchange of ligands between Zn and Cu complexes and leading to copper-alkyl species and zinc carboxylate. This technique led to the development of an active catalyst (as active as the commercial one) with small Cu particle size (1-4 nm) and organometallic zinc compounds. One of the advantages of this method is that no heating was used for synthesis and reproducible catalysts were prepared due to the simplicity of the preparation. The catalytic results are summarized in the Table 1-5.

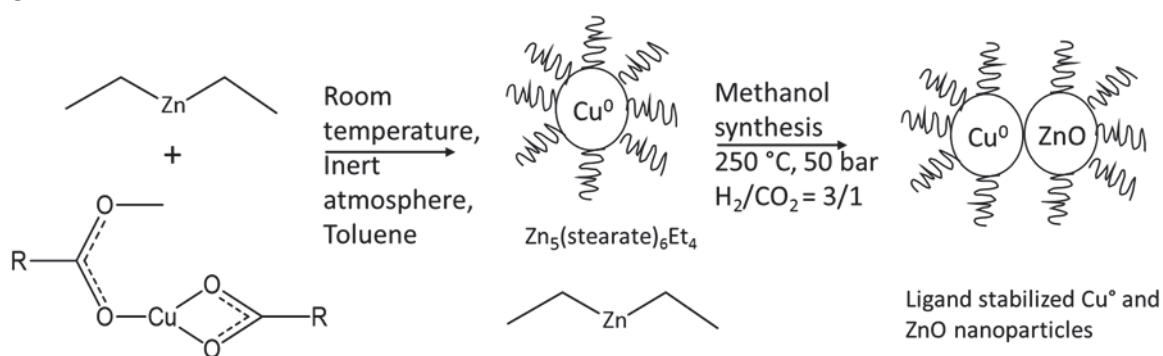
Scheme 1-7: One pot synthesis method for the elaboration of the ligand stabilized Cu and ZnO nanoparticles ¹¹⁸.

Table 1-5: Effect of the weight ratio of ZnO:Cu on the catalytic activity for CO₂ hydrogenation to methanol¹²⁰

Entry n°	Molar ratio precursors ZnEt ₂ : Cu(stearate) ₂	Theoretical weight ratio ZnO:Cu	Methanol maximum activity / mmol.g _{ZnOCu} ⁻¹ h ⁻¹	Methanol activity after 12h/ mmol.g _{ZnOCu} ⁻¹ h ⁻¹
1	1:3	30:70	39	39
2	1:1	55:45	60	58
3	2:1	70:30	43	37
4	7:1	90:10	18	13

Table 1-5 shows that the increase in the Zn content led to an increase in the methanol conversion from 39 mmol.g_{ZnOCu}⁻¹h⁻¹ with the 30:70 expected ZnO:Cu molar ratio to 60 mmol.g_{ZnOCu}⁻¹h⁻¹ with the 55:45 molar ratio followed by a decrease at higher content of ZnO. This means that there was an optimal value of ZnO:Cu weight ratio.

In conclusion, there are a multitude of methods for preparing Cu/ZnO catalysts, each with advantages and disadvantages. In general, the preparation and heat treatment conditions have a remarkable effect on the final structure of the catalyst and ultimately on its activity, but other conclusions can be summarized:

- the co-precipitation method is one of the simple and the most widely used, but its disadvantage is the high risk of non-replication of the synthesis.
- DPU leads to very small Cu crystallites and strong metal-support interaction
- Sol-gel process gives usually high metal homogeneity and high specific surface area

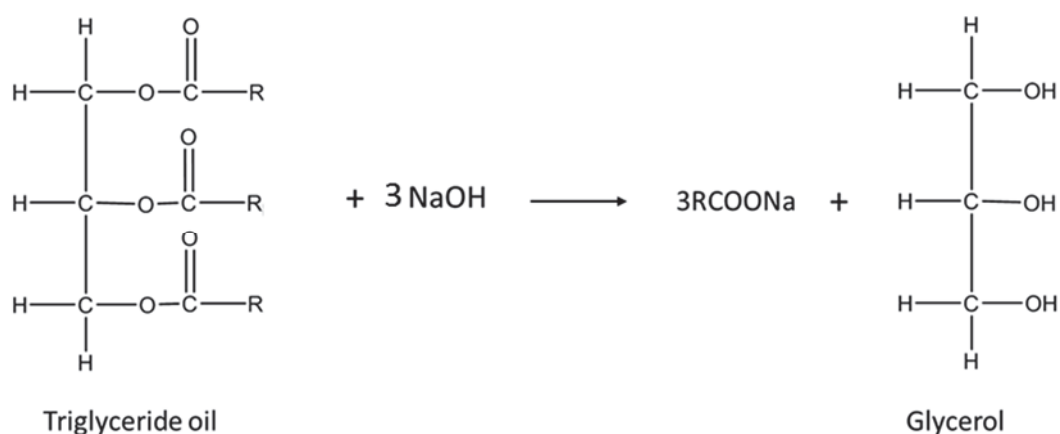
Al₂O₃ seems to be an essential promoter for increasing catalyst activity by:

- the increase in its surface area,
- increasing the long term stability of the catalyst,
- the increase in surface acidity,
- the decrease in particle size of the active metal

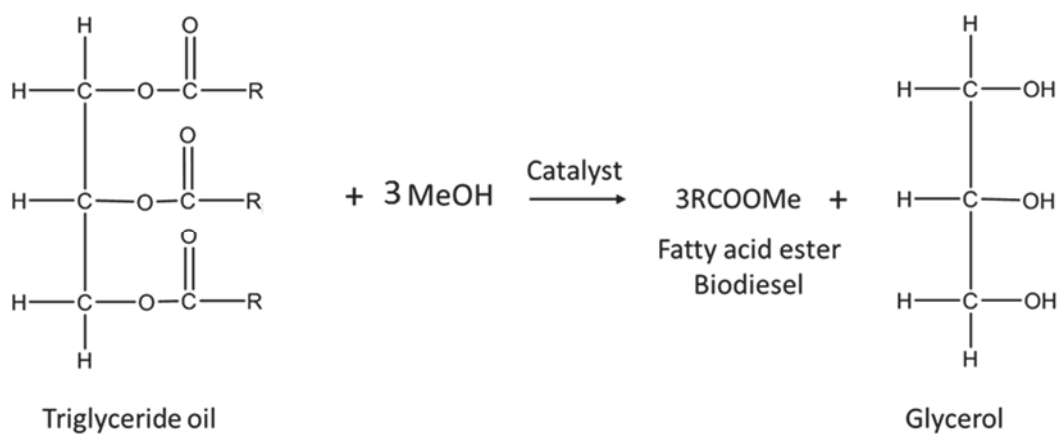
The post-treatment steps, i.e. washing, drying, calcination, reduction, must always be carried out carefully, whatever the method of preparation.

III. Glycerol as source for propanediols production

Glycerol is a component of triglyceride which can be found in most plant and animal oils and fats. Several routes contribute to glycerol production; it can be produced from saponification processes and from the biodiesel production as byproduct. In the first process, the hydrolysis of fats and vegetable oils in presence of an excess of sodium hydroxide or potassium hydroxide results in carboxylate salts (soap) and glycerol. The process is known as the traditional soap manufacturing and it is shown in Scheme 1-8. In the 2nd process, the transesterification of triglyceride under acid, basic or enzymatic catalysis leads to the formation of biodiesel but with a large excess of glycerol, in which glycerol represents about 10 wt% of the total biodiesel produced ¹²¹. Scheme 1-9 shows the production of glycerol from the transesterification process.

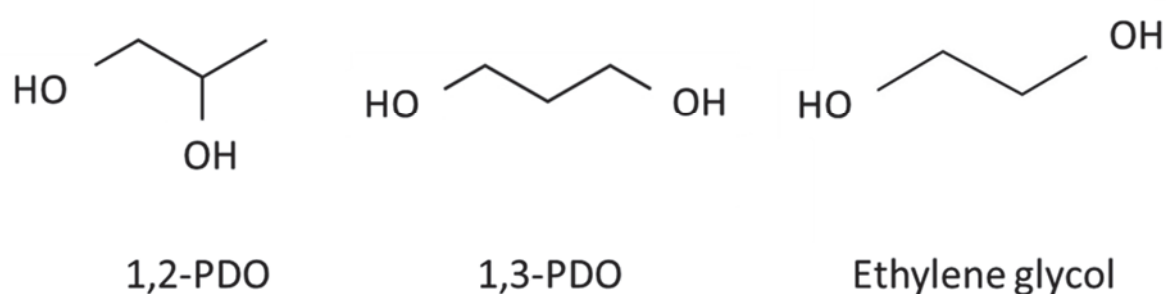


Scheme 1-8: Glycerol production by saponification process.



Scheme 1-9: Glycerol production from biodiesel.

In addition, biological fermentation processes for glycerol production from sugar are becoming useful route based on the inexpensive and abundant materials and cellulytic derivatives used for this production ^{122,123}. Glycerol has become more readily available as a renewable resource due to the increased production and application of biomass on one hand and the geopolitical benefit of this production on the other ¹²⁴. As a result, there is considerable interest in developing new technologies to convert glycerol into value-added chemicals such as propanediols and glycols with the following representation:



Glycerol hydrogenolysis has then been extensively studied in the recent years ^{125,126}, since main products obtained from this reaction are 1,2-propanediol (1,2-PDO) and 1,3-propanediol (1,3-PDO), isopropanol, n-propanol, ethylene glycol, propylene and propane. 1,2-propanediol is a synthetic organic compound widely used in industrial applications: polymer production, cosmetics, food industry, tobacco products and as de-icing fluid in aircrafts. In 2013 the global production of 1,2-PDO was 2.2 Million tons mainly in the USA and China ¹²⁷. 1,3-propanediol (1,3-PDO) ¹²⁸, is mainly used as a monomer for the production of: polytrimethylene terephthalate, a biodegradable polyester used in the manufacture of carpet and textile, polyethers and polyurethanes. The largest amount of propanediols is obtained by oxidation of propylene to propylene oxide. Nevertheless, more economical and less complicated routes can be applied.

The catalytic hydrogenolysis of glycerol consists in adding hydrogen to the substrate in order to break a C–C or C–O bond. Since the H–H bond is thermally stable, the addition of a metal catalyst is necessary in order to dissociate the H₂ molecule. The hydrogen adsorbed on the surface later reacts with the substrate and gives rise to new products. In the case of glycerol,

different products are obtained after hydrogenolysis depending on the catalyst and experimental conditions. Glycerol hydrogenolysis has been extensively studied in the recent decades and interesting results have been obtained ^{125,126}. Some groups studied the mechanism of this reaction, others focused on improving the activity and/or the selectivity toward propanediols. A summary of reported mechanisms is presented in the following pages, with a focus on 1,2-PDO as the main product.

III.1. Different mechanisms for the hydrogenolysis of glycerol into propanediol

Regarding the hydrogenolysis of glycerol to propanediols, catalysts based on noble metals (Pt, Pd, Rh and Ru) ^{129–132} and transition metals (Ni ^{133–135} and Cu ^{136–139}) have been studied in recent years. Depending on the experimental parameters (nature of the metal catalyst, nature of the support and solvent), different types of reaction mechanisms have been proposed in the literature. The most frequently cited are a 2 steps mechanism (dehydration followed by hydrogenation) and a 3 steps mechanism (dehydrogenation followed by dehydration and hydrogenation). The dehydration-hydrogenation mechanism is promoted by the presence of an acidic catalyst helping the first step of the mechanism to occur. The most used catalysts are Cu supported catalysts that can combine the acidic and the hydrogenation functions. While the 2nd mechanism is favored in neutral and alkaline conditions and it is more known with metal noble catalyst as (Ru, Pt...) ¹⁴⁰.

III.1.1. Dehydration of glycerol into 1,2-PDO and 1,3-PDO

The dehydration mechanism was first proposed by the group of Suppes ¹⁴¹ in 2005 using a copper-chromite (Cu-Cr) catalyst with 80 wt% glycerol solution, 14 bar at 200 °C and after 24 hours. Glycerol was first dehydrated to acetol, which reacted further with hydrogen and formed 1,2-PDO (Scheme 1-10). The catalyst was reduced in the reactor just before adding the reactants, which means that no surface hydroxyl groups could participate to the reaction. In order to validate their mechanism, they split the reaction into two steps. Initially, they isolated the acetol formed solely by the presence of the catalyst (without adding hydrogen). In the second step they added hydrogen to the acetol generated in the first step, and conducted the reaction with the same catalyst as previously. The yield of 1,2-PDO (around 50%) obtained by combining the two steps confirmed the mechanism.

This mechanism was also known for the acidic catalysts ^{142,143} or with metals catalysts with the

Other studies have shown a different pathway with bimetallic catalysts under the following reaction conditions: 67 wt% glycerol, 120 °C, 80 bar of H₂, 150 mg of catalyst and for 12 hours. The direct hydrogenolysis was proposed by Tomishige's group over Ir-ReO_x/SiO₂¹⁴¹ and Rh-M/SiO₂¹⁴² (M = Re, Mo or W) catalysts. Authors reported that glycerol was adsorbed at the interface between Ir or Rh metal surface and ReO_x cluster to form two terminal alkoxides: 2,3-dihydroxypropoxide and 1,3-dihydroxyisopropoxide. In a second step, the C-O bond was cleaved by nucleophilic attack on hydride, activated by iridium metal, on the positions 2 or 3 of dihydroxypropoxide (Figure 1-11). The last step was the release of the propanediols by hydrolysis of the resulting alkoxide. In this reaction, 1,3-PDO was obtained with a higher selectivity than 1,2-PDO which could be explained by the greater stability of the transition state of the intermediate alkoxide leading to 1,3-PDO.

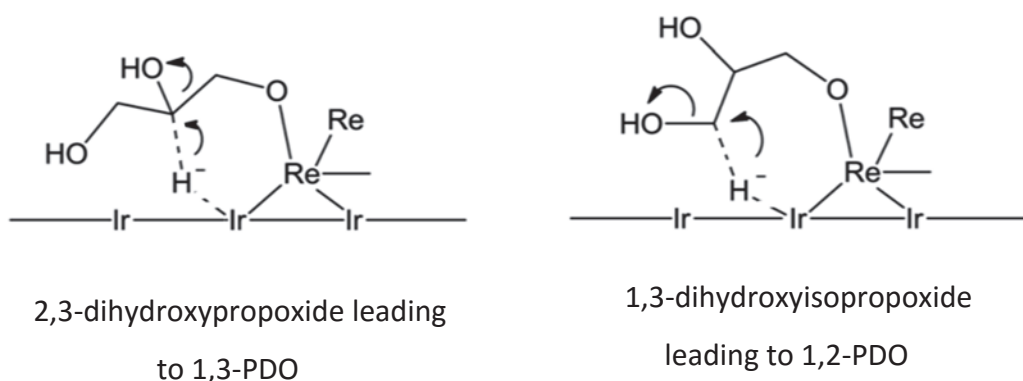


Figure 1-11: Model structures of the transition states of the hydride attack to the adsorbed substrate in the glycerol hydrogenolysis¹⁴¹.

III.2. List of copper catalysts for glycerol hydrogenolysis

Glycerol hydrogenolysis reaction has been extensively studied over catalysts based on Rh, Pt, Pd, Ru, Ni and the results have been summarized in different reviews¹⁴⁹⁻¹⁵². Table 1-6 shows a non-exhaustive list of some results from the literature using the metals cited above in a batch reactor.

Table 1-6: Short list for glycerol hydrogenolysis over noble metals and Ni supported catalysts

Catalyst	T(°C)/P _{H₂} (bar)/t(h)	Glycerol (wt%)/Cat(g)	Conversion (%)	Selectivity (%)	Ref
Rh/ZnO	180/20/12	2.5/0.2	98	28	129
Pt/TiO ₂	210/60/6	4.5/1	25	60	153
Pd/Fe ₂ O ₃	180/0/24	12/0.6	100	94	154
Ru/Al ₂ O ₃	240/80/5	1.27/0.9	69	38	155
Raney Ni	190/10/44	8/2	97	71	156

The main drawback of the noble metals catalysts is their high price compared to the transition metals but also their activity toward C-C cleavage resulting in high conversion of glycerol but low selectivity toward 1,2-PDO as seen in Table 1-6. Pd/Fe₂O₃ resulted in high conversion and high selectivity but it differs from the other listed experiments by removing external H₂ from the reaction medium and replaced it by inert gas and produce H₂ in-situ by dehydrogenation of 2-propanol or ethanol.

As we reported in the introduction, copper-based catalysts also have been extensively studied for glycerol hydrogenolysis and have a high selectivity towards 1,2-PDO under mild conditions. This can be explained by the low activity of Cu for C-C bond cleavage and high efficiency for C-O bond cleavage^{141,142,157} compared to noble metal catalysts.

III.2.1. Cu-Cr catalysts

The first report of copper as a catalyst for glycerol hydrogenolysis was from a Cu-Cr system by Adkins' group in 1932¹⁵⁸. The conversion was 55% and the selectivity to 1,2-PDO 85 % but the reaction conditions were harsh: 250 °C and 200 bar of H₂.

Later, less severe conditions were applied as in 2005 by Dasari et al.¹⁴¹. First, they tested different commercial catalysts including palladium, ruthenium, nickel, copper, and copper chromite in the form of metal oxides or supported metal on C or alumina at 200 °C and 14 bar of H₂ for 24 hours. The most active was a copper chromite supplied by Sud-Chemie, it showed

a conversion of 54.8 % with a selectivity of 85 % to 1,2-PDO. They studied different parameters for glycerol hydrogenolysis using this catalyst and proved the dehydration-hydrogenation mechanism by isolating the intermediate acetol. A summary of the best results, obtained in this publication, in term of conversion and selectivity is listed in the Table 1-7. All the results were obtained after 24 hours of reaction and at 80% weight concentration of glycerol for $\text{CuO}_x(\text{Cr}_2\text{O}_3)_y$ catalyst.

Table 1-7: Effect of the synthesis parameters and reaction conditions on the hydrogenolysis of glycerol¹⁴¹

Catalyst (wt%)	P (bar)	T (°C)	Water content (wt%)	Conversion (%)	Selectivity 1,2-PDO (%)
5	14	200	20	54.8	85.0
20	14	200	20	78.5	62.0
5	14	260	20	87	8.8
5	14	200	0	69.1	71.9
5	20.7	200	20	65.3	89.6

In 2009, Liang et al.¹⁵⁹ prepared Cu-Cr catalysts with high specific surface area (up to $88 \text{ m}^2 \text{ g}^{-1}$) via impregnation of $\text{Cu}(\text{NO}_3)_2$ and $\text{Cr}(\text{NO}_3)_3$ [Cu/Cr molar ratio = 1/5] on carbon followed by removal of the carbon template. Authors investigated the effect of the Cu/Cr ratio and found that the optimum molar ratio Cu/Cr was 1:5 in order to reach a conversion of 51% and a selectivity of 97.1% to 1,2-PDO, at 200 °C, under 14 bar H_2 and after 10 hours. **This study highlighted that an increase in specific surface area led to an increase in the conversion of glycerol.**

Later, other methods of preparation were studied. In 2010, Kim et al. reported different Cu/Cr catalysts prepared by a NaOH co-precipitation method¹⁶⁰. They studied the effect of the molar ratio by first testing a pure Cu catalyst (a conversion of 28% was obtained with a selectivity of 60% to 1,2-PDO) while a pure chromium catalyst was not very active (10% conversion) and not selective. The most active catalyst was a Cu/Cr catalyst with molar ratio 1:2 containing mainly the spinel phase of CuCr_2O_4 and achieving a 80.3% conversion with a selectivity of 83.9% toward 1,2-PDO. All catalysts were studied under the same conditions (50 g of concentrated glycerol at 90%, 220 °C, 80 bar of H_2 in presence of 1 g of catalyst and after 12 hours). It seems that the optimal metal ratio depends on the method of preparation.

In the two studies showing the spinel phase of CuCr_2O_4 , the effect of increasing the acidity of the catalyst due to that phase was reflected in higher conversion of glycerol.

Mane et al. in 2011¹⁶¹ studied the coprecipitation method with NH_4OH in order to prepare Cu/Cr catalysts. They also added Ba, Zn and Al as promoter where the conversion was low (16%) without Ba and reached 34% after adding the promoter with a selectivity of 82% to 1,2-PDO. The reaction conditions were 220 °C under 52 bar of H_2 and 5 hours using 20 wt% glycerol in 2-propanol and 1 g of catalyst. **Adding a promoter to the catalyst seems to be mandatory in some cases to enhance the activity of the catalyst due to the increase of surface area or the acidity by the promoting groups.**

A new preparation method was developed by Xiao et al. in 2012¹⁶² through an alkoxide-free sol-gel process. The aim was to produce small particle size of Cu and Cr, using $\text{Cu}(\text{NO}_3)_2$ and $\text{Cr}(\text{NO}_3)_3$ as precursors and precipitated by propylene oxide. Once again, the reaction conditions were mild (42 bar H_2 , 210 °C, 60 wt% aqueous glycerol solution, 5 wt% catalyst and 10 hours of reaction) and the conversion was 85.9% and the selectivity was 98.5% toward 1,2-PDO (only traces of propanol and acetol). **This method allowed the conservation of the small particles even after the catalytic conditions. The exact size is not given but from the XRD patterns, it could be seen that the only change is a slight increase in the intensity of the main copper peak (at 43°) after test.**

The last mention of Cu-Cr as catalyst for this liquid phase reaction was made by Yi et al. in 2016¹⁶³. The study focused on theoretical calculation to understand the mechanism of the reaction but they also compared a pure Cu catalyst with a Cu-Cr one prepared using the coprecipitation method. As other studies have showed, the Cu catalyst was less active than Cu-Cr. Indeed, the conversion increased from 19.6% to 32% and selectivity in 1,2-PDO increased from 52.6% to 73.8% by adding Cr under the same conditions (220 °C, 40 bar of H_2 , for 12 hours, 1 g of catalyst and 40 wt% glycerol solution).

III.2.2. Cu/ZnO catalysts

As mentioned above, the activity of Cu-Cr for this reaction was significant but the toxicity of chromium contributed to the search for a substitute. In order to maintain a high selectivity towards 1,2-PDO, Cu/ZnO proved to be an interesting candidate. This system has been widely applied in different industrial processes such as methanol synthesis, water gas shift reaction

and methanol steam reforming as it was cost-effective and easy to handle. Table 1-8 reports in chronological order the most significant results for the hydrogenolysis of glycerol over Cu-Zn systems and Cu based catalysts.

The first use of a copper-zinc catalyst for glycerol hydrogenolysis was reported in 2004 by Chaminand et al ¹⁶⁴ at IRCELYON. However, the activity of the catalyst was low with respect to the high catalyst loading and the long reaction time, the selectivity for 1,2-PDO was 100% at 19% of conversion. The reaction conditions are mentioned in the first entry of the Table 1-8.

Table 1-8: Different Cu based catalyst reported for glycerol conversion

Entry	Catalyst	$\frac{W_{\text{catalyst}}(\text{g})}{W_{\text{glycerol}}(\text{g})}$	C_{glycerol} (wt%)	P (bar)	T (°C)	Duration (h)	Conversion (%) ^a	Selectivity 1,2-PDO (%) ^a	Ref
1	CuO/ZnO	5/15	19	80	180	90	19.0	100	164
2	Cu-ZnO	4.7/15	20	42	200	12	33.9	77.5	145
3	Cu-ZnO	1.2/20	20	20	200	16	37.0	91.0	157
4	Cu/ZnO/Al ₂ O ₃	-	20	14	200	24	47.9	93.8	137
5	CuO/ZnO	3/156	100	50	200	7	46.0	90	147
	CuO/ZnO	3/80	50	50	200	7	55	86	
6	Cu/ZnO/Ga ₂ O ₃	2.8/88	90	50	220	7	96	82	165
7	Cu/ZnO/Al ₂ O ₃	0.6/20	80	40	180	10	85.8	92.1	166
8	Cu/Zn/Al	-	20	17	200	20	72.6	76.4	167

Entry	Catalyst	$W_{\text{catalyst}}/W_{\text{glycerol}}$ (g)	C_{glycerol} (wt%)	P (bar)	T (°C)	Duration (h)	Conversion (%) ^a	Selectivity 1,2-PDO (%) ^a	Ref
9	ZnO	0.4/40	80	24	200	8	0.4	0	168
	Cu	0.4/40	80	24	200	8	4.9	17.5	
	Cu/ZnO	0.4/40	80	24	200	8	16.2	60.2	
	Cu/Cu ₂ O/ZnO	0.4/40	80	24	200	8	24.6	44.6	
10	Cu _{0.4} /Mg _{5.6} /Al ₂ O _{8.6}	1/7.5	75	30	180	20	91.2	95.5	169
11	Cu _{0.4} /Mg _{5.6} /Al ₂ O _{8.6}	1/8	75	20	180	10	56.7	97.1	170
12	Cu/MWCNT	0.8/16	80	40	200	6	77.2	74.2	171
13	CuO/ZrO ₂	0.4/20	4	25	200	8	31.3	94.5	172
	Cu/ZrO ₂	0.4/20	4	25	200	8	94	95	

^a at final time

The catalyst preparation method appeared to have a significant contribution and effect on the results. The best results were obtained with Cu-ZnO prepared by the co-precipitation method as mentioned by the following groups: Wang & Liu in 2007 (Table 1-8, entry 2)¹⁴⁵ and Balaraju et al. in 2008 (Table 1-8, entry 3)¹⁵⁷. They studied different Cu/Zn molar ratio but both groups found that the 1:1 molar ratio gave the highest activity for the production of 1,2-PDO. Compared to the Cu-Cr system mentioned above, the activity of these catalysts was low.

Balaraju et al.^{145,157}, have also studied the effect of the weight of the catalyst on the conversion and the selectivity. The catalytic reaction was carried out at 200 °C, under 20 bar H₂ and 20 wt% of glycerol for 8 hours. The increase of the catalyst weight from 0.6 g to 1.8 g led to an increase in the conversion from 13% to 26% (not proportional) and an increase in the selectivity toward 1,2-PDO from 87% to 90%.

In 2009, Meher et al.¹³⁷ have tested different combinations of mixed metal oxides (Mg/Al, Zn/Al, Ni/Mg/Al, Co/Ni/Mg/Al, Cu/Zn/Al) and found that Cu/ZnO/Al₂O₃ prepared by co-precipitation gave the best performance. At 200 °C, under 14 bar of H₂ with a molar ratio of Cu/Zn/Al 1:1:4, 47.9% of glycerol were converted with a selectivity of 93.8% to 1,2-PDO after 24 hours (Table 1-8, entry 4).

Other groups focused on comparing the same catalyst compositions prepared by different methods such as Bienholz et al. in 2010¹⁴⁷. One of the catalysts was prepared by NaOH coprecipitation and the other by oxalate gel-coprecipitation. The oxalate gel-coprecipitation reduced the size of the Cu particles compared to the NaOH coprecipitation method and resulted in a better metal dispersion with 6 nm Cu size and 17% Cu dispersion versus 12 nm Cu size and 9% Cu dispersion, respectively. A conversion of 17% was obtained with the catalyst prepared by NaOH coprecipitation which increased to 46% with the catalyst prepared by oxalate-gel coprecipitation method, both having high selectivity to 1,2-PDO (87% and 90%, respectively) Table 1-8 (entry 5). The above results were obtained with 140 mL of 50 wt% glycerol in the presence of 3 g of catalyst at 200 °C, under 50 bar of H₂ and after 7 hours as shown in Table 1-8. They have also studied the effect of water as deactivating factor and replaced it with 1,2-butanediol and found that the conversion was increased from 5% to 55% under the same conditions with a selectivity of 86%. This was due to sintering phenomenon which were more important (75 nm) in presence of water than 1,2-butanediol (47 nm), (Table 1-8, entry 5).

In 2011, Bienholz et al. reported that by adding Ga to a Cu/ZnO catalyst, the catalyst activity improved significantly¹⁶⁵. In their report, compared to the use of the Cu/ZnO catalyst prepared by NaOH coprecipitation, when Ga was added, the glycerol conversion increased from 84% to 96%; the experimental conditions were 220 °C under 50 bar H₂; 80% aqueous glycerol was loaded and the reaction lasted 7 hours. However, Ga is an expensive metal, which will result in a higher production cost (Table 1-8, entry 6).

In 2013, Tan et al.¹⁶⁶ reported a new preparation method for a Cu/ZnO/Al₂O₃ catalyst, called evaporation-induced self-assembly (EISA), in which Pluronic P123 was used as a structure directing agent, copper-acetate as the precursor of CuO, zinc nitrate as the precursor of ZnO and aluminum isopropoxide as the precursor of Al₂O₃. The experimental conditions were reported to be 180 °C and 40 bar of H₂; 80% glycerol was loaded and 3 wt% of catalyst was used; within 10 hours the glycerol conversion was 85.8% and the selectivity to 1,2-PDO was 92.1% (Table 1-8, entry 7).

In 2015, Kim et al.¹⁶⁷ synthesized Cu-Zn-Al catalysts by microwave process. They have also studied the molar ratio of the materials and the effect of reduction after synthesis. Once again, reducing the catalyst led to increase the conversion and the selectivity to 1,2-PDO. The highest reported yield of 1,2-PDO was 76.4% and a conversion of 72.6% with a molar ratio Cu/Zn/Al of 2:2:1, at 200 °C, under 17 bar of H₂ and after 20 hours. (Table 1-8, entry 8).

In 2017, Mariscal et al.¹⁶⁸ studied two types of preparation: i) Coprecipitation method to elaborate: CuZn oxides with different atomic ratio of Cu and Zn and two monometallic oxides of Cu and Zn, and ii) Physical mixing of precursors: bimetallic catalyst with a molar ratio Cu/Zn = 2.5:1. Reaction conditions were chosen to be interesting for industrial application (solution of glycerol 80 wt% in water similar to crude glycerol from biodiesel production). All tests were done at 200 °C under 24 bar of H₂ and for 8 hours. ZnO as catalyst showed no activity, monometallic Cu showed a low conversion (5%) and low selectivity (17.5%) for 1,2-PDO. In the case of bimetallic oxide catalyst CuZn, the conversion of glycerol increased with the increase of the atomic ratio of Cu/Zn. Unlike the selectivity of the different products (1,2-PDO, acetol and ethylene glycol), no correlation was observed between selectivity and atomic ratio. The maximum selectivity values observed for 1,2-PDO were 63.8%, corresponding to the catalyst with 0.2 molar ratio Cu/Zn. The highest yield of 1,2-PDO (24.6% of conversion and 44.6% selectivity) was obtained with the Cu/Cu₂O/ZnO catalyst with a molar ratio Cu/Zn = 1:1

(Table 1-8, entry 9).

III.2.3. Cu/MgO catalysts

Recently, Cu/MgO catalysts have been reported for this reaction. It was found that the basicity of the catalyst also played an important role in its performance. In 2011, Yuan et al.¹⁶⁹ reported for the first time a Cu/MgO/Al₂O₃ catalyst for a glycerol hydrogenolysis process to produce 1,2-PDO. A Cu_{0.4}/Mg_{5.6}/Al₂O_{8.6} catalyst prepared using NaOH and Na₂CO₃ coprecipitation method, was reported as the optimal molar ratio. Under experimental conditions such as 180 °C, under 30 bar of H₂, 75% aqueous glycerol, the glycerol conversion was 91.2% and the 1,2-PDO selectivity 95.5% after 10 h. However, a significant copper 10 wt% loading of catalyst was required as shown in (Table 1-8, entry 10). It was also reported that when 5% to 10% NaOH were added to the reaction mixture, glycerol conversion was higher and 1,2-PDO selectivity decreased due to increased ethylene glycol production.

To improve the activity of the Cu/MgO/Al₂O₃ catalyst, another metal was added. In 2011, Xia et al.¹⁷⁰ reported that when Pd was added, the catalyst was active under milder conditions compared to a Cu/MgO/Al₂O₃ catalyst. In this report, the reaction conditions were: 180 °C, under 20 bar of H₂, 75% aqueous glycerol and for 10 hours and a glycerol conversion of 56.7% and a 1,2-PDO selectivity of 97.1% were obtained using the Cu/MgO/Al₂O₃ catalyst (Table 1-8, entry 11). The addition of 4 wt% Pd increased the glycerol conversion and 1,2-PDO selectivity to 76.9% and 97.2%, respectively. **The promotion effect of Pd was proposed to be due to H₂ spillover from Pd to Cu.**

III.2.4. Other Cu-based catalysts

Some copper-based supported catalysts prepared by impregnation method have also been reported. However, the activities of supported Cu-based catalysts were not as high as those prepared by coprecipitation method. The most frequently reported catalysts were Cu supported on γ -Al₂O₃^{173,174}, on SiO₂^{138,142,175,175,176} and other supports (MgO, Al hydrotalcite, ZrO₂, carbone nanotube...) ^{171,177,178}. In 2011, Wu et al.¹⁷¹ reported different Cu catalysts supported on multi-wall carbon nanotubes (MWCNT), which showed high activity for glycerol hydrogenolysis to produce 1,2-PDO. When the experimental conditions were 200 °C under 40 bar of H₂, 80 wt% aqueous glycerol with a reaction time of 6 hours, the glycerol conversion was reported to be 31.3% and the 1,2-PDO selectivity was 91.1% (Table 1-8, entry 12).

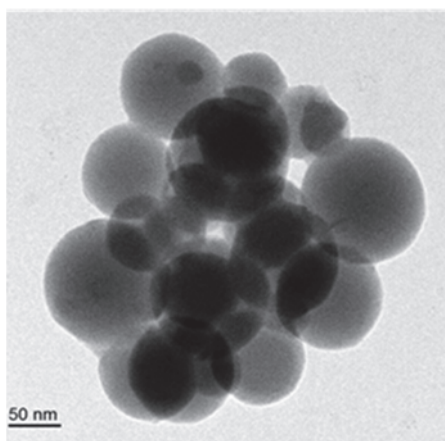
In 2018, Muhler et al.¹⁷² studied the effect of the reduction on Cu/ZrO₂ catalysts. They used the co-precipitation method to prepare different series with different metal loadings of catalysts. The reduction of the catalyst after the calcination step led to an increase in the conversion from 31% with 18% CuO/ZrO₂ to 95% with the same catalyst but reduced. The reaction conditions are shown in the last entry of the Table 1-8.

A summary of the listed results shows that the catalysts used for glycerol hydrogenolysis were mostly prepared by coprecipitation. In the case of Cu/ZnO, the most used zinc precursors were zinc nitrate and zinc acetate. Some groups used also commercial ZnO and elaborated inhomogeneous catalysts with undefined structure. The specific surface area of the catalyst showed an important effect on the conversion combined with the particle size of the Cu active phase.

In general, a high surface areas have resulted in smaller copper particle sizes and better dispersions leading to an increase in the catalytic activity. The solvents have also played an important role on the activity of the catalyst, and water seems to inhibit the activity of the catalyst by deactivating the copper particles. Nevertheless, adding a promoter to the catalyst, especially Al results in an increase in the acidity of the catalyst leading to a higher conversion.

IV. Objectives of the thesis

In our previous work ⁵⁸, a sol-gel route from reacting ZnEt_2 with an aqueous polyacrylic acid solution (PAAH) was developed and patented to obtain either highly luminescent ZnO nanocomposites or stable ZnO nano-suspensions with high quantum yield to be applied in LED devices. The co-precipitation method from zinc salts (acetate, nitrate, sulphate) in basic conditions (NaOH, KOH, LiOH) and in the presence of PAAH failed to reach the same performances. The efficiency of the resulting nanomaterials in terms of luminescence were correlated to the elaboration of hybrid systems ZnO/PAAH which self-assembled in 3D spherical morphologies.



Commercial ZnO have usually non-homogeneous shape with large particle size distributed randomly from 50 nm to 300 nm. Depending on the supplier, the properties of the material may change but most of them have very low specific surface areas of around $10 \text{ m}^2 \cdot \text{g}^{-1}$.

The starting point of our project was the use of our new hybrid ZnO-based nano-structured objects as supports for copper-based catalysts for glycerol hydrogenolysis. The study of different parameters such as the temperature, the washing setup, the chain length of the PAAH, the calcination temperature after synthesis and the weight percentage of PAAH had to be optimized in order to understand their synthesis mechanism, to control their morphologies and to reach high specific surface areas. This will be addressed in chapter 3 of this manuscript. Actually, one of the main property we had to optimize was the specific surface area because most of our materials elaborated by the sol-gel method were having small surface areas with an average of $20 \text{ m}^2 \cdot \text{g}^{-1}$.

Comparing to the literature as mentioned above, the Cu/ZnO catalysts were mostly prepared

by co-precipitation. In our project, we started by preparing catalysts by deposition precipitation with urea (DPU) in order to have small Cu particle size and well-dispersed on our hybrid ZnO matrix. Commercial ZnO support was first used and then substituted later by the novel hybrid ZnO-PAAH one. In a second time, a “one pot” synthesis was applied to decrease the preparation time and to limit the precipitation effects. These results will be presented in chapter 4.

The elaborated catalysts were used for the hydrogenolysis of glycerol into 1,2-PDO and the first catalytic tests were carried out with Cu/ZnO in order to increase the conversion of glycerol before adding a promoter. Since many studies showed the impact of adding promoters to the Cu/ZnO catalysts, we decided to add Al species to enhance the properties of our catalysts by increasing the acidity of the catalyst and the specific surface area (chapter 5).

The conversion of glycerol into 1,2-PDO with high selectivity is very challenging because of side reactions observed in literature leading to 1,3-PDO, ethylene glycol, acetol... Developing a catalyst selective toward 1,2-PDO was also one of our main target.

V. References

- Haider, A. J., Sultan, F. I. & Al-Nafiey, A. Controlled growth of different shapes for ZnO by hydrothermal technique. *AIP Conference Proceedings* **1968**, 33-38 (2018).
- Segets, D., Gradl, J., Taylor, R. K., Vassilev, V. & Peukert, W. Analysis of optical absorbance spectra for the determination of ZnO nanoparticle size distribution, solubility, and surface energy. *ACS Nano* **3**, 1703–1710 (2009).
- Wang, J., Cao, J., Fang, B. & Lu, P. Synthesis and characterization of multipod, flower-like, and shuttle-like ZnO frameworks in ionic liquids. *Mater. Lett.* **59**, 1405–1408 (2005).
- Bacaksiz, E., Parlak, M., Tomakin, M. & Altunbas, M. The effects of zinc nitrate, zinc acetate and zinc chloride precursors on investigation of structural and optical properties of ZnO thin films. *J. Alloys Compd.* **466**, 447–450 (2008).
- Chaari, M. & Matoussi, A. Electrical conduction and dielectric studies of ZnO pellets. *Phys. B Condens. Matter* **407**, 3441–3447 (2012).
- Wang, Z. L. Splendid one-dimensional nanostructures of zinc oxide: a new nanomaterial family for nanotechnology. *ACS Nano* **2**, 1987-1992 (2008).
- Bhattacharyya, S. & Gedanken, A. A template-free, sonochemical route to porous ZnO nano-disks. *Microporous Mesoporous Mater.* **110**, 553–559 (2008).
- Özgür, ü., Alivov, Ya. I., Liu, C., Teke, A. & Morkoç, H. A comprehensive review of ZnO materials and devices. *J. Appl. Phys.* **98**, 01- 103 (2005).
- Ludi, B. & Niederberger, M. Zinc oxide nanoparticles: chemical mechanisms and classical and non-classical crystallization. *Dalton Trans.* **42**, 35-47 (2013).
- Lu, P.-J., Huang, S.-C., Chen, Y.-P., Chiueh, L.-C. & Shih, D. Y.-C. Analysis of titanium dioxide and zinc oxide nanoparticles in cosmetics. *J. Food Drug Anal.* **23**, 587–594 (2015).
- Alhumdany, A. K. A., Al-Waily, M. L. & Mohammed, S. Q. Studying the thermal effect and nano zinc oxide load level on the adhesion between rubber compound and steel tire cords. *J. Univ. Babylon* **26**, 338–347 (2018).
- Frade, T., Melo Jorge, M. E. & Gomes, A. One-dimensional ZnO nanostructured films: Effect of oxide nanoparticles. *Mater. Lett.* **82**, 13–15 (2012).
- Wahab, R., Ansari, S. G., Kim, Y.-S., Seo, H.-K. & Shin, H.-S. Room temperature synthesis of needle-shaped ZnO nanorods via sonochemical method. *Appl. Surf. Sci.* **253**, 7622–7626 (2007).
- Perrin, M. D., Graham, J. R., Kalas, P. & Gates, E. L. Laser guide star adaptive optics imaging polarimetry of Herbig Ae/Be stars. *Science* **303**, 1345–1348 (2004).
- Nikoobakht, B., Wang, X., Herzing, A. & Shi, J. Scalable synthesis and device integration of self-registered one-dimensional zinc oxide nanostructures and related materials. *Chem Soc Rev* **42**, 342–365 (2013).
- Chen, W. J., Liu, W. L., Hsieh, S. H. & Tsai, T. K. Preparation of nanosized ZnO using α brass. *Appl. Surf. Sci.* **253**, 6749–6753 (2007).
- Chiu, W. S., Khiew, P. S., Cloke, M., Radiman, S. & Chia, C. H. Photocatalytic study of two-

- dimensional ZnO nanopellets in the decomposition of methylene blue. *Chem. Eng. J.* **158**, 345–352 (2010).
18. Bitenc, M. & Crnjak Orel, Z. Synthesis and characterization of crystalline hexagonal bipods of zinc oxide. *Mater. Res. Bull.* **44**, 381–387 (2009).
 19. Djurišić, A. B., Ng, A. M. C. & Chen, X. Y. ZnO nanostructures for optoelectronics: Material properties and device applications. *Prog. Quantum Electron.* **34**, 191–259 (2010).
 20. Sirelkhatim, A., Mahmud, S., Seeni, A & Mohamad, D. Review on zinc oxide nanoparticles: antibacterial activity and toxicity mechanism. *Nano-Micro Lett.* **7**, 219–242 (2015).
 21. Chen, J. T., Wang, J., Zhuo, R. F. & Yan, P. X. The effect of Al doping on the morphology and optical property of ZnO nanostructures prepared by hydrothermal process. *Appl. Surf. Sci.* **255**, 3959–3964 (2009).
 22. Park, H.-J., Lee, K. H., Sameera, I. & Kim, S.-W. Synthesis of highly crystalline Ga-doped zinc-oxide nanoparticles for hybrid polymer solar cells. *J. Korean Phys. Soc.* **66**, 1422–1425 (2015).
 23. Yuen, C., Yu, S. F., Lau, S. P. & Chen, T. P. Room temperature deposition of p-type arsenic doped ZnO polycrystalline films by laser-assist filtered cathodic vacuum arc technique. *J. Appl. Phys.* **101**, 94-102 (2007).
 24. Brauer, G., Kuriplach, J., Ling, C. C. & Djurišić, A. B. Activities towards p -type doping of ZnO. *J. Phys. Conf. Ser.* **265**, 12-17 (2011).
 25. Lin, C. Y., Wang, W. H., Lee, C.-S., Sun, K. W. & Suen, Y. W. Magnetophotoluminescence properties of Co-doped ZnO nanorods. *Appl. Phys. Lett.* **94**, 15-19 (2009).
 26. Pearton, S. J. *et al.* ZnO Doped With Transition Metal Ions. *IEEE Trans. Electron Devices* **54**, 1040–1048 (2007).
 27. Silvestre, C., Duraccio, D. & Cimmino, S. Food packaging based on polymer nanomaterials. *Prog. Polym. Sci.* **36**, 1766–1782 (2011).
 28. Lozada, E. V., Torchynska, T. & Castañeda, L. Photoluminescence emission at aging in ambient air of ZnO:Ag nanocrystals obtained by ultrasonic spray pyrolysis. *AIP Conference Proceedings* **1934**, 3-6 (2018).
 29. Liu, X., Wu, X., Cao, H. & Chang, R. P. H. Growth mechanism and properties of ZnO nanorods synthesized by plasma-enhanced chemical vapor deposition. *J. Appl. Phys.* **95**, 3141–3147 (2004).
 30. Qiu, J. *et al.* The growth mechanism and optical properties of ultralong ZnO nanorod arrays with a high aspect ratio by a preheating hydrothermal method. *Nanotechnology* **20**, 155-162 (2009).
 31. Shi, W. S., Cheng, B., Zhang, L. & Samulski, E. T. Influence of excitation density on photoluminescence of zinc oxide with different morphologies and dimensions. *J. Appl. Phys.* **98**, 83-90 (2005).
 32. ISO: Geneva, Switzerland, 2010. Rubber Compounding Ingredients—Zinc Oxide—Test Methods; ISO 9298:1995.
 33. Tsuzuki, T. & McCormick, P. G. Mechanochemical synthesis of nanoparticles. *J. Mater.*

- Sci.* **39**, 5143–5146 (2004).
34. Mahmud, S., Johar Abdullah, M., Putrus, G. A., Chong, J. & Karim Mohamad, A. Nanostructure of ZnO fabricated via French process and its correlation to electrical properties of semiconducting varistors. *Synth. React. Inorg. Met.-Org. Nano-Met. Chem.* **36**, 155–159 (2006).
 35. Moballegh, A., Shahverdi, H. R., Aghababazadeh, R. & Mirhabibi, A. R. ZnO nanoparticles obtained by mechanochemical technique and the optical properties. *Surf. Sci.* **601**, 2850–2854 (2007).
 36. Aghababazadeh, R., Mazinani, B., Mirhabibi, A. & Tamizifar, M. ZnO Nanoparticles Synthesised by mechanochemical processing. *J. Phys. Conf. Ser.* **26**, 312–314 (2006).
 37. Stanković, A., Veselinović, L., Škapin, S. D., Marković, S. & Uskoković, D. Controlled mechanochemically assisted synthesis of ZnO nanopowders in the presence of oxalic acid. *J. Mater. Sci.* **46**, 3716–3724 (2011).
 38. Ao, W., Li, J., Yang, H., Zeng, X. & Ma, X. Mechanochemical synthesis of zinc oxide nanocrystalline. *Powder Technol.* **168**, 148–151 (2006).
 39. Anas, S., Mangalaraja, R. V. & Ananthakumar, S. Studies on the evolution of ZnO morphologies in a thermohydrolysis technique and evaluation of their functional properties. *J. Hazard. Mater.* **175**, 889–895 (2010).
 40. Lee, J.-S. & Choi, S.-C. Crystallization behavior of nano-ceria powders by hydrothermal synthesis using a mixture of H₂O₂ and NH₄OH. *Mater. Lett.* **58**, 390–393 (2004).
 41. Podrezova, L. V., Porro, S., Cauda, V., Fontana, M. & Cicero, G. Comparison between ZnO nanowires grown by chemical vapor deposition and hydrothermal synthesis. *Appl. Phys. A* **113**, 623–632 (2013).
 42. Ehrentraut, D., Sato, H., Kagamitani, Y. & Sato, H. Solvothermal growth of ZnO. *Prog. Cryst. Growth Charact. Mater.* **52**, 280–335 (2006).
 43. Piticescu, R. R., Monty, C., Taloi, D., Motoc, A. & Axinte, S. Hydrothermal synthesis of zirconia nanomaterials. *J. Eur. Ceram. Soc.* **21**, 2057–2060 (2001).
 44. Mihaiu, S., Pokol, G., Toader, A & Zaharescu, M. Thermal behavior of ZnO precursor powders obtained from aqueous solutions. *Rev Roum Chim* **58**, 335–45 (2013).
 45. Lecarme, L., Nourdine, A., Alloin, F. & Leprêtre, J.-C. ZnO Nanowires as a promotor of high photoinduced efficiency and voltage gain for cathode battery recharging. *ACS Appl. Energy Mater.* **2**, 6254–6262 (2019).
 46. Debbarma, M., Das, S. & Saha, M. Effect of reducing agents on the structure of zinc oxide under microwave irradiation. *Adv. Manuf.* **1**, 183–186 (2013).
 47. Lamdab, U., Wetchakun, K., Kangwansupamonkon, W. & Wetchakun, N. Effect of a pH-controlled co-precipitation process on rhodamine B adsorption of MnFe₂O₄ nanoparticles. *RSC Adv.* **8**, 6709–6718 (2018).
 48. Raj, K. P. & Sadayandi, K. Effect of temperature on structural, optical and photoluminescence studies on ZnO nanoparticles synthesized by the standard co-precipitation method. *Phys. B Condens. Matter* **487**, 1–7 (2016).

49. López, C. & Rodríguez-Páez, J. E. Synthesis and characterization of ZnO nanoparticles: effect of solvent and antifungal capacity of NPs obtained in ethylene glycol. *Appl. Phys. A* **123**, 748–764 (2017).
50. Hong, R., Pan, T., Qian, J. & Li, H. Synthesis and surface modification of ZnO nanoparticles. *Chem. Eng. J.* **119**, 71–81 (2006).
51. Li, P., Wei, Y., Liu, H. & Wang, X. Growth of well-defined ZnO microparticles with additives from aqueous solution. *J. Solid State Chem.* **178**, 855–860 (2005).
52. Znaidi, L. Sol–gel-deposited ZnO thin films: A review. *Mater. Sci. Eng. B* **174**, 18–30 (2010).
53. Mahato, T. H., Singh, B., Acharya, J. & Vijayarghavan, R. Nanocrystalline zinc oxide for the decontamination of sarin. *J. Hazard. Mater.* **165**, 928–932 (2009).
54. You, H.-C. & Lin, Y.-H. Investigation of the sol-gel method on the flexible ZnO device. *Int J Electrochem Sci* **7**, 9085–9094 (2012).
55. Najafi, N. & Rozati, S. M. Resistivity reduction of nanostructured undoped zinc oxide thin films for Ag/ZnO bilayers using APCVD and sputtering techniques. *Mater. Res.* **21**, 15-22 (2018).
56. Carnes, C. L. & Klabunde, K. J. Synthesis, isolation, and chemical reactivity studies of nanocrystalline zinc oxide. *Langmuir* **16**, 3764–3772 (2000).
57. Monge, M., Kahn, M. L., Maisonnat, A. & Chaudret, B. Room-Temperature organometallic synthesis of soluble and crystalline ZnO nanoparticles of controlled size and shape. *Angew. Chem. Int. Ed.* **42**, 5321–5324 (2003).
58. Zhu, Y., Omar, L., Daniele, S. & Masenelli, B. Intense visible emission from ZnO/PAAX (X = H or Na) nanocomposite synthesized via a simple and scalable sol-gel method. *Sci. Rep.* **6**, (2016).
59. Zhang, Y., Theron, C., Daniele, S. & Masenelli, B. Doping of ZnO inorganic-organic nanohybrids with metal elements. *Sci. Rep.* **9**, (2019).
60. Grasza, K., Kopalko, K. & Mycielski, A. Effect of annealing atmosphere on the quality of ZnO crystal surface. *Phys. Status Solidi B* **244**, 1468–1472 (2007).
61. Wei, X. Q., Zhang, Z., Yu, Y. X. & Man, B. Y. Comparative study on structural and optical properties of ZnO thin films prepared by PLD using ZnO powder target and ceramic target. *Opt. Laser Technol.* **41**, 530–534 (2009).
62. Zhao, X., Zheng, B., Li, C. & Gu, H. Acetate-derived ZnO ultrafine particles synthesized by spray pyrolysis. *Powder Technol.* **100**, 20–23 (1998).
63. Hu, X.-L., Zhu, Y.-J. & Wang, S.-W. Sonochemical and microwave-assisted synthesis of linked single-crystalline ZnO rods. *Mater. Chem. Phys.* **88**, 421–426 (2004).
64. Kołodziejczak-Radzimska, A., Markiewicz, E. & Jesionowski, T. Structural characterisation of ZnO particles obtained by the emulsion precipitation method. *J. Nanomater.* **2012**, 1–9 (2012).
65. Kołodziejczak-Radzimska, A. & Jesionowski, T. Zinc oxide - From synthesis to application: A review. *Materials* **7**, 2833–2881 (2014).

66. <https://www.nanoshel.com/zinc-oxide-for-rubber-industry> consulted 21/06/2019.
67. Baysal, A., Saygin, H. & Ustabasi, G. S. Physicochemical transformation of ZnO and TiO₂ nanoparticles in sea water and its impact on bacterial toxicity. *Environ. Health Eng. Manag. J.* **6**, 73–80 (2019).
68. Espitia, P. J. P., Soares, N. F. F. & Medeiros, E. A. A. Zinc oxide nanoparticles: Synthesis, antimicrobial activity and food packaging applications. *Food Bioprocess Technol.* **5**, 1447–1464 (2012).
69. Jiang, J., Pi, J. & Cai, J. The Advancing of zinc oxide nanoparticles for biomedical applications. *Bioinorg. Chem. Appl.* **2018**, 1–18 (2018).
70. Mansouri, S., Bourguiga, R. & Yakuphanoglu, F. Analytic model for ZnO-thin film transistor under dark and UV illumination. *Curr. Appl. Phys.* **12**, 1619–1623 (2012).
71. Wang, M. & Wang, X. Electrodeposition zinc-oxide inverse opal and its application in hybrid photovoltaics. *Sol. Energy Mater. Sol. Cells* **92**, 357–362 (2008).
72. Gupta, S. M. & Tripathi, M. A review of TiO₂ nanoparticles. *Chin. Sci. Bull.* **56**, 1639–1657 (2011).
73. Qi, K., Cheng, B., Yu, J. & Ho, W. Review on the improvement of the photocatalytic and antibacterial activities of ZnO. *J. Alloys Compd.* **727**, 792–820 (2017).
74. Aponiene, K. & Luksiene, Z. Effective combination of LED-based visible light, photosensitizer and photocatalyst to combat Gram (–) bacteria. *J. Photochem. Photobiol. B* **142**, 257–263 (2015).
75. Zhang, Q., Liu, J. K. & Yang, X-H. Atmospheric self-induction synthesis and enhanced visible light photocatalytic performance of Fe³⁺ Doped Ag-ZnO Mesocrystals. *Ind. Eng. Chem. Res.* **53**, 13236–13246 (2014).
76. He, R., Hocking, R. K. & Tsuzuki, T. Co-doped ZnO nanopowders: Location of cobalt and reduction in photocatalytic activity. *Mater. Chem. Phys.* **132**, 1035–1040 (2012).
77. Yin, Q., Qiao, R., Li, Z., Zhang, X. L. & Zhu, L. Hierarchical nanostructures of nickel-doped zinc oxide: Morphology controlled synthesis and enhanced visible-light photocatalytic activity. *J. Alloys Compd.* **618**, 318–325 (2015).
78. Sin, J.-C., Lam, S.-M., Lee, K.-T. & Mohamed, A. R. Preparation of cerium-doped ZnO hierarchical micro/nanospheres with enhanced photocatalytic performance for phenol degradation under visible light. *J. Mol. Catal. Chem.* **409**, 1–10 (2015).
79. Khataee, A., Safarpour, M. & Ranjbar, H. G. Synthesis and characterization of dysprosium-doped ZnO nanoparticles for photocatalysis of a textile dye under visible light irradiation. *Ind. Eng. Chem. Res.* **53**, 1924–1932 (2014).
80. Kim, K.-J., Kreider, P. B., Choi, C., Chang, C.-H. & Ahn, H.-G. Visible-light-sensitive Na-doped p-type flower-like ZnO photocatalysts synthesized via a continuous flow microreactor. *RSC Adv.* **3**, 12702 (2013).
81. Etacheri, V., Roshan, R. & Kumar, V. Mg-Doped ZnO Nanoparticles for Efficient Sunlight-Driven Photocatalysis. *ACS Appl. Mater. Interfaces* **4**, 2717–2725 (2012).
82. Awasthi, G. P., Adihakari, S. P., Park, C. H. & Kim, C. S. Facile synthesis of ZnO flowers

- modified graphene like MoS₂ sheets for enhanced visible-light-driven photocatalytic activity and antibacterial properties. *J. Alloys Compd.* **682**, 208–215 (2016).
83. Pan, L., Shen, G-Q., Zou, J-J & Zhang, X. TiO₂–ZnO composite sphere decorated with ZnO clusters for effective charge isolation in photocatalysis. *Ind. Eng. Chem. Res.* **54**, 7226–7232 (2015).
 84. Yu, W., Zhang, J. & Peng, T. New insight into the enhanced photocatalytic activity of N-, C- and S-doped ZnO photocatalysts. *Appl. Catal. B Environ.* **181**, 220–227 (2016).
 85. Kuriakose, S., Satpati, B. & Mohapatra, S. Enhanced photocatalytic activity of Co doped ZnO nanodisks and nanorods prepared by a facile wet chemical method. *Phys. Chem. Chem. Phys.* **16**, 12741 (2014).
 86. Liao, L. C.-K. & Huang, J.-S. Energy-level variations of Cu-doped ZnO fabricated through sol-gel processing. *J. Alloys Compd.* **702**, 153–160 (2017).
 87. Carabineiro, S. A. C., Machado, B. F. & Figueiredo, J. L.. Catalytic performance of Au/ZnO nanocatalysts for CO oxidation. *J. Catal.* **273**, 191–198 (2010).
 88. Liao, F., Huang, Y & Tsang, S. C. Morphology-Dependent interactions of ZnO with Cu nanoparticles at the materials' interface in selective hydrogenation of CO₂ to CH₃OH. *Angew. Chem. Int. Ed.* **50**, 2162–2165 (2011).
 89. Lei, H., Nie, R., Wu, G. & Hou, Z. Hydrogenation of CO₂ to CH₃OH over Cu/ZnO catalysts with different ZnO morphology. *Fuel* **154**, 161–166 (2015).
 90. Lin, Y. G., Hsu, Y. K. & Chen, K-H. Nanostructured zinc oxide nanorods with copper nanoparticles as a microreformation catalyst. *Angew. Chem. Int. Ed.* **48**, 7586–7590 (2009).
 91. Blanc, B., Bourrel, A., Gallezot, P., Haas, T. & Taylor, P. Starch-derived polyols for polymer technologies: preparation by hydrogenolysis on metal catalysts. *Green Chem.* **2**, 89–91 (2000).
 92. Wang, X., Meng, L. & Mu, X. Efficient conversion of microcrystalline cellulose to 1,2-alkanediols over supported Ni catalysts. *Green Chem.* **14**, 758 (2012).
 93. Liu, F. & Zhang, Y. Controllable growth of 'multi-level tower' ZnO for biodiesel production. *Ceram. Int.* **37**, 3193–3202 (2011).
 94. Morales, M. V., Asedegbega-Nieto, E., Iglesias-Juez, A., Rodríguez-Ramos, I. & Guerrero-Ruiz, A. Role of exposed surfaces on zinc oxide nanostructures in the catalytic ethanol transformation. *ChemSusChem* **8**, 2223–2230 (2015).
 95. Toukoniitty, B., Kuusisto, J., Mikkola, J.-P., Salmi, T. & Murzin, D. Y. Effect of ultrasound on catalytic hydrogenation of D-Fructose to D-Mannitol. *Ind. Eng. Chem. Res.* **44**, 9370–9375 (2005).
 96. Zheng, H.-Y., Zhu, Y.-L. & Bai, Z-Q. Towards understanding the reaction pathway in vapour phase hydrogenation of furfural to 2-methylfuran. *J. Mol. Catal. Chem.* **246**, 18–23 (2006).
 97. Lee, J.-M. *et al.* Direct Hydrogenation of Biomass-Derived Butyric Acid to *n*-Butanol over a Ruthenium-Tin Bimetallic Catalyst. *ChemSusChem* **7**, 2998–3001 (2014).

98. Louis, C., Geus, J. W., Gates, B. et al. Synthesis of heterogeneous catalysts from "Catalyst preparation: science and engineering". Edited by Regalbuto, J. *CRC Press* **203**, Boca Raton, (2007).
99. Le Page, J-F. Developing industrial catalysts from "Applied heterogeneous catalysis: design, manufacture, use of solid catalysts". Edited by Limido, J. *Éditions Technip*, Paris, (1987).
100. Mota, N., Guil-Lopez, R., Pawelec, B. G., Fierro, J. L. G. & Navarro, R. M. Highly active Cu/ZnO–Al catalyst for methanol synthesis: effect of aging on its structure and activity. *RSC Adv.* **8**, 20619–20629 (2018).
101. Chinchen, G. & Spencer, M. Sensitive and insensitive reactions on copper catalysts: the water gas shift reaction and methanol synthesis from carbon dioxide. *Catal. Today* **10**, 293–301 (1991).
102. Klier, K. Methanol synthesis. *Adv. Catal.* **31**, 243–313 (1982).
103. Tanaka, Y., Utaka, T. & Eguchi, K. CO removal from reformed fuel over Cu/ZnO/Al₂O₃ catalysts prepared by impregnation and coprecipitation methods. *Applied Catalysis A: General* **11–18** (2003).
104. Geus, J. W., Grange, P. Preparation of Catalysts III. Edited by Poncelet, G. & Jacobs, P.A., *Elsevier Science Publishers, Prep. Catal.*, Amsterdam, **3**, (1982).
105. Geus, J.W. Production and thermal pretreatment of supported catalysts. *Prep. Catal. III*, **79**, 1–32 (1983).
106. Herman, R.G., Klier, K. & Kobylinski, T. P. Catalytic synthesis of methanol from COH₂: I. Phase composition, electronic properties, and activities of the Cu/ZnO/M₂O₃ catalysts. *J. Catal.* **56**, 407–429 (1979).
107. Gallei, E. F., Hesse, M. & Schwab, E. Preparation of solid catalysts from "Handbook of heterogeneous catalysis". Edited by Ertl, G., Knozinger, H., Weitkamp, J. & Schuth, F. *Wiley VCH*, Weinheim, **1**, (2008).
108. Louis, C. Deposition precipitation from "Gold Catalysis: Preparation, Characterization, and Applications". Edited by Prati, L. & Villa, A., *CRC Press*, Boca Raton (2016).
109. Huang, Z., Xue, J., Zuo, J. & Xia, C. Cu/SiO₂ catalysts prepared by hom- and heterogeneous deposition–precipitation methods: Texture, structure, and catalytic performance in the hydrogenolysis of glycerol to 1,2-propanediol. *Catal. Today* **183**, 42–51 (2012).
110. Delannoy, L., Reddy, B. & Louis, C. Selective hydrogenation of butadiene over TiO₂ supported copper, gold and gold–copper catalysts prepared by deposition–precipitation. *Phys Chem Chem Phys* **16**, 26514–26527 (2014).
111. Burattin, P., Che, M. & Louis, C. Molecular approach to the mechanism of deposition-precipitation of the Ni (II) phase on silica. *J. Phys. Chem. B* **102**, 2722–2732 (1998).
112. Derrouiche, S., Lauron-Pernot, H. & Louis, C. Synthesis and Treatment Parameters for Controlling Metal Particle Size and Composition in Cu/ZnO Materials—First Evidence of Cu₃Zn Alloy Formation. *Chem. Mater.* **24**, 2282–2291 (2012).
113. Wang, Z., Brouri, D., Casale, S., Delannoy, L. & Louis, C. Exploration of the preparation of Cu/TiO₂ catalysts by deposition–precipitation with urea for selective hydrogenation of

- unsaturated hydrocarbons. *J. Catal.* **340**, 95–106 (2016).
114. Behrens, M. & Schlögl, R. How to prepare a good Cu/ZnO catalyst or the role of solid state chemistry for the synthesis of nanostructured catalysts. *Z. Für Anorg. Allg. Chem.* **639**, 2683–2695 (2013).
115. Courty, P. & Marcilly, C. A scientific approach to the preparation of bulk mixed oxide catalysts from "Preparation of catalysts III". Edited by Poncelet, G, Grange, P & Jacobs, P. A, *Studies in Surface Science and Catalysis*, **16**, 485–519 (1983).
116. Schimpf, S. & Muhler, M. Methanol catalysts from "Synthesis of solid catalysts". Edited by Krijn, P. J., *WILEY-VCH*, Weinheim, **8**, 329–348 (2008).
117. Guo, Y., Weiss, R. & Epple, M. A. Straightforward route to copper/zinc oxide nanocomposites: The controlled thermolysis of Zn[Cu(CN)₃]. *Eur. J. Inorg. Chem.* **2005**, 3072–3079 (2005).
118. Weiss, R., Baltés, C., Muhler, M. & Epple, M. Copper/zinc L-Tartrates: Mixed crystals and thermolysis to a mixture of copper oxide and zinc oxide that is catalytically active in methanol synthesis. *Eur. J. Inorg. Chem.* **2006**, 4782–4786 (2006).
119. Guo, Y., Meyer-Zaika, W., Muhler, M., Vukojević, S. & Epple, M. Cu/Zn/Al xerogels and aerogels prepared by a sol–gel reaction as catalysts for methanol synthesis. *Eur. J. Inorg. Chem.* **2006**, 4774–4781 (2006).
120. Brown, N. J., Graça-Trenko, A & Williams, C. K. From organometallic zinc and copper complexes to highly active colloidal catalysts for the conversion of CO₂ to methanol. (2015).
121. Quispe, C. A. G., Coronado, C. J. R. & Carvalho Jr., J. A. Glycerol: Production, consumption, prices, characterization and new trends in combustion. *Renew. Sustain. Energy Rev.* **27**, 475–493 (2013).
122. Isikgor, F. H. & Becer, C. R. Lignocellulosic biomass: a sustainable platform for the production of bio-based chemicals and polymers. *Polym. Chem.* **6**, 4497–4559 (2015).
123. Muscatine, L. Glycerol excretion by symbiotic algae from corals and Tridacna and its control by the host. *Science* **156**, 516–519 (1967).
124. Anuar, M. R. & Abdullah, A. Z. Challenges in biodiesel industry with regards to feedstock, environmental, social and sustainability issues: A critical review. *Renew. Sustain. Energy Rev.* **58**, 208–223 (2016).
125. Mota, C. J. A., Peres Pinto, B. & de Lima, A. L. Glycerol utilization from "Glycerol, A versatile renewable feedstock for the chemical industry". *Springer International Publishing*, Cham, (2017).
126. Samudrala, S. P. Glycerol Transformation to value-added 1, 3-propanediol production: a paradigm for a sustainable biorefinery process from "Glycerine production and transformation, an innovative platform for sustainable biorefinery and energy" *IntechOpen*, (2019).
127. Saxena, R. K., Anand, P., Saran, S., Isar, J. & Agarwal, L. Microbial production and applications of 1,2-propanediol. *Indian J. Microbiol.* **50**, 2–11 (2010).
128. Vivek, N., Pandey, A & Binod, P. Production and application of 1,3-propanediol from

- "Current developments in biotechnology and bioengineering: production, isolation and purification of industrial products". Edited by Pandey, A., Negi, S. & Soccol, C. R. *Elsevier*, (2017).
129. Checa, M., Auneau, F., Pinel, C. & Urbano, J. F. Catalytic transformation of glycerol on several metal systems supported on ZnO. *Catal. Today* **196**, 91–100 (2012).
 130. Gallegos-Suarez, E., Pérez-Cadenas, M., Guerrero-Ruiz, A., Rodriguez-Ramos, I. & Arcoya, A. Effect of the functional groups of carbon on the surface and catalytic properties of Ru/C catalysts for hydrogenolysis of glycerol. *Appl. Surf. Sci.* **287**, 108–116 (2013).
 131. Rodrigues, R., Isoda, N. & Figueiredo, F. C. A. Effect of niobia and alumina as support for Pt catalysts in the hydrogenolysis of glycerol. *Chem. Eng. J.* **198-199**, 457–467 (2012).
 132. Pendem, C., Singh, S. & Bal, R. Aqueous phase reforming of glycerol to 1,2-propanediol over Pt-nanoparticles supported on hydrotalcite in the absence of hydrogen. *Green Chem.* **14**, 3107 (2012).
 133. Miranda, B. C., Santos, J. B. & Guirado, F. G. Conversion of glycerol over 10%Ni/ γ -Al₂O₃ catalyst. *Appl. Catal. B Environ.* **147**, 464–480 (2014).
 134. Gandarias, I., Requies, J., Arias, P. L., Armbruster, U. & Martin, A. Liquid-phase glycerol hydrogenolysis by formic acid over Ni–Cu/Al₂O₃ catalysts. *J. Catal.* **290**, 79–89 (2012).
 135. Hu, J., Liu, X. & Zong, B. Physically mixed ZnO and skeletal NiMo for one-pot reforming-hydrogenolysis of glycerol to 1,2-propanediol. *Chin. J. Catal.* **34**, 1020–1026 (2013).
 136. Tanielyan, S. K., Alvez, G. & Schmidt, R. An efficient, selective process for the conversion of glycerol to propylene glycol using fixed bed raney copper catalysts. *Org. Process Res. Dev.* **18**, 1419–1426 (2014).
 137. Meher, L. C., Gopinath, R., Naik, S. N. & Dalai, A. K. Catalytic hydrogenolysis of glycerol to propylene glycol over mixed oxides derived from a hydrotalcite-type Pprecursor. *Ind. Eng. Chem. Res.* **48**, 1840–1846 (2009).
 138. Vasiliadou, E. S. & Lemonidou, A. A. Kinetic study of liquid-phase glycerol hydrogenolysis over Cu/SiO₂ catalyst. *Chem. Eng. J.* **231**, 103–112 (2013).
 139. Chiu, C.-W., Tekeei, A., Ronco, J. M., Banks, M.-L. & Suppes, G. J. Reducing byproduct formation during conversion of glycerol to propylene glycol. *Ind. Eng. Chem. Res.* **47**, 6878–6884 (2008).
 140. Montassier, C., Giraud, D. & Barbier, J. Polyol conversion by liquid phase heterogeneous catalysis over metals. From "Heterogeneous catalysis and fine chemicals". Edited by Guisnet, M., Barrault, J., Montassier, C., Duprez, D., Pérot, G. *Elsevier*, **41**, 165–170 (1988).
 141. Dasari, M. A., Kiatsimkul, P.-P., Sutterlin, W. R. & Suppes, G. J. Low-pressure hydrogenolysis of glycerol to propylene glycol. *Appl. Catal. Gen.* **281**, 225–231 (2005).
 142. Huang, Z., Cui, F., Kang, H., Chen, J. & Xia, C. Characterization and catalytic properties of the CuO/SiO₂ catalysts prepared by precipitation-gel method in the hydrogenolysis of glycerol to 1,2-propanediol: Effect of residual sodium. *Appl. Catal. Gen.* **366**, 288–298 (2009).
 143. Chai, S.-H., Wang, H.-P., Liang, Y. & Xu, B.-Q. Sustainable production of acrolein:

- investigation of solid acid–base catalysts for gas-phase dehydration of glycerol. *Green Chem.* **9**, 1130–1136 (2007).
144. Kusunoki, Y., Miyazawa, T., Kunimori, K. & Tomishige, K. Highly active metal–acid bifunctional catalyst system for hydrogenolysis of glycerol under mild reaction conditions. *Catal. Commun.* **6**, 645–649 (2005).
 145. Wang, S. & Liu, H. Selective hydrogenolysis of glycerol to propylene glycol on Cu–ZnO catalysts. *Catal. Lett.* **117**, 62–67 (2007).
 146. Wang, S., Zhang, Y. & Liu, H. Selective hydrogenolysis of glycerol to propylene glycol on Cu–ZnO composite catalysts: Structural requirements and reaction mechanism. *Chem. - Asian J.* **5**, 1100–1111 (2010).
 147. Bienholz, A., Schwab, F. & Claus, P. Hydrogenolysis of glycerol over a highly active CuO/ZnO catalyst prepared by an oxalate gel method: influence of solvent and reaction temperature on catalyst deactivation. *Green Chem* **12**, 290–295 (2010).
 148. Montassier, C., Dumas, J., Granger, P. & Barbier, J. Deactivation of supported copper based catalysts during polyol conversion in aqueous phase. *Appl. Catal. Gen.* **121**, 231–244 (1995).
 149. Besson, M., Gallezot, P. & Pinel, C. Conversion of Biomass into Chemicals over Metal Catalysts. *Chem. Rev.* **114**, 1827–1870 (2014).
 150. Ruppert, A. M., Weinberg, K. & Palkovits, R. Hydrogenolysis goes bio: From carbohydrates and sugar alcohols to platform chemicals. *Angew. Chem. Int. Ed.* **51**, 2564–2601 (2012).
 151. Ma, J., Yu, W., Lu, F. & Xu, J. Advances in selective catalytic transformation of polyols to value-added chemicals. *Chin. J. Catal.* **34**, 492–507 (2013).
 152. Wang, Y., Zhou, J. & Guo, X. Catalytic hydrogenolysis of glycerol to propanediols: a review. *RSC Adv.* **5**, 74611–74628 (2015).
 153. Delgado, S. N., Yap, D., Vivier, L. & Especel, C. Influence of the nature of the support on the catalytic properties of Pt-based catalysts for hydrogenolysis of glycerol. *J. Mol. Catal. Chem.* **367**, 89–98 (2013).
 154. Musolino, M. G., Scarpino, L. A., Mauriello, F. & Pietropaolo, R. Selective transfer hydrogenolysis of glycerol promoted by palladium catalysts in absence of hydrogen. *Green Chem.* **11**, 1511 (2009).
 155. Vasiliadou, E. S., Heracleous, E., Vasalos, I. A. & Lemonidou, A. A. Ru-based catalysts for glycerol hydrogenolysis—Effect of support and metal precursor. *Appl. Catal. B Environ.* **92**, 90–99 (2009).
 156. Perosa, A. & Tundo, P. Selective hydrogenolysis of glycerol with raney nickel. *Ind. Eng. Chem. Res.* **44**, 8535–8537 (2005).
 157. Balaraju, M., Rekha, V., Sai Prasad, P. S., Prasad, R. B. N. & Lingaiah, N. Selective hydrogenolysis of glycerol to 1, 2 propanediol over Cu–ZnO Catalysts. *Catal. Lett.* **126**, 119–124 (2008).
 158. Connor, R., Folkers, K. & Adkins, H. The preparation of copper–chromium oxide catalysts for hydrogenation. *J. Am. Chem. Soc.* **3**, 1138–1145 (1932).

159. Liang, C., Ma, Z., Ding, L. & Qiu, J. Template preparation of highly active and selective Cu–Cr catalysts with high surface area for glycerol hydrogenolysis. *Catal. Lett.* **130**, 169–176 (2009).
160. Kim, N. D., Oh, S., Joo, J. B., Jung, K. S. & Yi, J. The promotion effect of Cr on copper catalyst in hydrogenolysis of glycerol to propylene glycol. *Top. Catal.* **53**, 517–522 (2010).
161. Mane, R. B., Ghalwadkar, A. A., Hengne, A. M., Suryawanshi, Y. R. & Rode, C. V. Role of promoters in copper chromite catalysts for hydrogenolysis of glycerol. *Catal. Today* **164**, 447–450 (2011).
162. Xiao, Z., Xiu, J. & Wang, X. Insights into the reaction pathways of glycerol hydrogenolysis over Cu–Cr catalysts. *J. Mol. Catal. Chem.* **365**, 24–31 (2012).
163. Yun, Y. S., Kim, T. Y. & Yi, J.. Understanding the reaction mechanism of glycerol hydrogenolysis over a CuCr_2O_4 catalyst. *ChemSusChem* **10**, 442–454 (2017).
164. Chaminand, J., Djakovitch, L., Gallezot, P. & Pinel, C. Glycerol hydrogenolysis on heterogeneous catalysts. *Green Chem.* **6**, 359–361 (2004).
165. Bienholz, A. *et al.* Prevention of catalyst deactivation in the hydrogenolysis of glycerol by Ga_2O_3 - modified copper/zinc oxide catalysts. *J. Phys. Chem. C* **115**, 999–1005 (2011).
166. Tan, H., Tall, O. & Han, Y. One-pot synthesis of $\text{Cu/ZnO/ZnAl}_2\text{O}_4$ catalysts and their catalytic performance in glycerol hydrogenolysis. *Catal. Sci. Technol.* **3**, 3360–3371 (2013).
167. Kim, D. W., Sh, H. & Hong, S. S. Hydrogenolysis of glycerol to propylene glycol on nanosized Cu–Zn–Al catalysts prepared using microwave process. *J. Nanosci. Nanotechnol.* **15**, 656–659 (2015).
168. Durán-Martín, D., Granados, M. L., Fierro, J. L. G., Pinel, C. & Mariscal, R. Deactivation of CuZn catalysts used in glycerol hydrogenolysis to obtain 1,2-Propanediol. *Top. Catal.* **60**, 1062–1071 (2017).
169. Yuan, Z. *et al.* Hydrogenolysis of glycerol over homogenously dispersed copper on solid base catalysts. *Appl. Catal. B Environ.* **101**, 431–440 (2011).
170. Xia, S., Yuan, Z., Wang, L., Chen, P. & Hou, Z. Hydrogenolysis of glycerol on bimetallic Pd–Cu/solid-base catalysts prepared via layered double hydroxides precursors. *Appl. Catal. Gen.* **403**, 173–182 (2011).
171. Wu, Z., Mao, Y., Wang, X. & Zhang, M. Preparation of a Cu–Ru/carbon nanotube catalyst for hydrogenolysis of glycerol to 1,2-propanediol via hydrogen spillover. *Green Chem.* **13**, 1311 (2011).
172. Gabrysch, T., Peng, B., Bunea, S., Dyker, G. & Muhler, M. The role of metallic copper in the selective hydrodeoxygenation of glycerol to 1,2-propanediol over Cu/ZrO_2 . *ChemCatChem* **10**, 1344–1350 (2018).
173. Zhou, J., Guo, L., Guo, X., Mao, J. & Zhang, S. Selective hydrogenolysis of glycerol to propanediols on supported Cu-containing bimetallic catalysts. *Green Chem.* **12**, 1835–1843 (2010).
174. Vila, F., López Granados, M., Ojeda, M., Fierro, J. L. G. & Mariscal, R. Glycerol hydrogenolysis to 1,2-propanediol with $\text{Cu}/\gamma\text{-Al}_2\text{O}_3$: Effect of the activation process.

- Catal. Today* **187**, 122–128 (2012).
175. Vasiliadou, E. S. & Lemonidou, A. A. Investigating the performance and deactivation behaviour of silica-supported copper catalysts in glycerol hydrogenolysis. *Appl. Catal. Gen.* **396**, 177–185 (2011).
176. Huang, Z., Cui, F. & Xia, C. Highly dispersed silica-supported copper nanoparticles prepared by precipitation–gel method: A simple but efficient and stable catalyst for glycerol hydrogenolysis. *Chem. Mater.* **20**, 5090–5099 (2008).
177. Mizugaki, T., Arundhathi, R., Mitsudome, T., Jitsukawa, K. & Kaneda, K. Selective hydrogenolysis of glycerol to 1,2-Propanediol using heterogeneous copper nanoparticle catalyst derived from Cu–Al hydrotalcite. *Chem. Lett.* **42**, 729–731 (2013).
178. Durán-Martín, D., Ojeda, M., Granados, M. L., Fierro, J. L. G. & Mariscal, R. Stability and regeneration of Cu–ZrO₂ catalysts used in glycerol hydrogenolysis to 1,2-propanediol. *Catal. Today* **210**, 98–105 (2013).

CHAPTER II

Experimental part

Table of contents

CHAPTER II	72
I. Synthesis of ZnO by hydrolysis of ZnEt ₂ in a solution of PAAH at 0.63%.....	75
I.1. Effect of the molecular weight of PAAH	75
I.2. Study of the influence of the washing set up after synthesis	76
I.3. Study of the influence of the concentration of PAAH.....	77
I.4. Synthesis of ZnO/PAAH at different temperature	77
I.5. Calcination after synthesis.....	78
II. Synthesis of ZnO-ZnAl ₂ O ₄ by hydrolysis of ZnET ₂ and AlMe ₃	78
III. Synthesis of supported Cu catalysts by deposition precipitation.....	80
III.1. Deposition precipitation of Cu on commercial ZnO.....	80
III.1.1. Synthesis of Cu/ZnO commercial with different concentration of Cu²⁺ and wt% Cu°	81
III.2. Synthesis of Cu/ZnO with the synthesized ZnO.....	82
III.2.1. Deposition precipitation with ZnO/PAAH :.....	82
III.2.2. Deposition precipitation with the calcined ZnO:	83
III.2.3. Deposition precipitation of Cu with ZnO-ZnAl₂O₄.....	84
IV. Synthesis of Cu/ZnO-ZnAl ₂ O ₄ by one pot.....	84
IV.1. Synthesis of Cu-ZnO and Cu/ZnO-ZnAl₂O₄ in one pot-one step:	84
IV.2. Synthesis of Cu/ZnO and Cu/ZnO-ZnAl₂O₄ in one pot-two steps:	86

IV.3.Synthesis of Cu/ZnO-ZnAl₂O₄ in one pot-two steps without adding urea:	87
V. Hydrogenolysis of glycerol in a batch reactor under H ₂ pressure	88
VI. Characterization techniques	89
VI.1.Powder X-Ray Diffraction (XRD)	89
VI.2.BET specific surface area	90
VI.3.Elemental analysis by ICP-OES.....	92
VI.4.Transmission Electronic Microscopy (TEM)	92
VI.4.1.Energy Dispersive X-Ray Spectroscopy (EDX) measurement.....	94
VI.5.Thermogravimetric analysis (TGA)	94
VI.6.Chromatographic analysis	95

Before developing the experimental conditions of each synthesis, a short list of the commercial products applied for the synthesis of ZnO, ZnAl oxides, the copper based catalysts and the glycerol is resumed in the Table 2-1.

Table 2-1: Properties of the chemical applied for the syntheses

Product	Formula	Acronym	Supplier	Purity (%)
Polyacrylic acid	$\text{CH}_3(\text{CH}_2\text{CHCOOH})_n\text{CH}_3$	PAAX	Sigma	50
Diethyl Zinc	$\text{Zn}(\text{CH}_2\text{-CH}_3)_2$	DEZ	Sigma	15
Trimethyl aluminium	$\text{Al}(\text{CH}_3)_3$	TMA	Sigma Alfa Aesar	97 25
Copper nitrate	$\text{Cu}(\text{NO}_3)_2 \cdot 3\text{H}_2\text{O}$	C.N	Sigma	99.9
Zinc oxide	ZnO	ZnO	Alfa Aesar	99.9
Urea	$\text{CH}_4\text{N}_2\text{O}$	U	Sigma	99
Glycerol	$\text{C}_3\text{H}_8\text{O}_3$	GLY	Sigma	99.5
1,2-Propanediol	$\text{C}_3\text{H}_8\text{O}_2$	1,2-PDO	Sigma	99.5

The first step of the work was the synthesis of the support (ZnO). Different parameters were studied such as the molecular weight of PAAH, the washing process, the weight concentration of PAA2...

I. Synthesis of ZnO by hydrolysis of ZnEt₂ in a solution of PAAH at 0.63%

I.1. Effect of the molecular weight of PAAH

The synthesis of ZnO was done via sol gel method, based on our previous work, by hydrolyzing one equivalent of ZnEt₂ (diethylzinc or DEZ) in a solution of PAAH under argon (schlenk system) due to the pyrophoric state of diethyl zinc.

The PAAH solutions were prepared using commercial PAAH with different molecular weight diluted in water. The commercial products used for ZnO synthesis and their detailed properties are listed in the table below:

Table 2-2: Commercial products used for the synthesis of ZnO

Properties	Diethyl zinc	Polyacrylic acid (PAAH)
Supplier	Sigma Aldrich	Sigma Aldrich
CAS No	557-20-0	9003-01-4
Formula	ZnC ₄ H ₁₀	CH ₃ (CH ₂ CHCOOH) _n CH ₃
Mw (g.mol ⁻¹)	123.5	1800 (PAA1.8), 2000 (PAA2), 5000 (PAA5), 100000 (PAA100)
Boiling T° (°C)	118	/
Melting T° (°C)	-28	/
Density (g.cm ⁻³)	1.2	/
Aspect	Liquid	Viscous liquids
Dangers	C*, F*, N*	Xi*
Purity	15% in toluene	50% in water

C*: corrosive, F*: inflammable, N*: dangerous for the environment, Xi*: irritant.

The procedure described in this paragraph is the classical method to synthesize 2 grams of ZnO (Figure 2-1):

2.52 g of PAA1.8 (Mw PAAH = 1800 g.mol⁻¹), PAA2 (Mw PAAH = 2000 g.mol⁻¹), PAA5 (Mw PAAH = 5000 g.mol⁻¹) and PAA100 (Mw = 100 000 g.mol⁻¹) initially concentrated at 50 wt%

were dissolved in 200 mL of distilled water to obtain 0.63 wt% PAAX/water. The solution was stirred at 1000 rpm under inert atmosphere (argon) at room temperature (15 - 25 °C). Then, 14.4 mL of DEZ was added in one shot with a syringe. The reaction is exothermic and fast, and produce ethane that is eliminated through a bubbler connected to the schlenk flask. After one hour of stirring, the solution was centrifuged at 8000 r.p.m for 20 minutes, washed (with water or ethanol) and the wet powder was dried in an oven under air at 80 °C.

To prepare 6 grams of ZnO, 600 mL of PAAX solution were used instead of 200 mL and 43.2 mL of DEZ were added under the same experimental conditions.

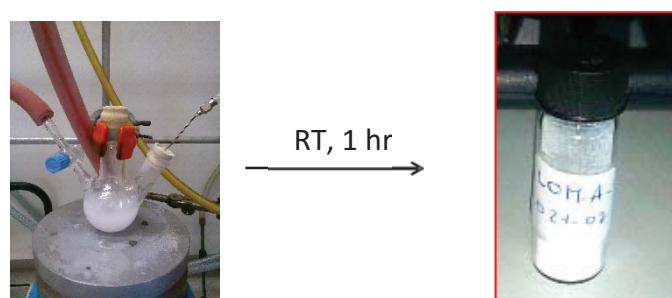


Figure 2-1: Synthesis of ZnO NPs

1.2. Study of the influence of the washing set up after synthesis

The effect of the washing process was studied for ZnO/PAA2 and ZnO/PAA5.

In order to recover the nanoparticles of ZnO, the suspensions were centrifuged at 4700 r.p.m for 40 minutes or 8000 r.p.m for 20 minutes depending on the total synthesized volume (200 mL and 600 mL, respectively).

After centrifugation the wet powder of ZnO/PAA2 was washed by three different ways:

- Unwashed,
- Ethanol,
- or by mixture of water/ethanol.

EtOH washings showed the best results in term of morphology and surface area, so all the ZnO NPs were washed by EtOH and it became important to study the effect of the volume of EtOH added on the properties of the final material.

Different volume of EtOH were used (30 mL, 60 mL and 90 mL) while using PAA2 and PAA5. Depending on the initial volume of PAAH solution, the time of washing varied

between 30 minutes for 200 mL of PAAH/water and one hour and a half for 600 mL PAAH/water. Volume of EtOH used for washing were fixed to 90 mL for 200 mL of PAAH/water and 270 mL for 600 mL PAAH/water.

I.3. Study of the influence of the concentration of PAAH

The study was done for PAA2, the weight percentage studied is shown in the following table.

Table 2-3: Weight of added PAA2 for different concentration

Percentage of PAA2 (wt%)	Weight of PAA2 added in 200 mL of water (g)
0	0
0.3	1.2
0.5	2.0
0.63	2.52
0.8	3.36
1	4.2
1.2	4.8

For each synthesis one equivalent of DEZ (14.4 mL) was added under argon at room temperature as described before. After synthesis, the suspension was centrifuged and the powder was washed with 90 mL of ethanol for half an hour and dried at 80 °C under air.

I.4. Synthesis of ZnO/PAAH at different temperature

The synthesis was conducted at three other temperatures: 0, 10 and 40 °C. Considering that the classical method was conducted at room temperature, i.e. around 20 °C.

The syntheses were done using PAA2 and PAA5, as before. In a schlenk flask of 1 L, 600 mL of PAA2 or PAA5 at 0.63 wt% were added. One equivalent of a solution of DEZ (43.2 mL, 0.16 mol) was added to the flask under argon.

For 0 °C, the flask was emerged in an ice bath for 30 minutes before adding the DEZ. The temperature of solution was measured before adding the reactant and it was stable after 20 minutes.

For 10 °C, the flask was emerged in a mixture of water and ice in order to maintain the

temperature stable at 10 °C.

For 40 °C, the flask was maintained in a metallic bath and heated at 40 °C.

The transformation of DEZ into ZnO was immediate at the three different temperatures, this is why it's important to have the temperature inside the flask stable before adding the reactant. As the solution was stirred for one hour, the temperature of the bath was maintained the same for one hour.

After synthesis, the suspensions were centrifuged and washed with 90 mL of ethanol for half an hour and dried at 80 °C under air.

For ZnO/PAA5, 60 °C was also added due to the experimental results and the procedure was always the same.

I.5. Calcination after synthesis

Some of the materials were calcined after drying. The materials were synthesized using the standards parameters: 0.63 wt% PAAH, room temperature, washing with water and centrifugation at 4700 r.p.m for 20 minutes. After drying, the materials were calcined in a static oven for four hours at different temperatures, starting from RT till attending the desired temperature with a heating rate of 5°C.min⁻¹. The choice of the temperature was related to the loss of the organic compound shown by TGA results, which occurs between 300 °C and 400 °C.

The study was done using PAA2 and PAA5:

For ZnO/PAA2, four temperatures were studied: 300, 325, 350 and 400 °C. For ZnO/PAA5, three temperatures were studied: 300, 350 and 400 °C.

II. Synthesis of ZnO-ZnAl₂O₄ by hydrolysis of ZnET₂ and AlMe₃

In order to enhance the catalytic properties of the support, aluminium was added by using trimethyl aluminium AlMe₃ (trimethylaluminium or TMA) as precursor. For the different synthesis, the hydrolysis was done at 0 °C. The effect of the molar ratio Zn:Al and the presence of PAA2 were studied.

1) Synthesis of ZnO-ZnAl₂O₄ with a theoretical molar ratio Zn:Al of 1:2 in presence of PAA2.

In a schlenk flask of 500 mL, 200 mL of a solution of PAA2 at 0.63 wt% was added. The flask was immersed in an ice bath for 30 minutes in order to decrease the solution temperature to 0 °C. On the other hand, in a 50 mL schlenk flask, 3.1 mL of TMA (97% from sigma Aldrich) was added to 14.4 mL of DEZ under argon. The transfer of the mixture of TMA and DEZ to the 500 mL flask was done slowly under argon with a syringe. In the seconds following the transfer, ethane and methane gases were generated and evacuated by the bubbler connected to the 500 mL flask. The reaction is highly exothermic and the color of the solution turned into white in a few minutes. After one hour, the stirring was stopped and the suspension was centrifuged with a rate of 8000 r.p.m for 30 minutes. 90 mL of ethanol was added to the wet powder obtained after centrifugation and the mixture was kept under stirring at room temperature for 30 minutes. A last centrifugation round was done as previously. To finish, the centrifuge tube was kept in the oven at 80 °C overnight and the powder obtained is divided in 3 batches: the as synthesized one was used as support for catalyst, a few mg were calcined at 400 °C and 600 °C for characterization.

2) Synthesis of ZnO-ZnAl₂O₄ with a molar ratio Zn:Al of 1:2 without PAA2

The same procedure was followed but without PAA2. Centrifugation, washing and drying steps were same as the 1st synthesis.

3) Synthesis of ZnO-ZnAl₂O₄ with a molar ratio Zn:Al of 1:2 without PAA2

The first bottle of TMA had been opened for a long time, or it is readily oxidized. For that reason, a new bottle of TMA was purchased from Alfa Aesar (25 wt% in hexane). The synthesis steps were same as the previous one but the corresponding volume of TMA was 4 times higher since the bottle was not pure (12.27 mL).

4) Synthesis of ZnO-ZnAl₂O₄ with a molar ratio Zn:Al of 1:2 in presence of PAA2

The synthesis was done now with PAA2. No change in the procedure was done.

5) Synthesis of ZnO-ZnAl₂O₄ with a molar ratio Zn:Al of 2:1 in presence of PAA2

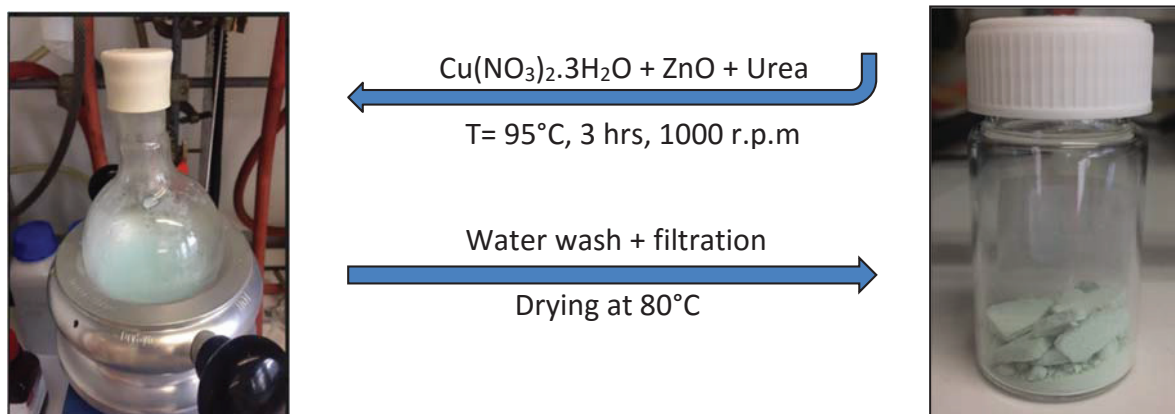
This time we synthesized the material by adding more DEZ than TMA to obtain a molar

ratio of 2:1. Instead of 12.27 mL of TMA, 3.06 mL of the new bottle of TMA was added to the schlenk flask containing 14.4 mL of DEZ under argon. The transfer, centrifugation and washing steps were the same as before.

III. Synthesis of supported Cu catalysts by deposition precipitation

III.1. Deposition precipitation of Cu on commercial ZnO

A commercial ZnO (Alfa Aesar) was first used to set up the parameters of the synthesis. 7.6 g of $\text{Cu}(\text{NO}_3)_2 \cdot 3\text{H}_2\text{O}$ was dissolved in 200 mL of water to obtain a solution of Cu^{2+} at $0.157 \text{ mol}\cdot\text{L}^{-1}$. According to the nominal weight percentage of copper, a specific volume of the Cu^{2+} prepared solution (from 0.26 to 25 mL) was added to 1 g of ZnO in a flask of 500 mL with 4 g of urea, used as precipitating agent. Depending on the concentration of Cu^{2+} in the final solution, different volumes of water were added. The mixture was heated at $5 \text{ }^\circ\text{C min}^{-1}$ to $95 \text{ }^\circ\text{C}$ and kept under stirring for 3 hours while connecting the flask to a refrigerator to maintain the same volume of solution during heating. After synthesis, the solution was filtrated and washed with 100 mL of distilled water to remove any urea residues and dried in the oven under air at $80 \text{ }^\circ\text{C}$ for one night.



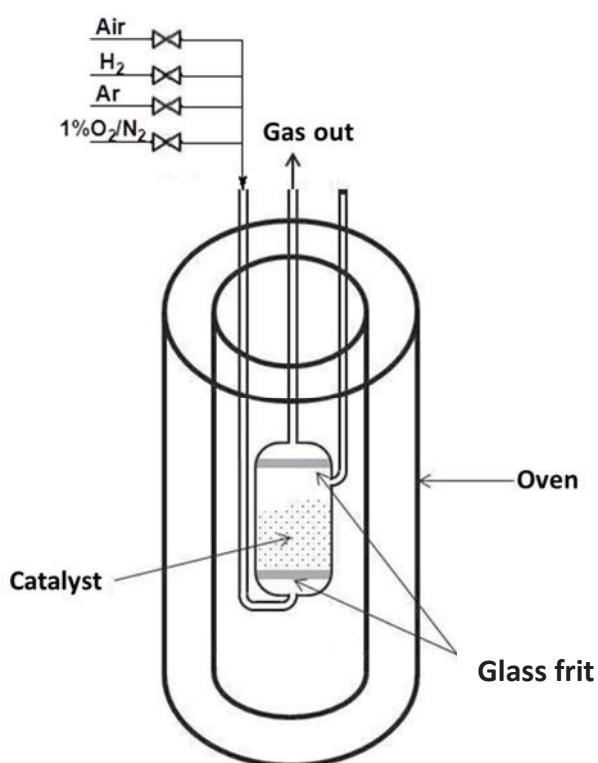
Scheme 2-1: Example of synthesis of Cu/ZnO by DPU

After DPU, thermal treatments under air and reductive atmosphere were conducted to obtain Cu based catalysts.

The first step was the calcination, to eliminate the organics and to transform the copper

precursor into copper oxide, at 400 °C for four hours in a static oven with a heating rate of 5 °C.min⁻¹. Once the heating was over, the sample was removed from the oven after cooling down. The second step was the reduction to transform Cu²⁺ to Cu⁰; the powder was transferred to a cell as in the scheme below. First the cell was purged with argon for 10 minutes before H₂ flow with an output of 50 mL.min⁻¹ and the oven was heated till 300 °C or 350 °C for one hour with a heating rate of 5 °C.min⁻¹.

After cooling down under argon and at room temperature, a passivation step was needed in order to form a protective oxide layer on the surface of the catalyst. The passivation was conducted for half an hour with a mixture of gas flow of 1% O₂/N₂ with 50 mL.min⁻¹ flow rate.



Scheme 2-2: Glass cell for reducing the catalyst under a gas flow

III.1.1. Synthesis of Cu/ZnO commercial with different concentration of Cu²⁺ and wt% Cu⁰

As mentioned above, the catalysts were first prepared using a commercial ZnO. In order to define the best synthesis parameters, different catalysts were prepared by changing

the concentration of the solution containing Cu^{2+} in the mixture and the weight percentage of Cu^0 . In order to obtain different weight percentage, 2 solutions of Cu^{2+} were prepared.

Solution 1: 2.416 g of $\text{Cu}(\text{NO}_3)_2 \cdot 3\text{H}_2\text{O}$ were dissolved in 50 mL of water to obtain a 0.2 M concentration of Cu^{2+} .

Solution 2: 7.6 g of $\text{Cu}(\text{NO}_3)_2 \cdot 3\text{H}_2\text{O}$ were dissolved in 200 mL of water to obtain a 0.157 M concentration of Cu^{2+} .

The tables below show the different catalysts synthesized using the commercial support:

Table 2-4: Volume of the added solution for each copper concentration

Cu^0 weight percentage (%)	Added volume of Cu^{2+} solution (mL)
2.5	2.02 of solution 1
5	5.27 of solution 2
10	11.1 of solution 2
15	17.7 of solution 2
20	25 of solution 2

After synthesis the filtration and thermal treatment were as described above.

III.2. Synthesis of Cu/ZnO with the synthesized ZnO

III.2.1. Deposition precipitation with ZnO/PAAX :

The hybrid ZnO (ZnO-PAAX uncalcined) were used after drying at 80 °C. The same DPU method was used with the hybrid ZnO as previously.

However, TGA results showed that 50% of weight was lost by heating at 400 °C. The syntheses were conducted before calcination, hence in order to respect the same quantities (wt% Cu/ZnO) as for the commercial ZnO, two grams of hybrid ZnO were used instead of 1 g of commercial ZnO. Catalysts with different Cu^0 weight percentage were synthesized (from 10 wt% to 30 wt%). Table 5-2 resumes the studied parameters of ZnO/PAAX used as support for copper catalysts.

Table 2-5: Different ZnO used as supports for catalysis

Parameters	ZnO/PAA2	ZnO/PAA5	ZnO/PAA100
Weight percentage	10, 20 and 30% Cu ⁰	10 and 20% Cu ⁰	10 and 20% Cu ⁰
Synthesis temperature	0, 10, 40 °C and RT	0, 40 °C and RT	RT
Washing	Water, EtOH	Water, EtOH	Water, EtOH

III.2.2. Deposition precipitation with the calcined ZnO:

The deposition was also conducted on calcined ZnO.

As the aim is to compare the results between commercial support and the synthesized one, the same nominal Cu weight percentage was aimed.

For that reason, the same quantity of ZnO was supposed to be added in order to have the same weight percentage. Once again, that was a little bit hard because the weight loss calculated by TGA can have a 5% error. As the catalyst will be calcined at 400 °C after synthesis, the weight of ZnO initially added to prepare the catalyst should be calculated according to the TGA results in order to obtain in the end one gram of ZnO. The easier way was to calcine 2 g of ZnO at the selected temperature and after calcination adding the powder to the flask containing the copper and the urea to prepare the catalyst.

The protocol was the same as previously, different volume of Cu²⁺ solution at 0.157 M were added to the calcined ZnO with 4 g of urea and different volumes of water depending on the weight percentage of Cu in order to have the same concentration as before (20 mmol.L⁻¹). The table below shows different parameters studied for ZnO/PAA2 and ZnO/PAA5 calcined samples.

Table 2-6 Synthesis parameters for Cu/calcined ZnO catalyst

Parameters	ZnO/PAA2	ZnO/PAA5
Weight percentage	10, 15, 20 and 35% Cu°	10 and 17% Cu°
Calcination temperature	300, 325, 350 and 400 °C	300 and 350 °C

III.2.3. Deposition precipitation of Cu with ZnO-ZnAl₂O₄

As it was the last part of the work, all the parameters were fixed. For that reason, all the syntheses were done with 20 wt% of Cu. The different kind of ZnO-ZnAl₂O₄ synthesized were used as support for catalysts. In addition to the as-synthesized support, a deposition precipitation was done with a calcined material.

For the as synthesized one without PAA2, 1.1 g of support was suspended in 163 mL of water in presence of urea and 25 mL of Cu²⁺ solution of 0.157 M was added under stirring. For the supports synthesized with PAA2, based on TGA results, 1.8 g of the supports were added to obtain 1 g after calcination at 400 °C. The volume of water and Cu²⁺ were kept the same. For the support calcined at 400 °C, 1 g was used.

IV. Synthesis of Cu/ZnO-ZnAl₂O₄ by one pot

IV.1. Synthesis of Cu-ZnO and Cu/ZnO-ZnAl₂O₄ in one pot-one step:

Cu-ZnO were synthesized by mixing all the precursors at once:

In order to have 20 wt% of Cu, 25 mL of Cu²⁺ solution (157 mmol/L or 10 g/L of Cu²⁺) prepared by dissolving 7.6 g of Cu(NO₃)₂·3H₂O in 200 mL of water were added in a flask of 500 mL; 4 g of urea was added to this solution to keep the same parameters as before; 2.52 g of PAA2 (50 wt% in water) dissolved in 200 mL of water was added to prepare the ZnO suspension inside the mixture. The temperature was increased to 60 °C (the temperature of decomposition of urea) before adding 14.4 mL of the DEZ and stirring

under argon. The heating continued till 60 °C for 3 hours. During this time, the solution was having the same color (blue) during all the process. After three hours, the solution was centrifuged at 8000 r.p.m for 20 minutes and washed with 90 mL of ethanol and centrifuged again before drying under air at 80 °C for one night. After synthesis, the powder was calcined at 400 °C for 4 hours under air and reduced with H₂ flow at 350 °C for one hour, as previously. The color of the dried and calcined powder is same as the catalyst obtained by DPU method showed in the picture below.

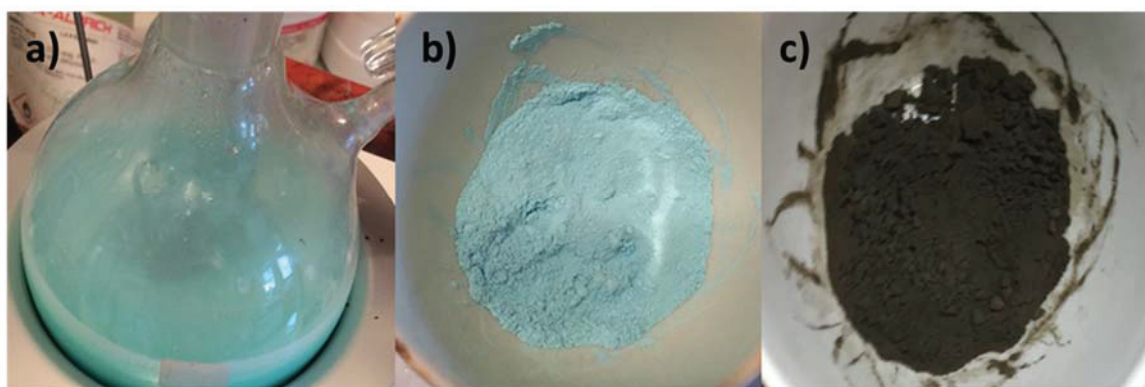


Figure 2-2: Color of the sample a) in solution, b) after drying and c) after calcination, for Cu-ZnO

In the 2nd family of catalysts aluminium was incorporated. The precursor used was the old bottle of AlMe₃ purchased from sigma Aldrich (97% in hexane). Different methods of syntheses were used. In a first trial, 30 wt% of copper was added, for that 37.5 mL of Cu²⁺ solution was mixed with the solution of PAA2 and urea. As for Cu/ZnO, 14.4 mL of DEZ was added to the hot solution of Cu²⁺ and PAA2 under argon, followed by 5.11 mL of TMA at 60 °C, the stirring took place for 3 hours.

At the beginning the color of the solution was blue as before and it turned into green at the end of the reaction indicating the presence of Al in the suspension. The washing and thermal treatment were the same as described above.

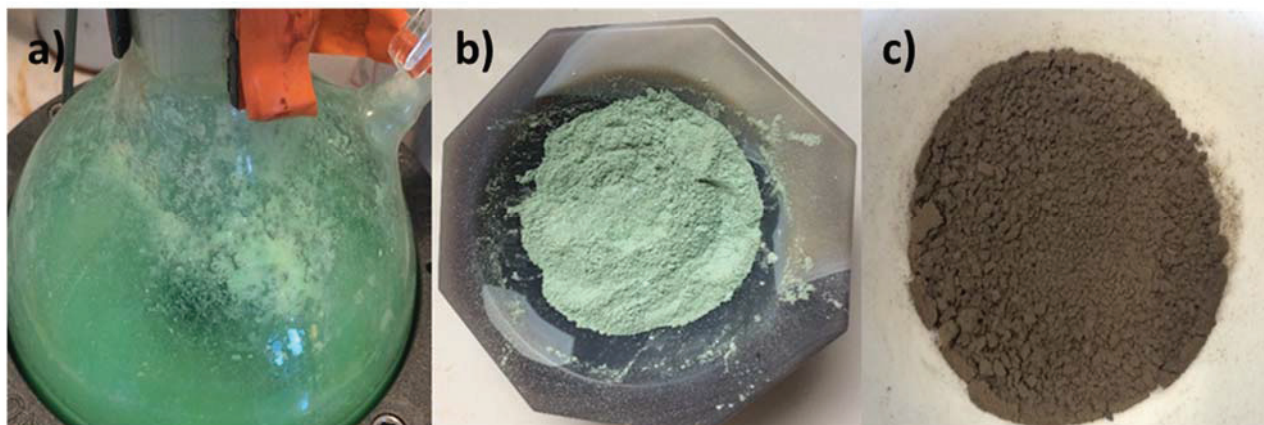


Figure 2-3: Color of the sample a) in solution, b) after drying and c) after calcination for Cu-ZnO-ZnAl₂O₄

The temperature of the synthesis can have a big impact on the properties of the ZnO, so other one pot syntheses were done by dividing the synthesis into 2 steps.

IV.2. Synthesis of Cu/ZnO and Cu/ZnO-ZnAl₂O₄ in one pot-two steps:

The first step was the synthesis of ZnO at 0 °C: in a schlenk flask of 500 mL, 4 grams of urea were mixed with 0.63 wt% PAA2 in water and the appropriate volume of Cu²⁺. The flask was in a glace bath for half an hour to reach 0 °C. The corresponding volume of DEZ was added to the flask by a syringe under argon and the stirring at 0 °C continued for one hour. The second step was the heating at 60 °C for 3 hours to dissolve urea and to enhance the precipitation of copper on the support. Washing with 90 mL of EtOH was done as for ZnO NPs and thermal treatments are the same as before. At 0 °C, the solution was light green and after heating it turned into yellow.



Figure 2-4: Color of the sample for the two steps method; a) in solution at 0°C, b) in solution at 60 °C and c) after drying

For Cu/ZnO-ZnAl₂O₄ catalyst, the two steps synthesis was conducted in two schlenk systems: a schlenk tube containing 14.4 mL of DEZ and 5.11 mL of TMA kept under argon and a schlenk flask containing the appropriate amount of Cu²⁺ solution, PAA2 in water and 4 g of urea. We changed the volume of TMA depending on the molar ratio Zn:Al aimed. The addition of the aluminium precursor and DEZ on the solution of Cu²⁺ and PAA2 was done with a syringe after cooling down the solution temperature of the schlenk flask to 0 °C.

After one hour of stirring the suspension was heated till 60 °C for 3 hours. The solution had a light green color during all the reaction time. The washing and thermal treatment were same as before.

After calcination the color of the powder was brown indicating the presence of CuO and the weight of the powder is the half because of removing the nitrates of Cu and the PAAH from the as-synthesized sample. It turns into dark black after reduction under H₂ due to the presence of Cu⁰ species.

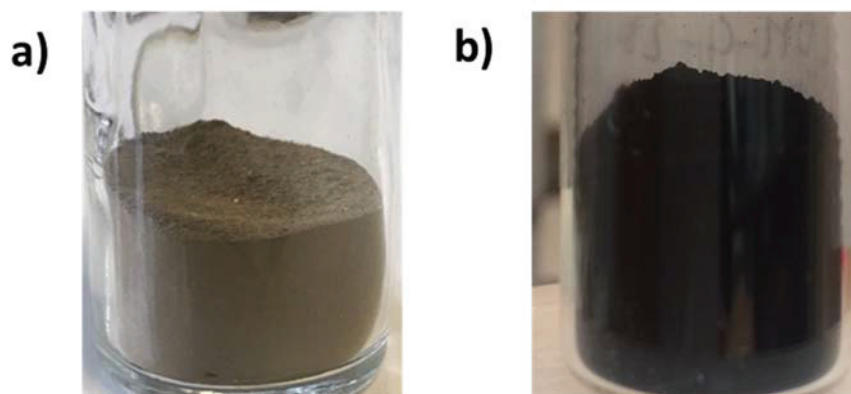


Figure 2-5: a) Calcined CuO/ ZnO-ZnAl₂O₄ and b) reduced Cu/ZnO-ZnAl₂O₄

IV.3. Synthesis of Cu/ZnO-ZnAl₂O₄ in one pot-two steps without adding urea:

Some experiments were done without adding urea with different Cu wt%.

The procedure was kept the same: transfer of Zn and Al precursors at 0 °C under argon into the PAA2/Cu²⁺ solution and after one hour of stirring, heating of the solution at 60 °C for 3 hours without adding urea. The color of the powder obtained after drying depended on the percentage of Cu added into the solution.

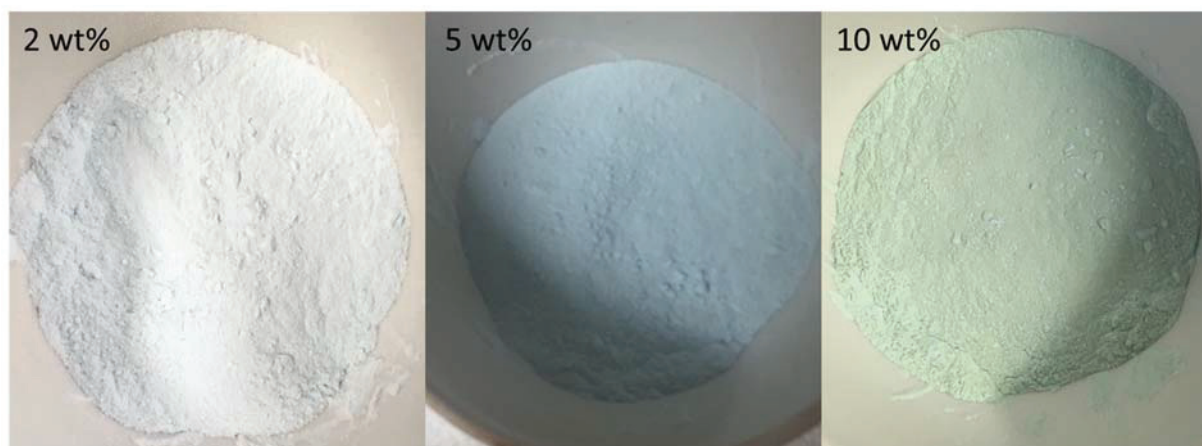


Figure 2-6: Dependence of the color on the weight percentage of copper

V. Hydrogenolysis of glycerol in a batch reactor under H₂ pressure

The hydrogenolysis reactions were performed in a 300 mL batch Hastelloy Parr 4560 autoclave set-up. It was equipped with a 0-200 bar pressure gauge, a 150 bar safety rupture disc and a thermocouple. The seal between the tank and the lid was ensured by a Teflon® seal. After sealing, the autoclave was surrounded by an electrical heating jacket controlled by a control box indicating the temperature of the heating jacket as well as the temperature of the reaction medium via the thermocouple. A magnetically coupled drive system overcame the reactor and drove the self-suction turbine agitator. A removable cage made of stainless steel supported on the walls of the tank was equipped with counter-blades. This assembly improved the gas-liquid contact in order to facilitate the solubilization of hydrogen which was essential for hydrogenolysis reactions. Finally, samples were taken through a tube dipping into the tank via a valve and provided at its end with a filter Hastelloy® of 8 µm.

A solution of glycerol 0.23 M was prepared by dissolving 2.15 g of glycerol (Alfa Aesar) in 100 mL of water. The catalyst and the solution were added simultaneously in the reactor. After closing the reactor, the lines and the reactor were purged 3 times with 50 bar of argon. Then the heater was turned on to reach 200 °C under a stirring rate of 1000 r.p.m. When the reactor temperature was stable at 200 °C, the valve of hydrogen was open and the pressure was maintained at 50 bar. After heating the pressure was already around 20 bar. Sampling was done at room temperature and once the temperature reached 200 °C before adding H₂. Once the reaction was started, every 2 hours a sampling was done till 6

hours and the next day at $t = 23$ h and $t = 24$ h. A last sampling was done after cooling down the reactor at $t = 26$ h. Those samples were characterized by GC-FID in order to identify all the products obtained and their percentage. The solution containing the catalyst was filtrated and the catalyst was dried under air at $80\text{ }^{\circ}\text{C}$ in order to be regenerated.

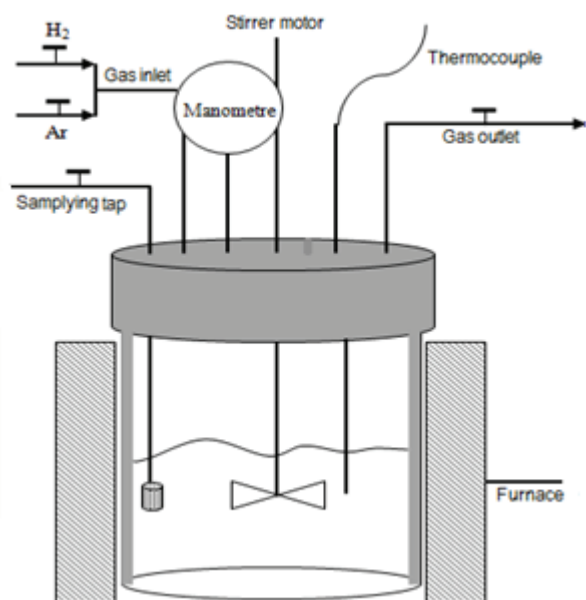


Figure 2-7: Photo (left) and scheme (right) of the batch reactor

VI. Characterization techniques

VI.1. Powder X-Ray Diffraction (XRD)

X-ray diffraction (XRD) of powders is used to identify the nature of crystalline phases present in a solid and to determine the mean crystallite size of each phase present in the sample. The measurement consists of sending X-ray beams (λ known) at an angle θ on the sample. These rays may be diffracted by the lattice planes at angle 2θ if Bragg's law is satisfied. The diffracted rays interfere constructively and they are detected by a detector in the form of intensity peaks. This technique is based on the Bragg's law is given by equation (1).

$$n \cdot \lambda = 2d_{hkl} \cdot \sin \theta \quad (1)$$

With

- λ : Wavelength of the incident light (\AA);
- d_{hkl} : Lattice interplanar spacing of crystal (\AA);
- θ : Diffraction angle (degree);
- n : Order of diffraction line.

Powder X-ray diffraction patterns (XRD) of the samples were recorded using a Bruker Advance Diffractometer D8A25 equipped with a nickel filter, a copper tube ($\lambda K\alpha$ (Cu) = 1.54184 \AA) and a multi-channel fast detector (LynxEye 192 channels an active length of 2.947 $^\circ$). Samples were scanned at 0.04 $^\circ \text{ s}^{-1}$ over the range $5 \leq 2\theta \leq 80^\circ$.

With heterogeneous catalysts, it is possible to estimate the size of the crystallite by X-ray diffraction. But if the metal particles are too small (< 5 nm) and well dispersed, the diffraction lines are not observed. If they are visible, the mean crystallite sizes (d_M) were estimated using the Scherrer equation **(2)** from the half-width of the XRD broadening peak in a diffraction pattern.

$$d_M = \frac{0.9\lambda}{\beta \cos\theta} \quad (2)$$

With

- λ : X-ray wavelength ($\lambda = 1.54184 \text{\AA}$);
- θ : Bragg angle (degree);
- β : Line broadening at half-maximum of diffraction peak, in radians.

VI.2. BET specific surface area

Nitrogen adsorption/desorption is an important analytical technique for porous solid. It is based by physical adsorption of a gas (most commonly, nitrogen) on the surface of the

solid. Nitrogen adsorption/desorption isotherms allow us to determine the BET surface area of a solid (which defines the total surface area per unit of mass accessible to molecules), as well as the volume of the adsorbed monolayer (V_m). The data are treated according to the Brunauer, Emmett and Teller (BET) adsorption isotherm equation **(3)**:

$$\frac{P}{V_{ads}(P_0-P)} = \frac{C-1}{V_m.C} \times \left(\frac{P}{P_0}\right) + \frac{1}{V_m.C} \quad (3)$$

With

- P : Pressure at equilibrium (mmHg);
- P_0 : Saturation pressure of adsorption of the sample (mmHg);
- C : constant obtained from adsorption and desorption rates;
- V_{ads} : Volume adsorbed at 77K (cm^3);
- V_m : Volume of adsorbed monolayer (cm^3).

The determination of the steering coefficient as well as the intercept at the origin by plotting $\frac{P}{V_{ads}(P_0-P)}$ as a function of $\left(\frac{P}{P_0}\right)$ allow us to access the value of V_m . Then the total area of the solid is then deduced by using equation **(4)**:

$$S = 4.35 \times V_m \text{ (m}^2\text{)} \quad (4)$$

This surface relative to the mass of the degassed solid used during the analysis is called specific surface area (S.S.A). It is expressed in $\text{m}^2 \text{g}^{-1}$. The BET specific surface area of the samples was determined by N_2 physisorption at 77K, using an ASAP 2020 Micromeritics apparatus. Prior to the measurements, catalysts were degassed at 150 °C for 3 h under nitrogen (10^{-4} mbar) with a heating rate of $5 \text{ }^\circ\text{.min}^{-1}$ in with Smart VacPrep Micromeritics.

VI.3. Elemental analysis by ICP-OES

After each catalyst preparation, the chemical analysis is used in order to access the exact content of metal deposited on the support, and to detect any leaching of the active species into solution during the chemical reaction. In the case of copper, zinc and aluminum, solid sample is dissolved in a mixture of H₂SO₄ and HNO₃ under heating temperature between 250 and 300 °C.

After mineralization, the resulting sample solution is then nebulized into the core of inductively coupled argon plasma, where temperatures of approximately 9000 K are attained. At such high temperatures, the nebulized solution is vaporized, and the analyte species are atomized, ionized and thermally excited. The analyte species can then be detected and quantitated with an optical emission spectrometer (OES), which measures the intensity of radiation emitted at the element-specific, characteristic wavelength from thermally excited analyte atoms or ions. Intensity measurements are converted to elemental concentration by comparison with calibration standards. The device used is ACTIVA spectrophotometer by Horiba JOBIN YVON.

VI.4. Transmission Electronic Microscopy (TEM)

Transmission electron microscopy (TEM) is a technique which allow the direct observation of metal particles. The size distribution of these particles can be established as well as the dispersion of the metal can be calculated. TEM images are obtained on a JEOL 2010 LaB₆ microscope operating at 200 kV. The resolution of electronic microscopy is much higher than the optical ones due to the very short De Broglie wavelength of electrons (resolution of 0.19 nm in Jeol 2010 microscopy).

Sample preparation involves grinding of the material in ethanol in a mortar and depositing a drop of the suspension on a Cu TEM holey carbon grid for samples with no copper, whereas for the latter Ti TEM holey carbon grids were used. In case of the supported catalyst, this procedure allows for a very thin layer of the sample to deposit on the grid, avoiding overlap between the catalyst particles and making it easier to image the metal particles on the support.

A picture and scheme of the TEM equipment is showed in Figure 2-8. An electron beam is

emitted by an electron gun containing an emission source (LaB₆ single crystal in JEOL 2010) connected to a high voltage source (200 Kv in JEOL 2010) under vacuum. The beam is converged by the different electromagnetic lenses of the TEM, typically the condenser, objective and projector lenses. The condenser lenses are responsible for primary beam formation and focus the beam on the sample. When passing through the sample, electrons are scattered due to collisions with the atoms in the sample and the beam is focused by the objective lenses to form the image of the sample. The projector lenses magnify the image and project them on an imaging device (a CCD camera in the case of JEOL 2010). The images are then recorded using Digital Micrograph software.

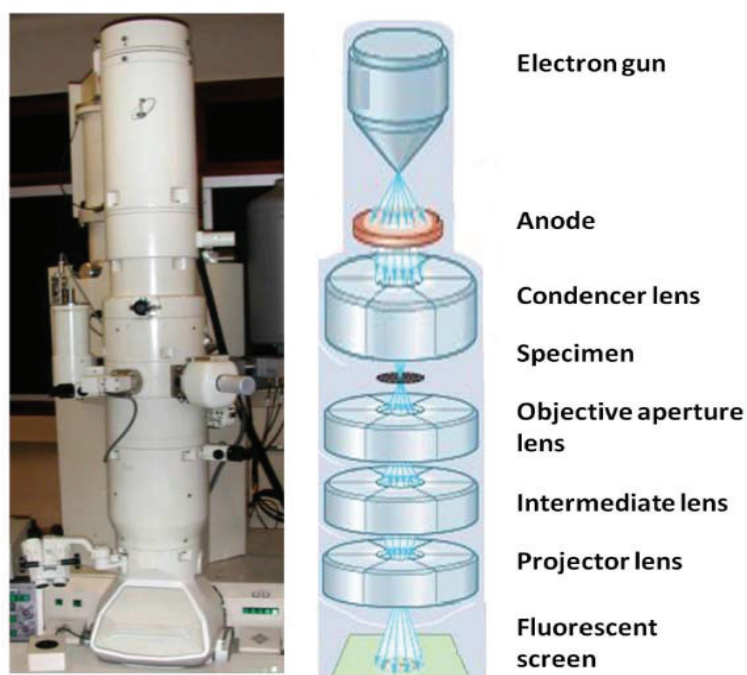


Figure 2-8 Photo (left) and scheme (right) of JEOL-2010 TEM apparatus.

The resolution of the TEM is determined by the speed and wavelength of the electrons. The magnification of the TEM is determined by the ratio of the distances between the specimen and the image plane of the objective lens; the contrast is due to the absorption of electrons by the solid depending on the thickness and composition of the material. JEOL 2010 can also operate under high resolution (HRTEM) mode for direct imaging of the atomic structure of the sample. In this mode, the image formation is based on a different principle than conventional ones.

In this work, microscopy has been mainly used for the characterization of the particular

structure of the ZnO and ZnAl₂O₄ before adding copper. Moreover, TEM images have been used to evaluate particle size distribution, using Image J software.

VI.4.1. Energy Dispersive X-Ray Spectroscopy (EDX) measurement

JEOL 2010 microscope is equipped with an EDX Link ISIS analyzer (Oxford Instruments). It is possible to identify the elements present in the sample by performing EDX. When the electron beam passes through the sample, X-rays are generated and emitted from the sample. X-rays escaping from the sample can be detected and measured from the characteristic spectrum of each element. In addition, the number of photons emitted is proportional to the mass concentration of this species.

Hence, EDX can provide precise constitution of a part of the sample at the nanometer scale. The aim of this technic is to locate, when it's possible, the position of the different elements.

VI.5. **Thermogravimetric analysis (TGA)**

Thermogravimetric Analysis (TGA) of materials is commonly used to provide information on the weight loss as a sample is heated or held isothermally under different gases. The apparatus used for this study was TGA/DSC 1 thermal analysis MX1 from Mettler Toledo, Stare system, gas controller GC200. Few milligrams of the sample are weighed inside an alumina crucible following this method:

- 5°C.min⁻¹ heating rate till 700°C, under an air flow of 50 mL.min⁻¹ for ZnO and ZnAl₂O₄
- 5°C.min⁻¹ heating rate till 1000°C, under argon flow of 50 mL.min⁻¹ for the reduced and used catalyst.

The decomposition of the material (ZnO and ZnAl₂O₄) is then determined by the weight loss during the heating. As the solvent is water the first loss is at 100°C and later the organic compounds start decomposing between 300°C and 400°C. The percentage of the inorganic material at the end of the process lead to the final composition of the product between: solvent, organic and inorganic species. For the catalyst the TGA was used to check if there's any difference in term of mass for the catalyst before and after the catalytic test.

VI.6. Chromatographic analysis

The gas chromatography (GC) is based on the interaction of a sample with a stationary phase located inside a capillary column and the detection of the separated components by a detector. There are a lot of different detectors and one of the most common is the flame ionization detector (FID). FID detects the presence of a molecule by the formation of charged species in a hydrogen flame by the variation of the flame potential. This charged species are created when one component from the sample reaches the detector. GC can be easily used for quantitative analysis by the introduction of an internal standard. The internal standard is very important due to the different response factor of different analytes and also because the injection can lead to different amount of sample introduced in the capillary column. The internal standard is used to give a relative response factor and, then, through a calibration curve recover the sample quantitative composition.

The identification of the products by gas chromatography was done by their characteristic retention time in the developed method. The retention times were determined by the injection of a sample containing the desired analyte. The response factors were obtained with a calibration curve with standard reactants and products. The calibration curve gives the relationship between the concentration of standards and the respective ratio of their peak area corrected by the internal standard area. The correction of the analyte signal area is performed because the amount of sample that enters the capillary column can be different for several reasons. The internal standard is an inert compound that is present in all samples in a known concentration. The peak area is linearly proportional to the product amount enabling the calculation of conversion following this equation:

$$A = K.C$$

A: Area of the compound at a given molar concentration

K: Correlation coefficient of the compound

C: molar concentration of the compound (mol.L⁻¹)

After the hydrogenolysis of glycerol, the 1,2-PDO formation was measured using a Shimadzu GC-2010 system equipped with a flame ionization detector and an autosampler AOC-20i. A Phenomenex FFAP 30 x 0.25 μm is used for the separation of products. The

carrier gas is N₂, the injector and detector temperature are 250 °C and 300 °C respectively. 1,4-Butan-diol was chosen as internal standard for this reaction and a list of the possible products was calibrated (Appendix 1-11). Their retention time is shown in the table below.

Table 2-7: Possible products of hydrogenolysis of glycerol and their retention time

Products	Formula	M.W. (g.mol ⁻¹)	Retention time (min)
Glycerol	C ₃ H ₈ O ₃	92.08	22.8
1.2 PDO	C ₃ H ₈ O ₂	76.09	15.2
1.3 PDO	C ₃ H ₈ O ₂	76.09	17.5
Lactic acid	C ₃ H ₆ O ₃	90.07	21.7
Ethylen glycol	C ₂ H ₆ O ₂	62.06	15.8
n-butanol	C ₄ H ₁₀ O	74.12	8.7
Acetol	C ₃ H ₆ O ₂	74.07	11
EtOH	C ₂ H ₅ OH	46.07	4.4
MeOH	CH ₃ OH	32.04	3.9
1.4 BDO	C ₄ H ₁₀ O ₂	90.12	18.9
2-propanol	C ₃ H ₈ O	60.10	4.3

The conversion and the selectivity were calculated based on these equations:

$$Conv_t(\%) = \frac{C_0^{substrate} - C_t^{substrate}}{C_0^{substrate}} \times 100$$

With :

- C₀^{substrate} : Initial concentration of substrate (in mol.L⁻¹);
- C_t^{substrate} : Concentration of substrate at time t (in mol.L⁻¹).

The carbon selectivity S_t^i to a desired product was calculated according to equation (5):

$$S_t^i(\%) = \frac{C_t^{\text{product } i} \times N_C^{\text{product } i}}{(C_0^{\text{substrate}} - C_t^{\text{substrate}}) \times N_C^{\text{substrate}}} \times 100 \quad (5)$$

With

- $C_t^{\text{product } i}$: Concentration of product i at time t (in mol.L⁻¹);
- $N_C^{\text{product } i}$: Number of carbon atoms in the product i;
- $N_C^{\text{substrate}}$: Number of carbon atoms in the substrate.

CHAPTER III

ZnO-PAAX: study of synthesis parameters

Table of contents

CHAPTER III	98
I. Effect of the synthesis parameters on ZnO-PAAX.....	99
I.1. Effect of the molecular weight of PAAH	99
I.2. Effect of the washing process after hydrolysis.....	110
I.2.1. ZnO-PAA2 system	111
I.2.2. ZnO-PAA5 system	114
I.3. Effect of PAA2 concentration during synthesis.....	116
I.4. Effect of the synthesis temperature	121
I.4.1. Effect of the synthesis temperature on ZnO-PAA2	121
I.4.2. Effect of the synthesis temperature on ZnO-PAA5	123
I.5. Effect of calcination temperature after synthesis.....	128
I.5.1. Effect of calcination temperature on ZnO-PAA2	128
I.5.2. Effect of calcination temperature on ZnO-PAA5.....	133
II. Conclusion	136
III. References.....	137

As mentioned in Chapter I, ZnO nanoparticles can be synthesized using different approaches and the surface can be modified with many types of additives. The method chosen in our study is sol-gel with the addition of polyacrylic acid (PAAH) as a modifying agent during the synthesis of ZnO-PAAH hybrid systems as described in our publication ¹. The hydrolysis of diethyl zinc in an aqueous PAAH solution is following the reaction below:



Previous works done in our laboratory demonstrated that such ZnO-PAAH hybrid systems may have original spherical self-assembly structures, depending on the nature and the concentration of the polyacrylic polymer, that could be used as efficient nano-luminophors for LED applications ¹. The starting point of this PhD project was to evaluate the interest of such system as support for copper-based catalyst for glycerol hydrogenolysis.

One of the first aim of this study was to find synthesis conditions that allow a control of the specific surface area of the final ZnO-PAAH support and in particular to obtain high values in order to disperse Cu⁰ effectively. Several parameters were studied such as the molecular weight and the concentration of the polymer, the washing and the drying phase and the synthesis temperature. We have also studied the thermal behaviour of ZnO-PAAH hybrid supports to evaluate the evolution of their characteristics after calcination. Another important parameter that we focused on was the reproducibility of these syntheses.

I. Effect of the synthesis parameters on ZnO-PAAX

I.1. Effect of the molecular weight of PAAH

The samples will be labelled "ZnO-PAAX", where X denotes the molecular weight of the polymer (X = 1.8 for PAA with Mw = 1 800 g.mol⁻¹, 2 for PAA with Mw = 2 000 g.mol⁻¹, 5 for PAA with Mw = 5 000 g.mol⁻¹ and 100 for PAA with Mw = 100 000 g.mol⁻¹). ZnO without PAAX will be used as a reference.

First, it should be noted that the synthetic yields compared to zinc moles are a function of the molecular weight of the PAAH (under the same operating conditions) with the particularity of being quantitative without PAAH and with PAA1.8, of being greater than 100% with PAA2 and PAA100 and of being only 50% with PAA5. For this latter, the centrifugation step only allowed to precipitate half of the solid, the rest remaining in suspension in water. The materials

characterized in the following section are those resulting from centrifugation and rinsing. A study on the stable suspension obtained for PAA5 will also be discussed at the end of this sub-chapter.

X-ray powder diffractograms (XRD) for hybrid ZnO-PAAX nanoparticles synthesized by sol-gel method at room temperature with different PAAX ($X = 1.8, 2, 5, 100$) at a concentration of 0.63 mol.l^{-1} are shown in Figure 3-1. XRD patterns showed either amorphous ZnO, crystallized ZnO (hexagonal phase: zincite, PDF 01-083-6338 and Appendix 1) or Zn(OH)_2 (orthorhombic phase: wulffingite PDF 04-012-2300 and Appendix 2). Average crystallite sizes were calculated using the Debye-Scherrer equation on the diffrac.eva software with peaks at $47.5, 57$ and 63° . Well-crystallised ZnO with average crystallite sizes of 16 or 11 nm were obtained for ZnO without PAAX and ZnO-PAA1.8 respectively (Figure 3-1 a, b). Moreover, diffraction peaks exhibited similar relative intensity between the two samples, hence there was no significant effect of PAA1.8 on the crystallinity of the material.

On the other hand, the use of PAA2 (Figure 3-1 c) led to a mixture of a poorly crystalline zincite phase with an average crystallite size of 19 nm calculated with the peaks at $47.5, 57$ and 63° and an unidentified phase with two peaks at 33 and 59° . ZnO-PAA5 exhibited mainly an amorphous ZnO structure and again the unidentified phase with two broad peaks at 33 and 59° (Figure 3-1 d).

A well-crystallized mixture of ZnO and Zn(OH)_2 was observed when PAA100 was added to the solution with an average crystallite size of 12 nm for ZnO calculated with the peaks at $32, 35$ and 63° and 30 nm for Zn(OH)_2 calculated with the peaks at 41 and 53° (Figure 3-1 e). In this last case, it was hard to know whether ZnO was transforming into Zn(OH)_2 or if Zn(OH)_2 was obtained first by the hydrolysis step of ZnEt_2 followed by a condensation. The second proposal seemed more likely with the presence of such a long polymer chain that partially blocked the further dehydration of Zn(OH)_2 especially when the synthesis was done at room temperature. The XRD results have shown that all the crystallized samples had similar crystallite average size but the main difference was the crystallinity of the samples and the appearance of Zn(OH)_2 with PAA100.

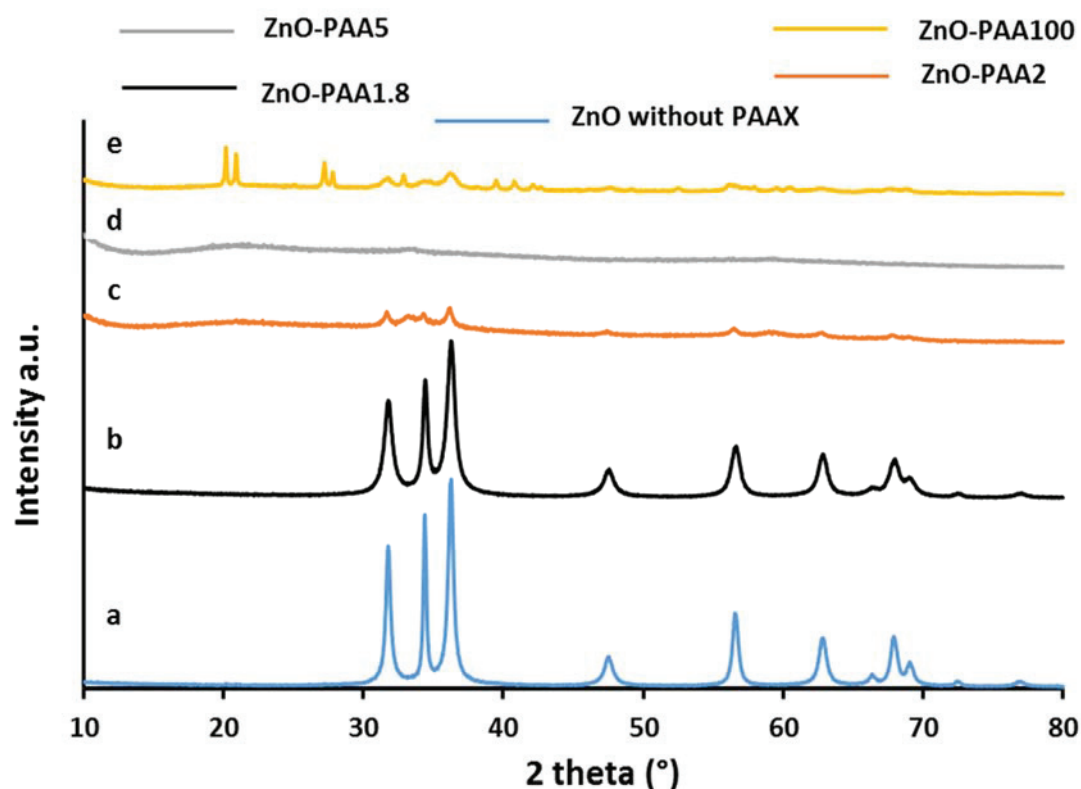


Figure 3-1: XRD diffraction patterns of (a) ZnO without PAA, (b) ZnO-PAA1.8, (c) ZnO-PAA2, (d) ZnO-PAA5 and (e) ZnO-PAA100

TEM analysis of the five samples were conducted and representative images are shown in Figure 3-2. The morphologies and particle size changed drastically as the molecular weight of the polymer changed. ZnO without PAA (Figure 3-2 a) and ZnO-PAA1.8 (Figure 3-2 b) had similar morphologies with nanoparticles of indefinite forms below 30 nm, in agreement with the XRD data. These results proved once again that adding PAA1.8 did not have a significant influence on the synthesis and morphology of ZnO nanoparticles. Increasing the molecular weight to 2 000 and 5 000 $\text{g}\cdot\text{mol}^{-1}$ gave self-assembled spherical aggregates of ZnO nanoparticles (Figure 3-2 c and Figure 3-2 d) of size in ranges of 150-200 nm and 50-100 nm, respectively. The molecular weight of the polymer seemed to have an impact on the size of the self-assembled aggregates but we did not know whether this could be attributed to lower size of the ZnO crystallites. At a larger scale, ZnO-PAA2 and ZnO-PAA5 showed a combination of two morphologies spherical particles and 2D nano-sheets; moreover some particles agglomerated had higher particle size in Figure 3-3 proving that the two materials were not so homogeneous.

Finally, ZnO-PAA100 (Figure 3-3 e) exhibited two morphologies: irregular platelets and spherical aggregates of different sizes between 10 and 50 nm, which could be related to the presence of two phases as seen in XRD.

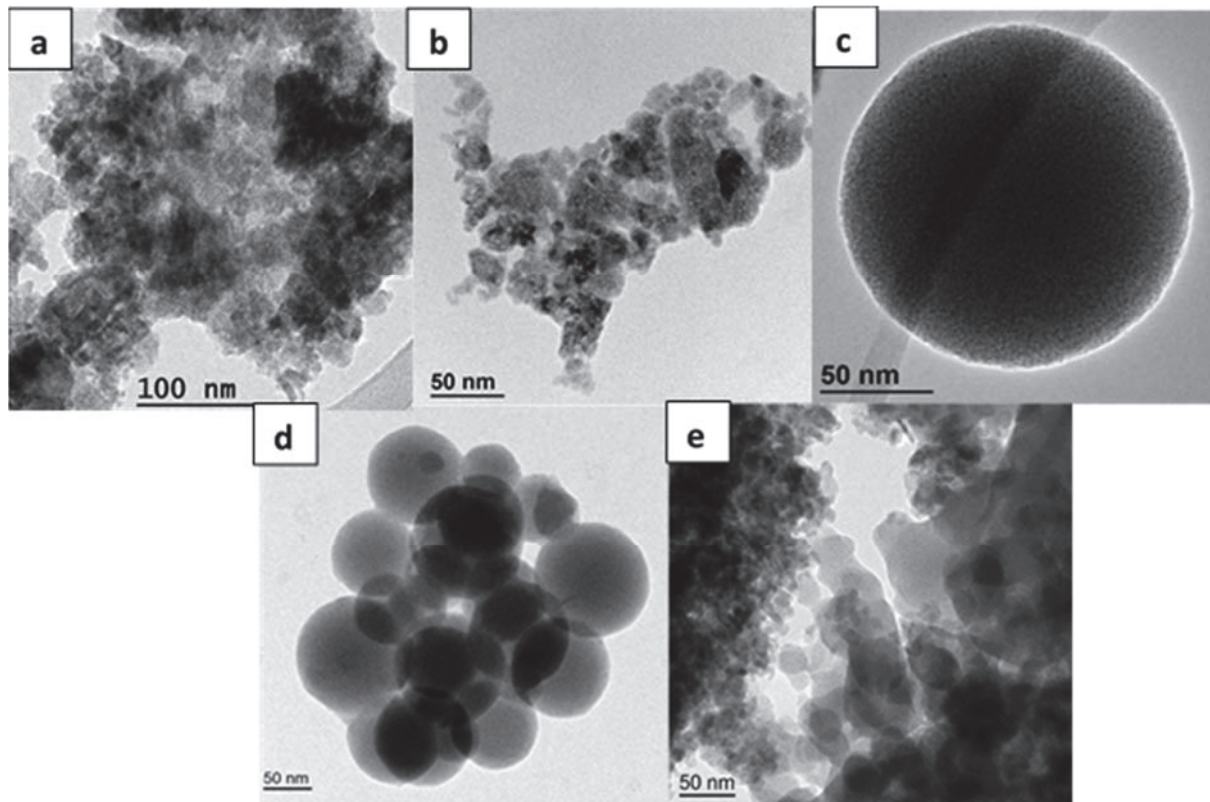


Figure 3-2: TEM images of: a) ZnO without PAA, b) ZnO-PAA1.8, c) ZnO-PAA2, d) ZnO-PAA5 and e) ZnO-PAA100

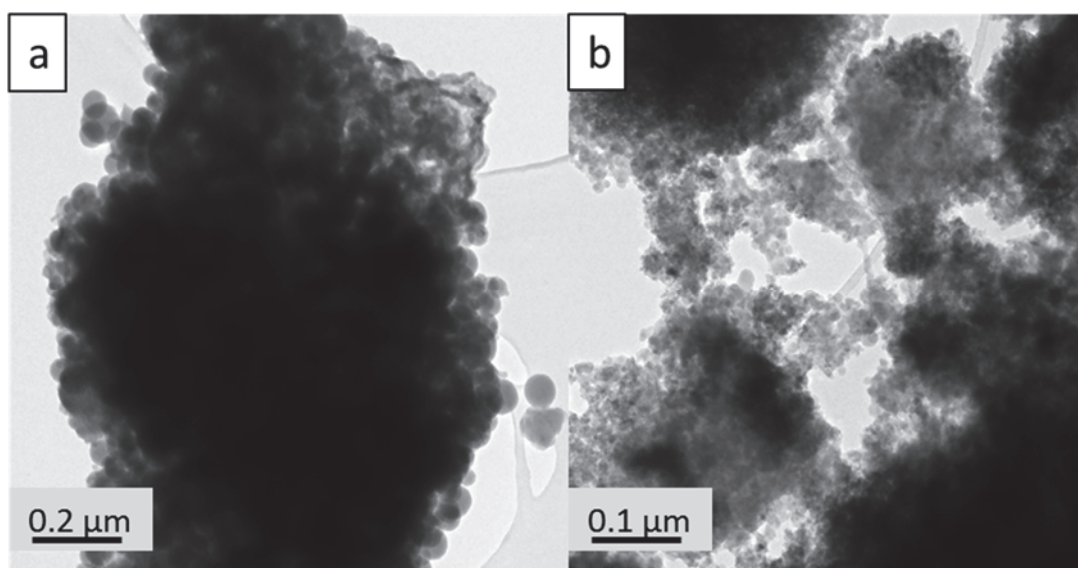


Figure 3-3: TEM images of a) ZnO-PAA2 and b) ZnO-PAA5 at large scale

TG analyses, carried out under air till 700 °C at a rate of 5 °C.min⁻¹, demonstrated that polyacrylic acid was present for all the sample but in different quantities (Figure 3-4). In theory, if all the polymer was integrated into the hybrid system, we should have a weight loss of about 46% above 200 °C. This value was very close to the ones for the samples obtained with PAA2 and PAA5 while for PAA100 and in particular PAA1.8, this one was quite far. Indeed, ZnO-PAA2 and ZnO-PAA5 showed weight loss of 40% and 41% above 200 °C, respectively, while ZnO-PAA100 exhibited a weight loss of 30%. ZnO-PAA1.8 displayed a low organic weight loss indicating that a very small amount of PAA1.8 was in interaction with ZnO NPs (Figure 3-4). The comparison between the TGA spectra of pure polymers (Figure 3-5) and hybrid materials (Figure 3-4) showed that these latter were more thermally robust because the temperatures onset of weight loss were much higher (320 °C instead of 200 °C). Evaporation of water/solvent occurred below 200 °C and above 200 °C, TGA of the two pure polymers showed several weight losses corresponding to their pyrolysis. While degradation was complete at 500 °C for PAA2, 20 wt% of residue were still present for PAA5 and the total degradation occurred at temperature higher than 800 °C. The remaining 5 wt% was found as black carbon residue in the crucible.

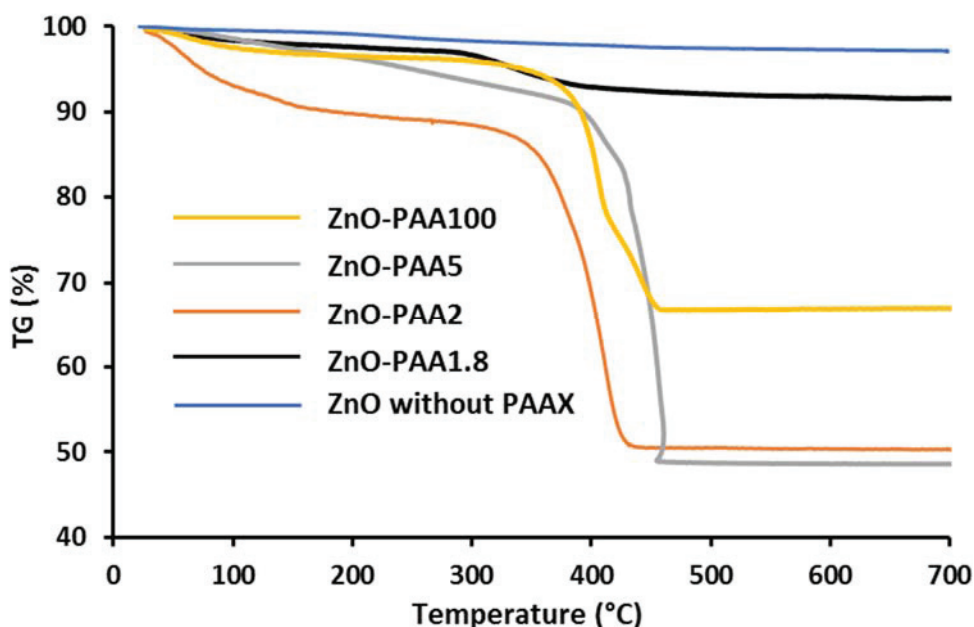


Figure 3-4: TGA curves for the different ZnO-PAAX

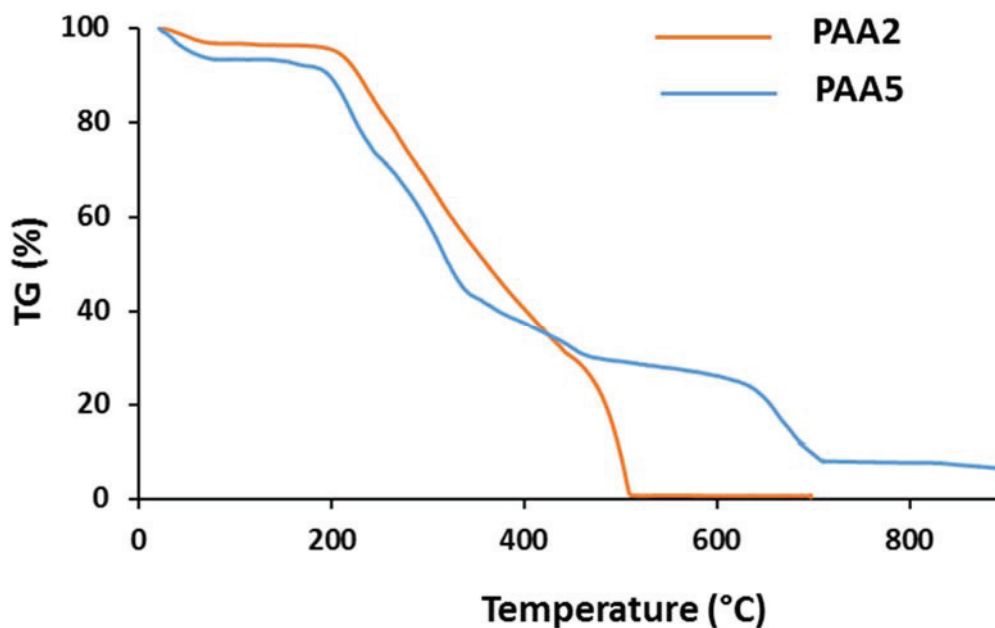


Figure 3-5: TGA curves of pure PAA2 and PAA5

The FTIR spectra of the samples (Figure 3-6) showed that polyacrylic acid was mainly present as polyacrylate confirming the presence of Class II hybrid systems (in sol-gel classification) and a strong interaction (via a deprotonation reaction) of the polymer on the surface of the ZnO nanoparticles. It should be noted that the use of polyacrylate ester (PAAME) instead of polyacrylic acid during synthesis led to ZnO without any organic content and confirmed the lack of interaction between the ester and the surface of ZnO. In the case of polyacrylic acid, this interaction was strong and resulted in a very different flocculation phenomenon depending on its molecular weight. One possible explanation would be that partial deprotonation of polyacrylic acid led to hydrophobic systems, which could be noted as ZnO-(PAAH)_x-(PAA)_y, which precipitated in aqueous solution as self-assembled spherical hybrid nano-objects. These objects would only be obtained if the final hydrophobic/hydrophilic balance was appropriate, which would not be the case for a polymer that it was too short or too long.

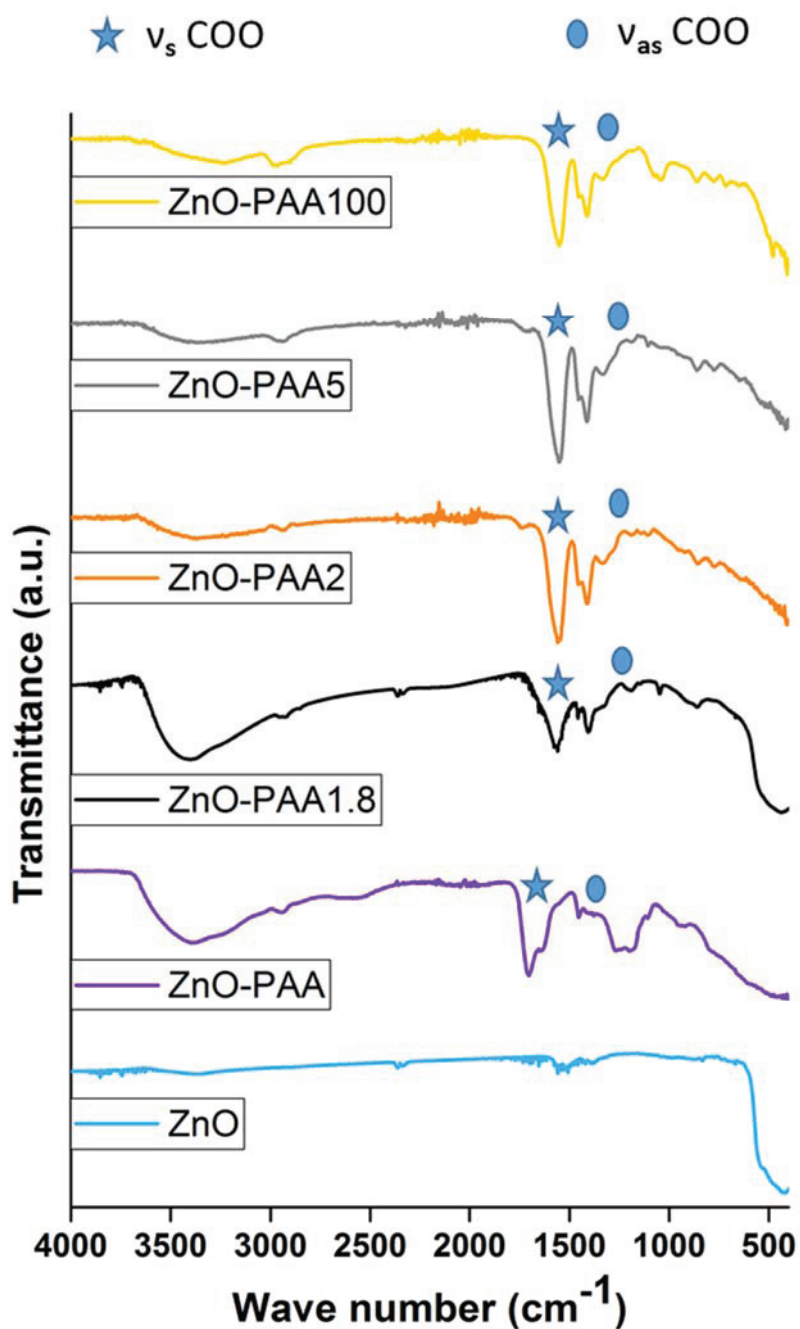


Figure 3-6: FTIR spectra for the different ZnO-PAA

The BET specific surface area were determined by N₂ adsorption analysis (the values are given with an uncertainty of 5%). The values reported in Table 3-1 showed that the largest specific surface area of 50 m².g⁻¹ was obtained with ZnO-PAA100. ZnO-PAA2 and ZnO-PAA5 had similar values around 20 m².g⁻¹. ZnO without PAA and ZnO-PAA1.8 had similar specific surface area of around 40 m².g⁻¹. The main pore diameter of the three samples ZnO-PAA2, ZnO-PAA5 and

ZnO-PAA100 was around 4 nm proving that all the NPs were mesoporous (Appendix 3-5). No data has been published on the relationship between the specific surface area of ZnO and the length of PAAH, but related study such as S. Park et al. ², demonstrated that an increase in the chain (carbon or nitrogen) of the added fuel resulted in an increase in the specific surface area of the ZnO NPs: 27 m².g⁻¹ with urea as additive (CH₄N₂O), 32 m².g⁻¹ with carbohydrazide (CH₆N₄O) and 120 m².g⁻¹ with glycine (C₂H₅NO₂). The main characteristics of the ZnO-PAAX are compiled in Table 3-1.

Table 3-1: ZnO-PAAX characteristics.

Sample	S.S.A./ BET (m ² .g ⁻¹)	Pore diameter / BET (nm)	Crystallite size / XRD (nm)	Aggregate size / TEM (nm)	TGA weight loss [200-600 °C] (%)
ZnO without PAAH	43	--	16	20-30	2
ZnO-PAA1.8	38	--	11	15-25	5
ZnO-PAA2	20	3	19	150-200	40
ZnO-PAA5	23	4	Amorphous	50-100	41
ZnO-PAA100	50	3 -10	ZnO: 12 Zn(OH) ₂ : 30	10-50	30

The synthetic yield with PAA5 was only of 50%. In order to collect all the ZnO material during the synthesis of ZnO-PAA5, the aqueous suspension obtained after centrifugation was freeze-dried. The powder obtained was naturally less dense than the one obtained after drying. In addition, the XRD analysis of the lyophilized powder of ZnO-PAA5 (Figure 3-7) showed the two broad peaks at 33 and 59° associated with the unknown phase previously observed in Figure 3-1.

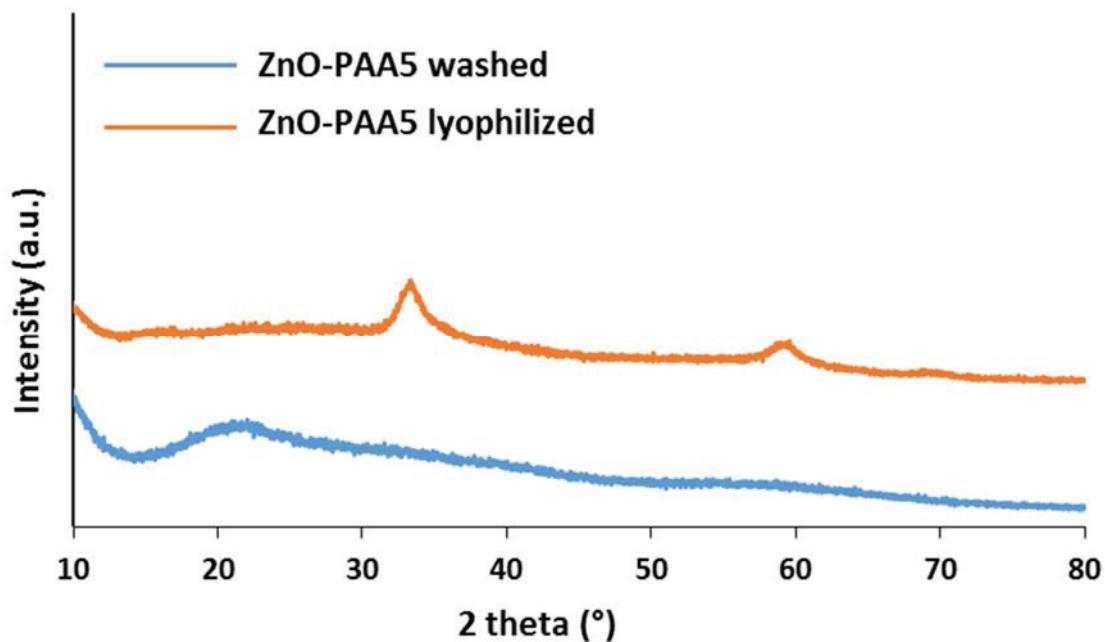


Figure 3-7: XRD diffraction patterns of ZnO-PAA5 dried after washing or lyophilized

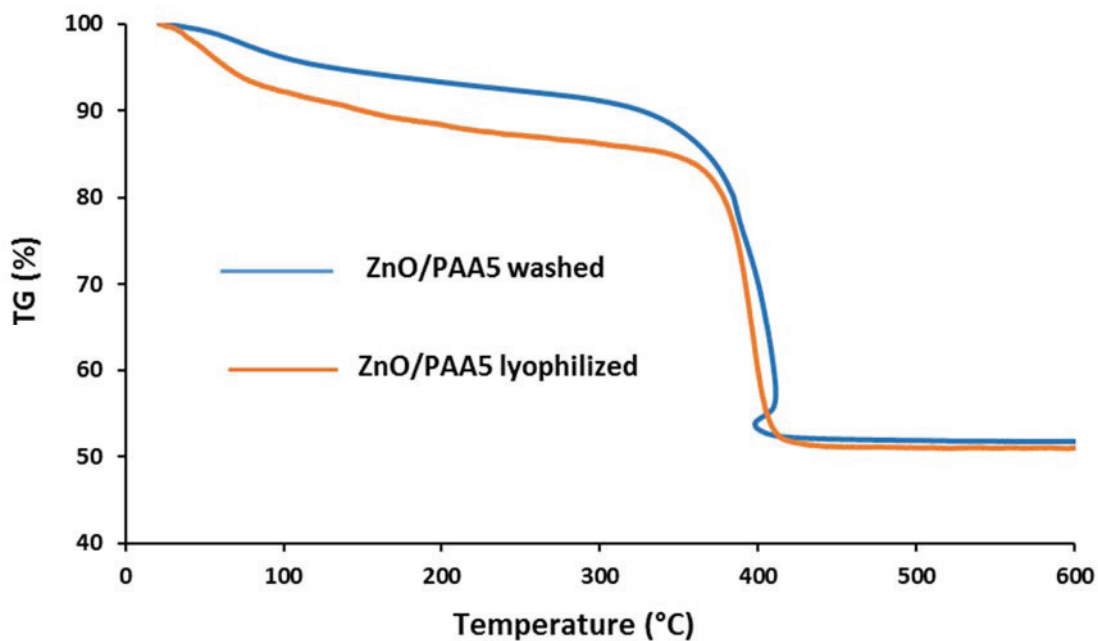


Figure 3-8: TGA curves of ZnO-PAA5 dried after washing or lyophilized

TGA of the two ZnO-PAA5 fractions (precipitate and suspension), either dried or freeze-dried, did not show any significant differences in terms of thermal stability (onset temperature of

degradation around 380 °C) and organic/inorganic ratio (about 50% of each). It could therefore be assumed that the two fractions were very similar in nature and composition.

Aqueous solutions of PAA2 and PAA5 polymers at the same concentration as those of the syntheses were freeze-dried and the powders obtained were studied by XRD. The data showed an amorphous structure with two broad peaks at 20 and 38° (Figure 3-9).

It seemed that the unknown phase found on some XRD spectra of ZnO-PAA2 and ZnO-PPA5 might come from a hybrid species Zn(OH)-PAAX. Indeed, on the EVA software, the two files Zn(OH)₂ (PDF 04-012-2300) and Zn₅(CO₃)₂(OH)₆ (PDF 04-036-1475, in appendix 6) were the ones that fit the most and two of the peaks fit those of the unknown phase.

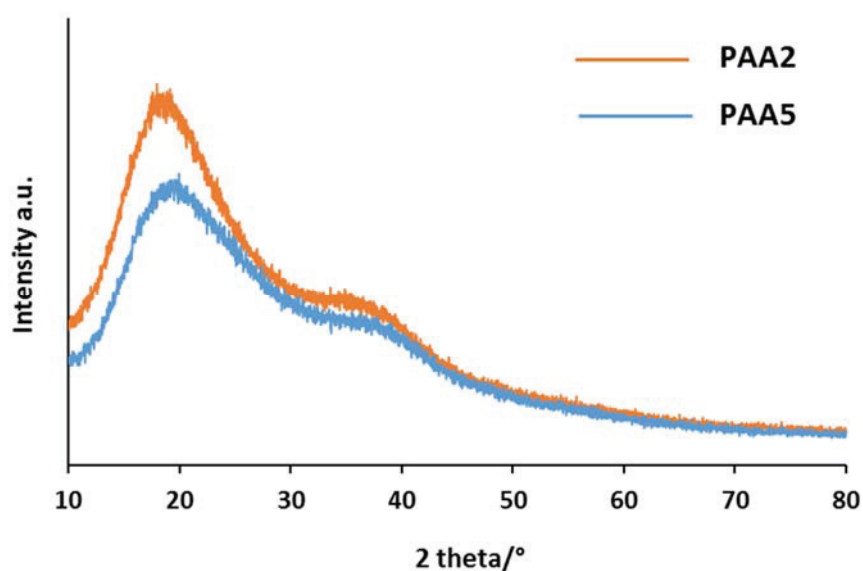


Figure 3-9: XRD diffraction patterns of PAA2 and PAA5

The BET analysis of the freeze-dried ZnO-PAA5 solid showed a smaller specific surface area of about 16 m².g⁻¹, compared to 23 m².g⁻¹ after washing. Moreover the images obtained by the TEM and SEM analyses showed few mesospheres and a continuous polymer film containing nanocrystallites smaller than 100 nm (Figure 3-10). This morphology was different from ZnO-PAA washed presented in Figure 3-2 d. At this stage of our study, we could assume that the unidentified phase present on XRD spectra could be associated with a 2D structure combining PAAH and nanoparticles of ZnO or Zn(OH)₂. Therefore, the drying mode was also an important parameter to consider when synthesizing the different ZnO-PAAX materials in order to generate materials with high specific surface area.

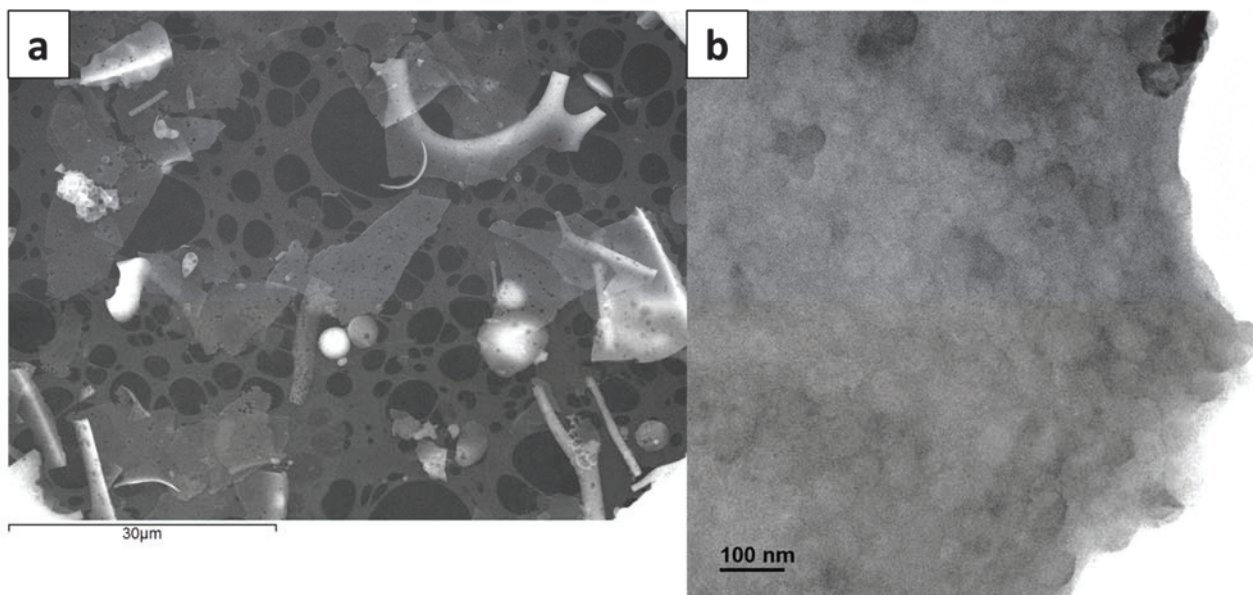


Figure 3-10: Images of ZnO-PAA5 after freeze-drying obtained by: a) SEM and b) TEM

The impact of freeze-drying on ZnO nanomaterials has already been mentioned in the literature for a synthesis of ZnO by reaction between zinc nitrate and sodium carbonate ³. After synthesis, the batch was separated into two parts; one part was dried in an oven at 110 °C and the other one was freeze-dried. The powders obtained were then calcined at different temperatures and the results are summarized in the table below:

Table 3-2: ZnO NPs properties after different treatments ³

Temperature (°C)	SSA (m ² g ⁻¹)	True Density (g.cm ⁻³)	Total pore volume (10 ⁻³ cm ³ g ⁻¹)	Average particle size (nm)	Average crystallite size by XRD(nm)
<i>Controlled drying</i>					
110	39.1	3.8	48	40	12
200	27.2	3.9	35	57	29
400	17.1	4.2	23	84	35
600	7.2	4.5	10	185	45
800	2.1	4.8	2	595	64
<i>Freeze drying</i>					
As-prepared	20.1	2.5	31	119	46
200	7.2	3.0	8	278	35
400	2.0	3.3	1	909	66
600	1.5	3.8	2	1051	82
800	1.0	5.0	2	1200	91

The results presented in this study were quite similar to those obtained for ZnO-PAA5. Freeze-drying was accompanied by a decrease in specific surface area associated with an increase in particle size (Figure 3-10). In the rest of our study, only conventional drying in an oven at 80 °C for 14 hours will be used.

The original spherical morphology of the 3D hybrids ZnO-PAA2 and ZnO-PAA5 nano-structured aggregates was further investigated to determine the synthesis parameters, such as washing/rinsing process, concentration of polymer and synthesis temperature, that would influence the final characteristics of these hybrid objects and in particular their specific surfaces that were sought to be maximized for use as supports for copper-based catalysts.

1.2. Effect of the washing process after hydrolysis

Washing steps are known to be an important step in the synthesis of hybrid nanoparticles as they can affect the specific surface area by removing organic matter that would not be effectively grafted onto the surface ⁴.

In a typical synthesis, after one hour of reaction, the ZnO-PAAX slurry was centrifuged to obtain a wet powder of ZnO-PAAX which was rinsed for a few minutes with a small amount of ethanol. Due to a lack of reproducibility of the structural characteristics (BET for instance from 20 to 40 m².g⁻¹), we decided to carry out different washing by using two solvents (water and/or ethanol) and different washing volumes. Wet samples were then washed with a specific volume of solvent (from 30 to 90 mL for an initial volume of 200 mL of PAAX solution) for 30 minutes under stirring. When the volumes of PAAX solution were higher, the volume of solvent was proportionally increased, as was the washing time. For all samples (unwashed and washed), a centrifugation step and oven drying at 80°C in ambient air were performed to obtain the final powder.

I.2.1. ZnO-PAA2 system

The ZnO-PAA2 samples obtained without washing or after washing with different volumes of ethanol (30 mL, 60 mL, 90 mL) or ethanol/water (60 mL) have shown very similar XRD diffractograms (Figure 3-11) and ATG curves (Figure 3-12). Only the intensity of the peak at 33° (unidentified phase) seemed to increase with the amount of ethanol. It would therefore be concluded that the washing step did not impact the crystallinity of the sample, the ZnO crystallite size, or the amount of organic matter (Table 3-3). The latter was predictable due to the insolubility of PAA2 in ethanol.

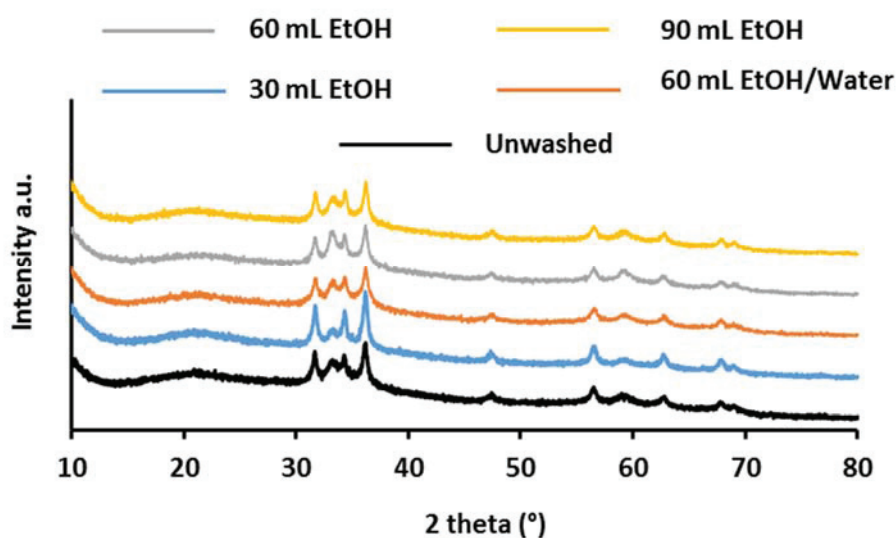


Figure 3-11: XRD patterns of ZnO-PAA2 using different washing

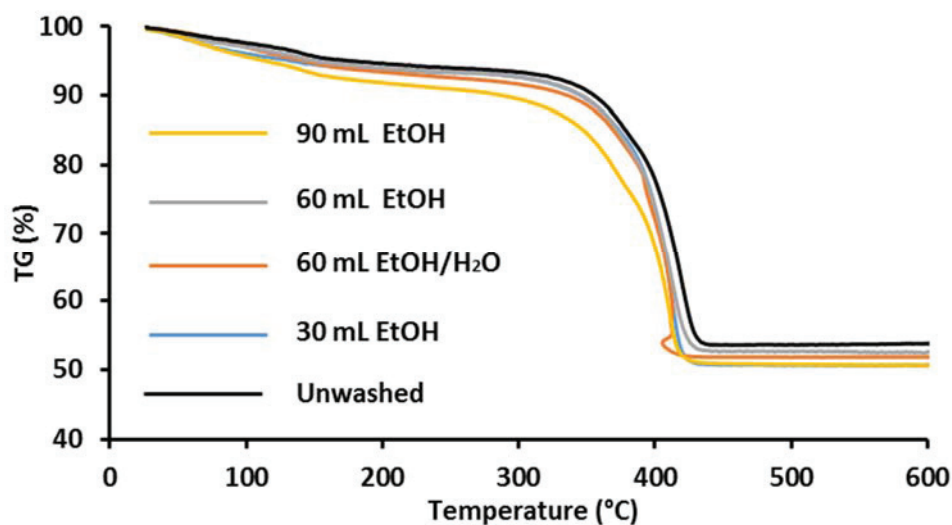


Figure 3-12: TGA curves of ZnO-PAA2 using different washing

Nevertheless, the BET and TEM results show that the samples were structurally different. Indeed, the BET results (Table 3-3) showed that washing with ethanol significantly increased the specific surface area of ZnO-PAA2 samples from 20 to 91 $\text{m}^2\cdot\text{g}^{-1}$, especially when the volume of ethanol was large. TEM images before and after washing with 90 mL of ethanol provided a possible explanation for this increase in specific surface area (Figure 3-13). These showed that ethanol washing induced the "appearance" of a larger quantity of 2D nano-sheet structures composed of zinc and polymer according to EDX.

If we combined all these data, we could consider that ethanol only removed water whose presence would result in folding these 2D structures onto themselves via hydrogen interactions, for example. The elimination of water would therefore make it possible to unfold these structures which would be at the origin of the increase in the specific surface area observed after washing. The presence of water when washing with a water/ethanol mixture (1:1) confirmed this effect with a lower specific surface area of 41 $\text{m}^2\cdot\text{g}^{-1}$.

Table 3-3: Effect of EtOH volume on ZnO-PAA2 NPs properties

Solvent volume (mL)	S.S.A. / BET (m ² .g ⁻¹)	ZnO crystallite size / XRD (nm)	TG / weight loss [200-600°C] (%)
Un-washed	20-40	19	40
30 EtOH	60	18	50
60 EtOH/H ₂ O (1:1)	41	16	51
60 EtOH	68	22	52
90 EtOH	91	20	50

Morphological changes in ZnO nanoparticles due to the ethanol/water ratio in a double solvent system were reported by Yin et al. in 2015⁵. The study showed that spherical ZnO was obtained without adding water while the addition of different volumes of water transformed the morphology into hexagonal discs with a low water content (2 mL) and micro rods with 8 mL of water.

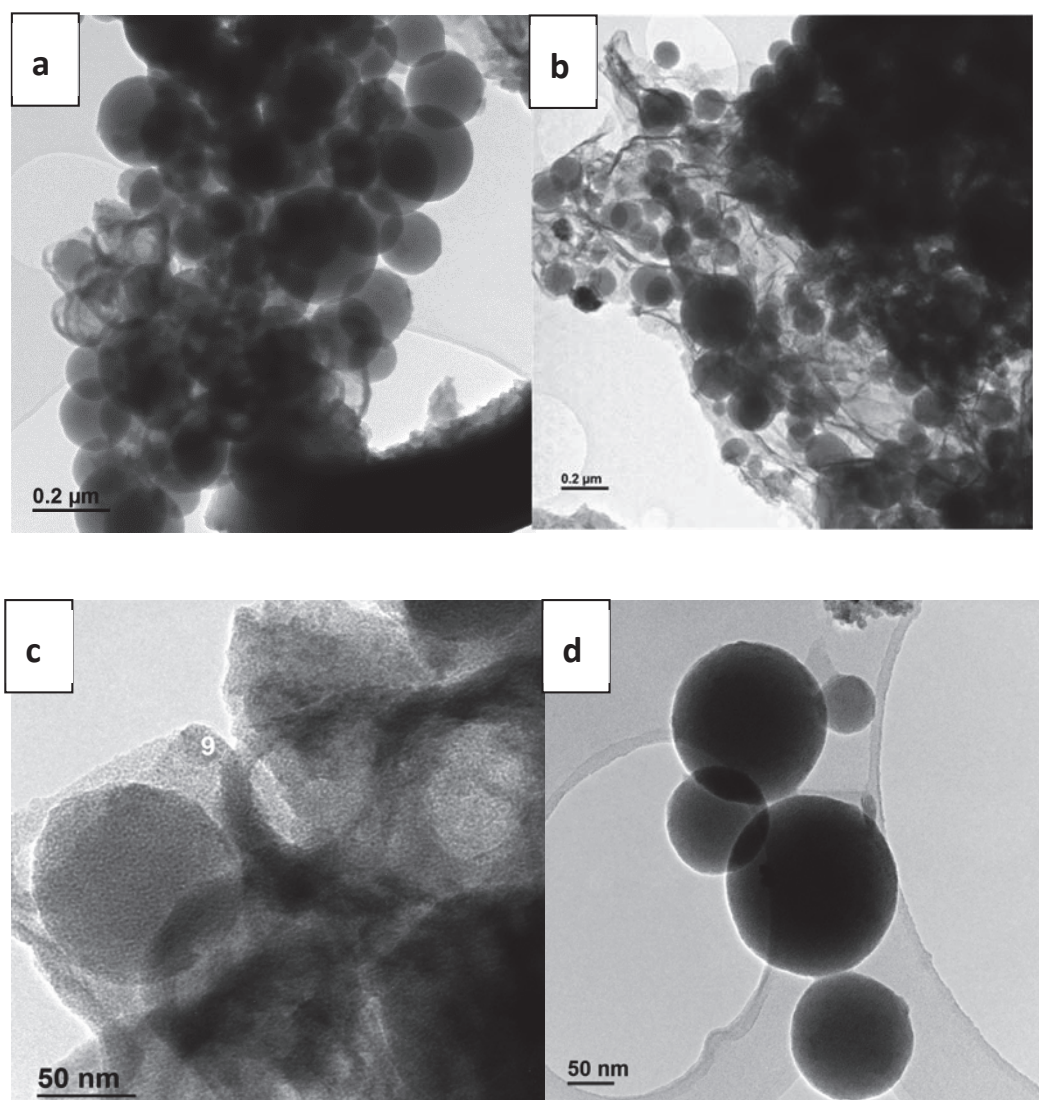


Figure 3-13: TEM images of ZnO-PAA2: a,c) unwashed and b,d) washed with 90 mL of EtOH

I.2.2. ZnO-PAA5 system

The effect of ethanol washing on the properties of ZnO nanoparticles was extended to ZnO-PAA5. As before, the XRD diffractograms showed no impact on the crystallinity of the material as shown in Figure 3-14. ZnO-PAA5 washed with different volumes of EtOH was amorphous like ZnO-PAA5 rinsed with EtOH (Figure 3-1 d). Similarly, the TGA also showed an average loss of 50% for the three volumes (Figure 3-15, Table 3-4) as for the ZnO-PAA2 samples (Table 3-3).

As for ZnO-PAA2, there was an increase in specific surface area with the increase in the volume of EtOH from 20 to 75 $\text{m}^2 \cdot \text{g}^{-1}$ (Table 3-4).

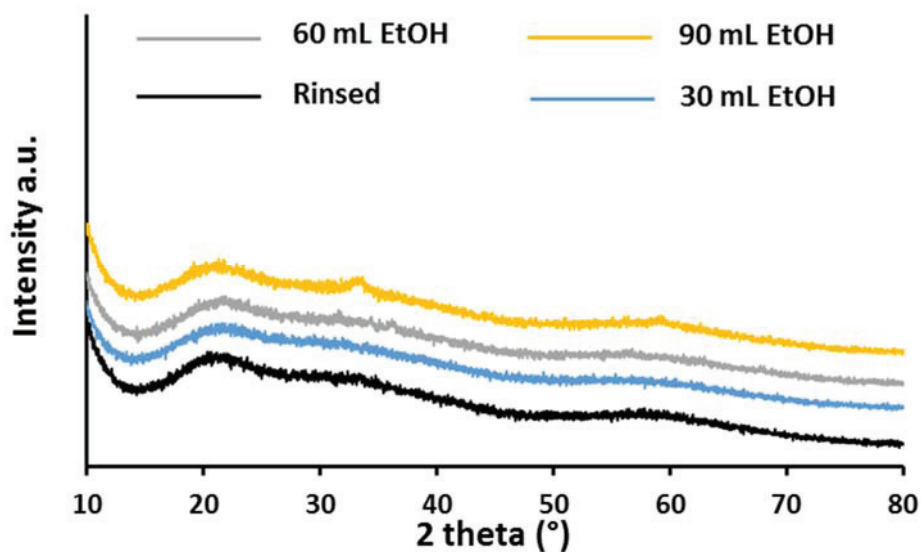


Figure 3-14: XRD diffraction patterns for ZnO-PAA5 washed with different volume of EtOH

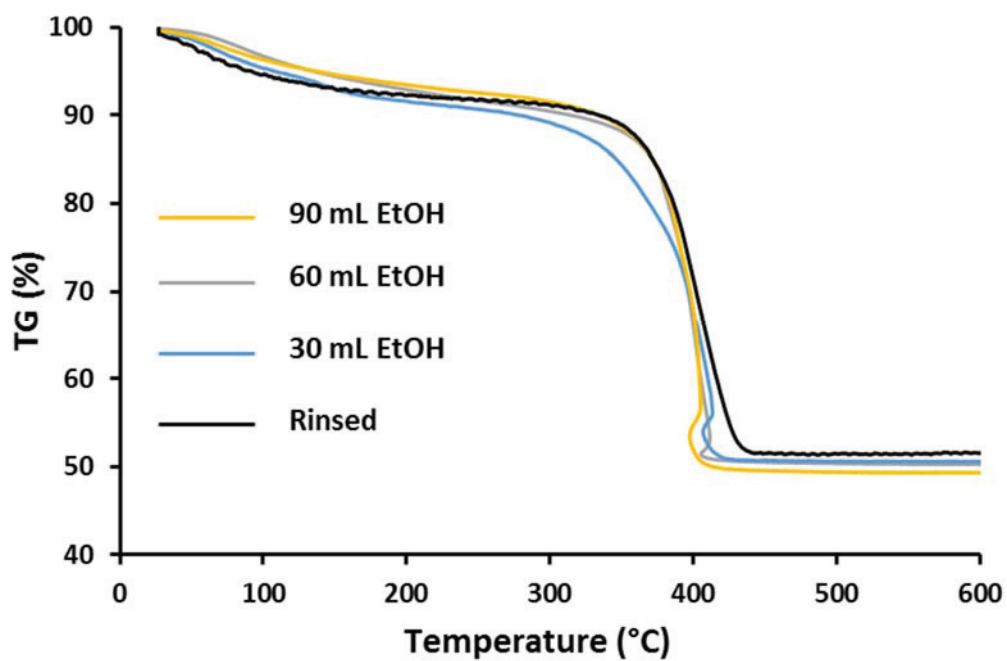


Figure 3-15: TGA curves for ZnO-PAA5 washed with different volume of EtOH

Table 3-4: Effect of EtOH volume on the properties of ZnO-PAA5 NPs

Solvent volume (mL)	S.S.A. / BET (m ² .g ⁻¹)	TG / weight loss [200-600°C] (%)
Rinsed	23	41
30 EtOH	53	42
60 EtOH	58	42
90 EtOH	75	44

In conclusion, as both materials, ZnO-PAA2 and ZnO-PAA5, have shown an improvement in their structural properties and in particular a larger specific surface area when washed with EtOH, all up-coming materials were washed with 90 mL EtOH when synthesizing 2 grams of ZnO-PAAX.

I.3. Effect of PAA2 concentration during synthesis

The length of the polymer chain having shown a significant impact on the morphology of the ZnO-PAA material, it was interesting to study the effect of the mass percentage of PAA2, only, during the synthesis on the material.

As mentioned in the experimental section, the polyacrylic acid solution used to produce the majority of ZnO-PAAX nanoparticles had a concentration of 0.63 wt% (the commercial solution having a concentration of 63wt%). Different PAA2 solutions were therefore prepared with concentrations ranging from 0.3 to 1.2 wt% and a synthesis without PAA2 was carried out as a reference.

As the washing step improved the properties of the material, all samples were washed with 90 mL EtOH. As shown in Figure 3-16, peaks of the unknown phase at 33° and 59° were present when PAA2 was added, compared to ZnO without PAA2. The increase in the weight percentage of PAA2 resulted in a decrease in the crystallinity of the material to a quasi-amorphous structure with 1.2 wt% of PAA2 (Figure 3-16).

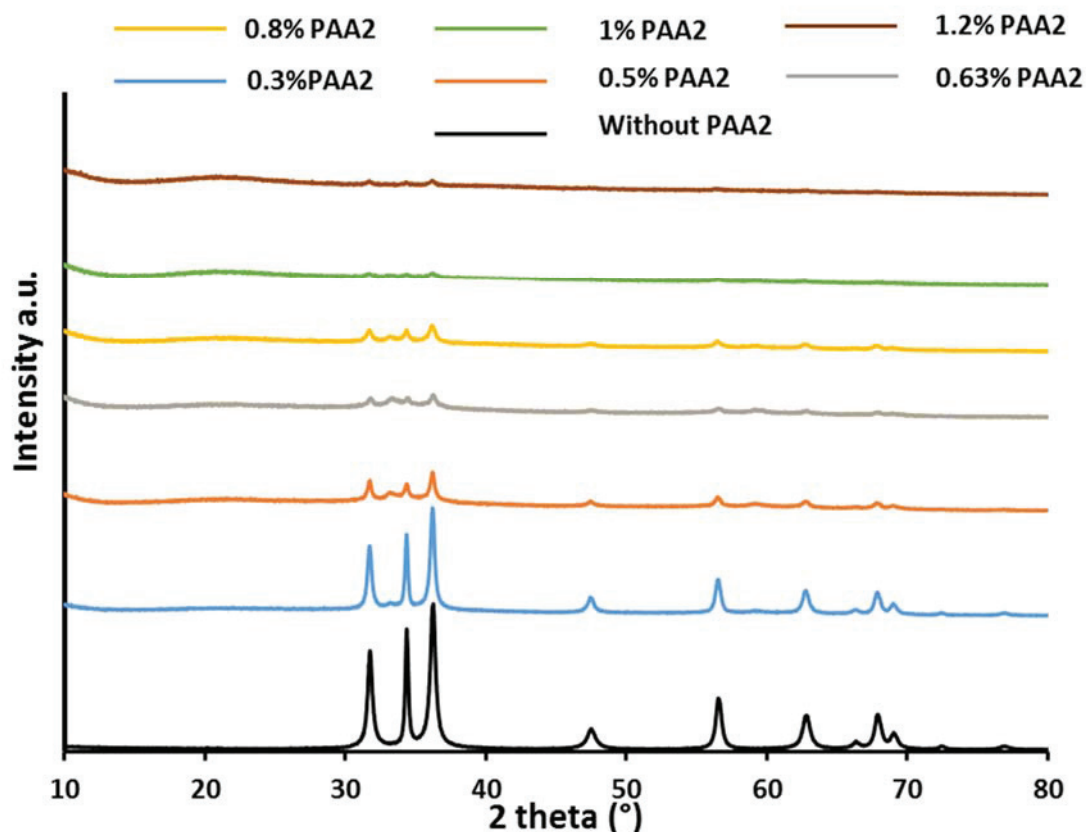


Figure 3-16: XRD diffraction patterns for ZnO-PAA2 synthesized with different weight percentage of PAA2

The BET specific surfaces are summarized in Table 3-5 and the values are plotted according to the weight percentage of PAA2 in Figure 3-17. The results showed that the increase in the specific surface area of ZnO-PAA2 hybrid NPs followed a Gaussian with a maximum around $75 \text{ m}^2 \cdot \text{g}^{-1}$ between 0.3 and 0.6 wt%. For higher PAA2 concentrations, the specific surface area decreased to $17 \text{ m}^2 \cdot \text{g}^{-1}$ for 1.2 wt%. TEM images for 0.3 wt% and 1.2 wt% of PAA2 (Figure 3-18) showed that a high initial concentration of PAA2 generated large aggregates in size with some mesospheres but no more 2D nano-structures such as nano-sheets.

The same behaviour was found in an article studying the effect of raw rice as a bio-model for the synthesis of ZnO by hydrothermal method using zinc acetate and sodium hydroxide as reactants⁶. The authors found that the increase in raw rice concentration led to an increase in the specific surface area of ZnO nanoparticles up to a maximum where it then decreased. Figure 3-19 shows the relationship between the specific surface area of ZnO nanoparticles and the rice concentration. They also observed a modification of the surface associated with a change in specific surface area of the nanoparticles when the additive concentration was

varied. Figure 3-20 shows the flake assembly structures obtained when no raw rice was added (a) compared to the rods and agglomerated particles of ZnO without specific form with high raw rice concentration (b).

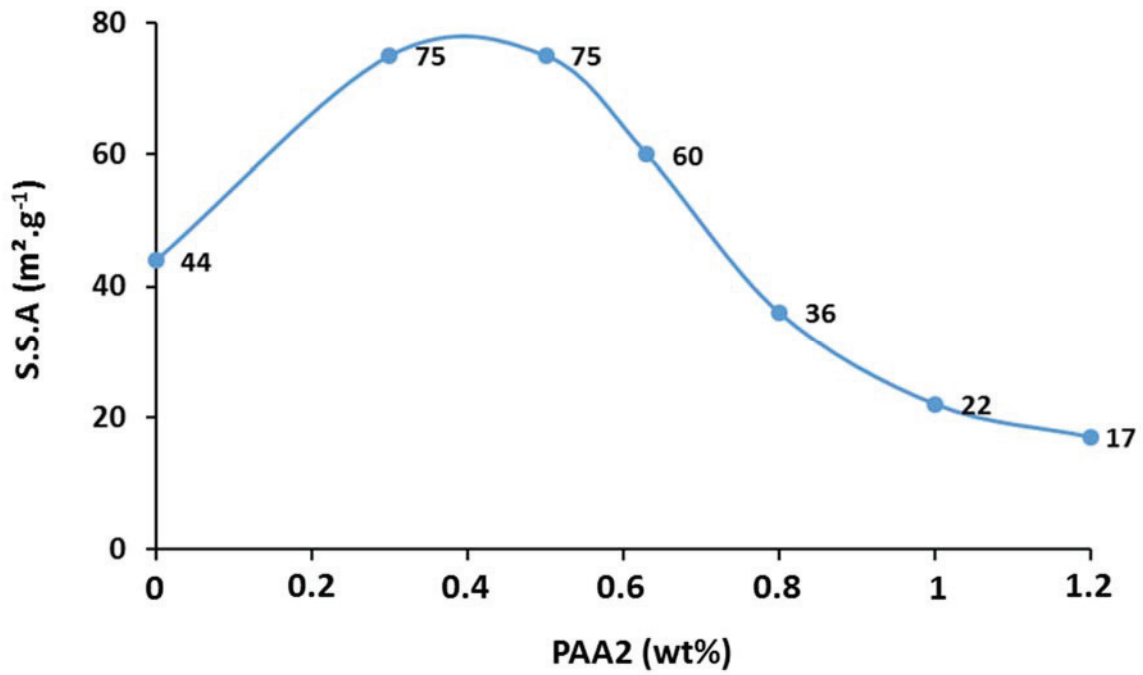


Figure 3-17: Relation between specific surface area and PAA2 weight percentage

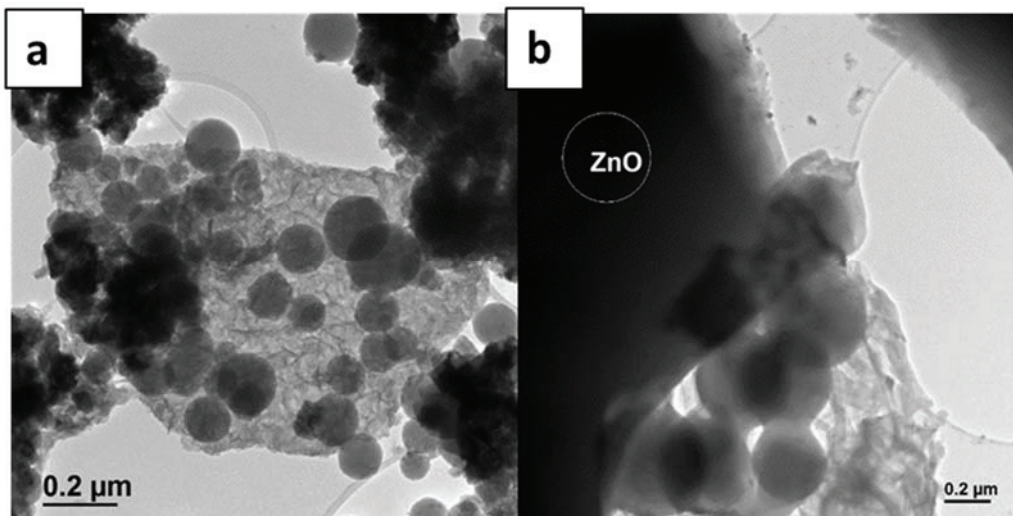


Figure 3-18: TEM images of ZnO-PAAX with: a) 0.3 wt% and b) 1.2 wt% of PAAH

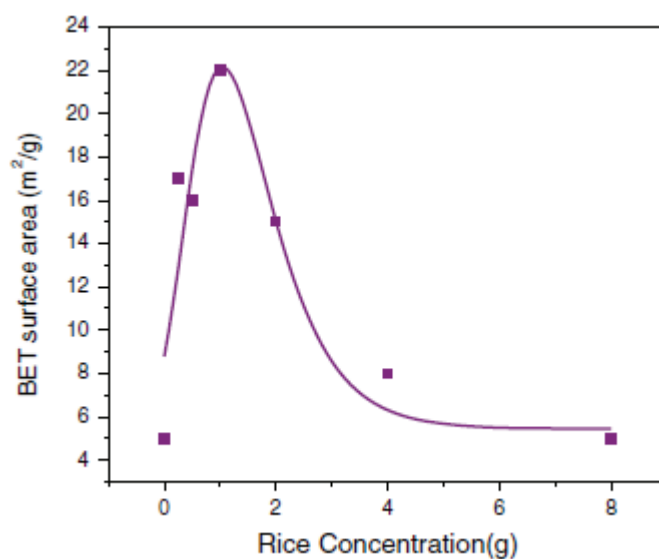


Figure 3-19: Relation between ZnO specific surface area and rice concentration ⁶

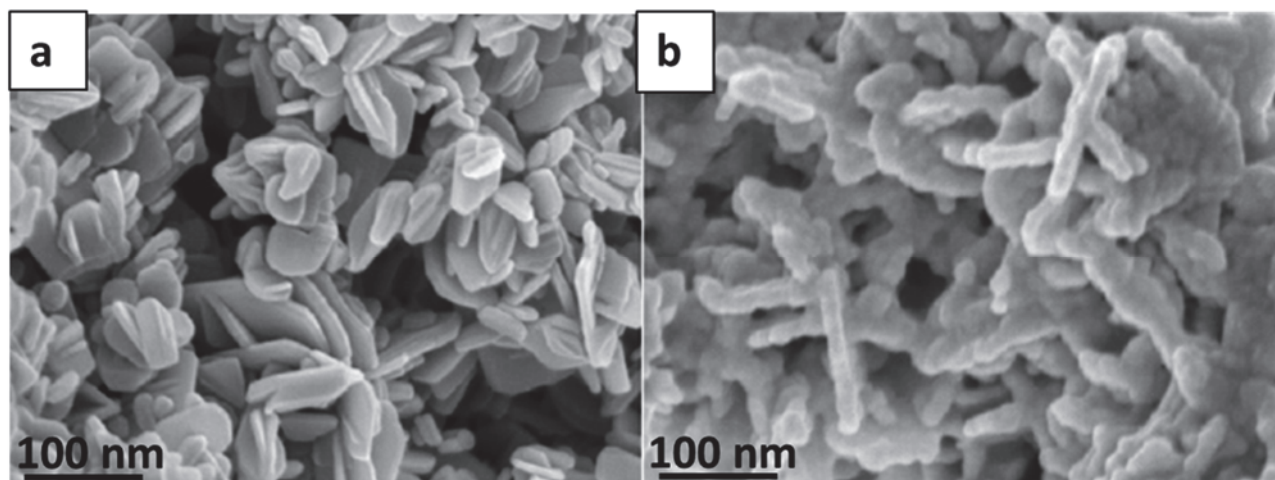


Figure 3-20: SEM images of ZnO prepared with a) 0 g of rice and b) 8 g of rice ⁶

The TGA curves under air (Figure 3-21) showed that weight losses between 200 and 600 °C (Table 3-5) were proportional to the weight percentage of PAA2 added initially. With 0.3 wt% of PAA2, the proportion of inorganic components was 67%, while it is only 39% for 1.2 wt% of PAA2.

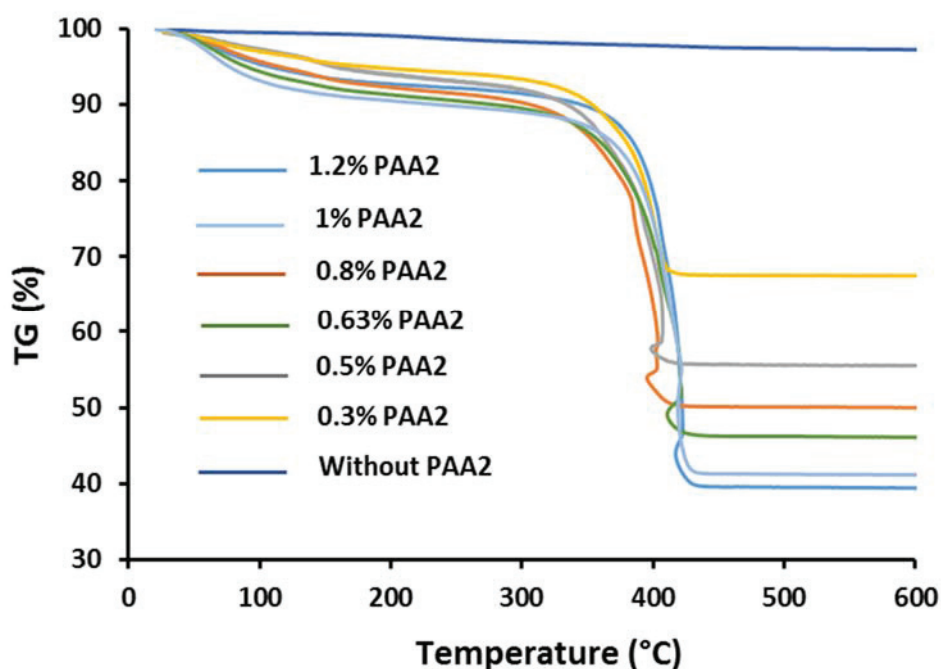


Figure 3-21: TGA curves for ZnO-PAA2 synthesized with different weight percentage of PAA2

Table 3-5: Effect of the weight percentage of PAA2 on the properties of ZnO NPs.

PAA2 (wt%)	S.S.A. BET ($\text{m}^2\cdot\text{g}^{-1}$)	ZnO crystallite size / XRD (nm)	Agregate size / TEM (nm)	TG / weight loss 200-600 (%)
0	44	16	20-30	3
0.30	75	18	100-150	33
0.50	75	19	X	45
0.63	60	19	X	50
0.80	36	13	X	54
1.00	22	17	X	59
1.20	17	Amorphous	250-300	61

It should be noted that the current specific surface area ($60 \text{ m}^2\cdot\text{g}^{-1}$) associated with ZnO-PAA2 synthesized with 0.63wt% did not correspond to that indicated in previous works in Table 3-3 ($90 \text{ m}^2\cdot\text{g}^{-1}$), whereas it should be the same. These two sets of samples (Table 3-5 and Table 3-3) were synthesized within a few months of each other. **This suggested the influence of another parameter that had been neglected so far, namely the synthesis temperature.**

I.4. Effect of the synthesis temperature

One of the major problems with ZnO-PAA_X synthesis was undoubtedly the reproducibility of the results and, in particular, the measurement of the specific surface area which seemed extremely sensitive to subtle changes of parameters.

Therefore, after having set some parameters in the previous sections, the synthesis temperature was finely controlled in order to minimize its impact on the structural properties of the hybrid ZnO. All the experiments described earlier in this chapter were performed at room temperature (between 15 and 20 °C), so we focused on studying the influence of a temperature range of 0 to 40 °C on the structural properties of ZnO-PAA_X materials (X = 2 and 5). Other parameters such as washing with 90 mL EtOH and 0.63wt% of PAA2 concentration were kept constant.

I.4.1. Effect of the synthesis temperature on ZnO-PAA2

For ZnO-PAA₂, syntheses were performed at 0 °C, 10 °C and 40 °C. The XRD results showed no difference in crystallinity and crystallite size between the three materials (Figure 3-22, Table 3-6) which were comparable to those of ZnO-PAA₂ synthesized at room temperature (Figure 3-11).

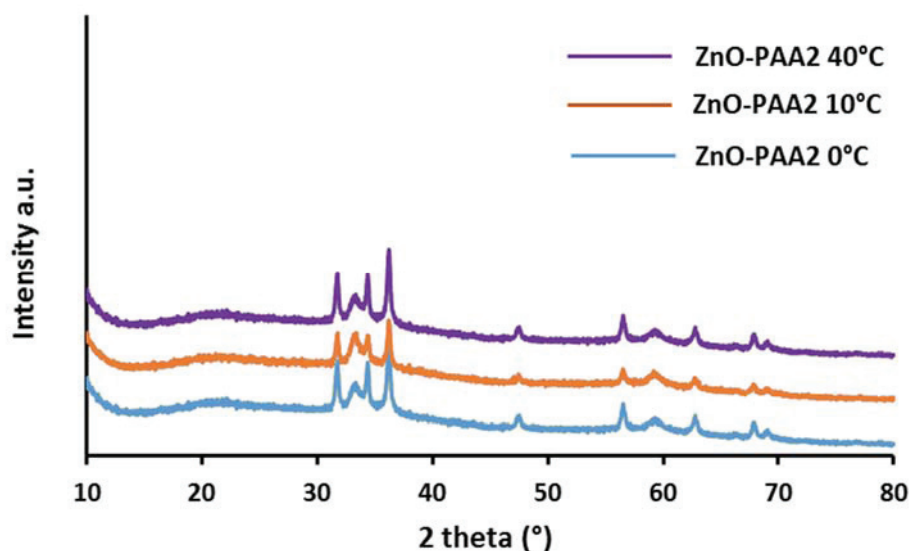


Figure 3-22: XRD diffraction patterns for ZnO-PAA₂ synthesized at different temperatures (0.63 wt% of PAA₂)

BET specific surface area measurements showed differences between materials (Table 3-6), with the highest surfaces ($80\text{-}90\text{ m}^2\cdot\text{g}^{-1}$) being obtained at low temperature ($0\text{-}10\text{ }^\circ\text{C}$), in the same range than values obtained previously at room temperature. On the other hand, a temperature of $40\text{ }^\circ\text{C}$ had the effect of reducing by two the specific surface area ($37\text{ m}^2\cdot\text{g}^{-1}$).

The TG analyses (Figure 3-23) did not show any effect of the synthesis temperature on the inorganic/organic ratios since they were identical for materials produced at the same concentration of PAA2 of $0.63\text{ wt}\%$. Temperature therefore did not affect the thermodynamics of the system since the same raw material was formed overall but it affected the material's morphological evolution through the 60 minutes of synthesis.

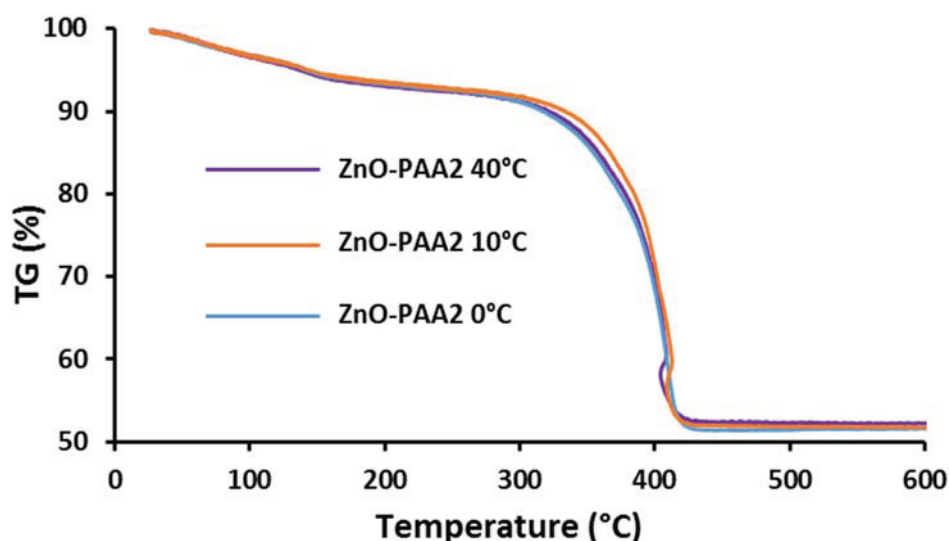


Figure 3-23: TGA curves for ZnO-PAA2 synthesized at different temperatures ($0.63\text{wt}\%$ of PAA2)

Table 3-6: Effect of the synthesis temperature on ZnO-PAA2 properties

Synthesis T° (°C)	S.S.A. BET ($\text{m}^2\cdot\text{g}^{-1}$)	ZnO crystallite size / XRD (nm)	TG / Weight loss [200-600°C] (%)	Aggregate size / TEM (nm)
0	89	23	40	100-200
10	91	25	40	--
40	37	24	40	250-350

By comparing TEM images obtained for samples synthesized at 0 °C (Figure 3-24 a) and 40 °C (Figure 3-24 b), the decrease in specific surface area could result from the lower amount of 2D nano-sheets and the fusion of some mesospheres into larger aggregates. At low temperatures, it was also possible to find hollow mesospheres, but in very limited numbers.

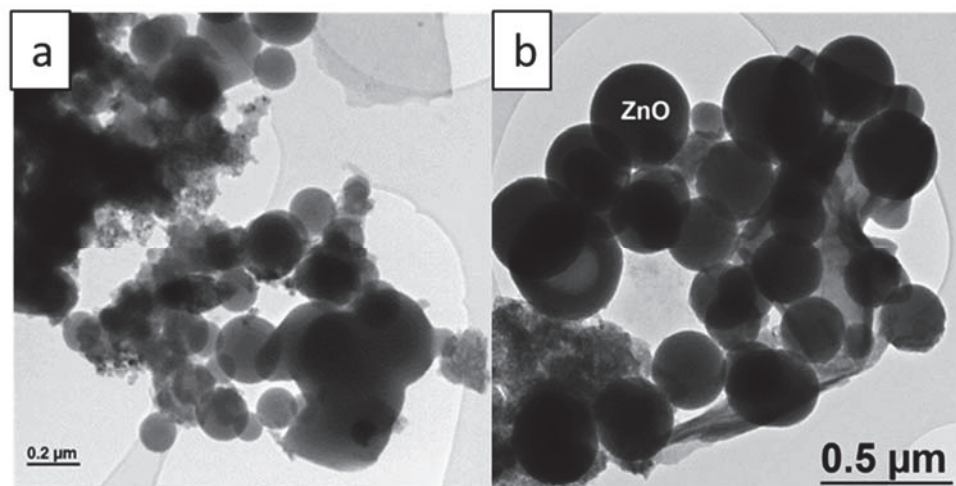


Figure 3-24: TEM images of ZnO-PAA2 synthesized at a) 0 °C and b) 40 °C

In order to have a general idea of the behaviour of ZnO-PAAX NPs and the relationship between nucleation growth and synthesis temperature, the study was extended to ZnO-PAA5 to verify if there was also an effect of the nature of the polymer.

I.4.2. Effect of the synthesis temperature on ZnO-PAA5

The results obtained for ZnO-PAA5 were in the opposite direction to those obtained with ZnO-PAA2. Indeed, based on XRD measurements (Figure 3-25), the structure of ZnO crystallites was strongly influenced by the synthesis temperature. At low temperatures, ZnO-PAA5 nanoparticles were mainly amorphous or very small, while an increase in temperature led to an increase in the degree of crystallinity or size of crystallites. The synthesis temperature of 60 °C was added to the three previously selected values to visualize the evolution in terms of structure over a larger temperature range. Table 3-7 summarizes the different physico-chemical characteristics of the four samples and shows that the specific surface area tends to increase with the synthesis temperature with a maximum of 120 m².g⁻¹ at 40 °C, which is the opposite for PAA2. The latter surface area was the highest value that has been obtained so far in our study. The average crystallite sizes of ZnO around 20 nm and the percentages of organic

around 50% (measured by TGA, Figure 3-26) were close to those obtained for PAA2.

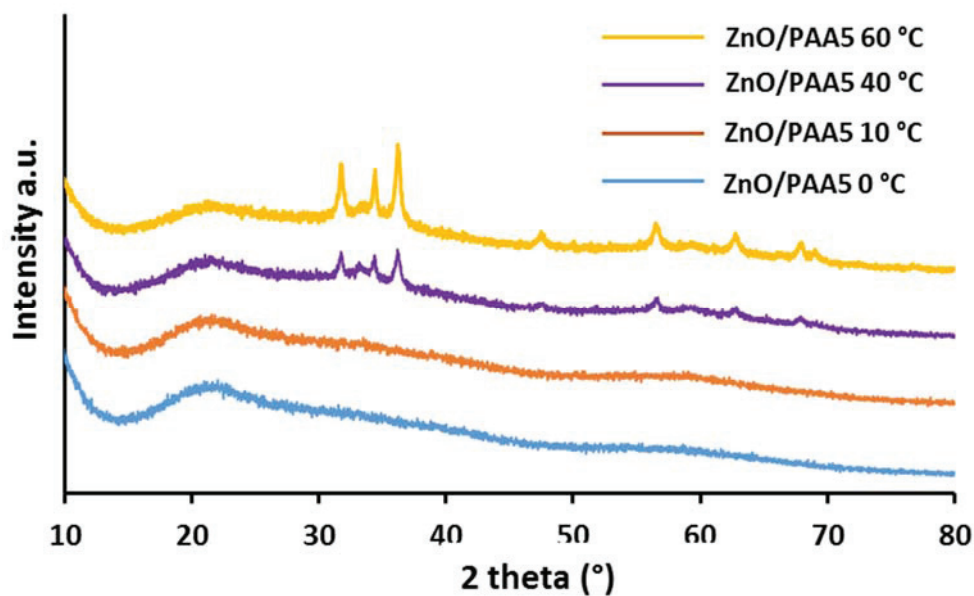


Figure 3-25: XRD diffraction patterns of ZnO-PAA5 at different synthesis temperature (0.63 wt% of PAA5)

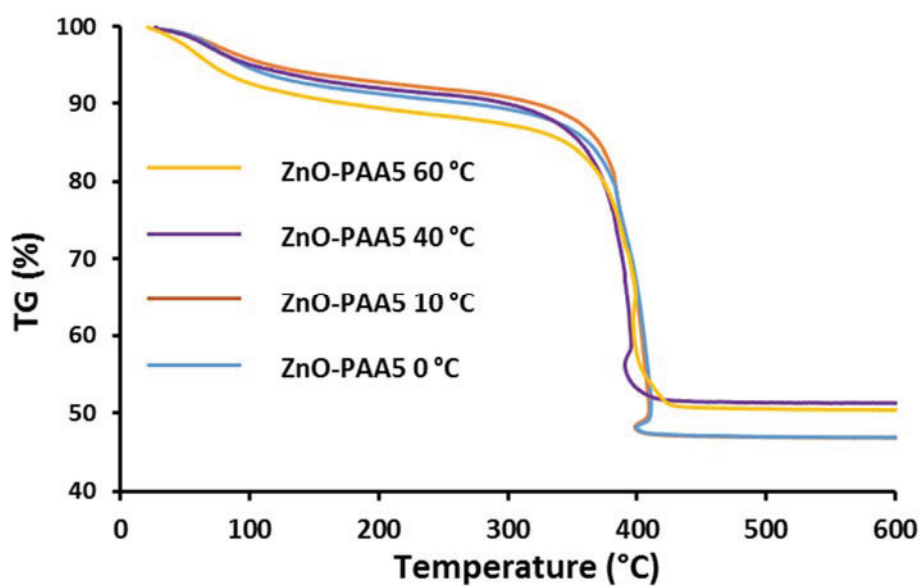


Figure 3-26: TGA cuves of ZnO-PAA5 at different synthesis temperature (0.63 wt% of PAA5)

Table 3-7: Effect of the synthesis temperature on ZnO-PAA5 characteristics

Synthesis T° (°C)	S.S.A. BET (m ² .g ⁻¹)	ZnO crystallite size XRD (nm)	Aggregate size TEM (nm)	TG / Weight loss [200-600°C] (%)
0	73	Amorphous	60	41
10	70	Amorphous	--	41
40	120	21	40	38
60	89	18	--	37

--: not determined

TEM and SEM analyses (Figure 3-27 and Figure 3-28) of the samples synthesized at 0 °C and 40 °C showed that this increase in specific surface area was once again accompanied by the appearance of a 2D nano-sheet phase, a phenomenon already observed in the ZnO-PAA2 system study when washing with 90 mL ethanol (Section I.2.1) or with 0.3 wt% of PAA2 (Section I.3). TEM images showed that at 0 °C, the material was essentially composed of spherical aggregates of an average size of 60 nm associated with a very interesting monodispersity (Figure 3-27 a). This observation was confirmed by the SEM images obtained on this same material where the monodispersity was visualized on a larger scale (Figure 3-28). At 40 °C, there was a majority of spherical aggregates on average smaller (40 nm) but also more polydispersed. This smaller size could also explain the increase in specific surface area, but it also seemed plausible to explain it by the presence of 2D nano-sheet structures. SEM images of the material obtained at 40 °C showed that there was an intimate mixture between spherical aggregates and 2D nano-sheets.

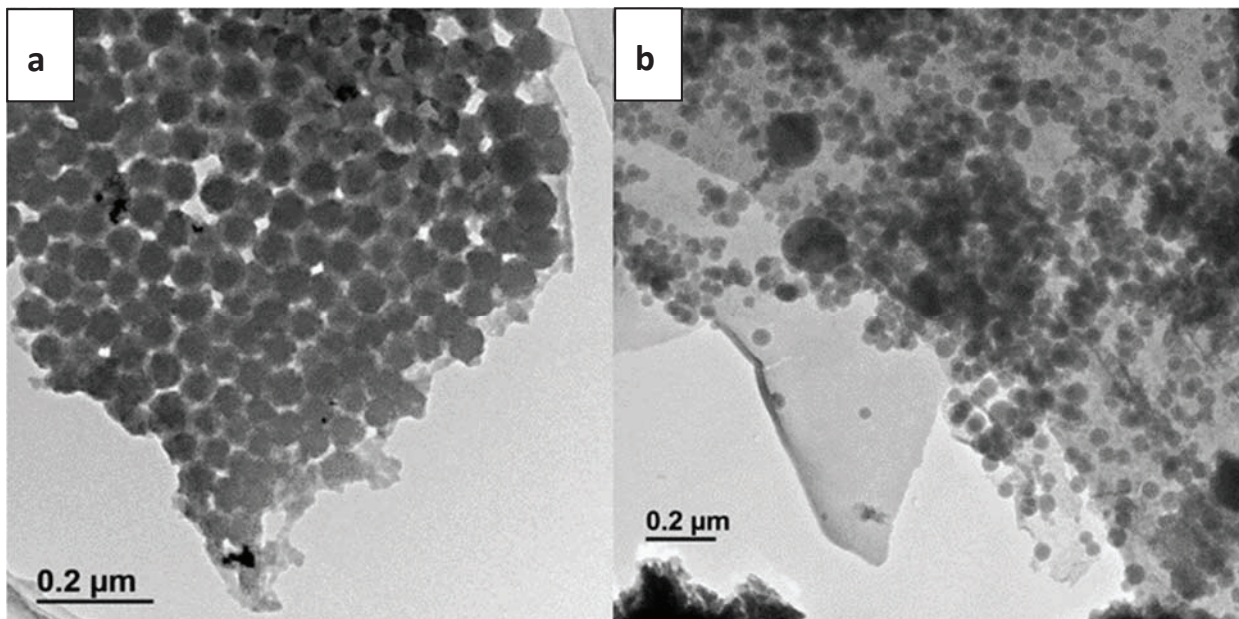


Figure 3-27: TEM images of ZnO-PAA5 synthesized at: a) 0 °C and b) 40 °C

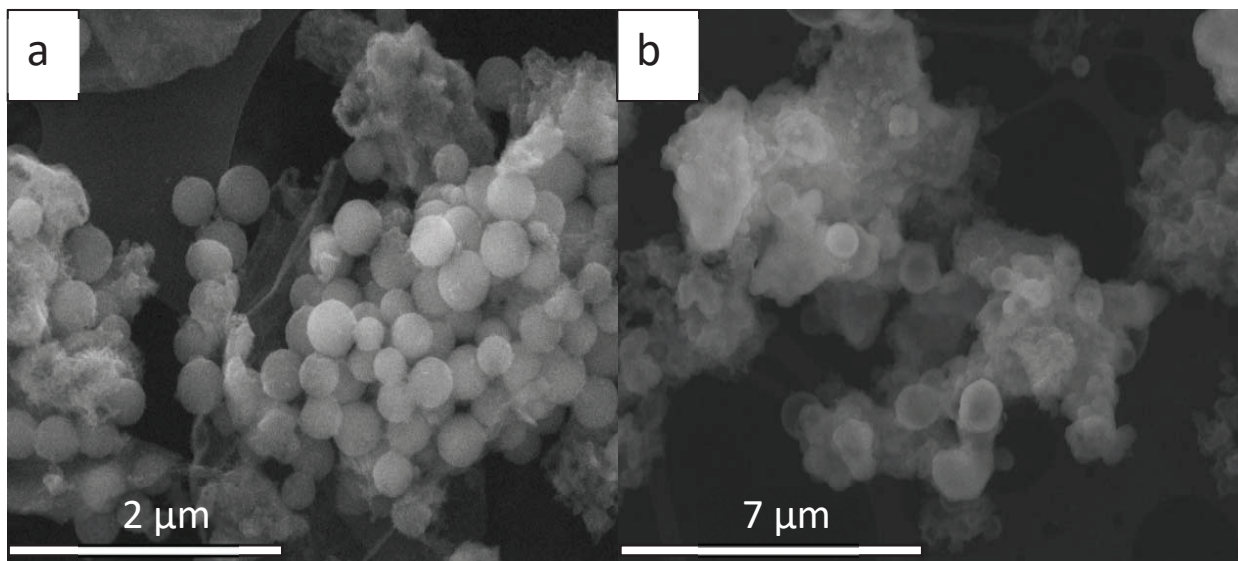


Figure 3-28: SEM images of: a) ZnO-PAA5 at 0 °C and b) ZnO-PAA5 at 40 °C

The change in morphology of ZnO nanoparticle assemblies as a function of temperature was reported by different groups. For instance, in article of Samei et al. ⁷, the effect of three different temperatures on the size of ZnO crystallites and their morphology was studied. All materials were prepared by precipitation of zinc acetate with 2-methoxyethanol and

monoethanolamine in the presence of NaOH at 30, 60 and 90 °C. While the crystallite size remained virtually unchanged for the three samples (37 nm on average), the morphology of the particles went from spheres at the lowest temperature to bars and ellipsoids at 90 °C (Figure 3-29).

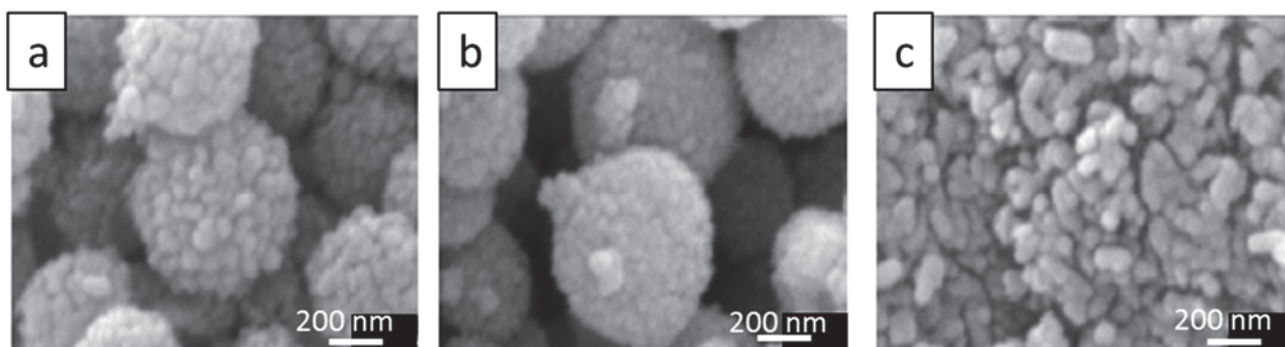


Figure 3-29: SEM images of ZnO synthesized at: a) 30 °C , b) 60 °C and c) 90 °C ⁷

In conclusion, the various synthesis parameters previously studied showed that the presence of PAAH, its nature and its concentration during the hydrolysis of ZnEt₂ generated a large variability of physico-chemical characteristics in terms of morphology and specific surface area. First, it would appear that the removal of residual water by washing with ethanol was the reason for the increase in the specific surface area of both PAA2 and PAA5 systems. While they also have in common the thermodynamics that led to almost total use of PAAH, the nucleation/growth mechanisms appeared very different, or even in the opposite direction, between PAA2 and PAA5. The temperature parameter was therefore extremely important to control the morphology of the objects obtained as well as the specific surface area. Having a large specific surface area would therefore require the presence of nano-sheet-like structures, which are obtained at low temperature with PAA2 and at high temperature with PAA5.

This could be very interesting for different applications but also delicate in order to develop a robust method for the production of catalyst supports with a high specific surface area. Nevertheless, these hybrid supports will have to undergo calcination steps between 300 and 400 °C when developing copper-based catalysts, so it is also necessary to evaluate the thermal behavior of these structures in the temperature range up to 400 °C.

I.5. Effect of calcination temperature after synthesis

As shown in the TG analyses in Figure 3-4, ZnO-PAA2 and ZnO-PAA5 began to degrade thermally at around 300 °C. We therefore studied the thermal behaviour of ZnO-PAA2 and ZnO-PAA5 substrates between 300 and 400 °C since they will be calcined at 400 °C after copper deposition. ZnO-PAAX powders were thus characterized after calcination at 300, 325, 350 and 400 °C under air in a static furnace at a heating rate of 5 °C.min⁻¹ until the desired temperature was reached and maintained for 4 hours.

It is important to mention that this thermal behaviour study was carried out on substrates obtained at room temperature with a PAAX mass concentration of 0.63 wt% and rinsing with ethanol. It should therefore be dissociated from the previous sections on synthesis parameters but it will nevertheless make it possible to evaluate, in a relative way, the thermal behaviour of the different ZnO-PAA2 and ZnO-PAA5 structures.

I.5.1. Effect of calcination temperature on ZnO-PAA2

The XRD diffractograms associated with the four samples obtained after calcination of ZnO-PAA2 at 300 °C, 325 °C, 350 °C and 400 °C (Figure 3-30) showed an increase in crystallinity with increasing calcination temperature. The crystallinity was calculated by Rietveld refinement with FullProf software and the results are presented in Table 3-8. Indeed, at 300 °C, ZnO-PAA2 was 90% amorphous and the 10% of the crystallized phase corresponded to hexagonal ZnO with a crystal size between 9 nm (calculated with peaks at 47°, 57° and 63°) and 15 nm (calculated with peaks at 31.5°, 34° and 36°). The increase in calcination temperature to 325 °C resulted in a 90% increase in crystallinity with small crystallites of an average size of 4.4 nm. For temperatures above 325 °C, ZnO-PAA2 was fully crystallized with the same hexagonal structure with an average size of 12 nm for ZnO-PAA2 calcined at 350 °C and 19 nm after calcination at 400 °C calculated with all the peaks. The increase in the size and degree of crystallinity of the crystallites with the increase in the calcination temperature has been reported in several studies on ZnO nanoparticles and ZnO films.^{8,9}

It therefore seemed that 350 °C was a transition temperature for the ZnO-PAA2 system, which was confirmed by the TG analyses since the organic content became very low above 325 °C.

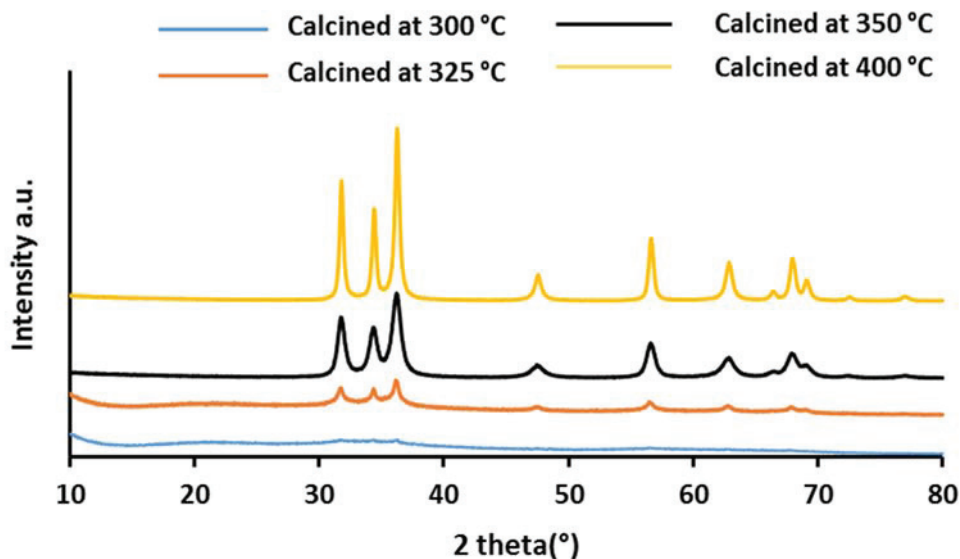


Figure 3-30: XRD diffraction patterns of ZnO-PAA2 calcined at different temperatures

Indeed, the TGA curves (Figure 3-31) confirmed the presence of a large part of the polymer after calcination at 300 °C and 325 °C with respective total weight losses of 47 and 53% for ZnO-PAA2 (Table 3-8). The increase in the calcination temperature led to an increase in the degradation of the polymer. After calcination at a temperature above 350 °C, ZnO-PAA2 had almost completely lost its organic component. A weight loss of less than 10% was observed at 350 °C and 400 °C by TG analysis. Another change occurred at high calcination temperature, the onset of degradation temperature shift to a lower value (250 °C instead of 350 °C) indicating a change in the ZnO-PAA interaction.

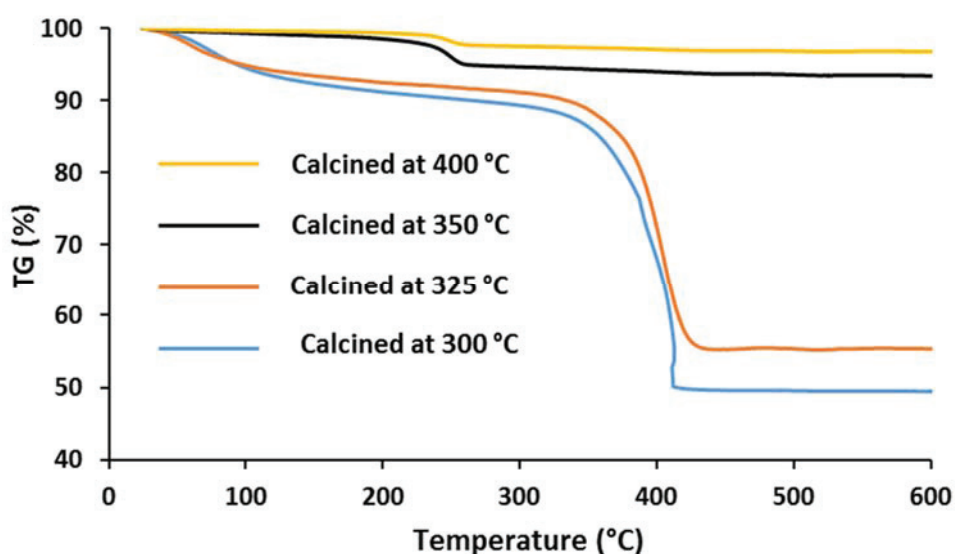
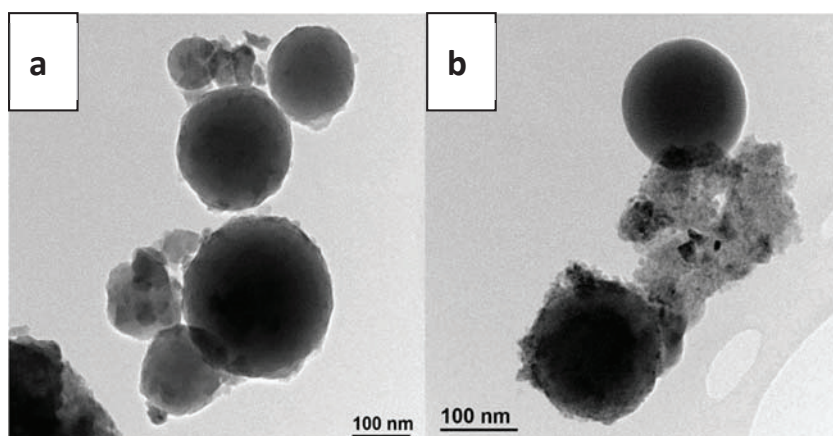


Figure 3-31: TGA curves for ZnO-PAA2 calcined at different temperatures and PAA2

Table 3-8: Properties of ZnO-PAA2 calcined at different temperature

Calcination temperature (°C)	S.S.A. / BET (m ² .g ⁻¹)	ZnO crystallite size / XRD (nm)	ZnO Crystallinity (%)	Aggregate size (TEM nm)	TG / weight loss [200-600°C] (%)
300	28	Amorphous	10	120-220	40
325	38	4.4	90	150-200	45
350	51	12.0	100	10-20	5
400	18	19.0	100	20-40	2

TEM images associated with samples calcined at different temperatures are shown in Figure 3-32. ZnO-PAA2 calcined at 300 °C and 325 °C (Figure 3-32: TEM images of ZnO-PAA2 calcined at: a) 300 °C, b) 325 °C, c) 350 °C and d) 400 °C Figure 3-32 a,b) showed the conservation of 3D mesospheric nanoparticle assemblies as for ZnO-PAA2. Heating to a temperature above 325 °C resulted in the total destruction of this morphology (although some spherical aggregates could still be observed in Figure 3-32 c and d) which was associated with an increase in crystallite size, as shown in Table 3-8. This observation showed the need to have the polymer inside the aggregate matrix to maintain the self-assembled morphology.



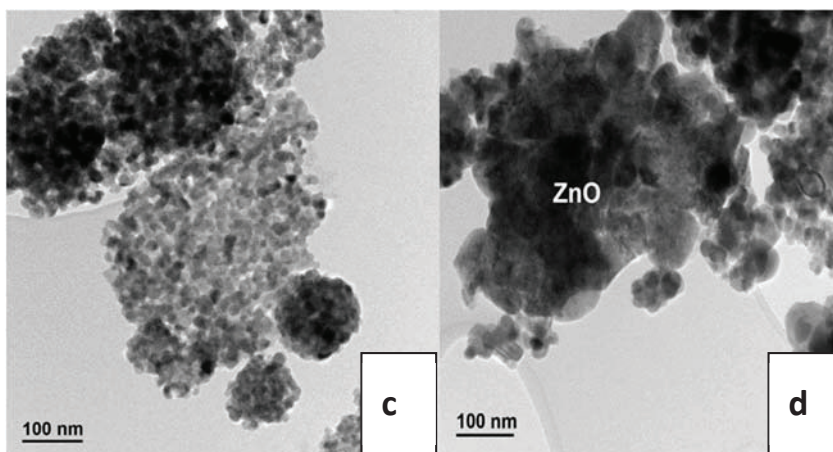


Figure 3-32: TEM images of ZnO-PAA2 calcined at: a) 300 °C, b) 325 °C, c) 350 °C and d) 400 °C

Compared to as-prepared ZnO-PAA2 sample, the BET surface area increased from $20 \text{ m}^2 \cdot \text{g}^{-1}$ to 28 and $38 \text{ m}^2 \cdot \text{g}^{-1}$ after calcination at 300 °C and 325 °C, respectively. BET showed an increase in specific surface area with the increase in calcination temperature up to a maximum of $51 \text{ m}^2 \cdot \text{g}^{-1}$ after calcination at 350 °C. At 400 °C, the specific surface area was the lowest, indicating that ZnO nanoparticles started sintering.

The increase in the specific surface area of ZnO nanoparticles for low calcination temperatures followed by a decrease at higher temperatures was reported by Shohel et al.⁹ They prepared ZnO by electrolysis of zinc plates in a sodium bicarbonate solution for 1 hour under a fixed current of 2A. The precipitates were then centrifuged, air-dried and crushed in a mortar and calcined at 200-800 °C. Table 3-9 summarizes the values obtained in their article for the effect of the calcination temperature on the specific surface area of ZnO NPs. The specific surface area of ZnO increased from $40 \text{ m}^2 \cdot \text{g}^{-1}$ to $51 \text{ m}^2 \cdot \text{g}^{-1}$ with an increase in the calcination temperature from room temperature to 300 °C followed by a decrease in the specific surface area for temperatures above 400 °C (Table 3-9). Indeed, at low calcination temperatures, the particles were smaller than at high temperatures, which led to an increase in pore volume and specific surface area. At higher calcination temperatures, the particles tended to sinter due to inter-crystalline growth resulting in a decrease in pore volume and therefore a decrease in specific surface area.

Table 3-9: Effect of the calcination temperature on ZnO NPs properties ⁹

Sample	Surface area (m ² .g ⁻¹)	Total pore volume (cm ³ .g ⁻¹)	Particle size (BET; nm)	Mean pore diameter (nm)
ZnO-air dried	40.32	0.4029	26.56	39.99
ZnO-200	49.70	0.4759	21.53	38.29
ZnO-300	51.11	0.5601	20.92	43.81
ZnO-400	40.63	0.4848	26.38	47.79
ZnO-500	19.95	0.4744	53.68	95.19
ZnO-600	14.31	0.2073	74.65	57.84
ZnO-700	10.81	0.1176	98.88	43.47
ZnO-800	2.82	0.0151	379.56	21.42

The decrease in the specific surface area of ZnO nanoparticles when calcined at temperature above 400 °C seemed to be frequent, it had also been reported in Bai's article ¹⁰. Authors prepared ZnO NPs by sol-gel method by reacting a zinc acetate solution with a potassium hydroxide solution in the presence of tetraethylorthosilicate as a surface modifier. The colloid as prepared was separated from the unreacted molecules by centrifugation and washed with methanol and water. Figure 3-33 shows the relationship between the calcination temperature of ZnO nanoparticles and the specific surface area. The specific surface area decreased for calcination temperature above 400 °C. Between 200 °C and 400 °C, the specific surface area was approximately 65 m².g⁻¹ and decreased to 27 m².g⁻¹ at 800 °C. Again, the authors attributed this behaviour to the increasing size of crystallites at higher temperatures.

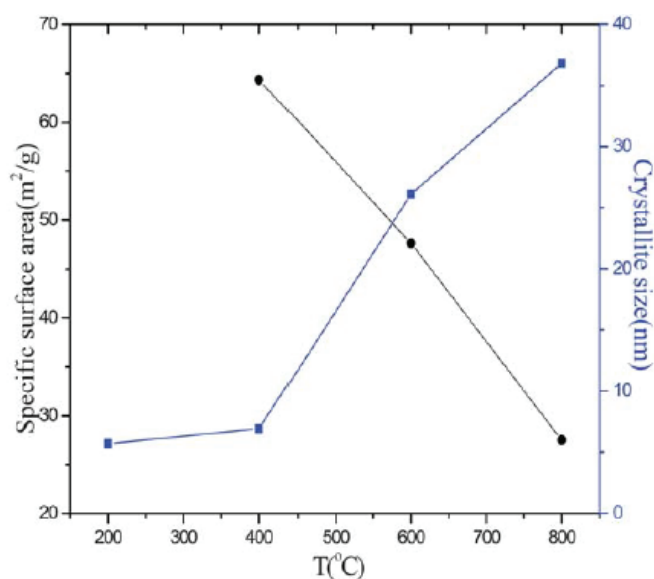


Figure 3-33: Relation between ZnO NPs specific surface area and calcination temperature ¹⁰

I.5.2. Effect of calcination temperature on ZnO-PAA5

For the material ZnO-PAA5, changes in morphology could already be observed after calcination at 300 °C. The XRD diffractograms of the powders calcined at 300, 350 and 400 °C (Figure 3-34) showed a well-crystallized zincite-type ZnO phase with an average crystallite size of 20 nm for the three samples. TEM images (Figure 3-35) have shown that 3D hybrid self-assemblies were destroyed at 300 °C to give overall ZnO nanoparticles of hexagonal shapes with an average size between 20 and 30 nm in accordance with XRD results. Therefore, over this temperature range targeted for catalyst synthesis and unlike ZnO-PAA2, the morphology, size of the objects and specific surface area did not change and remained around 20-30 m².g⁻¹.

The TGA curves of solids calcined at 300, 350 and 400 °C showed one weight loss, between 200 and 600 °C, of less than 10%, confirming the almost total degradation of the polymer from 300 °C and a slight evolution of the overall composition (Organic/Inorganic) of the materials obtained at these three temperatures (Figure 3-36). The same result as for ZnO-PAA2 was found with an onset of weight loss temperature that was lowered by 100 °C, proving again that the organic component was of a totally different nature from the original PAA5.

Compared to ZnO-PAA2, the structure of the ZnO-PAA5 hybrid material has appeared less robust. This observation could be correlated to the smaller size of the aggregates for PAA5 and therefore to a larger area of exposure to thermal degradation. Table 3-10 summarizes the characteristics of the materials obtained.

Table 3-10: properties of ZnO-PAA5 calcined at different temperature

Calcination T° (°C)	S.S.A. / BET (m ² .g ⁻¹)	ZnO crystallite size / XRD (nm)	ZnO particle size / TEM (nm)	TG / Weight loss [200-600] (%)
300	26	20	20-30	6
350	31	18	20-30	5
400	20	24	20-30	2

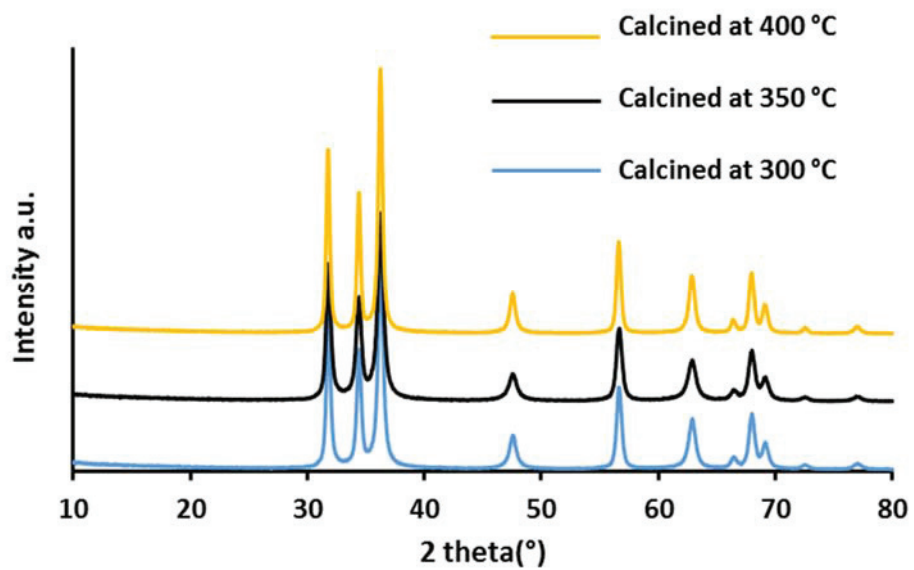


Figure 3-34: XRD diffraction patterns of ZnO-PAAX calcined at different temperature

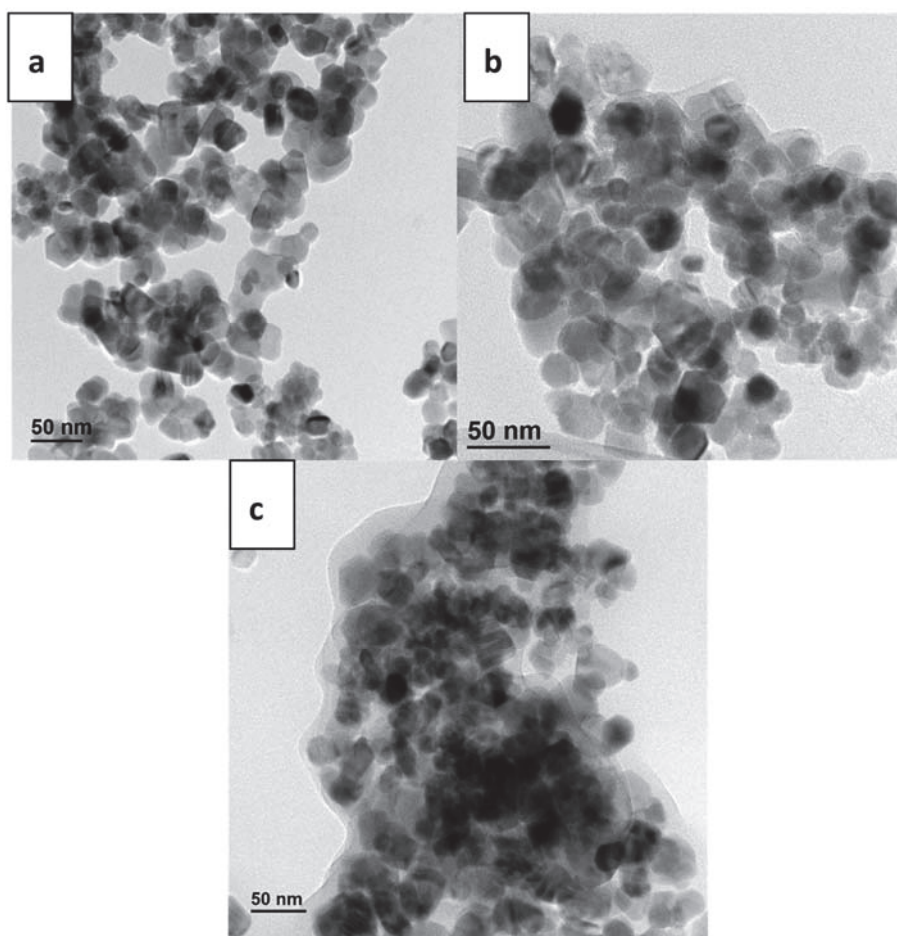


Figure 3-35: TEM images of ZnO-PAAX calcined at: a) 300 °C, b) 350 °C and c) 400 °C

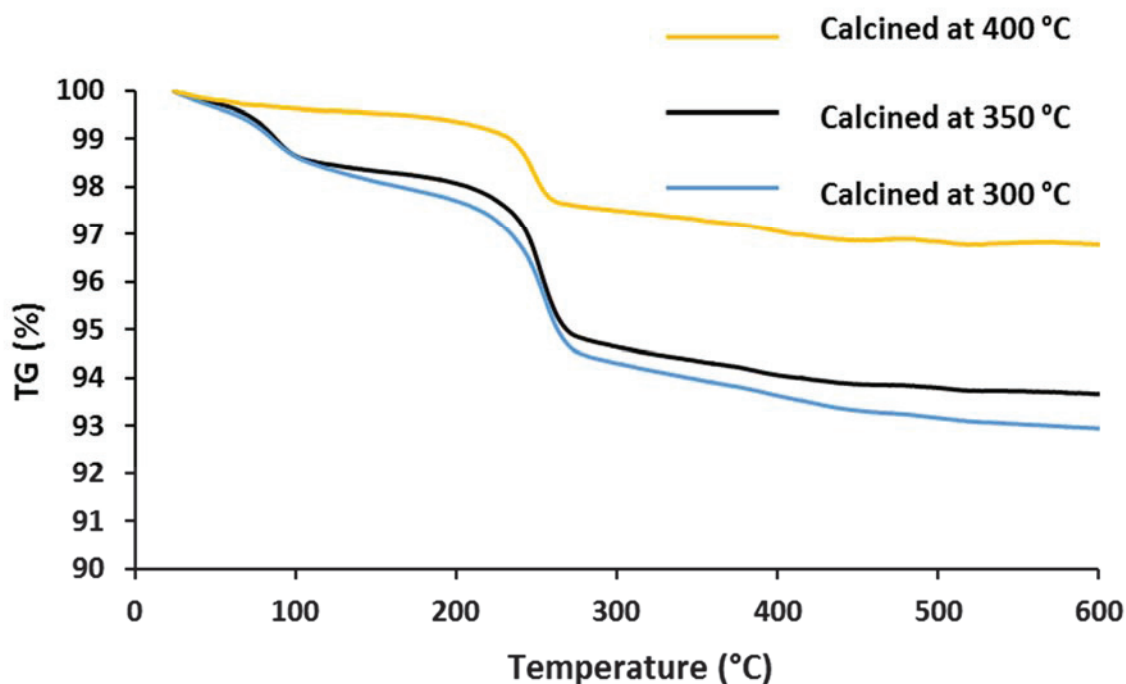


Figure 3-36: TGA curves for ZnO-PAA5 calcined at different temperatures

In conclusion, ZnO-PAA2 has appeared to be more thermally resistant since the hybrid particles are agglomerated in larger spheres, protecting more the polymer from thermal degradation. This has resulted in the retention of mesospheric morphology even after calcination at 325 °C, whereas ZnO-PAA5 lost 3D morphology after calcination at 300 °C. The increase in the calcination temperature led to an increase in the specific surface area with a maximum of 51 m².g⁻¹ obtained for ZnO-PAA2 calcined at 350 °C and destruction of the mesospheric morphology. In the case of ZnO-PAA5, the particle size was in the same 20 nm range after calcination between 300 °C and 400 °C as well as the specific surface area (20-30 m².g⁻¹) showing high material stability after polymer removal and destruction of the 3D spherical morphology.

But as mentioned above, these hybrid materials will be used as a support for the development of heterogeneous catalysts for glycerol hydrogenolysis via the deposition of copper molecular compounds followed by a first calcination step at 400 °C. If we refer to the specific surfaces obtained at this temperature, they were around 20 m².g⁻¹ for the two supports developed. It was therefore the impact of the morphology and the nature of the interactions between the different hybrid carriers ZnO-PAA2 and ZnO-PAA5 and copper precursors that must be studied in detail and these results will be described in Chapter IV.

II. Conclusion

In conclusion of this chapter, it was demonstrated that the development of reproducible batches of ZnO-PAAX hybrid nanomaterials with well-defined properties (large specific surface area in particular) involved the fine control of many parameters such as synthesis temperature, polymer quantity and powder washing.

Weight concentrations of PAA2 or PAA5 in the range of 0.5 to 0.63 wt% were appropriate to obtain a 3D mesospheric morphology following the self-assembly phenomena of the ZnO-PAAX hybrid nanoparticles. Their syntheses were generally accompanied by a secondary phase in the form of 2D nano-sheets. The latter, which seemed to be preferred at high temperature for PAA5 and low temperature for PAA2, led to a significant increase in the specific surface area of the final material. Thus, for ZnO-PAA2, low temperature synthesis (0-10 °C) was associated with a high specific surface area of 91 m².g⁻¹ and for ZnO-PAA5, a maximum specific surface area of 120 m².g⁻¹ was obtained at 40 °C.

Ethanol washing seemed to affect the surface dehydration of aggregates, which led to a decrease in inter-aggregate (or even inter-nano-sheet) interactions of Van der Waals (hydrogen interactions), allowing an increase in the specific surface area.

The thermal stability of the ZnO-PAA2 and ZnO-PAA5 systems depended on the size of the aggregates and therefore on the molecular weight of the polymer. ZnO-PAA5, forming smaller aggregates, was less thermally stable with total degradation of the hybrid system from 300 °C while the mesospheres of ZnO-PAA2 were still observable at 325°C.

In the following chapters, ZnO-PAA2 and ZnO-PAA5 will be used as starting materials for copper-based catalysts in order to study the effect of certain support synthesis parameters on the catalytic results (conversion, selectivity) in the hydrogenolysis of glycerol. Specific attention will be given to ZnO-PAA2 synthesized at 0 °C, washed with ethanol and not calcined as a support for Cu nanoparticles.

III. References

1. Zhu, Y., Omar, L., Daniele, S. & Masenelli, B. Intense visible emission from ZnO/PAAX (X = H or Na) nanocomposite synthesized via a simple and scalable sol-gel method. *Sci. Rep.* **6**, (2016).
2. Park, S., Choi, G. R., Kim, J. H., Lee, J. C. & Kim, S.-J. Dispersion effect of sodium hexametaphosphate on the photocatalytic efficiency of a solution-combusted ZnO nanopowder. *J. Korean Phys. Soc.* **61**, 1400–1403 (2012).
3. Rezende, C., da Silva, J. & Mohallem, N. D. Influence of drying on the characteristics of zinc oxide nanoparticles. *Brazilian journal of physics* **39**, 248–251 (2009).
4. Le Page, J-F. The preparation of catalysts from "Applied heterogeneous catalysis: design, manufacture, use of solid catalysts". Edited by Limido, J. *Éditions Technip*, Paris, (1987).
5. Yin, J., Gao, F., Wei, C. & Lu, Q. Water amount dependence on morphologies and properties of ZnO nanostructures in double-solvent system. *Sci. Rep.* **4**, (2015).
6. Ramimoghadam, D., Bin Hussein, M. & Taufiq-Yap, Y. Hydrothermal synthesis of zinc oxide nanoparticles using rice as soft biotemplate. *Chem. Cent. J.* **7**, 136-146 (2013).
7. Samei, J., Shokufhar, A., Esmailzadeh Kandjani, A. & Vaezi, M. Effect of Synthesis Temperature on the Morphology of ZnO Nanoparticles Obtained via a Novel Chemical Route. *Defect and diffusion forum* **273**,192–197 (2008).
8. Alibe, I., Matori, A., Saion, E., Ali, A. & Zaid, M. The influence of calcination temperature on structural and optical properties of ZnO nanoparticles via simple polymer synthesis route. *Sci. Sinter.* **49**, 263–275 (2017).
9. Shohel, M., Miran, M. S., Susan, M. A. B. H. & Mollah, M. Y. A. Calcination temperature-dependent morphology of photocatalytic ZnO nanoparticles prepared by an electrochemical-thermal method. *Res. Chem. Intermed.* **42**, 5281–5297 (2016).
10. Bai, S., Hu, J. & Liu, C. C. Quantum-sized ZnO nanoparticles: Synthesis, characterization and sensing properties for NO₂. *J. Mater. Chem.* **21**, 12288-12294 (2011).

CHAPTER IV

Development of Cu/ZnO catalysts: support effect

Table of contents

CHAPTER IV.....	138
I. Commercial ZnO as support.....	139
I.1. Effect of Cu⁰ weight percentage	145
I.2. Effect of Cu²⁺ concentration	150
II. ZnO-PAA _X (X = 2, 5, 100) as supports.....	154
II.1. ZnO-PAA₂ non calcined.....	154
II.1.1. Effect of the synthesis parameters (support and copper wt%)	154
II.1.2. Effect of the weight of the catalyst.....	159
II.1.3. Recyclability of Cu/ZnO-PAA₂	162
II.2. ZnO-PAA₂ calcined.....	164
II.3. ZnO-PAA₅ as support	167
II.3.1. Non Calcined ZnO-PAA₅	167
II.3.1. Calcined ZnO-PAA₅	169
II.4. ZnO-PAA₁₀₀ as support	169
III. Cu-ZnO by a “one pot” method	170
III.1. Cu-ZnO synthesis by a “one pot - one step” approach.....	171
III.2. Cu-ZnO synthesis by a “one pot - two steps” approach	173
IV. Conclusions.....	177
V. References.....	178

This chapter is dedicated to the synthesis of Cu/ZnO catalysts and their use for the hydrogenolysis of glycerol into 1,2-PDO. We first started by synthesizing Cu/ZnO with different weight percentage and concentration of copper by deposition-precipitation with urea method (DPU). This first screening was done using a commercial ZnO in order to choose the synthesis parameters for copper deposition that led to the highest conversion.

In a second time, the home-made ZnO/PAAH was used as support in order to check the effect of the synthesis parameters of ZnO on the activity of the catalyst. We ended the chapter by elaborating Cu-ZnO with a novel one pot method.

I. Commercial ZnO as support

The first set of catalysts was developed using commercial ZnO purchased from Alfa Aesar as a support. Figure 4-1 shows the XRD patterns of this material, it was very well crystallized with the hexagonal phase (PDF number 01-083-6338) of zincite. The size of the crystallites calculated using the Scherrer equation showed that crystallites had a size of about 50 nm when calculated with all the peaks, except with the one at 33°, corresponding to the crystallographic plane (002), i. e. 72 nm. On the other hand, TEM images (Figure 4-2) showed large particles ranging from 50 to 200 nm with a heterogeneous shape. The high particle size was reflected in the specific surface area measured by BET which was very low with a value of 13 m².g⁻¹.

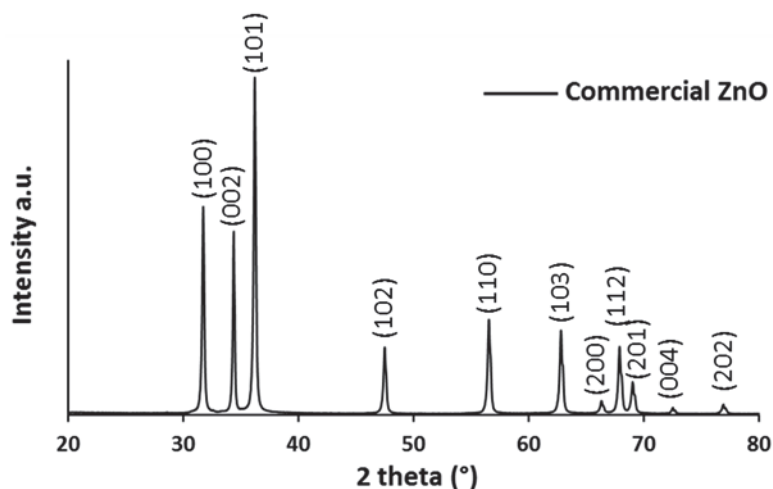


Figure 4-1: XRD diffraction pattern of commercial ZnO

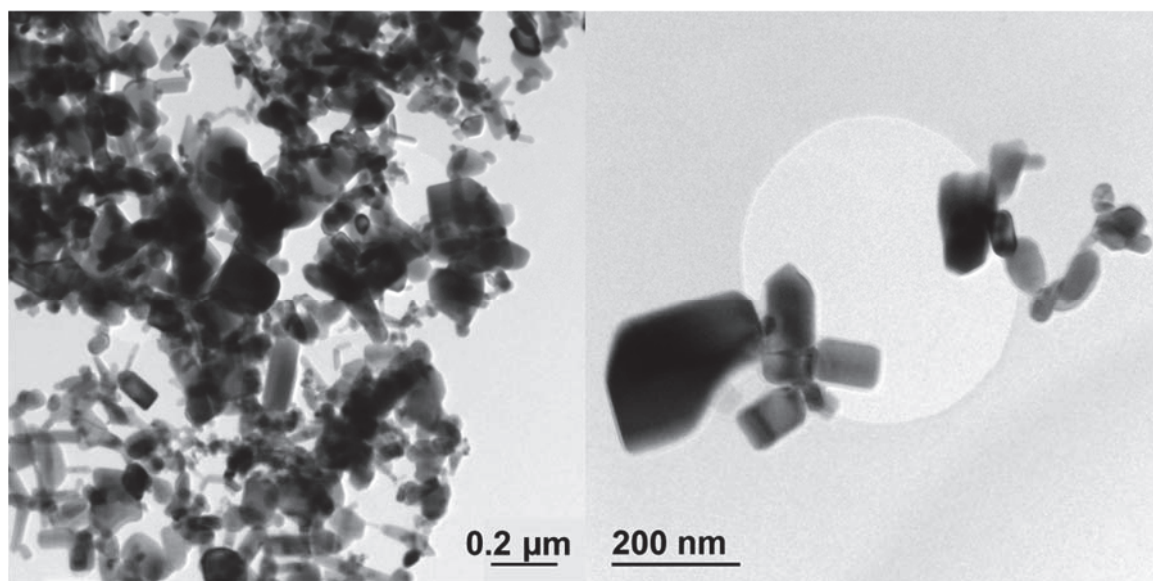
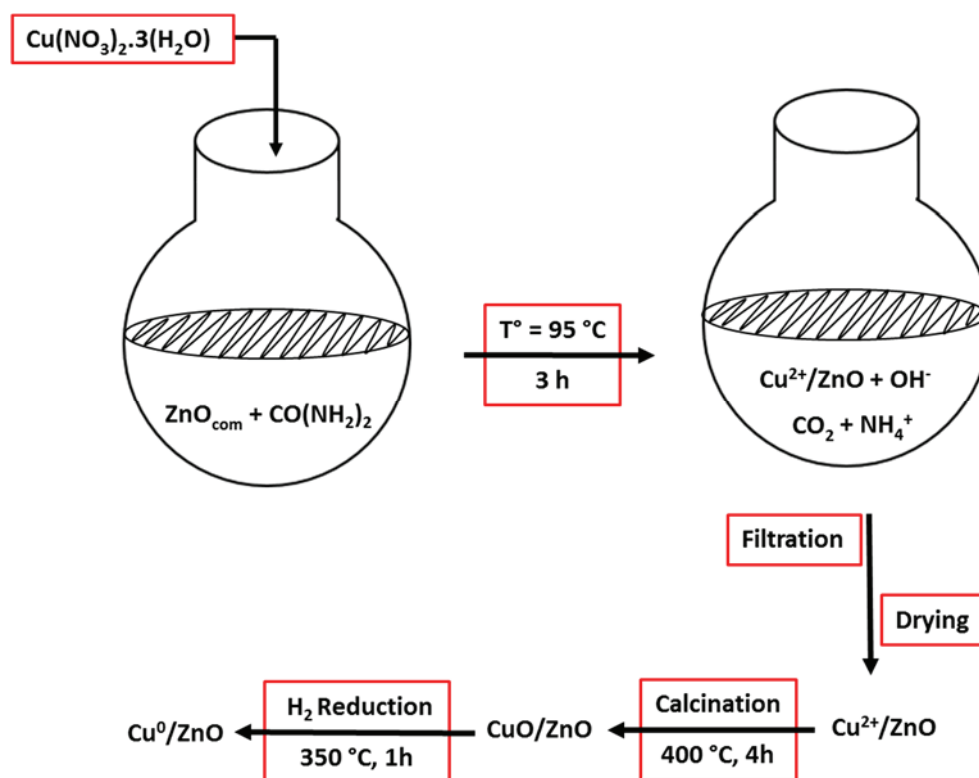


Figure 4-2: TEM images of commercial ZnO support

Different weight percentages of copper (from 2.5 to 20 wt%) were deposited by DPU on the support according to the synthesis parameters described in the experimental part (chapter II, page 80). Briefly, the copper solution was added to 1 g of commercial ZnO and 4 g of urea under stirring. The flask was heated at $5\text{ }^{\circ}\text{C}\cdot\text{min}^{-1}$ to $95\text{ }^{\circ}\text{C}$ for 3 hours. Solutions with varied $[\text{Cu}^{2+}]$ were used, from 5.2 to $81.6\text{ mmol}\cdot\text{L}^{-1}$. The volume of the Cu^{2+} solution depended on the desired $[\text{Cu}^{2+}]$ of the solution and the desired loading of copper in the catalyst. The amount of urea was chosen after a preliminary study conducted by a master student (Ms Constance Lecourt) who observed that for 1 g of commercial ZnO, 4 grams of urea allowed the highest deposition loading of copper (20 wt%) associated with the smallest Cu particle size (11 nm). The pH of the solution before adding urea was neutral and reached 8 at the end of the deposition step. After heating, the solution was filtered, washed with water and dried in the oven overnight in air. The dry powder mentioned as "After DPU" was calcined at $400\text{ }^{\circ}\text{C}$ for 4 hours in air and reduced at $300\text{ }^{\circ}\text{C}$ under H_2 for 1 hour followed by a passivation step with 1% O_2/N_2 flow at room temperature during 30 minutes.

The reaction of deposition of copper on ZnO support in presence of urea is proposed in scheme 4-1 (the stoichiometry is not shown). T° corresponds to the temperature of deposition-precipitation and it was chosen according to the temperature of degradation of urea ($> 60\text{ }^{\circ}\text{C}$).



Scheme 4-1: Synthesis of Cu/ZnO catalysts by DPU on commercial ZnO

As a first screening, twenty catalysts were synthesized using various $[\text{Cu}^{2+}]$ during the synthesis to get different final Cu loading (Table 4-1). The XRD patterns shown in Figure 4-3 correspond to the crystallographic states of 5 wt% Cu/ZnO, synthesized with $[\text{Cu}^{2+}] = 20.8 \text{ mmol}\cdot\text{L}^{-1}$, at different stages of the synthesis (after DPU, after calcination and after reduction), as representative examples of all the catalysts. The hexagonal phase of ZnO was present for all three steps with an average crystallite size of 60 nm (based on the three main peaks). After DPU, a new peak appears at 28° corresponding to the monoclinic phase $\text{Cu}_2(\text{NO}_3)(\text{OH})_3$ (PDF number 00-045-094). In this first stage copper ions precipitated onto the support in presence of urea. As it was mentioned in the first chapter, urea played a role of a delay base by decomposing first into ammonium and cyanate leading to an increase in the pH. Hence, Cu ions precipitated with the nitrates ions in the form of $\text{Cu}_2(\text{NO}_3)(\text{OH})_3$ onto the surface of ZnO, as previously reported by Louis et al. over TiO_2 ¹. We cannot exclude the formation of $(\text{Cu,Zn})(\text{CO}_3)(\text{OH})_2$ (PDF number 00-036-1475 appendix 7) which overlaid with $\text{Cu}_2(\text{NO}_3)(\text{OH})_3$ on Diffrac.Eva software. This phase would result from a partial dissolution of ZnO in basic media followed by co-precipitation. After calcination, the later phase transformed into

monoclinic CuO (PDF number 00-045-0937 appendix 8) where the main peak was at 38°. Hydrogen reduced CuO to cubic Cu⁰ (PDF number 04-013-9963 appendix 9) with the two main peaks at 43° and 51°. A third peak for Cu⁰ appeared at 74° for higher copper loadings. The intensity of the peaks depended on the weight percentage of copper.

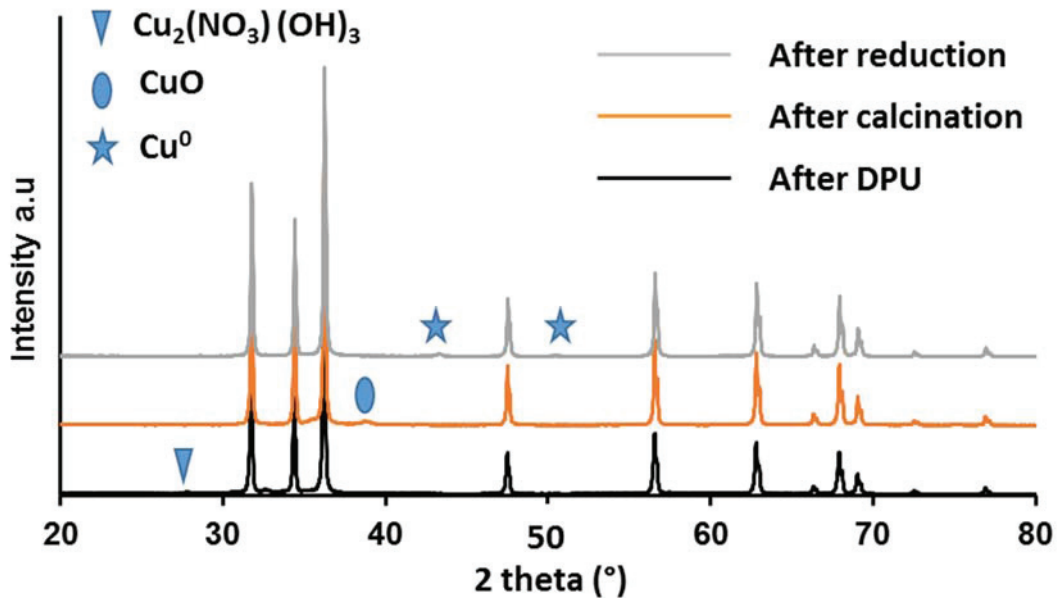


Figure 4-3: Representative XRD diffraction patterns of Cu/ZnO at different step of catalyst synthesis

It is worth noting that the ICP results (Cu_{exp}) are consistent with the theoretical weight percentage proving that the DPU method (in our conditions) was guarantying the total deposition of copper onto the support (Table 4-1). The crystallite sizes of Cu⁰ are also shown in Table 4-1. The estimation of the crystallite size might not always be accurate, as the peaks were broad and small, especially at low Cu loading but the error did not exceed 5 % of the value. At the same weight percentage, the crystallite main size showed a decrease in the size when increasing the Cu²⁺ concentration. This phenomenon did not seem to be random because it occurred for different copper loadings. To our knowledge, there is no study showing the effect of precursor concentration at the same weight percentage for the synthesis of Cu catalysts by DPU. At higher concentration and lower volume, the kinetic was different and the precursor should precipitate more rapidly. Or the temperature and pH increased with time; therefore, the precipitation might occur at lower temperature and / or lower pH at higher concentration. This might result in the formation of a larger number of nuclei and / or a better

support/precursor interaction, which would result on the formation of smaller particles.

Table 4-1: Cu/ZnO catalysts with different initial $[Cu^{2+}]$ and copper loadings.

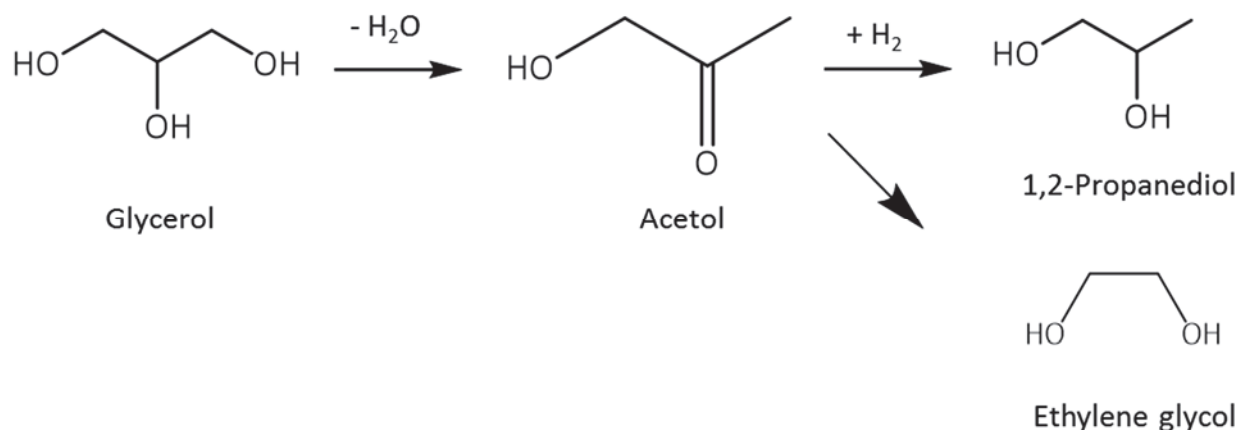
Cu_{theo} (wt%) ^a	2.5		5		10		15		20	
$[Cu^{2+}]$ (mmol.L ⁻¹)	C.S. ^b (nm)	Cu_{exp} ^c (wt%)	C.S. (nm)	Cu_{exp} (wt%)	C.S. (nm)	Cu_{exp} (wt%)	C.S. (nm)	Cu_{exp} (wt%)	C.S. (nm)	Cu_{exp} (wt%)
5.2	20	2.4	24	5.1	23	11.1	23	15.5	--	--
10.4	15	2.4	22	5.0	20	10.3	20	16.5	--	--
20.8	13	2.3	13	4.9	15	9.7	14	15.5	20	19.2
40.8	13	2.3	13	5.0	15	10.3	14	14.3	--	--
81.6	--	--	12	4.7	11	9.3	16	14.2	--	--

^a Theoretical copper weight percentage

^b Copper crystallite size based on Scherrer equation

^c Experimental copper weight percentage obtained by ICP analysis

After characterizing the main properties of these catalysts, the conversion of glycerol into 1,2-propanediol (1,2-PDO) was studied in a batch reactor, under 30 bar of H₂ and 200 °C, for 24 hours. 100 mL of an aqueous solution of 0.23 M glycerol and 500 mg of catalyst were used. As it was mentioned in the chapter I, when using Cu/ZnO in water, the reaction follows the dehydration hydrogenation route as shown in Scheme 4-2. As a first step, the dehydration takes place on the surface of ZnO due to its acidic properties resulting in acetol as intermediate, detected in our case as well. It is then transformed over the copper surface into 1,2 propanediol (1,2-PDO) as major product and ethylene glycol (EG) as secondary product with low selectivity (< 10 %), depending on the conversion. The conversions after 24 hours obtained with all the catalysts prepared with the commercial ZnO with different copper weight percentage and $[Cu^{2+}]$ are summarized in Table 4-2. For all the catalysts studied in this chapter, the carbon balance was always above 95%.



Scheme 4-2: Mechanism of glycerol hydrogenolysis over Cu/ZnO catalysts

Table 4-2: Conversions of glycerol after 24hrs for Cu/ZnO catalysts with different initial $[Cu^{2+}]$ and copper loadings

Cu_{theo} (wt%)	2.5	5	10	15	20
$[Cu^{2+}]$ (mmol.L ⁻¹)	Conversion /24h (%)				
5.2	2	14	19	18	--
10.4	2	8	20	20	--
20.8	2	10	25	22	15
40.8	2	20	22	17	--
81.6	--	17	16	15	--

At low weight percentage (2.5%) of copper, the conversion was very low, only 2% of glycerol was converted, and thus independently of the different initial concentrations of Cu^{2+} . The increase in the weight percentage of copper to 5% resulted in an increase in catalyst conversion, as the same mass of catalyst was used for all the reactions (500 mg). Nevertheless, there was no homogeneous behavior for the catalyst at this percentage where conversion increased and/or decreased without having a defined relationship with Cu^{2+} concentration. When the weight percentage of copper was higher, the catalyst began to behave according to a defined trend. The increase in the concentration of the Cu^{2+} solution for 10 wt% Cu/ZnO resulted in an increase, followed by a decrease in catalyst conversion, with an optimum of 25% for a Cu^{2+} concentration of 20.8 mM. At higher weight percentage of copper (15% and 20%), the support began to be highly charged and might be inaccessible to glycerol molecules,

which prevented an increase in conversion. Actually, the surface density² of Cu per nm² was around 8 atoms/nm for a weight percentage of copper higher than 8 wt%, calculated by considering an average surface area of the catalyst of 20 m².g⁻¹. A monolayer of copper had a surface density around 8 atoms/nm²² which meant that the catalyst's surface might be saturated by copper and ZnO might be inaccessible. As shown in scheme 4-2, the catalyst was bifunctional and the first step of the mechanism involved the acidic properties of ZnO. That was why, if the surface of the support was highly charged with copper, the interaction between the molecules of glycerol and ZnO particles decreased leading to a decrease in the glycerol conversion.

An important point to mention was that all catalysts were highly selective (> 90%) towards 1,2-PDO as shown by GC (see appendix 10) and the remaining 10% was mainly EG and traces of ethanol and unknown product. This was in agreement with the literature^{3,4} where Cu/ZnO were known to exhibit high selectivity to 1,2-PDO under these reaction conditions, as shown in chapter I (Table 1-8).

In the same paper cited above, showing the formation of the copper nitrates after DPU, the effect of the weight percentage of copper in the solution during synthesis was also studied for Cu/TiO₂¹ and authors observed an increase in the copper crystallite size with the increase in the copper weight percentage. It was a common phenomenon and we got the same results.

The effects of copper weight percentage on catalyst properties and structures were then studied in depth using the "20.8 mM Cu²⁺ concentration" series (in grey in Table 4-2). As we could not find a published work dealing with the effect of the precursor concentration in the solution at the same weight percentage, the effect of [Cu²⁺] will then be discussed in more details for 10 wt% Cu/ZnO.

1.1. Effect of Cu⁰ weight percentage

Table 4-3 summarizes data on elemental copper analysis, specific surface area, size of ZnO and Cu⁰ crystallites of catalysts prepared with a Cu²⁺ concentration of 20.8 mM and different copper weight percentage.

Table 4-3: Characteristics of the catalysts synthesized at 20.8 mM of Cu²⁺

Cu _{theo} (wt%)	Cu _{exp} (wt%)	S.S.A. (m ² .g ⁻¹)	ZnO Size (nm)		Cu ⁰ Size (nm)		Conversion (%)	Selectivity (%)	
			B.T.	A.T.	B.T.	A.T.		1,2 PDO	EG
2.5	2.3	18	58	55	13	20	2	99	1
5	4.9	22	51	51	13	21	10	92	8
10	9.7	22	46	54	15	20	25	90	10
15	15.5	20	45	67	14	45	22	91	9
20	19.2	18	48	69	20	35	15	91	9

(B.T. : before test and A.T. : after test)

As we already observed, the copper weight percentage measured by ICP corresponded to the theoretical percentage indicating the total copper deposition on ZnO. With regard to the specific surface area of the catalyst, there was no change to note since all catalysts were prepared with the same commercial support having a surface area around 13 m².g⁻¹. In the last stage of catalyst elaboration, the specific surface area increased to an average of 20 m².g⁻¹ due to copper deposition and heat treatment.

Figure 4-4 shows the XRD diffractograms of the Cu/ZnO materials before catalysis with a zoom on the main Cu⁰ peaks. Sizes of the ZnO crystallites before catalysis were between 45 and 58 nm in accordance with the size of the starting support (50 nm) indicating no sintering during catalyst synthesis. Intensities of ZnO peaks were not affected by the change in copper weight percentage but the size of the crystallite decreased slightly from 58 nm at 2.3 wt% to 48 nm at 19.2 wt% of copper. For copper contents less than or equal to 15 wt%, the size of Cu⁰ crystallites (C.S.) before catalysis was constant (ca. 14 nm). On the other hand, at 20 wt%, the size of Cu⁰ crystallites increased from 14 to 20 nm. When the weight percentage of copper was high (19.2 wt%), there were not only an increase in the size of the crystallite, but also in the intensity of the Cu⁰ peaks.

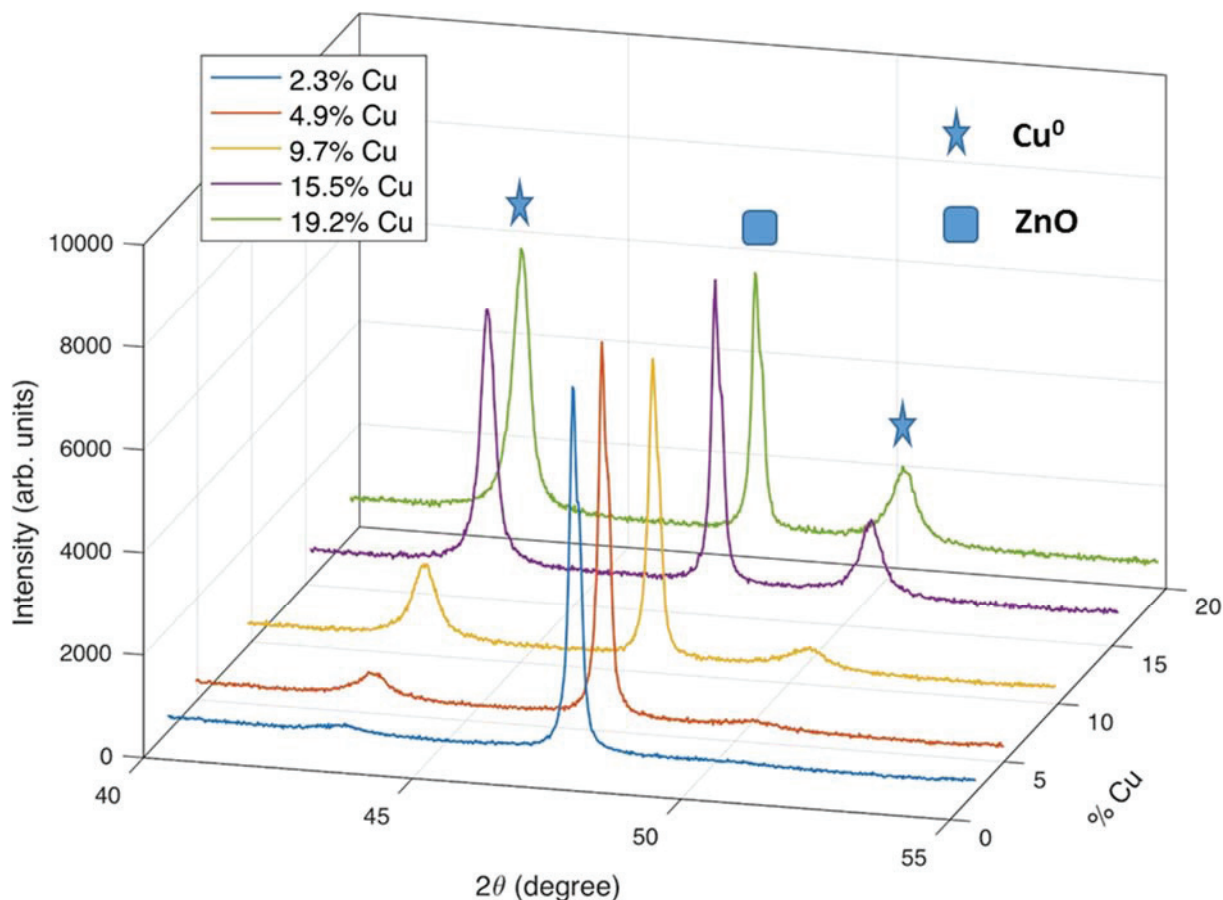


Figure 4-4: XRD diffraction patterns of Cu/ZnO with different copper weight percentage

The increase in crystallite size for a high copper charge has been reported in several studies using different preparation methods. Karelavic et al. have prepared Cu/ZnO by wet impregnation and obtained Cu^0 crystallites from 25 to 35 nm at 3 and 15 wt% of Cu, respectively.⁵

The evolution of the conversion and selectivity to 1,2-PDO versus time are shown in Figure 4-5. For all the catalysts the conversions were low with a maximum of 25% after 24 h for 10%Cu/ZnO. These catalysts had identical kinetic profiles, with a linear increase in conversion with the increase in reaction time (Figure 4-5) suggesting a zero order reaction. The coefficient R^2 of the equation was greater than 0.99 for all catalysts.

At low conversion (2 %; associated with 2.3%Cu/ZnO), 1,2-PDO was the only product detected by GC analysis; the selectivity is presented in Figure 4-5 by the grey curve. The selectivity toward 1,2-PDO was high for all the other catalysts ($\geq 90\%$) with selectivity toward EG $\leq 10\%$

(black curve, Figure 4-5).

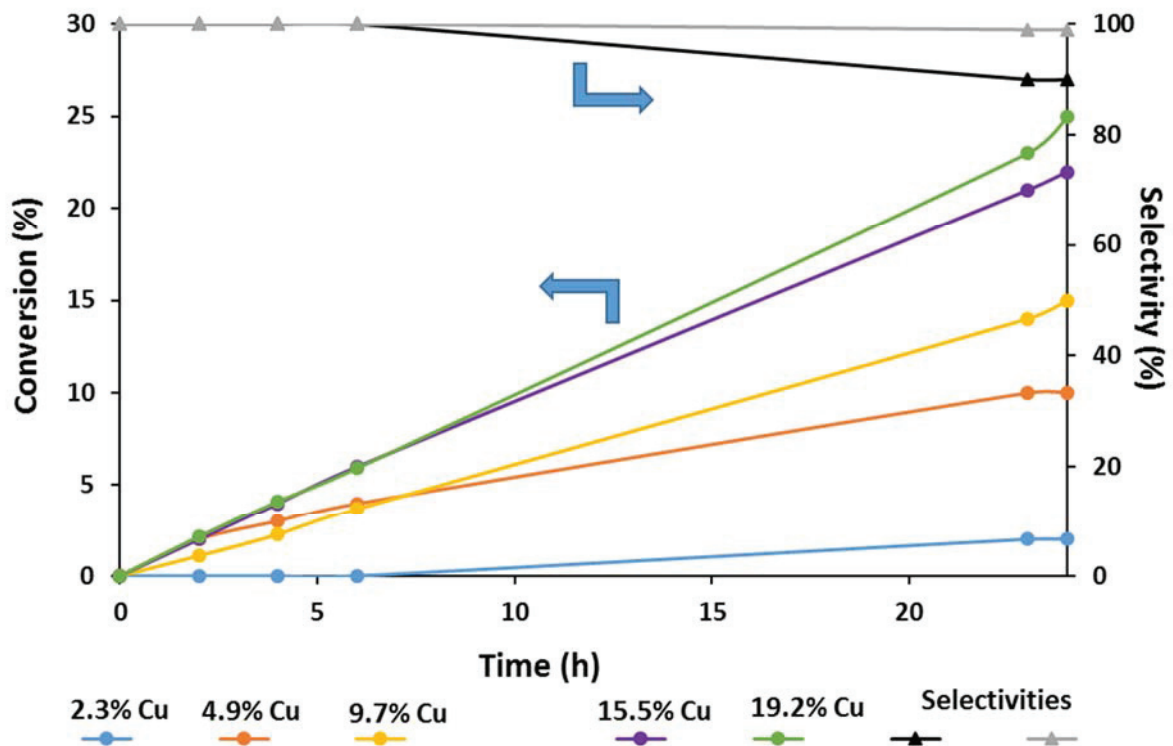


Figure 4-5: Conversion and selectivity in function of time for Cu/ZnO with different copper weight percentage. Grey curve: selectivity for 2.3%Cu/ZnO; black curve: selectivity for the other catalysts

It would therefore appear that between 15 and 20 wt% of copper, copper particles saturate the catalyst surface, resulting in a drop in conversion. Since the support played a major role in this reaction by hydrolyzing glycerol to acetol in a first step, as we already concluded, saturation of its surface led to a decrease in reaction rate. Another factor contributing to this low conversion was the sintering of copper and ZnO particles. Indeed, Figure 4-6 shows the diffractograms associated with 2.3%Cu/ZnO and 19.2%Cu/ZnO after test. The crystallite sizes after reaction were reported for all the catalysts in Table 4-3. For the catalysts with low Cu loading, the crystallites did not show any strong structural changes. However, for the catalysts with 15 and 20 wt% of copper, the crystallite sizes showed a greater sintering of ZnO and, more specifically, Cu⁰ nanoparticles.

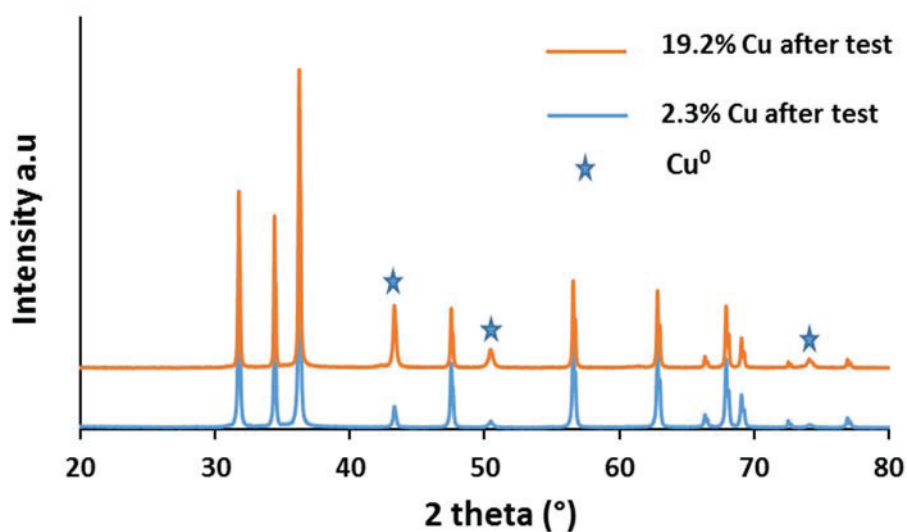


Figure 4-6: XRD patterns of Cu/ZnO at 2.3 wt% and 19.2 wt% after catalysis

This behavior was reported by Gao et al. ⁶ who demonstrated that increasing the Cu/Zn molar ratio from 0 to 1.86 led to an increase in glycerol conversion from 0 to 48% followed by a decrease to 33% with increasing copper content. Nevertheless, selectivity towards 1,2-PDO increased continuously up to 67% with increasing copper content. The results published by the authors are listed in Table 4-4.

Table 4-4: Effect of Cu/Zn molar ratio on the conversions and selectivities of the catalysts from reference 6.

Cu/Zn (molar ratio)	Glycerol conversion (mol%)	Selectivity (mol%)					
		1,2-PDO	Acetol	1-PO	EG	Et-OH	Me-OH
ZnO	/	/	/	/	/	/	/
0.39	15.8	42.3	51.2	0.1	1.7	0.3	0.3
1.08	25.2	41.8	49.1	0.1	2.3	0.2	0.3
1.86	47.9	50.4	29.8	0.1	2.3	0.6	0.5
3.01	43.1	53	29.1	0.3	5.7	0.9	0.7
4.03	41.9	57.8	28	0.2	4.5	0.7	0.7
4.88	33.1	67.6	17.9	0.2	5.3	0.5	0.6
CuO	9.8	40.5	52.7	/	3.3	0.5	0.6

At this point of our study, it would therefore be desirable to investigate the impact of the concentration of the copper precursor solution for the same final content of 10 wt%, which led, under our experimental conditions, to the best glycerol hydrogenolysis Cu/ZnO catalyst.

1.2. Effect of Cu²⁺ concentration

In the following section, the two catalysts studied are at the same percentage by weight of copper (10 wt%) but synthesized with different Cu²⁺ concentrations (20.8 and 81.6 mM). They are labeled by the weight percentage and the first number of their concentrations (10%Cu/ZnO_{com-2} designates the catalyst at 10 wt% of copper synthesized with [Cu²⁺] = 20.8 mM). The characteristics and the catalytic results obtained with these two catalysts are summarized in Table 4-5.

Table 4-5: Characteristics of 10%Cu/ZnO catalysts synthesized with [Cu²⁺] of 20.8 mM and 81.6 mM.

Catalyst	ZnO C.S. (nm)		Cu ⁰ C.S. (nm)		Conversion (%)	Selectivity (%)	
	B. T.	A. T.	B. T.	A. T.		1,2-PDO	EG
10%Cu/ZnO _{com-2}	46	54	15	20	25	90	10
10%Cu/ZnO _{com-8}	55	55	11	40	16	98	1

(B.T : before test and A.T : after test)

XRD diffractograms shown in Figure 4-7 for catalysts before catalysis showed fairly similar crystallite sizes for ZnO and Cu⁰. 10%Cu/ZnO_{com-8} has an average size of ZnO crystallites of 55 nm which was slightly larger than with 10%Cu/ZnO_{com-2} (46 nm) but Cu⁰ was smaller with an average size of 11 nm with 10%Cu/ZnO_{com-8} instead of 15 nm with 10%Cu/ZnO_{com-2}.

The two catalysts did not have the same behavior for the hydrogenolysis of glycerol. 10%Cu/ZnO_{com-2} showed a higher conversion (25%) versus 16% for 10%Cu/ZnO_{com-8}. In order to understand the difference in catalyst activity, since no significant difference could be observed for freshly prepared catalysts, the same characterizations were made for catalysts after use (mentioned as after test). The catalyst characterized after test was simply recovered by filtration and dried in an oven at 80 °C under air overnight.

The XRD diffractograms after catalysis presented in Figure 4-7 showed the appearance of a new phase containing carbon, (Cu,Zn)₅(CO₃)₂(OH)₆ (PDF 00-038-0154 appendix 11), for 10%Cu/ZnO_{com-2}. This observation meant that a C-C cleavage occurred during the catalytic reaction. To our knowledge, few studies showed what happened to the catalyst after test and if they did, they conducted thermal treatment before characterization. Recently, Biswas group ⁷ published an article showing the change in the nature of the catalyst by XRD after testing

their catalyst (Cu-Zn/MgO) without being retreated for the same catalytic reaction. The question of whether or not the new phase was carbonaceous was not discussed in this article. However, some peaks were not attributed and the mention of methanol as a by-product indicated a C-C cleavage. In our case, ethylene glycol and traces of ethanol and methanol (less than 0.001 M) were detected by GC analysis for the most efficient catalyst (10%Cu/ZnO_{com-2}), confirming C-C cleavage under our experimental conditions. The phase containing carbon was not observed after reaction for the less active 10%Cu/ZnO_{com-8}.

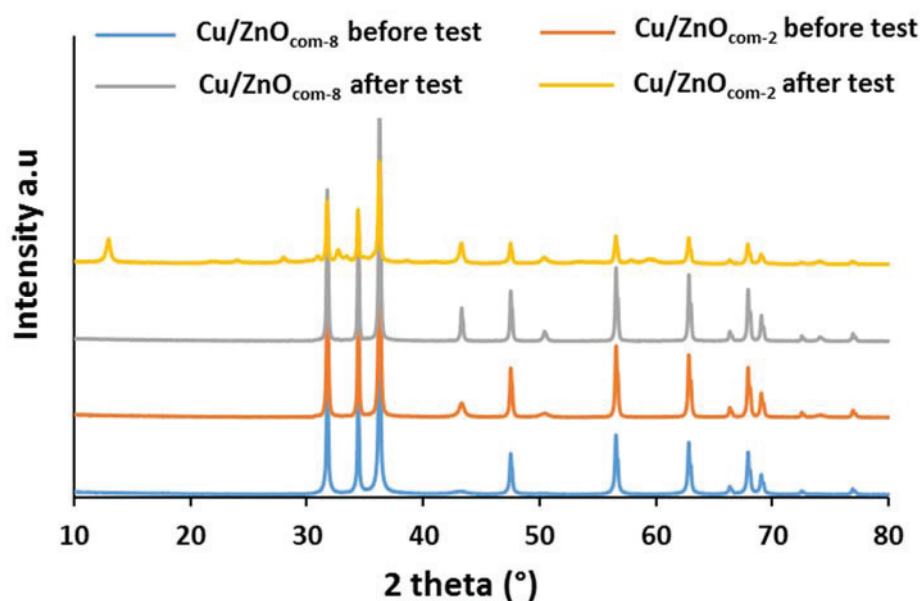


Figure 4-7: XRD patterns of 10%Cu/ZnO before and after catalysis

The lower conversion obtained for 10%Cu/ZnO_{com-8} could be explained by the sintering of copper particles during reaction. The size of Cu⁰ crystallites increases from 11 to 40 nm for 10%Cu/ZnO_{com-8} compared to a slight increase from 15 to 20 nm for 10%Cu/ZnO_{com-2}. The sintering of copper particles during reaction was a common phenomenon for copper-based catalysts and has been reported by many groups. In the article of Bienholz et al.,⁸ copper particle size increases from 15 nm before catalysis (CuO/ZnO) to 40 nm after catalysis (Cu/ZnO) for the same catalytic reaction with 46% of conversion after 7 hours of reaction.

The TEM images of the catalysts before catalysis (Figure 4-8 a for 10%Cu/ZnO_{com-2} and Figure 4-8 b for 10%Cu/ZnO_{com-8}) showed a similar particle size for both concentrations, although it was difficult to measure it because copper and ZnO could not be easily distinguished by TEM

due to their close atomic number. But the overall size and morphological aspect of the two catalysts were similar.

TEM images of catalysts after reaction, in agreement with XRD data, showed significant differences in morphology in two aspects. 10%Cu/ZnOcom-₂ (Figure 4-8 c) exhibited lamellar structures characteristic of Layered Double Hydroxides (LDH) while for 10%Cu/ZnOcom-₈, the sintering of copper nanoparticles was clearly visible (Figure 4-8 d).

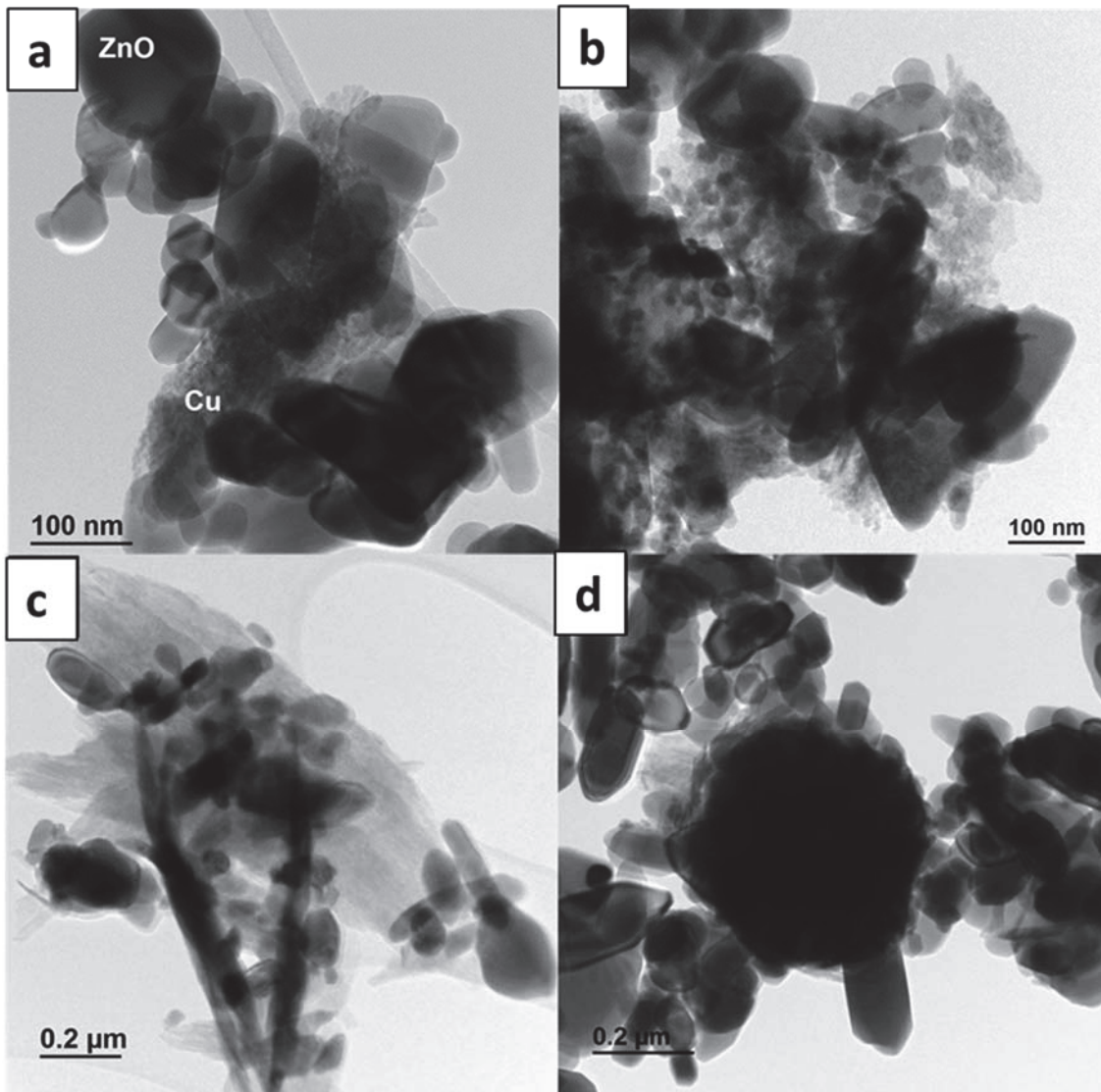


Figure 4-8: TEM images of 10%Cu/ZnO catalysts: a,c) 10%Cu/ZnOcom-₂ b,d) 10%Cu/ZnOcom-₈ before and after catalysis, respectively

The TGA curves of the catalysts before catalysis in Figure 4-9 showed a similar thermal behavior, in terms of weight loss. A slight shift in thermal events to higher temperatures could

be noted for 10%Cu/ZnO_{com-8}. Theoretically, no weight loss should be recorded because the catalysts were already calcined at 400 °C and reduced at 300 °C and the TGA was performed under nitrogen. Nevertheless, the weight gain after 300 °C could be attributed to the contamination of the TG gas line with O₂ leading to CuO_x. Then, the weight remained constant until high temperatures (900 °C) where some carbon species could be degraded, contributing to the small weight loss of 2%. From a global point of view, these two catalysts with 10% by weight of copper were thermally stable up to 900 °C.

The TGA curves also showed differences in thermal behavior between the two catalysts after reaction. As shown in Figure 4-9, for 10%Cu/ZnO_{com-8} the data were very close to those of the starting catalyst. However, for 10%Cu/ZnO_{com-2} there was a significant and unprecedented loss of weight of about 11% between 200 and 600 °C, confirming the presence of CO₃ and OH on the used catalyst.

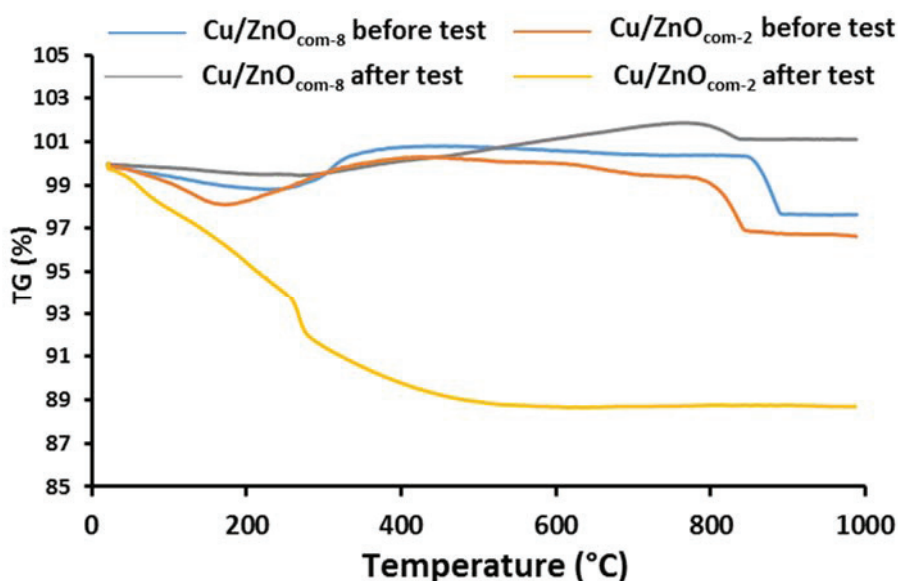


Figure 4-9: TGA curves under nitrogen of Cu/ZnO catalysts at 10 wt% of Cu⁰ before and after catalysis

To conclude on the commercial ZnO as a support for Cu/ZnO catalysts for glycerol hydrogenolysis, under our experimental conditions:

- The small specific surface area of the support led to deactivation of the catalyst for

copper loads greater than 10 wt% due to sintering of the copper particles during catalysis and saturation of the surface.

- The increase in the concentration of the Cu²⁺ precursor solution allowed a better dispersion of copper nanoparticles, resulting in smaller copper crystallite size, but this did not assure a higher activity at higher copper weight percentage.

- When highly active, C-C bond cleavages occurred and it was accompanied by a structural change of the catalyst after reaction.

- At low conversion (2%), the catalyst was highly selective (99%) towards 1,2-PDO while at higher conversion (25%), selectivity decreased to 90% with the appearance of ethylene glycol.

We have then decided to study the different ZnO-PAAX hybrid systems (X = 2, 5, 100) with high specific surface area, described in chapter 3, as supports instead of commercial ZnO, using the optimal concentration of Cu²⁺ (20.8 mM).

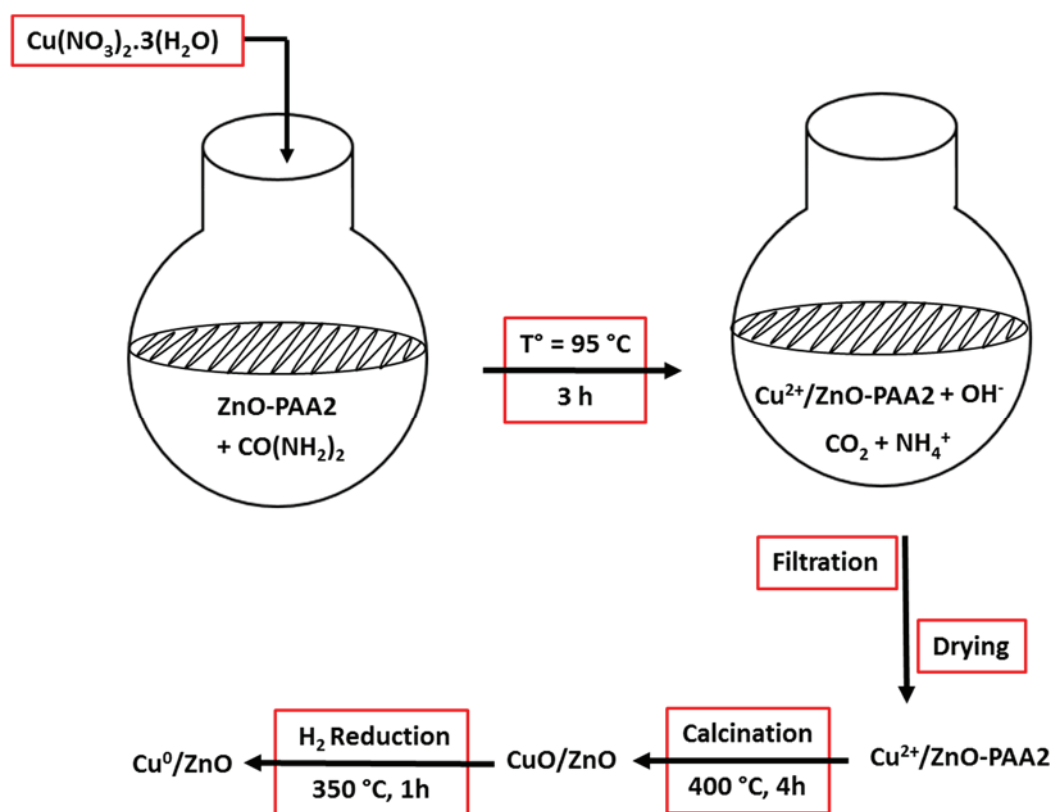
II. ZnO-PAAX (X = 2, 5, 100) as supports

II.1. ZnO-PAA2 non calcined

The catalysts were prepared from a non-calcined ZnO-PAA2 support, washed with 90 mL EtOH and by adding copper according to the DPU method described in the upper section, with [Cu²⁺] = 20.8 mM. We will address the effect of the synthesis temperature of the support and the weight percentage of copper loaded on the different support on the catalytic conversion of Cu/ZnO-PAA2 catalysts.

II.1.1. Effect of the synthesis parameters (support and copper wt%)

The catalysts were synthesized with different wt% of Cu, using different hybrid ZnO supports, following scheme 4-3 identical to the DPU method described in the first section with the commercial ZnO.



Scheme 4-3: Synthesis of Cu/ZnO catalysts by DPU of copper on hybrid non-calcined ZnO-PAA2

Table 4-6 presents some of the properties of the catalysts, as well as the conversion and selectivity at 24 h. The ZnO-PAA2 were synthesized at different temperature (0, 10, RT and 40 °C). The specific surface areas presented in Table 4-6 were for the support after drying. After DPU, calcination and reduction, all the catalysts exhibited the same specific surface area of about 25 m².g⁻¹. The difference in specific surface area for supports synthesized at the same temperatures came from the reproducibility problems when elaborating the ZnO supports, as discussed in Chapter III, because the supports were not synthesized at the same time.

The catalysts are labelled XCu/ZnO-PAA2_{y-z} where X is the theoretical weight percentage of copper, y is the temperature of synthesis of the support and, when needed, z is the number of the experiment (to differ between two catalysts having the same loading of copper and the same synthesis temperature of support but not produced from the same batch). For example, 10Cu/ZnO-PAA2₀₋₂ is the catalyst prepared with 10 wt% of copper, with a support elaborated at 0 °C and different from 10Cu/ZnO-PAA2₀₋₁.

The selectivities towards 1,2-PDO were similar for all the catalysts, independently of the support. It went from 98% towards 1,2-PDO at low conversion, down to 86-90% at high

conversion. Ethylene glycol was formed as a by-product.

When comparing the effect of the copper percentage on the conversion, we noticed an increase in the conversion with the increase of copper loading under the same parameters till 20 wt% of copper. This was attributed to the higher ratio $n_{\text{Cu}}/n_{\text{glycerol}}$ at higher loading of copper since the catalytic reaction conditions were the same for all the catalysts (weight of catalyst and glycerol loading). 20Cu/ZnO-PAA2_{RT-1} and 20Cu/ZnO-PAA2_{RT-2} had very similar properties: The two batches of ZnO-PAA2 were synthesized at room temperature and exhibited very similar S.S.A. (80 and 82 m².g⁻¹). Moreover, Cu crystallite sizes were in the same range (19-21 nm) however both catalysts showed different conversions (44% vs. 55%) due to the difference in actual copper loading (18.0% vs. 21.2%). When comparing the catalysts based on support synthesized at 0 °C (Cu/ZnO-PAA2₀), Cu⁰ sizes were around 12 nm for 5, 10, and 20 wt% of Cu, and the conversion increased from 4% to 70% when increasing Cu loading. However, Cu crystallite size increased up to 20 nm when increasing the loading to 38 wt% (40Cu/ZnO-PAA2₀). This was associated with a decrease in conversion from 70% to 4%. The high copper load could have blocked the active sites on the ZnO and caused the activity to decrease compared to a lower weight percentage of copper. If we calculate the number of atoms of copper occupying the surface of ZnO-PAA2 with a SSA = 80 m².g⁻¹, 41.6 wt% of copper correspond to 8 atoms of Cu per nm² which was more or less the number of atoms before saturating the surface. The second main reason for this low conversion might be the deactivation of 40Cu/ZnO-PAA2₀ due to the sintering of copper particles during the catalysis as Cu⁰ increased from 20 nm to 40 nm.

Table 4-6: Properties of the support ZnO-PAA2, the catalysts Cu/ZnO-PAA2 and the associated catalytic results after 24h.

Catalyst	S.S.A. / BET (m ² .g ⁻¹)	Cu ⁰ size (nm)		Cu _{exp} (wt%)	Conversion /24hrs (%)	Selectivity (%)	
		B. T.	A. T.			1,2-PDO	EG
5Cu/ZnO-PAA2 ₀	80	12	12	5.5	4	98	2
10Cu/ZnO-PAA2 _{RT}	72	15	40	9.8	13	93	7
10Cu/ZnO-PAA2 ₀	86	13	14	10.2	48	90	11
20Cu/ZnO-PAA2₀	105	12	16	19.3	70	87	12
20Cu/ZnO-PAA2 ₁₀	91	15	18	20.9	60	89	11
20Cu/ZnO-PAA2 _{RT-1}	82	19	22	18.0	44	86	13
20Cu/ZnO-PAA2 _{RT-2}	80	21	25	21.2	55	88	12
20Cu/ZnO-PAA2 ₄₀	37	21	26	21.0	27	89	11
40Cu/ZnO-PAA2 ₀	86	20	40	37.9	4	94	6

(B.T. : before test and A.T. : after test)

An important result was the possibility of depositing a very high copper charge, about 38 wt%, on the surface of such supports. Unfortunately, catalyst activity decreased strongly for this high loading, but this could be beneficial for other catalytic reactions where ZnO had no role in the reaction mechanism. Compared to commercial ZnO, the same phenomenon was observed but at lower copper loading (15 wt%) due to its lower specific surface.

Regarding the effect of the synthesis temperature of the support. If we compared 10Cu/ZnO-PAA2_{RT} and 10Cu/ZnO-PAA2₀, the support specific surface area and the Cu dispersion were slightly higher for the second one. The catalyst with the support synthesized at 0 °C was more active (13% vs. 48% of conversion). The same trend was observed for the catalysts with 20 wt% of copper. Comparing the support synthesized at 0 °C (20Cu/ZnO-PAA2₀), 10 °C (20Cu/ZnO-PAA2₁₀), RT (20Cu/ZnO-PAA2_{RT}) and 40 °C (20Cu/ZnO-PAA2₄₀), when the temperature decreased, the specific surface area increased (37, 80, 91, 105 m².g⁻¹), and the crystallite size decreased (from 21 to 12 nm). This resulted in an increase in the conversion, from 27% to 70%. If we looked back to the effect of the synthesis temperature on the NPs of ZnO, the main difference laid in the morphology of the material. It appeared that the presence of 2D nano-sheets at low temperature generated a higher dispersion of Cu particles than the support synthesized at high temperature.

Figure 4-10 shows the XRD diffractograms after reaction of the two catalysts 10Cu/ZnO-PAA2₀ and 10Cu/ZnO-PAA2_{RT} synthesized at 0 °C and RT (20-25 °C), respectively. The main difference laid in the size of the copper nanoparticles after the reaction and in the appearance of the new phase for the catalyst with the highest conversion as already observed with 10%Cu/ZnO_{com-2}. 10Cu/ZnO-PAA2₀₋₁ showed a conversion of 48% with no increase in the copper crystallite size after reaction while 10Cu/ZnO-PAA2_{RT-1} displayed 13% of conversion and a drastic sintering of copper crystallite from 15 to 40 nm. Once again, the phase containing carbon was associated with good activity (48% conversion) and cleavage of C-C bonds. Selectivity at 1,2-PDO was 90% and the main by-product was ethylene glycol.

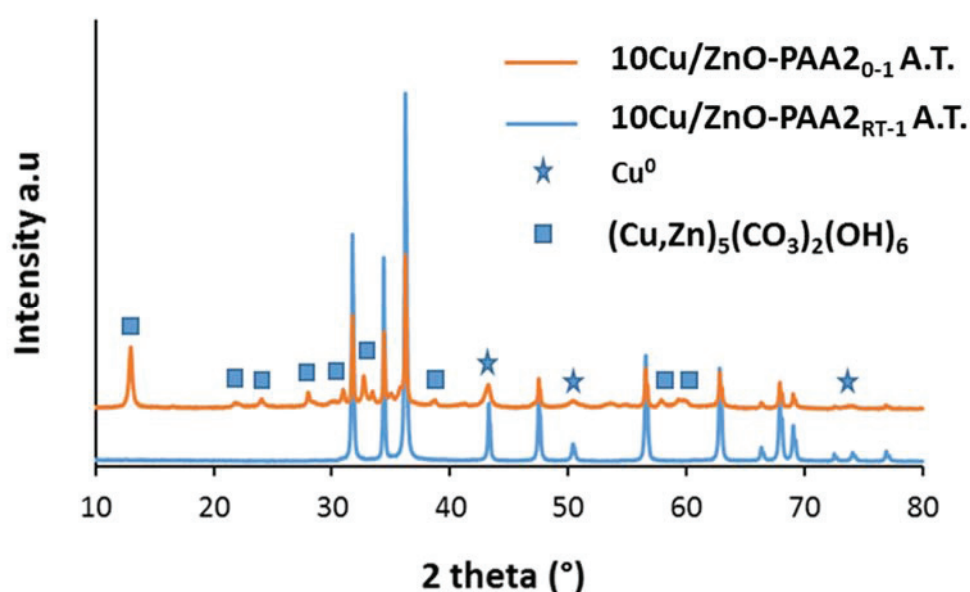


Figure 4-10: XRD diffraction patterns of 10Cu/ZnO-PAA2_{RT-1} and 10Cu/ZnO-PAA2₀ after catalysis

It was difficult to uncorrelate the influence of the different factors on the conversion, i.e. the temperature of the supports, the specific surface area of the supports, the Cu charge and the size of the Cu crystallites, because they were all interdependent. Generally, the increase in the specific surface area of the support led to a decrease of the deposited metal particle size and an increase in glycerol conversion. The most active catalyst, with a 70% glycerol conversion after 24 hours of reaction at 30 bar of hydrogen and 200 °C, was the one synthesized with ZnO elaborated at 0 °C and loaded with 20 wt% of copper (20Cu/ZnO-PAA2₀) which was also the one with the highest specific surface area of 105 m².g⁻¹. This remarkable value in terms of specific surface area for a ZnO-based system allowed a high dispersion of copper and the

achievement of the smallest Cu⁰ sizes around 12 nm.

Moreover, an increase in Cu loading was also associated with an increase in activity up to 20 Cu wt%. The results obtained showed that there was a compromise to be found in terms of copper percentage in order to accommodate both a reasonable amount of copper and a high dispersion.

Comparing the properties of Cu/ZnO_{com} to Cu/ZnO-PAA2, the two families of catalysts showed similar copper crystallite size which ranged between 11 and 20 nm depending on the copper weight percentage. However, under the same conditions, the conversion was always higher when the support used was the one developed instead of the commercial one.

II.1.2. Effect of the weight of the catalyst

As the highest conversion was obtained at 20 wt% of copper and 20.8 mM Cu²⁺ with ZnO-PAA2 synthesized at 0 °C and washed with 90 mL of EtOH (20Cu/ZnO-PAA2₀, Table 4-6), the synthesis was up-scaled from 1 gram of catalyst to 3 grams. Two catalysts were synthesized using two different batches of ZnO/PAA2 supports, synthesized under the above conditions. The Cu loading were determined by ICP and are included in Table 4-7 and the XRD diffractograms are shown in Figure 4-11. The main difference between the two reduced catalysts was the size of the Cu⁰ crystallites which was 20 nm for the 20.6 wt% Cu catalyst and 28 nm for the 19.8 wt% Cu catalyst.

Table 4-7: Cu loading, ZnO and Cu⁰ size for two batches of Cu/ZnO-PAA2 and their associated catalytic results after 24h using different mass.

Cu _{exp} (wt%)	Mass of catalyst (g)	ZnO size (nm)		Cu ⁰ size (nm)		Conversion (%)	Selectivity (%)	
		B. T.	A. T.	B.T.	A. T.		1,2-PDO	EG
20.6	0.3	21	39	20	38	15	96	4
	1	21	--	20	24	66	88	11
	1.5	21	35	20	25	73	85	14
19.8	0.5	21	38	28	30	32	99	1
	1	21	40	28	35	60	90	8
	0.5	21	33	28	29	12 (6h)	99	1

(--: not determined)

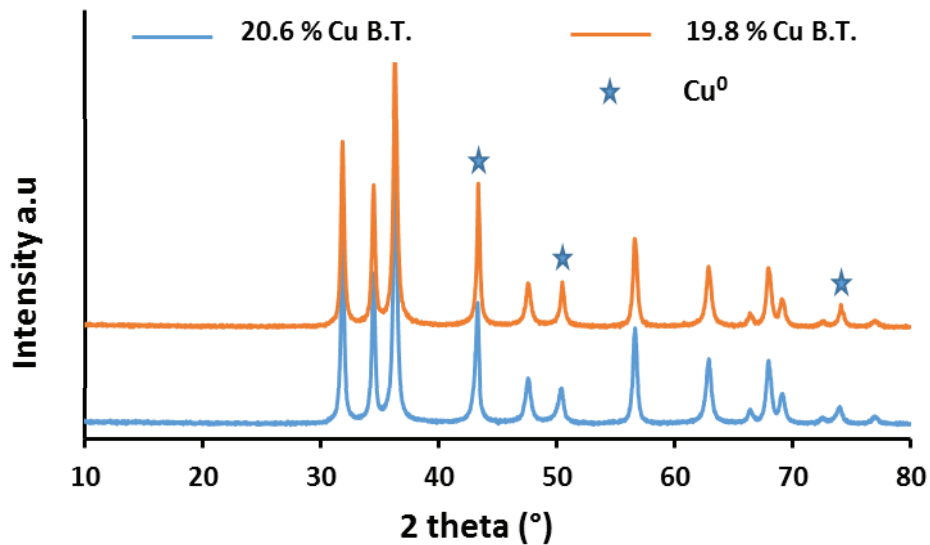


Figure 4-11: XRD patterns of Cu/ZnO catalysts with 19.8 wt % and 20.6 wt% of copper, before reaction

Two reactions were performed with 20.6%Cu/ZnO and 19.8%Cu/ZnO using 1 g under the same reaction conditions (0.23 M glycerol, under 30 bar H₂, 200 °C and 24 hours). Despite the difference in Cu main crystallite size, the two catalysts exhibited the same kinetic profiles up to 24 hours as shown in Figure 4-12 and a final conversion of ca. 63%. Figure 4-13 shows the XRD patterns associated with 20.6%Cu/ZnO and 19.8%Cu/ZnO after reaction using 1 g where the two catalysts exhibit the carbonic phase (Cu,Zn)₅(CO₃)₂(OH)₆. Another reaction was conducted with 1 g of 19.8%Cu/ZnO but this time the reaction was stopped after 6 h and the catalyst was recovered, dried and analyzed by XRD (Figure 4-13). After 6 hours of reaction, the catalyst was not showing any structural changes, the carbonic phase was not present. This confirmed the hypothesis that the phase was appearing at high conversion due to the formation of products resulting from C-C cleavage. However, after all the reactions, the ZnO crystallite sizes increased from ca. 20 nm to 33 nm (after 6h) and ca. 39 nm (after 24h). This showed that despite the thermal stability of the catalysts (as shown by TGA under N₂, Figure 4-9) the hydrothermal stability of the ZnO particles was limited.

Reactions were then conducted using 0.3 g, 0.5 g, 1 g and 1.5 g of the catalysts. We could observe an increase in conversion (from 15% to 73%) with an increase in mass, which was expected as the ratio $n_{\text{Cu}}/n_{\text{glycerol}}$ increased. This increase was proportional between 0.3 g and 1 g, however the result was lower than expected with 1.5 g. As before, the increase in

conversion was followed by a slight decrease of selectivity in 1,2 PDO.

The catalytic results obtained with 20Cu/ZnO-PAA2₀ synthesized in a batch of 1 g (Table 4-6) or 3 g (Table 4-7) were quite different (70% vs. 32%). Hence the up-scaling of the method of synthesis was accompanied with problems of reproducibility.

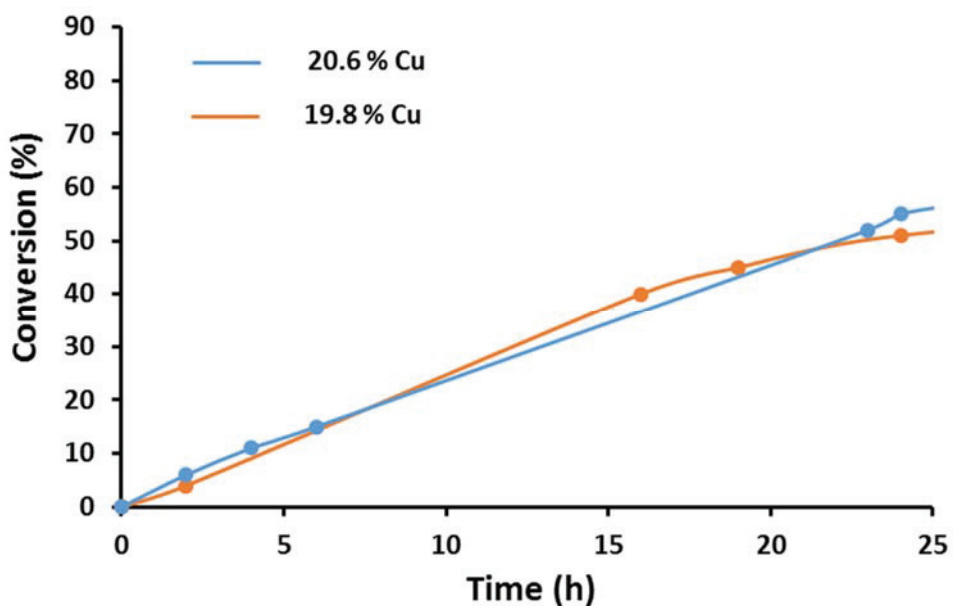


Figure 4-12: 24 hours' kinetic profile with 1g of 19.8%Cu/ZnO and 20.6%Cu/ZnO catalysts

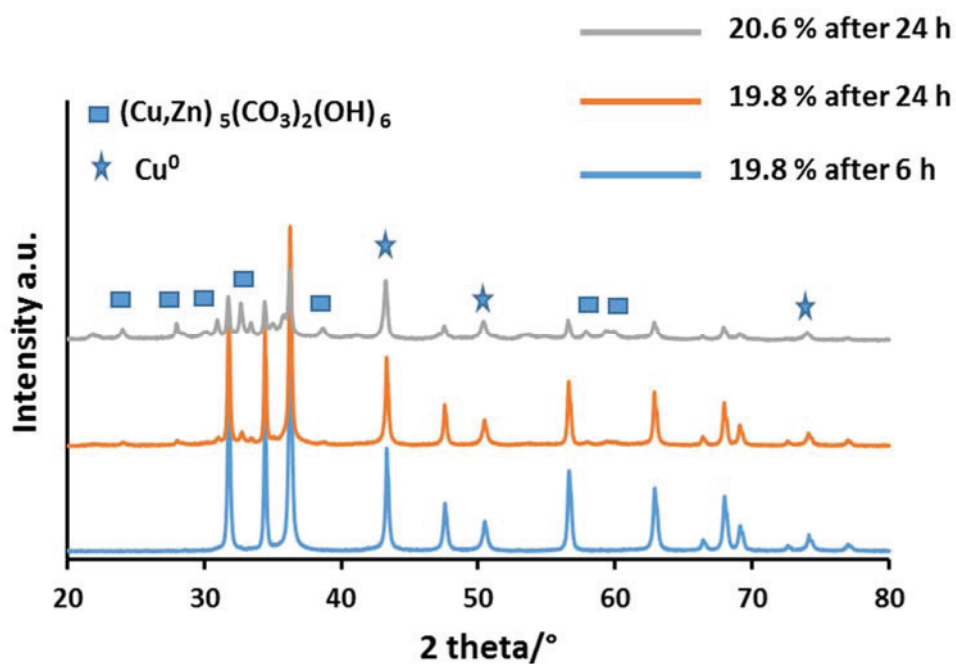


Figure 4-13: XRD patterns of Cu/ZnO catalysts with 19.8 wt % and 20.6 wt% of copper after reaction

II.1.3. Recyclability of Cu/ZnO-PAA2

The first recyclability test was carried out with 20Cu/ZnO-PAA2₀. The selected catalyst, the one with the highest activity indicated in Table 4-6 (section II.1.1.), was collected after a first reaction with 0.5 g, filtered and dried in an oven at 80 °C and reused without pre-treatment. Only 0.25 g was recovered from the first reaction but the ratio $n_{\text{glycerol}}/n_{\text{catalyst}}$ (7.8) was respected for the second reaction, by diluting the solution. While the fresh catalyst gave 70% conversion, its reuse led to a decrease to 34% conversion. It was difficult to know if the results were comparable, as even if the ratio $n_{\text{glycerol}}/n_{\text{catalyst}}$ was the same, the amount of substrate and catalyst were lower in the second reaction. Deactivation due to water molecules has been reported in different studies such as in the article by Jean et al.⁹ where the conversion decreased with increasing water content in glycerol solution with concentration varying from 80 to 100 wt% in water.

In order to conduct the recyclability test with the same mass, the catalyst in Table 4-7 (section II.1.2.) used for the reaction with 1.5 g was recovered. The conversion of this fresh catalyst was around 40 % for 0.5 g and 73% with 1.5 g (Table 4-8). The catalyst was recycled without pre-treatment and once again the catalyst was not as active as the freshly reduced one. The Table 4-8 shows the properties and the conversion of the recycled catalysts. The conversion decreased to 8 % and the selectivity toward 1,2-PDO decreased to 75 % while the selectivity toward EG increased till 22 % with appearance of many unknown products. In a second time, the used catalyst was calcined at 400 °C and reduced at 350 °C. The conversion was as expected 48 % instead of 8 % and the selectivity toward 1,2-PDO went back to its initial value of 90 %.

Table 4-8: Structural properties and activity of reused Cu/ZnO catalysts

Catalysts	ZnO size (nm)		Cu ⁰ size (nm)		Conversion / 24 hrs (%)	Selectivity (%)	
	B. T.	A. T.	B. T.	A. T.		1,2-PDO	EG
Fresh / 1.5 g	21	35	20	25	73	85	14
Reused / 0.5 g	35	46	25	26	8	75	22
Retreated and reused / 0.5 g	22	35	20	24	48	90	10

XRD diffractograms (Figure 4-14) showed that the catalyst after the first reaction (reused B. T.) and after the second reaction (reused A. T.) exhibited the same diffractograms, i.e. there was the presence of $(\text{Cu,Zn})_5(\text{CO}_3)_2(\text{OH})_6$ phase. However, after calcination and reduction, the retreated catalyst had the same structure as the fresh catalyst. This result meant that this Cu/ZnO catalyst could be regenerated and this was proven by maintaining the conversion at the same level. The catalyst reused without treatment was not very active, hence $(\text{Cu,Zn})_5(\text{CO}_3)_2(\text{OH})_6$ phase might be detrimental for the activity.

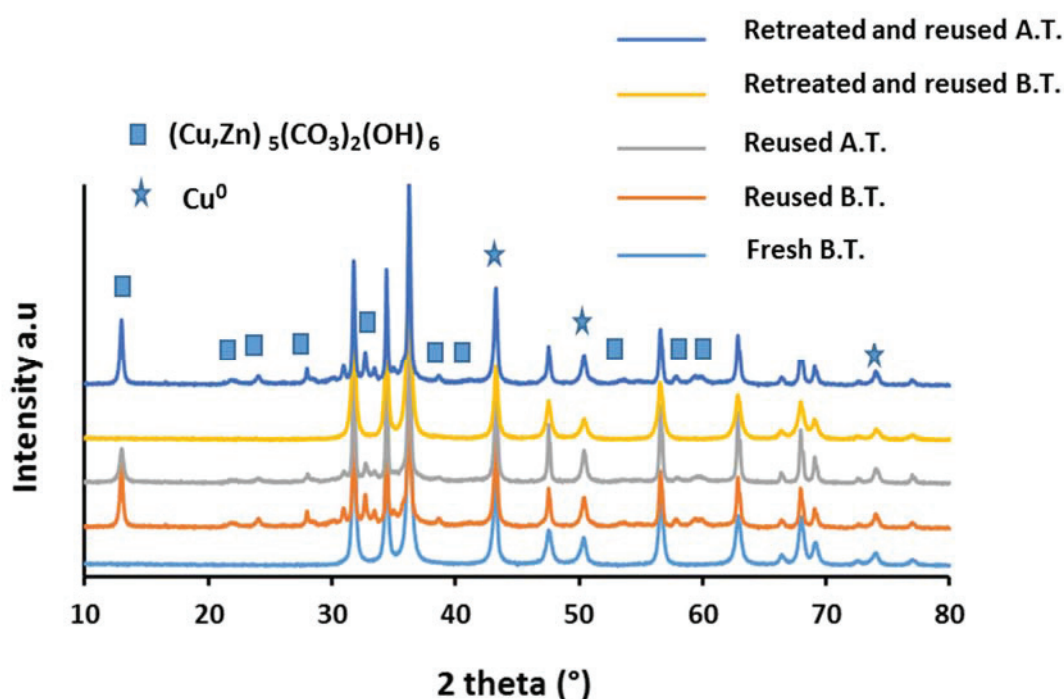


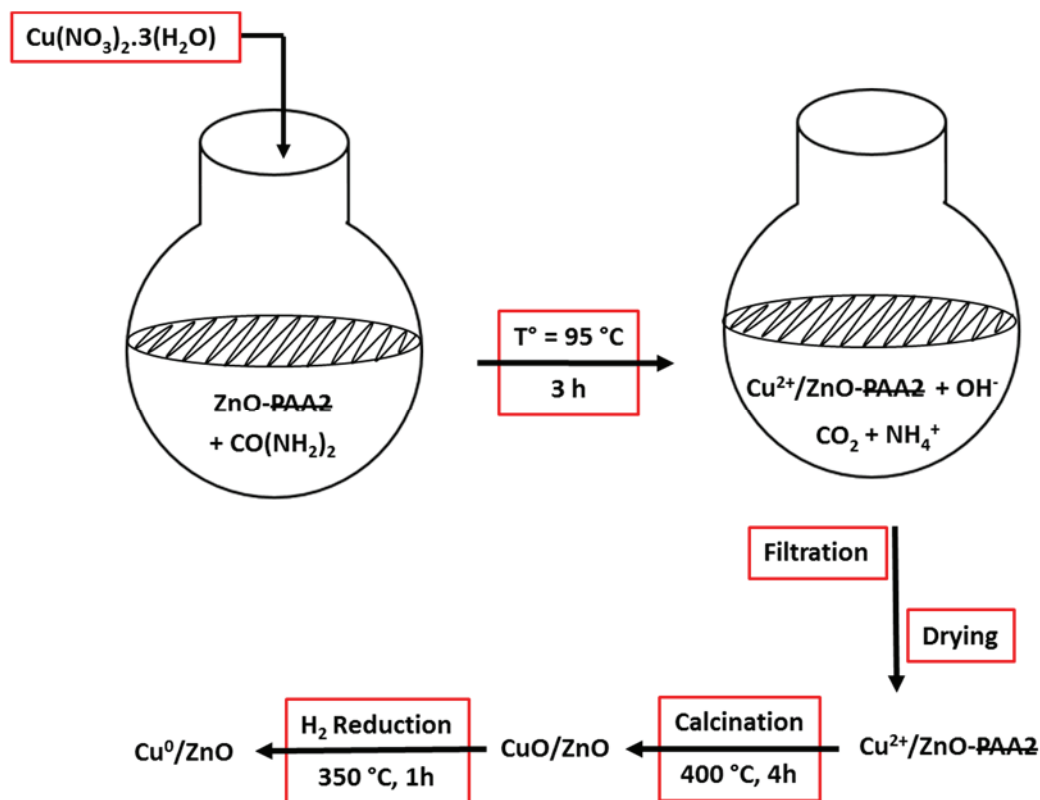
Figure 4-14: XRD patterns of the fresh and reused catalysts (20%Cu/ZnO-PAA2). (B.T. : before test and A.T. : after test)

Although the conversion results were excellent for some of the catalysts presented in section II.1, their reproducibility in term of S.S.A. of the support and Cu crystallite size were nevertheless sometime random which was time-consuming and difficult to manage. This major difficulty for rational application in catalysis seemed inherent to the use of the ZnO-PAA2 hybrid as support for Cu deposited by DPU method. To improve the reproducibility of the results, we have therefore decided to use ZnO-PAA2 supports calcined at different temperatures (300-400 °C) in the next section.

II.2. ZnO-PAA2 calcined

The table below summarizes the results obtained for glycerol hydrogenolysis using calcined ZnO-PAA2 supports synthesized at room temperature (the non-calcined ZnO-PAA2 is used as reference). The value of the specific surface area corresponded to the support before calcination. The supports were then calcined at 300, 325, 350 or 400 °C. The final catalysts were synthesized by depositing either 10 or 20 wt% of Cu. The specific surface area of the catalyst were not measured but the specific surface area of all the catalysts should be in the same range after calcination and reduction, around 25 m².g⁻¹, as in chapter II.1.1.

The DPU method was the same as before but the commercial ZnO and the ZnO-PAA2 were substituted that time by calcined ZnO-PAA2, noted ZnO-PAA2, as presented in scheme 4-4.



Scheme 4-4: Synthesis of Cu/ZnO catalysts by DPU of copper on calcined ZnO-PAA2

Catalysts are labeled according to the theoretical copper weight percentage and the calcination temperature of the support. For example, 10Cu/ZnO-PAA2₃₀₀ is the catalyst presented in the first entry of the table with a theoretical copper weight percentage of 10 wt% and prepared using the ZnO-PAA2 calcined at 300 °C.

Table 4-9: Effect of the calcination temperature of ZnO-PAA2 on the catalysts structural properties and the catalytic results

Entry	S.S.A. BET (m ² .g ⁻¹)	Cu ⁰ size (nm)		Cu _{exp} (wt %)	Conversion / 24 hrs (%)	Selectivity (%)	
		B. T.	A. T.			1,2-PDO	EG
10Cu/ZnO-PAA2 ₃₀₀	34	14	21	16.5	18	88	11
10Cu/ZnO-PAA2 ₃₂₅	57	15	18	16.4	18	87	13
10Cu/ZnO-PAA2 ₃₅₀	72	13	14	13.6	54	90	9
20Cu/ZnO-PAA2 ₃₅₀	80	24	30	23.4	35	90	10
10Cu/ZnO-PAA2 ₄₀₀	72	16	18	9.2	10	88	12
20Cu/ZnO-PAA2 ₄₀₀	80	19	21	22.1	55	88	12
20Cu/ZnO-PAA2 _{RT-2}	80	21	25	21.2	55	88	12

It was difficult to accurately manage the amount of final copper based on the speculated remaining organic weight loss, which was why the copper ICP results were far from the theoretical targets of 10 and 20 wt% of copper (Cu_{exp}, Table 4-9). Nevertheless, a comparison of the last two entries in the table showed that the catalyst based on a support calcined at 400 °C had a similar activity to the non-calcined support; their characteristics were identical. We could therefore deduce that the calcination of the support at 400 °C before DPU or at the end of the synthesis of the catalyst produced the same properties. Figure 4-15 shows the XRD of Cu/ZnO calcined at 400 °C with the highest conversion (20Cu/ZnO-PAA2₄₀₀) before and after test and compared to the reference catalyst 20Cu/ZnO-PAA2_{RT-2}. XRD patterns are showing the same phases and crystallite size for the two catalysts, before and after reaction.

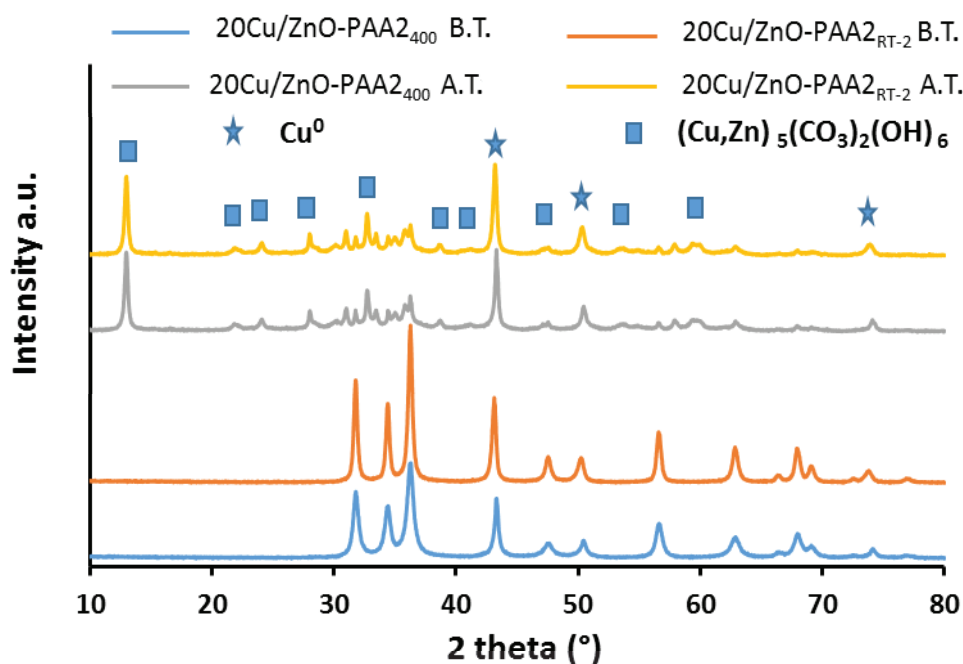


Figure 4-15: XRD patterns for 20Cu/ZnO-PAA2_{RT-2} and 20Cu/ZnO-PAA2₄₀₀ before and after catalysis. (B. T. : before test, A. T. : after test)

The lower conversion observed for 20Cu/ZnO-PAA2₃₅₀ in comparison with 20Cu/ZnO-PAA2₄₀₀ might be attributed to the higher Cu⁰ crystallite size. If we compared the effect of the temperature of calcination of the support with 10 wt%Cu, the best conversion of 54% after 24 hours of reaction was obtained for a support calcined at 350 °C (10Cu/ZnO-PAA2₃₅₀, in grey), associated with a low Cu⁰ size (13 nm) and a high specific surface area of the support (72 m².g⁻¹). Below 350 °C, the retention of a large quantity of organic matter did not seem to be favorable for good activity even with low Cu⁰ size (14-15 nm). The lower activity of 10Cu/ZnO-PAA2₄₀₀ compared to 10Cu/ZnO-PAA2₃₅₀ might be attributed to the larger Cu particles and the lower Cu loading. The selectivities toward 1,2-PDO and EG were almost the same for all the catalysts, 90% and 10% respectively.

In conclusion, the effect of the calcination of the support on the catalytic activity of Cu/ZnO seemed a little delicate because it was difficult to control the remaining organic content. Calcining the ZnO-PAA2 support at 400 °C appeared to be the best way to obtain a good conversion in agreement with the study on non-calcined supports and this in a more reproducible way. Indeed, different batch of 20Cu/ZnO-PAA2₄₀₀ were prepared and they exhibited the same structural properties and gave the same conversion (results not shown).

II.3. ZnO-PAA5 as support

II.3.1. Non Calcined ZnO-PAA5

As mentioned in Chapter III, the synthesis conditions and in particular the synthesis temperature could strongly influence the specific surface area of ZnO-PAA5 supports. 20 wt% of copper were deposited on ZnO-PAA5 synthesized at 0 °C, RT and 40 °C for the synthesis of catalysts. A fourth sample was synthesized with 10 wt% of Cu, on ZnO-PAA5 synthesized at room temperature. The samples were labeled as previously. As we mentioned in the previous chapter, the yield of ZnO-PAA5 obtained by sol-gel method was around 50 wt%. For that reason, the number of experiments done with that support compared to ZnO-PAA2 was lower.

The surface area associated with the support, the crystallite size of Cu before and after reaction, the Cu weight percentage, along with the catalytic results are included in Table 4-10. The results showed that the S.S.A. of the support and Cu crystallite size had little effect on the conversion of Cu/ZnO catalysts, the best conversion being obtained with 20Cu/ZnO-PAA5_{RT-2}, the catalyst having neither the highest specific surface area nor the smallest copper crystallite size. It was difficult at this stage to explain this lack of trend, but several observations could be made. First, despite extremely high specific surfaces (120-135 m².g⁻¹), the size of copper crystallites remained relatively important (18-20 nm). This could be explained by weak interactions between copper precursors and ZnO-PAA5. Therefore, the morphology of the support might affect the activity of the catalyst since at room temperature the ZnO-PAA5 was mostly spherical while at 40 °C it was aggregated in 2D nanosheets. It was worth noting that the catalyst obtained from the support synthesized at 0 °C was extremely selective with respect to the 1,2-PDO (99%) at high conversion (64%). This was not the case when using ZnO commercial or ZnO-PAA2. Hence, the combination of high surface area of the support and clean morphology (20Cu/ZnO-PAA5₀) led to 64 % conversion with almost total selectivity toward 1,2-PDO.

Total selectivity at high conversion when using copper based catalysts has been reported in few studies but in presence of organic solvents as in the article by Mizugaki et al.¹⁰ where authors used copper nanoparticles supported on AlO_x. The reaction conditions were the following: 0.35 mmol of glycerol with 25 mg of catalyst (0.19 mmol of copper), in presence of

5 mL of 1,4-dioxane as solvent after 6 hours of reaction under 10 bar H₂ pressure and 180 °C. The difference between our catalyst and the other Cu/ZnO catalysts reported could come from our original support ZnO-PAA5 which made it highly selective even in the presence of water.

Table 4-10: effect of the ZnO-PAA5 support on the Cu/ZnO activity.

Catalyst	S.S.A. / BET (m ² .g ⁻¹)	Cu ⁰ size (nm)		Cu _{exp} (wt%)	Conversion/ 24hrs (%)	Selectivity (%)	
		B. T.	A. T.			1,2-PDO	EG
20Cu/ZnO-PAA5 ₀	135	18	20	23.2	64	99	1
10Cu/ZnO-PAA5 _{RT-1}	49	15	24	10.8	48	88	11
20Cu/ZnO-PAA5 _{RT-2}	75	17	20	20.5	70	87	13
20Cu/ZnO-PAA5 ₄₀	120	20	25	19.9	56	89	11

(B.T. : before test and A.T. : after test)

Figure 4-16 shows the XRD diffractograms before and after catalysis using Cu/ZnO with the highest activity (20Cu/ZnO-PAA2_{RT-2}). The copper particles were not sintered after the reaction but once again, the phase (Cu,Zn)₅(CO₃)₂(OH)₆ was present at 62%, based on a semi-quantitative analysis.

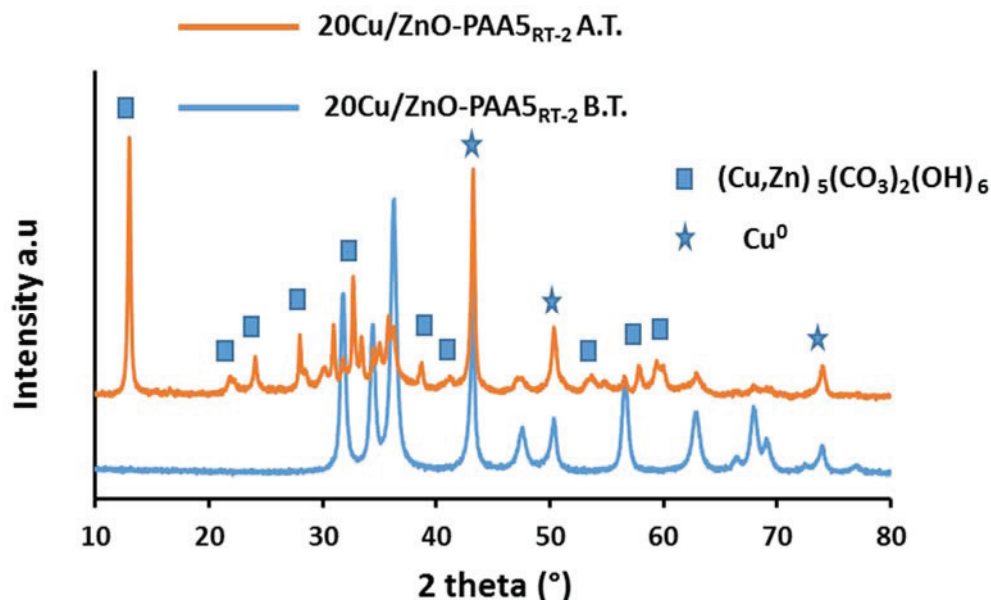


Figure 4-16: XRD of 20Cu/ZnO-PAA5_{RT-2} before and after test (B. T. = before test, A. T. = after test)

II.3.1. Calcined ZnO-PAA5

As with ZnO-PAA2, the effect of the calcination temperature of the support on the catalytic activity was studied. After being synthesized at RT, the supports were calcined at 300 °C and 350 °C. Since ZnO-PAA5 was already completely transformed after calcination at 350 °C, no calcination was conducted at 400 °C, in contrary to ZnO-PAA2.

The results are reported in Table 4-11. The conversions after 24 h were very low, 4 % and 27 % for 10 wt% and 17 wt% of copper, respectively, compared to non-calcined supports (48-70% of conversion; Table 4-10). The decrease in conversion might again be due to the morphological change of the support. The specific surface areas of the catalysts were not measured but should be around 20-30 m².g⁻¹ (cf Chapter 3, section I.5.2.). In any case, it appeared that the calcination of ZnO-PAA5 before copper deposition had a negative impact on catalyst activity.

Table 4-11: Effect of the calcination of the support ZnO-PAA5 on the Cu/ZnO catalytic results

Calcination temperature (°C)	Cu ⁰ size (nm)	Cu (wt %) ICP	Conversion / 24 hrs (%)	Selectivity (%)	
				1,2-PDO	EG
			300	13	17.0
350	17	10.3	4	95	5

For ZnO-PAA5, the catalyst activities were higher when the support was not calcined, which meant that the polymer (PAA5) played a beneficial role in depositing copper and it might either contribute to the formation of new active sites or it could help the Cu-ZnO interaction.

II.4. ZnO-PAA100 as support

Two catalysts were synthesized with ZnO-PAA100 at 10 and 20 wt% of copper. None activity were detected even with a material with high specific surface area (70 m².g⁻¹) and small copper crystallite size (11 nm) as shown in the Table 4-12.

Table 4-12: Properties and catalytic results of Cu/ZnO-PAA100

Synthesis temperature	S.S.A. / BET ($\text{m}^2\cdot\text{g}^{-1}$)	Cu ⁰ size (nm)	Cu ICP (wt %)	Conversion / 24 hrs (%)
RT	70	11	12.9	0.9
RT	49	13	22.4	1

After reaction, the XRD diffractogram (Figure 4-17) showed that the catalyst was unchanged which was linked to the inactivity of the catalyst. A slight increase in copper particle size occurred from 13 to 18 nm due to the reaction conditions.

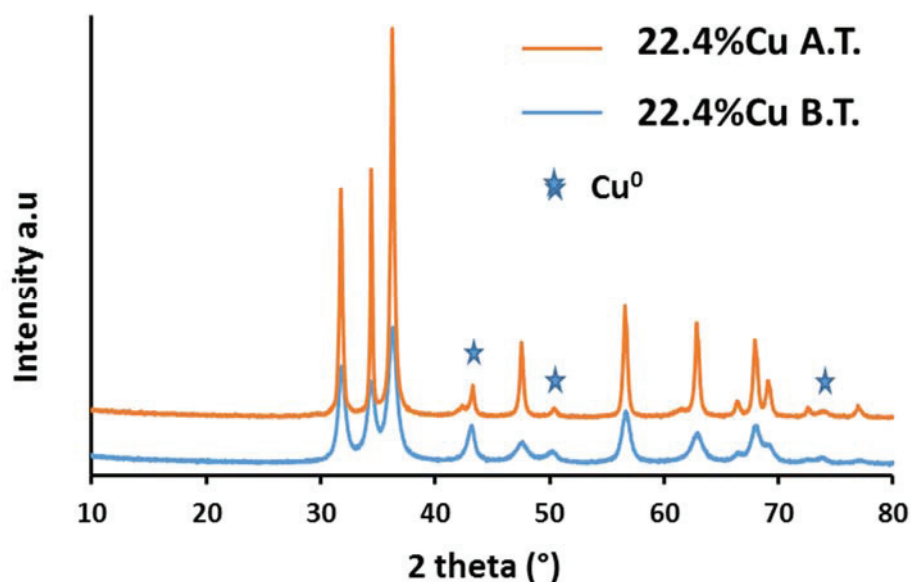


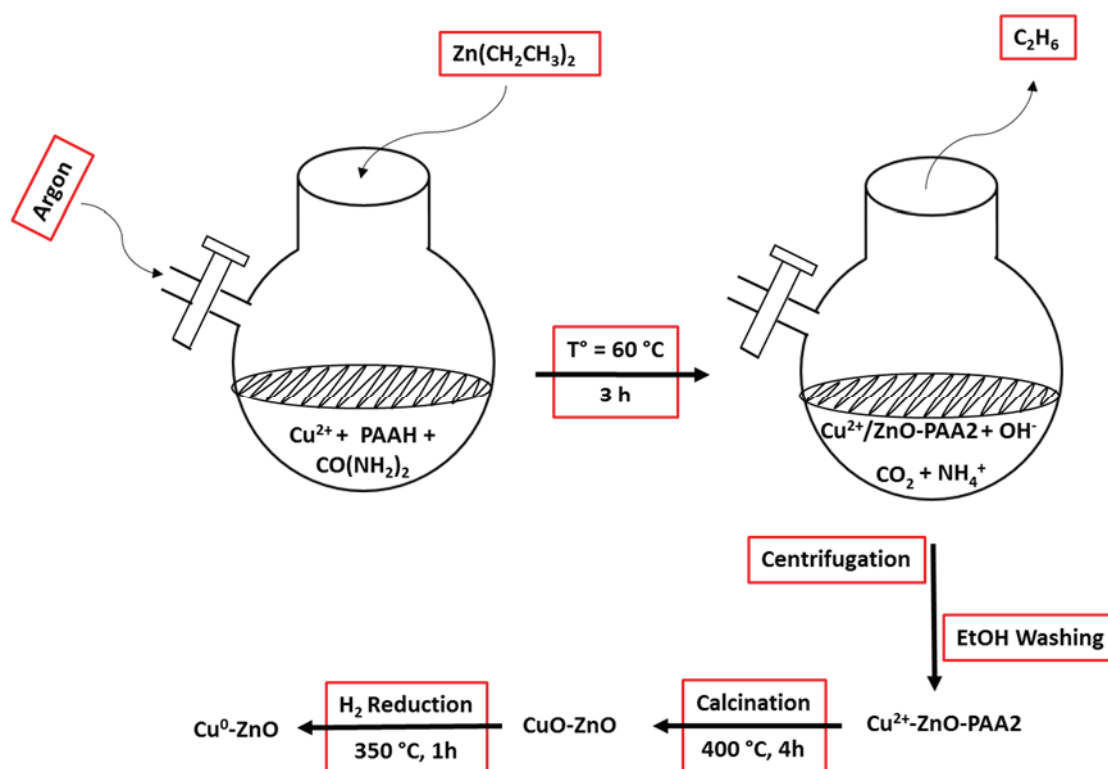
Figure 4-17: XRD diffraction patterns of 22.4%Cu/ZnO-PAA100 before and after reaction. (B.T. : before test and A.T. : after test)

III. Cu-ZnO by a “one pot” method

In order to save time and in an attempt to obtain reproducible Cu/ZnO catalysts, a one pot method was implemented. Two approaches, a “one step” and a “two steps”, were investigated and the various synthesis parameters optimized. Since the best catalytic results were obtained with the catalysts elaborated with ZnO-PAA2 supports, only PAA2 was studied in this section.

III.1. Cu-ZnO synthesis by a “one pot - one step” approach

The first test of Cu-ZnO production by a one-pot method was performed by mixing all the precursors in the same schlenk flask. At room temperature, copper precursor, urea and PAA2 solution were mixed together and heated till 60 °C. After 20 minutes at 60 °C, the ZnEt₂ was added to the solution under argon as described in the experimental part of Chapter 2. After 3 hours of heating at 60 °C, the suspension was centrifuged and the wet powder was washed with 90 mL of EtOH (for 1 g of catalyst). As before, the powder underwent calcination and reduction to elaborate the final catalyst labelled as Cu-ZnO to differ it from the one prepared by DPU (Cu/ZnO). A representative scheme of the “one pot - one step” approach is shown in scheme 4-5.



Scheme 4-5: Synthesis of Cu-ZnO by “one pot - one step” approach

We called it a “one pot - one step” approach to distinguish it from the next approach where we divided the synthesis into two steps.

Table 4-13 summarizes the catalyst properties at different stages. The specific surface after synthesis was similar to the ZnO-PAA2 support synthesized at high temperature (40 °C) since the elaboration of the ZnO-PAA2 was happening at 60 °C leading to a small surface area of 28

$\text{m}^2.\text{g}^{-1}$. The catalyst was tested: 41 % of conversion with a selectivity of 88% towards 1,2-PDO were obtained after 24h (Table 4-15). An increase from $24 \text{ m}^2.\text{g}^{-1}$ to $43 \text{ m}^2.\text{g}^{-1}$ occurred after the catalytic reaction associated with the formation of the new carboxylate phase. The size of the crystallite of ZnO was almost the same during all stages of synthesis, even after the reaction.

Table 4-13: Properties and catalytic results of “one pot - one step approach Cu-ZnO” at different steps

Catalyst	S.S.A. / BET ($\text{m}^2.\text{g}^{-1}$)	ZnO size (nm)	Cu size (nm)	Cu _{exp} (wt%)
After synthesis	28	11	--	--
After calcination	25	16	CuO	--
After reduction	24	14	13	21.2
After test	43	18	14	--

The XRD diffractograms of the catalyst prepared by this approach are shown in Figure 4-18. Compared to Cu/ZnO_{com} (ca. 60 nm, Figure 4-3) or Cu/ZnO-PAA2 (ca. 20 nm), the catalyst after synthesis had an average ZnO crystallite size of 11 nm. After calcination CuO crystallites were around 15 nm and remained in the same range after reduction (13 nm) and catalysis (14 nm). The results indicated that neither ZnO, nor Cu sintered during the reaction. However, as for Cu/ZnO-PAA2 prepared by DPU, Cu-ZnO prepared by “one pot – one step” method was showing a phase change after the catalytic reaction.

The catalyst could be compared to 20Cu/ZnOPAA2 with ZnO synthesized at 0 °C, 10 °C, RT and 40 °C (Table 4-6). The conversion was 41%, higher than 20Cu/ZnOPAA2₄₀ (27%) but lower than 20Cu/ZnOPAA2_{RT-2} (55%), 20Cu/ZnOPAA2₁₀ (60%) and 20Cu/ZnOPAA2₀ (70%). The selectivities to 1,2-PDO were 88% and 11% for EG similar to those obtained by the processing methods described above.

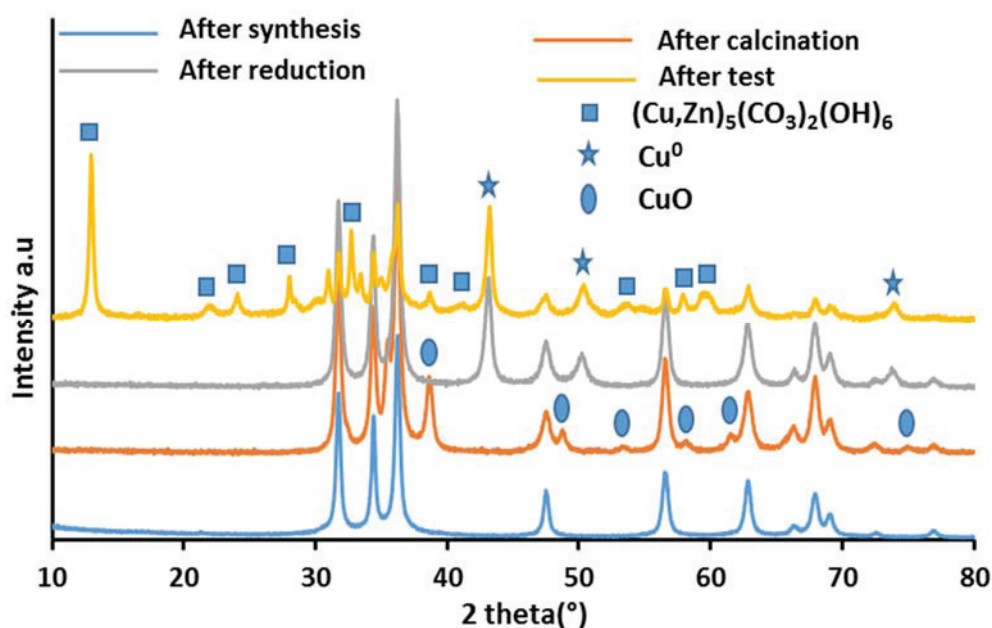
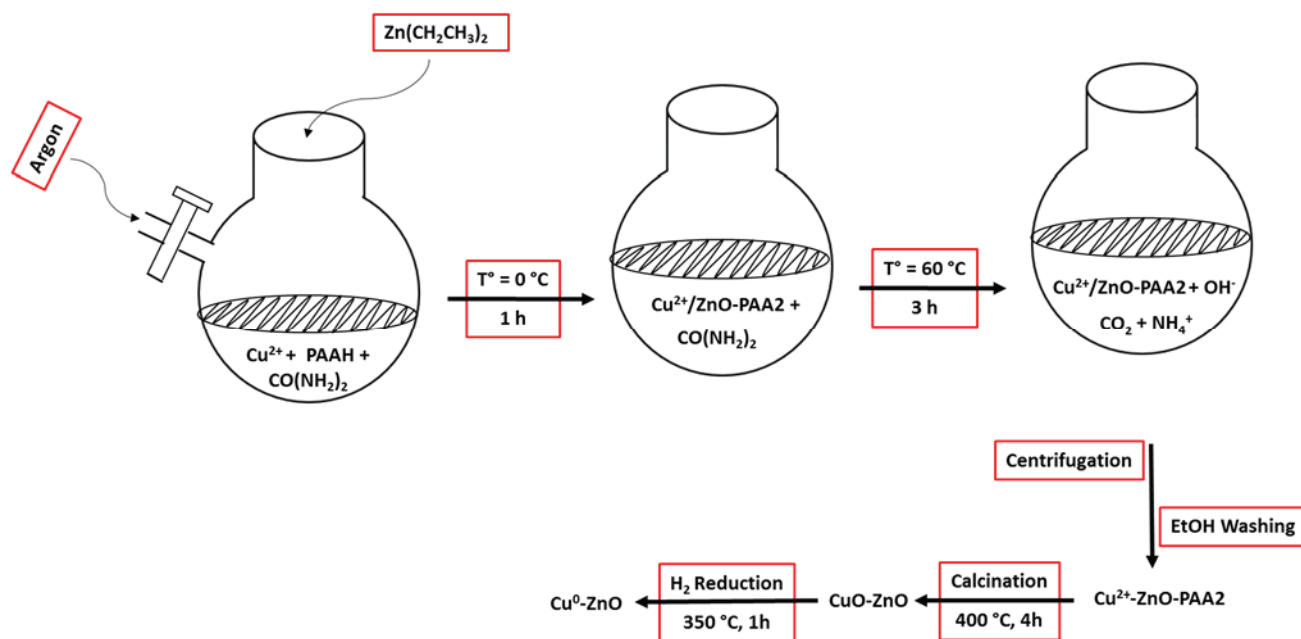


Figure 4-18: XRD patterns at different step of the “one pot - one step approach Cu-ZnO”

III.2. Cu-ZnO synthesis by a “one pot - two steps” approach

Since the most outstanding properties of ZnO-PAA2 were obtained at low synthesis temperature and the highest conversion was obtained with 20Cu/ZnO-PAA2₀, the second one-pot method was divided into two steps. The first step was the in-situ preparation of the support at 0 °C in presence of the copper solution and urea and the second step was the decomposition of urea at 60 °C. As for the “one pot - one step” approach, centrifugation, washing and thermal treatments were needed to elaborate the final catalyst. scheme 4-6 shows the “one pot - two steps” approach.



Scheme 4-6: Synthesis of Cu-ZnO by one pot - two steps approach

Table 4-14 shows the catalyst properties after different steps. The specific surface area after synthesis ($89 \text{ m}^2 \cdot \text{g}^{-1}$) was much higher than the one elaborated with the one step method ($28 \text{ m}^2 \cdot \text{g}^{-1}$) reminding the surface area of ZnO-PAA2 synthesized at $0 \text{ }^\circ\text{C}$. Nevertheless, after reduction the specific surface area were similar (ca. $23 \text{ m}^2 \cdot \text{g}^{-1}$). However, the conversion was higher with 61 % and selectivity of 89 % for 1,2-PDO and 11 % for EG (Table 4-15).

Table 4-14: Properties of “one pot - two steps” approach Cu-ZnO at different steps

Catalyst	S.S.A. ($\text{m}^2 \cdot \text{g}^{-1}$)	ZnO size (nm)	Cu size (nm)	Cu ICP (wt%)
After synthesis	89	30	--	--
After calcination	24	18	CuO	--
After reduction	23	16	15	--
After reaction	33	55	24	20.6

The XRD diffractograms of the catalyst prepared with this approach are shown in Figure 4-19. As expected, after calcination CuO was formed and after reduction Cu^0 was obtained with a crystallite main size of 15 nm. Moreover, Cu^0 crystallite size increased slightly from 15 nm to 24 nm and ZnO crystallite size increased drastically from 16 nm to 55 nm. It was worth noting that even if the conversion was relatively high and the crystallite sizes of copper and ZnO were

not the same, the XRD of the catalyst after test did not show any phase change (Figure 4-19). The new synthesis method seemed to be beneficial for the elaboration of a robust catalyst, partially stable under hydrothermal condition.

Table 4-15: Catalytic results associated with the one pot Cu-ZnO

Catalysts Cu/ZnO	Conversion / 24h (%)	Selectivity / 24h (%)	
		1,2-PDO	EG
“one pot - one step” approach	41	88	11
“one pot - two steps” approach	61	89	11

The conversion was higher (61%) with the “one pot - two steps” approach compared to 41% for the one pot – one step. It could be attributed to a stronger interaction between copper and ZnO since the first step of the synthesis, where the surface area was relatively high ($89 \text{ m}^2.\text{g}^{-1}$) leading to a conservation of the ZnO nanoparticles after the catalytic test and just resulting in sintering of the particles. Nevertheless, the one pot – one step catalyst also seemed to be a robust catalyst, even that the ZnO is transforming, no sintering is occurring. That can be explained by an almost total coverage of the surface of ZnO by the copper particles leading to a protection one by the other.

Comparing our results to studies found in literature for Cu-ZnO prepared by co-precipitation, considering the one pot similar to that synthesis method, we can say that the activity of our system can be considered in the middle or relatively high.

Some studies showed low activity of the system as in the article of Wang et al.¹¹ where authors have prepared Cu-ZnO by co-precipitation of copper nitrate and zinc nitrate in presence of urea. For a molar ratio of Cu:Zn (1:1) and under the following catalytic conditions: 200 °C, 42 bars of H₂, glycerol content of 20 wt% (15 g of glycerol in 65 mL of water), in presence of 7.5 mM of copper [equivalent of 1.1 g of catalyst, resulting in $n_{\text{glycerol}}/n_{\text{catalyst}} = 9.4$ a bit higher than our system (7.8)] and after 12 hours, the conversion of their system was 22.5% with a selectivity toward 1,2-PDO of 83.6%. The crystallite size of ZnO increased from 19 to 28 nm and those of copper from 10 to 33 nm.

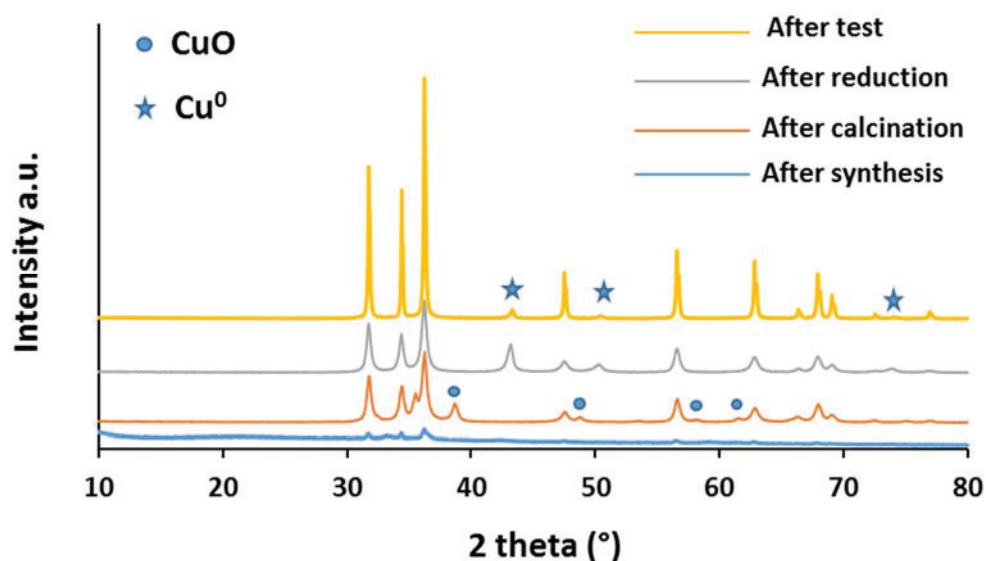


Figure 4-19: XRD patterns at different steps for the “one pot - two steps approach Cu-ZnO”

Other studies showed very high activity like in the article of Bienholz et al.¹² where authors have prepared Cu-ZnO catalysts by co-precipitation with the same copper and zinc precursors as Wang et al. but the precipitating agent was sodium carbonate instead of urea. The hydrogenolysis of glycerol was done with 90 wt% of glycerol (177 g of glycerol in 200 mL of water), under 50 bar of H₂, in presence of 2.8 g of catalyst ($n_{\text{glycerol}}/n_{\text{catalyst}} = 44$) and after 7 hours. At 200 °C, the conversion was 55 % with 82% selectivity toward 1,2-PDO while the same catalyst at 220 °C gave a conversion of 84% with maintaining the selectivity (81%) under the same catalytic conditions cited above. The recyclability test resulted in a decrease in the conversion from 55% to 38% but the selectivity stayed in the same range (79%).

In conclusion, our new “one pot-two steps” succeeded to elaborate a robust system with high conversion and high selectivity toward 1,2-PDO competitive for the hydrogenolysis of glycerol under mild conditions.

As we mentioned in the literature, the Cu/ZnO catalysts were often accompanied by a promoter as Al¹³, Ga¹²... and these systems showed higher activity compared to the simple Cu/ZnO. For that reason, the addition of Al on the Cu/ZnO catalyst will be studied in the following chapter.

IV. Conclusions

The synthesis of copper-based catalysts using commercial ZnO has shown that the activity of these catalysts was strongly influenced by the weight percentage of copper and the concentration of Cu^{2+} . The small specific surface area of the commercial support led to sintering of the copper particles with high loadings. The highest conversion of 25% was obtained when using this support with 10 wt% of copper and 20.8 mM Cu^{2+} after 24 hours and at 200 °C and under 30 bar H_2 . The selectivity to 1,2-PDO in this case was 90% and 10% for the ethylene glycol (EG). The catalyst after the catalytic reaction had a new carbon-containing phase, associated with C-C cleavage.

By replacing commercial ZnO with ZnO-PAA2, glycerol conversion increased. Moreover, it was possible to charge the catalyst with 35 wt% by weight of copper.

In the case of ZnO-PAA5, the best catalytic results were obtained with the support synthesized at 0 °C as the selectivity was almost total for 1,2-PDO at 64% conversion, which was not the case with all the other supports studied. These results show that the nature of the polymer used to develop ZnO nanoparticles seemed to have a significant impact on the catalyst activity. In comparison, the catalyst synthesized with ZnO-PAA100 as support was totally inactive.

The recyclability tests conducted with Cu/ZnO-PAA2 gave similar conversions when the catalysts were reactivated and retested under the same conditions as for the fresh catalyst. In parallel, scaling-up was possible but the catalyst prepared by the DPU method was not easily reproducible.

This was why a “one pot” method was developed to avoid this problem. At first, a “one pot - one step” approach was not very interesting because the activity decreased compared to that of the conventional DPU and the only improvement was avoiding the sintering problem of copper and ZnO particles. On the other hand, a “one pot-two-steps” approach helped to maintain conversion and selectivity with a more robust catalyst showing an increase in ZnO crystallite size but without changing the phase.

In the next chapter, this last method will be further developed by adding alumina to increase specific surface area and then catalyst activity.

V. References

1. Wang, Z., Brouri, D., Casale, S., Delannoy, L. & Louis, C. Exploration of the preparation of Cu/TiO₂ catalysts by deposition–precipitation with urea for selective hydrogenation of unsaturated hydrocarbons. *J. Catal.* **340**, 95–106 (2016).
2. Van den Berg, R., Thesis “Formation, Activity and Growth of Copper Nanoparticles in Methanol Synthesis Catalysts”. ISBN: 978-94-6233-278-2, (2016).
3. Chaminand, J., Djakovitch, L., Gallezot, P. & Pinel, C. Glycerol hydrogenolysis on heterogeneous catalysts. *Green Chem.* **6**, 359–361 (2004).
4. Balaraju, M., Rekha, V., Sai Prasad, P. S., Prasad, R. B. N. & Lingaiah, N. Selective hydrogenolysis of glycerol to 1, 2-propanediol over Cu–ZnO catalysts. *Catal. Lett.* **126**, 119–124 (2008).
5. Karelavic, A. & Ruiz, P. The role of copper particle size in methanol synthesis via CO₂ hydrogenation over Cu/ZnO catalysts. *Catal. Sci. Technol.* **5**, 869–881 (2015).
6. Gao, Q. Xu, B., Tong, Q., & Fan, Y. Selective hydrogenolysis of raw glycerol to 1,2-propanediol over Cu–ZnO catalysts in fixed-bed reactor. *Biosci. Biotechnol. Biochem.* **80**, 215–220 (2016).
7. Pandey, D.K. & Biswas, P. Production of propylene glycol (1,2-propanediol) by the hydrogenolysis of glycerol in a fixed-bed downflow tubular reactor over a highly effective Cu–Zn bifunctional catalyst: effect of an acidic/basic support. *New J. Chem.* **43**, 10073–10086, (2019).
8. Bienholz, A., Schwab, F. & Claus, P. Hydrogenolysis of glycerol over a highly active CuO/ZnO catalyst prepared by an oxalate gel method: influence of solvent and reaction temperature on catalyst deactivation. *Green Chem.* **12**, 290–295, (2010).
9. Jean, D., Nohair, B., Bergeron, J-Y., & Kaliaguine, S. Hydrogenolysis of glycerol over Cu/ZnO-Based catalysts: Influence of transport phenomena using the Madon–Boudart Criterion. *Ind. Eng. Chem. Res.* **53**, 18740–18749, (2014).
10. Mizugaki, T., Arundhathi, R., Mitsudome, T., Jitsukawa, K. & Kaneda, K. Selective hydrogenolysis of glycerol to 1,2-Propanediol using heterogeneous copper nanoparticle catalyst derived from Cu–Al hydrotalcite. *Chem. Lett.* **42**, 729–731, (2013).
11. Wang, S. & Liu, H. Selective hydrogenolysis of glycerol to propylene glycol on Cu–ZnO catalysts. *Catal. Lett.* **117**, 62–67 (2007).
12. Bienholz, A. *et al.* Prevention of catalyst deactivation in the hydrogenolysis of glycerol by Ga₂O₃ modified copper/zinc oxide catalysts. *J. Phys. Chem. C* **115**, 999–1005 (2011).
13. Tan, H. *et al.* One-pot synthesis of Cu/ZnO/ZnAl₂O₄ catalysts and their catalytic performance in glycerol hydrogenolysis. *Catal. Sci. Technol.* **3**, 3360–3371 (2013).

CHAPTER V

Cu-Zn-Al: Effect of Al on the hydrogenolysis

Table of contents

CHAPTER V.....	179
I. Synthesis of Zn_xAl_yO -PAA2: Study of the molar ratio of metals.....	180
I.1. Zn:Al (2:1) molar ratio in presence of PAA2 (Zn_2Al_1O-PAA2₂).....	181
I.2. Zn:Al (1:2) molar ratio in presence of PAA2 (Zn_1Al_2O-PAA2₂).....	185
I.3. Zn:Al (2:1) molar ratio without PAA2 (Zn_2Al_1O-z).....	190
I.4. Zn-Al (1:2) molar ratio without PAA2 (Zn_1Al_2O-z).....	192
II. Synthesis of Cu/ZnAl by DPU: study of the Zn-Al effect.....	196
II.1. Deposition of 20 wt% of copper on Zn_2Al_1O-PAA2 and Zn_2Al_1O materials by DPU	197
II.2. 20 wt% of copper on Zn_1Al_2O-PAA2 and Zn_1Al_2O materials by DPU.....	200
III. Synthesis of $Cu-Zn_xAl_yO_z$ by a “one pot method”: Study of the synthesis parameters	205
III.1.Synthesis of $Cu-Zn_xAl_yO_z$ by a “one pot - one step” route	205
III.2.Synthesis of $Cu-Zn_xAl_yO_z$ by a “one pot -two steps” route	207
III.3.Catalytic results over $Cu-Zn_xAl_yO_z$ prepared by “one pot” routes	211
III.4.Effect of synthesis parameters on $Cu-Zn_xAl_yO_z$ by “one pot-two steps” route:	213
IV. Conclusions.....	220
V. References.....	222

After obtaining promising results on the hydrogenolysis of glycerol with Cu/ZnO catalysts prepared either by DPU or by a "one-pot" method, we were interested in adding aluminium to this system in an attempt to increase the conversion. As shown in Chapter 1, Cu-Zn-Al system is well-known for this reaction and many Zn:Al ratios have been investigated. Some studies showed that the 1:2 Zn:Al¹ molar ratio gave the highest conversion while others found that 1:0.5 Zn:Al gave better results².

In this chapter, we will start by synthesizing Zn_xAl_yO oxide supports and study the effect of the synthesis parameters on the properties of the support. In a second step, we will add Cu to the Zn_xAl_yO mixed support using the previously optimized DPU method and we will test the catalyst activity on glycerol hydrogenolysis. Finally, we will synthesize the Cu-Zn_xAl_yO catalyst by a "one-pot" method and will also study the effect of the synthesis parameters on the activity of the catalyst for the same reaction.

In the literature, mixed oxides of ZnAl have been produced by different approaches such as hydrothermal³⁻⁵ or Sol-gel⁶ methods. Sol-gel did not lead to specific surface area as high as when produced by hydrothermal or other sophisticated methods. This is why, in this project, we have tried to make a compromise between the good properties of the materials obtained by hydrothermal and the ease of the sol-gel method. For this reason, and after setting the ZnO-PAA2 synthesis parameters in Chapter III, the same conditions were applied to produce Zn-Al with two different molar ratios.

The samples will be named Zn_xAl_yO-PAA2_z, with:

- x, y : molar content of zinc and aluminium, corresponding to the actual loading
- z : the calcination temperature after synthesis.

For example, in the following chapter, the as-prepared sample will be named Zn_xAl_yO-PAA2 and the sample calcined at 600 °C, Zn_xAl_yO-PAA2₆₀₀.

I. Synthesis of Zn_xAl_yO-PAA2: Study of the molar ratio of metals

As the material will be used as a support for copper catalysts, the molar ratio Zn:Al is an important factor to study. Nevertheless, for reasons of time remaining, we carried out this study only with two stoichiometries Zn:Al (1:2 and 2:1) keeping in mind that the 1:2

stoichiometry would be likely to give the spinel phase ZnAl_2O_4 .

As mentioned in the experimental part, the bottle of AlMe_3 used for some of these syntheses was pure (97% in hexane), purchased from Sigma Aldrich, however it had been opened for a long time. For that reason the theoretical molar ratio of Zn:Al was not equal to the experimental one because the bottle was partially oxidized. For Zn-Al, two samples were prepared using this bottle and used later as supports for Cu/Zn-Al. While for Cu-Zn-Al (last section of the chapter, prepared by the “one pot” method), seven catalysts were elaborated with the old bottle. The concerned samples will be appointed in the chapter.

1.1. Zn:Al (2:1) molar ratio in presence of PAA2 ($\text{Zn}_2\text{Al}_1\text{O-PAA}_2$)



Initially, the molar ratio used to synthesize the Zn-Al support was 1:2 in the presence of aqueous PAA2 solution. As described in the experimental section, the synthesis was carried out as for ZnO-PAA2 after setting the synthesis parameters at 0 °C and 0.63 wt% of PAA2. For this purpose, the PAA2 solution was cooled in an ice bath before adding a mixture of ($\text{ZnEt}_2 + \text{AlMe}_3/\text{old bottle}$) with a respective ratio Zn:Al of 1:2. The powder obtained after washing with 90 mL EtOH and drying steps (centrifugation and night drying in the oven) was calcined at 400 and 600 °C in order to study the effect of calcination on the nature of the material. Indeed, a spinel phase of ZnAl_2O_4 might form at high calcination temperature^{3,7}. No EDX measurements were made on the samples but the molar ratios were measured by ICP analysis for the sample calcined at 400 °C and gave formula of $\text{Zn}_{1.95}\text{AlO}_{4.67}$. Therefore, this sample was labelled $\text{Zn}_2\text{Al}_1\text{O-PAA}_2$. Data are summarized in Table 5-1.

Table 5-1: Characteristics of $\text{Zn}_2\text{Al}_1\text{O-PAA}_2$

Temperature (°C)	S.S.A. / BET ($\text{m}^2\cdot\text{g}^{-1}$)	Crystallite size / XRD (nm)		Particle size / TEM (nm)	Metal loading (weight %)		Zn:Al (molar ratio)	TG / weight loss [200-600 °C] (%)
		ZnO	ZnAl_2O_4		Zn	Al		
As-prepared	71	22	--	--	--	--	--	35
400	234	8	--	10-100	55.8	11.8	2:1	4
600	98	9	12	5-20	--	--	--	1

(--: not determined)

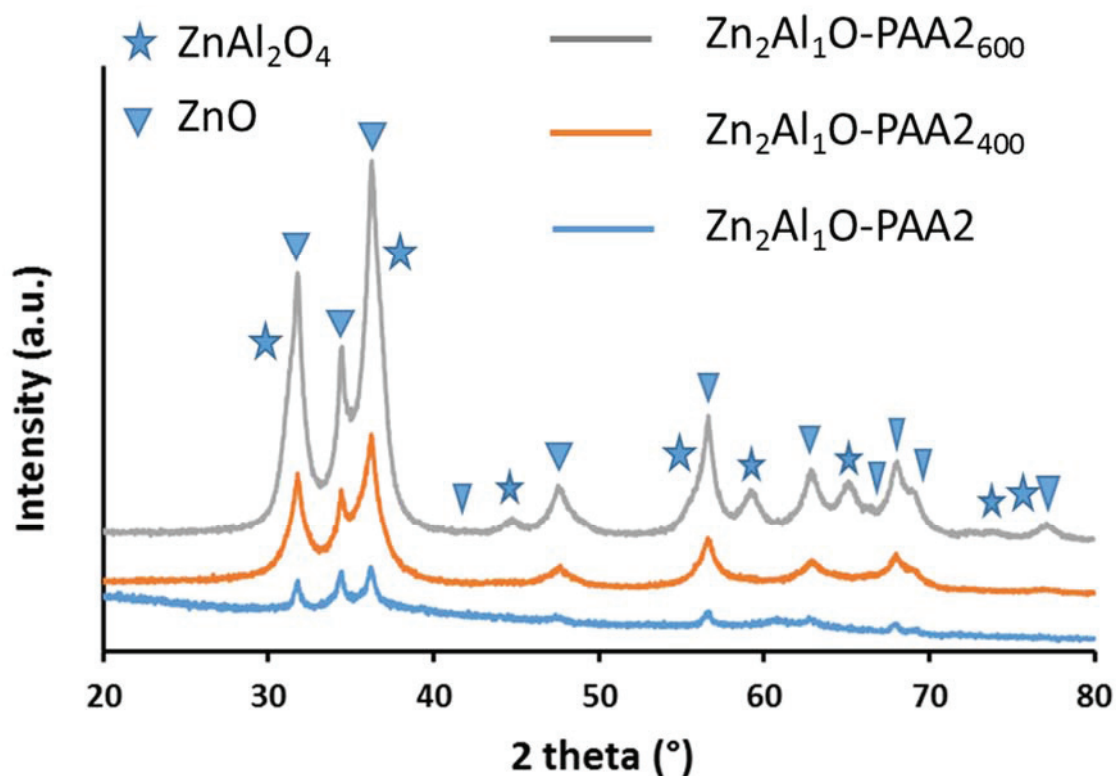
ICP results showed a higher content of zinc from what was expected, with a molar ratio 2:1 instead of 1:2. At first, we did not know if the difference was coming from the synthesis (i.e. leaching of Al) or if the bottle was oxidized resulting in a lower content of Al.

Powder X-ray diffractograms of $\text{Zn}_2\text{Al}_1\text{O}$ -PAA2, $\text{Zn}_2\text{Al}_1\text{O}$ -PAA2₄₀₀, $\text{Zn}_2\text{Al}_1\text{O}$ -PAA2₆₀₀ are shown in Figure 5-1. XRD pattern indicates that as-prepared material is composed of crystalline ZnO (hexagonal phase: zincite, PDF number 01-083-6338) with an average crystallite size of 22 nm, calculated by using the peaks at 47°, 57° and 63°, very similar to the ones obtained without aluminium (19 nm) in chapter III - section I. The main difference comes from the absence of peaks at 33 and 59° from the “unidentified” phase.

The calcination of the powder at 400 and 600 °C, at a heating rate of 5 °C per minute for 4 hours in a static furnace, led to an increase in the crystallinity of ZnO and the appearance of large peaks corresponding to ZnAl_2O_4 (cubic phase, PDF number 04-014-1594 appendix 12), slightly visible at 400 °C. At 600 °C, the mean crystallite sizes of ZnO decreased to 9 nm and the one of ZnAl_2O_4 was estimated at 12 nm with peaks at 59°, 65° and 74°.

For the material $\text{Zn}_2\text{Al}_1\text{O}$ -PAA2₆₀₀, calculations with Diffrac.Eva software gave a proportion of 58% ZnO and 42% ZnAl_2O_4 . This ratio did not reflect the ICP Zn:Al ratio of 2:1, which could be due to the fact that part of the solid was amorphous. For clarification, we should also mention that the proportions obtained with Diffrac.Eva software were semi-quantitative and should mainly be used for comparing the samples between each other.

For the upcoming diffractograms we will just label the peaks associated with ZnAl_2O_4 phase as ZnO one was present in most samples. In the following XRD patterns (Figure 5-1), all peaks of ZnAl_2O_4 are represented, even those that are not well crystallized and/or overlap with ZnO, in order to distinguish between the two crystallographic phases. Actually, the two main peaks of ZnAl_2O_4 at 31° (Intensity: 80%) and 37° (100%) were really close to the major peaks of ZnO at 32° (71%) and 36° (100%). Therefore, an easy way to distinguish between the two phases was the presence of a peak at 34° (56%) which was associated with ZnO and peaks at 59° (40%) and 65° (40%) which were associated with ZnAl_2O_4 .

Figure 5-1: XRD diffraction patterns of $\text{Zn}_2\text{Al}_1\text{O-PAA2}_z$

Compared to the aluminium-free system, the materials $\text{Zn}_2\text{Al}_1\text{O-PAA2}_z$ had much higher specific surfaces after calcination; indeed at 400 °C we obtained a specific surface area of the order of $234 \text{ m}^2.\text{g}^{-1}$ which dropped to $98 \text{ m}^2.\text{g}^{-1}$ after calcination at 600 °C. While ZnO-PAA2 after calcination at 400 °C resulted in a surface area of $18 \text{ m}^2.\text{g}^{-1}$ (Chapter III, Table 3-8). In terms of similarities, those as-prepared with or without aluminium were similar (between 70 and $90 \text{ m}^2.\text{g}^{-1}$) and the same temperature-dependent evolution was observed for both systems. The result showed that the addition of aluminium during synthesis was responsible for increasing the specific surface area of the materials.

TG analyses were performed as for ZnO-PAA2 (under air at a heating rate of 5 °C per minute up to 700 °C) to study the content of organic compounds in the material before and after calcination, as shown in Figure 5-2. It showed that the same amount of the polymer PAA2 was incorporated into the hybrid mixed material $\text{Zn}_2\text{Al}_1\text{O-PAA2}$ and ZnO-PAA2 with a total 51% weight loss between 200 and 600 °C. Weight loss at low temperature (60-200 °C) corresponded to the evaporation of the solvent. At higher temperatures, degradation could be attributed to the decomposition of the formed oxides into ZnO_x and/or $\text{Zn}_x\text{Al}_y\text{O}_z$. Organic

compounds started to decompose at the same temperature (around 300 °C) as for ZnO-PAA2 (Figure 3-4 in Chapter III on page 103), suggesting no impact of Al on the synthesis and the thermal behaviour of the mixed oxide.

After calcination at 400 °C, the TGA showed that the compound $\text{Zn}_2\text{Al}_1\text{O-PAA2}_{400}$ had lost a large part of the organic matter. The decomposition of the organic residue began at a temperature below that of $\text{Zn}_2\text{Al}_1\text{O-PAA2}$, of about 150 °C and the final total loss of weight was of 13%. The increase in calcination temperature to 600 °C logically resulted in a decrease in the amount of organic compounds present in the compound with a total weight loss of 6%, indicating an absence of residue for $\text{Zn}_2\text{Al}_1\text{O-PAA2}_{600}$.

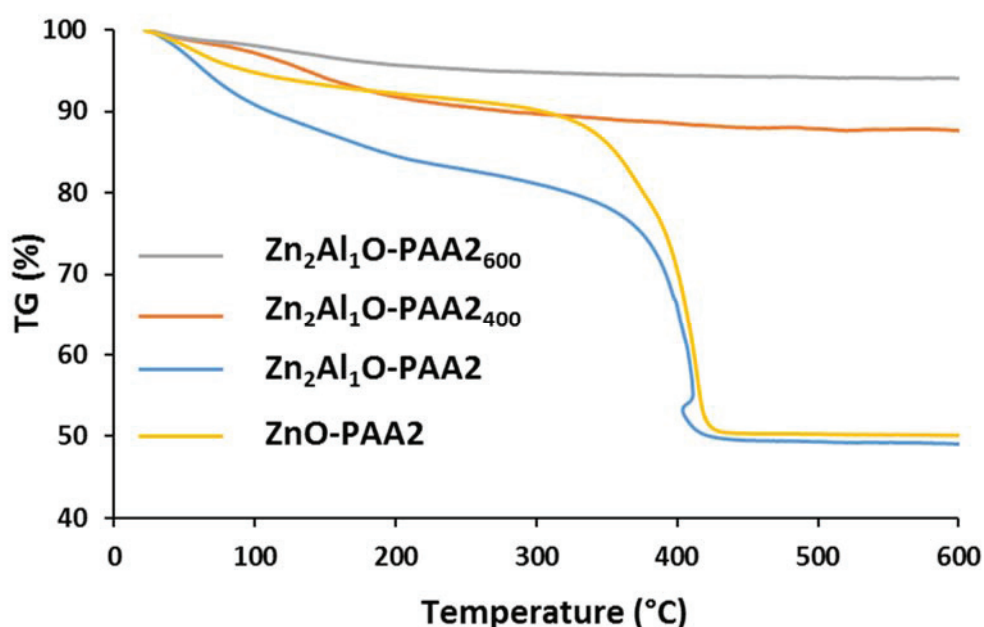


Figure 5-2: TGA curves of ZnO-PAA2 and $\text{Zn}_2\text{Al}_1\text{O-PAA2}_z$

The TEM images for $\text{Zn}_2\text{Al}_1\text{O-PAA2}_{400}$ and $\text{Zn}_2\text{Al}_1\text{O-PAA2}_{600}$ (Figure 5-3) showed two different morphologies. For $\text{Zn}_2\text{Al}_1\text{O-PAA2}_{400}$, the material was mainly in the form of a 2D nano-sheets and nanoparticles mixture while $\text{Zn}_2\text{Al}_1\text{O-PAA2}_{600}$ was mainly composed of aggregated spherical nanoparticles. The sizes of the nanoparticles that composed $\text{Zn}_2\text{Al}_1\text{O-PAA2}_{400}$ and $\text{Zn}_2\text{Al}_1\text{O-PAA2}_{600}$ were between 10-100 nm and 5-20 nm, respectively. Figure 5-3 (c and d) showed different interplanar orientations, spacings and network fringes proving the formation of the spinel phase ZnAl_2O_4 .

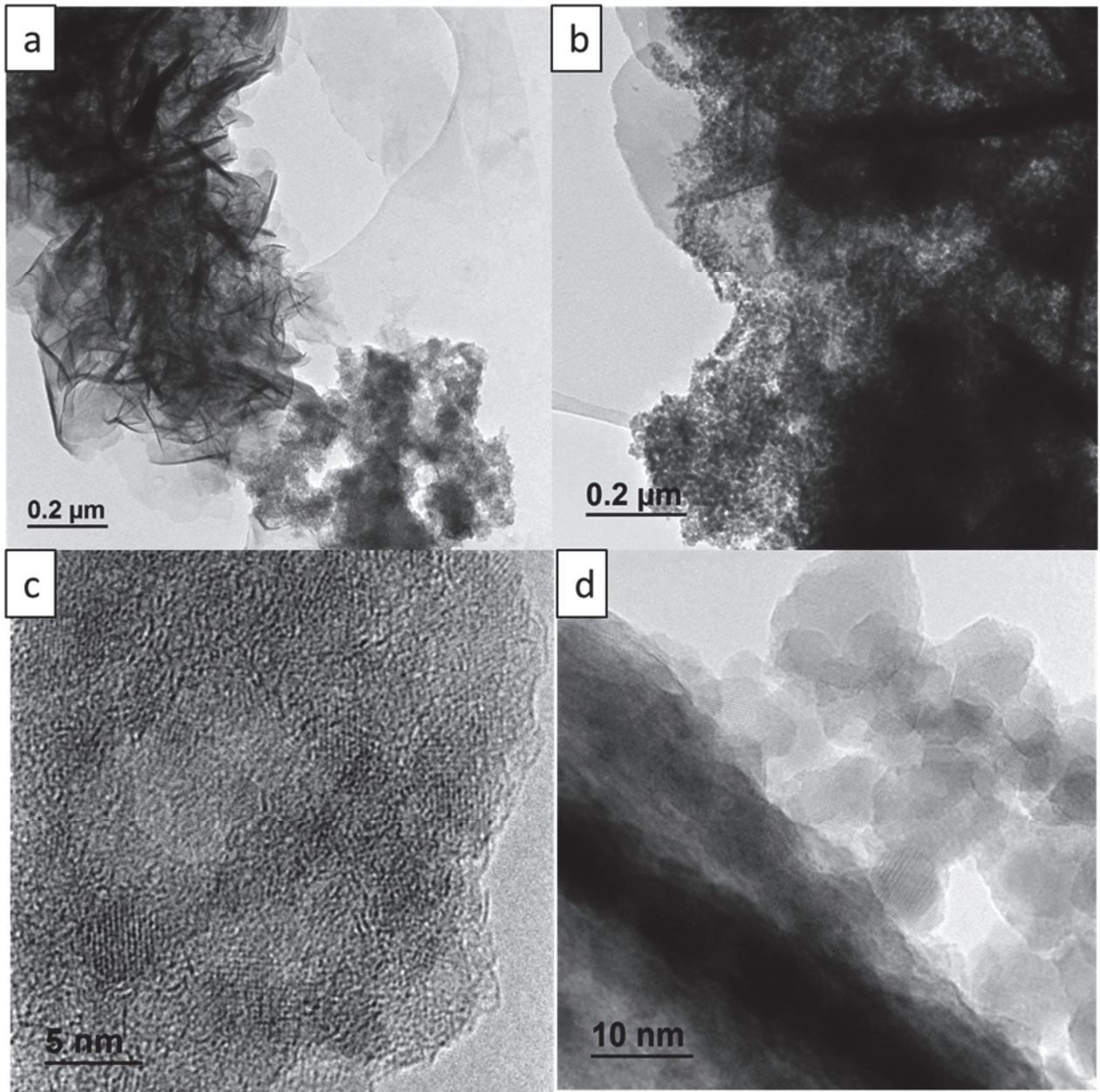


Figure 5-3: TEM images of a,c) Zn_2Al_1O -PAA₂₄₀₀ and b,d) Zn_2Al_1O -PAA₂₆₀₀

Again, a correlation between the presence of 2D nano-sheets and a large specific surface area could be highlighted.

1.2. Zn:Al (1:2) molar ratio in presence of PAA2 (Zn_1Al_2O -PAA_{2z})

Since the first attempt to elaborate ZnAl oxides with Zn:Al molar ratio 1:2 did not work, we bought a new bottle of TMA as mentioned previously and aimed once again for this molar ratio.

Under the same operating conditions as above ($T = 0\text{ }^\circ\text{C}$ and PAA2 at 0.63 wt%), the increase

in the quantity of aluminium in the material was accompanied by a loss of crystallinity of the as-prepared powder as shown by XRD (Figure 5-4). Calcination at 400 °C ($\text{Zn}_1\text{Al}_2\text{O-PAA2}_{400}$) slightly increased crystallinity and showed the appearance of large peaks corresponding mainly to ZnAl_2O_4 . Calculations on Diffrac.Eva software gave a 50:50 mixture of ZnO and ZnAl_2O_4 . The peaks of the two phases were not separated well enough and the crystallites remained too small to be calculated by Debye-Scherrer equation. After calcination at 600 °C, the material exhibited the crystallized phase ZnAl_2O_4 at 80% with an average crystal size of 13 nm calculated with peaks at 45°, 59° and 65° and 20% of ZnO (not suitable for crystallite size measurement).

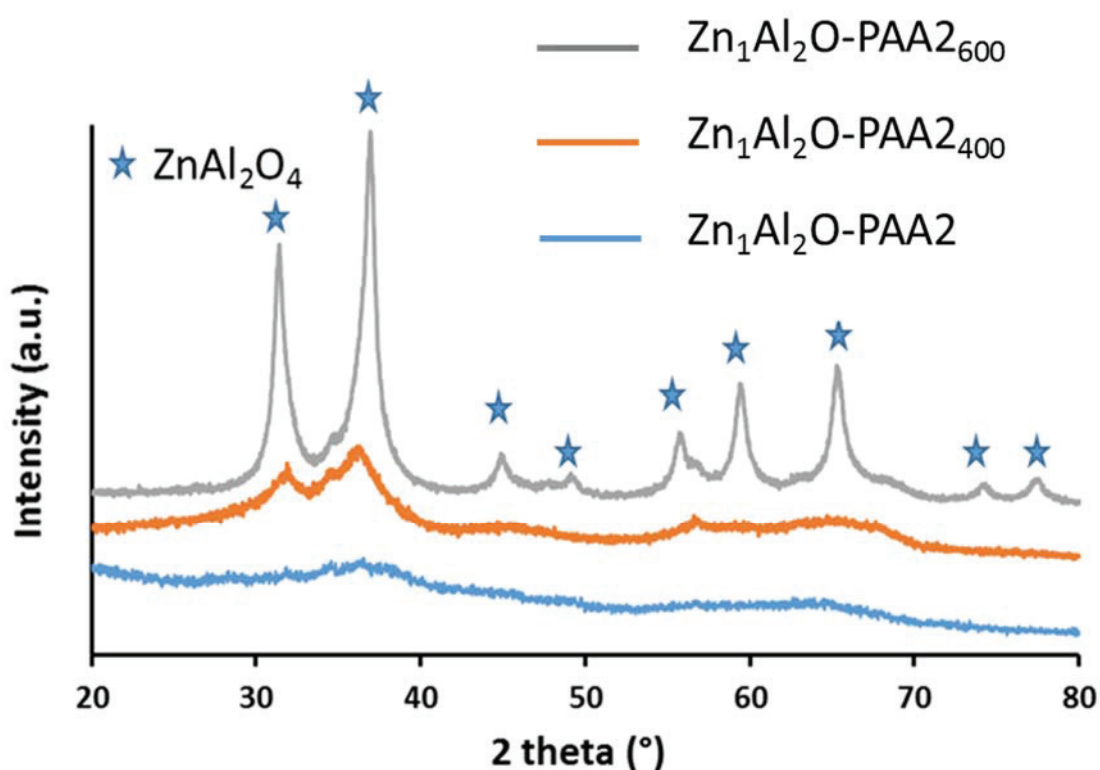


Figure 5-4: XRD diffraction patterns of $\text{Zn}_1\text{Al}_2\text{O-PAA2}_z$

ICP measurements of the compound $\text{Zn}_1\text{Al}_2\text{O-PAA2}_{400}$ yielded a formula $\text{ZnAl}_{2.46}\text{O}_{7.79}$ with an excess of aluminium in comparison to the nominal stoichiometry but much closer than the stoichiometry obtained with the old bottle. Table 5-2 summarizes the properties of the materials obtained. Once again, the ratio obtained by ICP was not in agreement with the phase calculations made on Diffrac.Eva. Indeed, for an ICP ratio of Zn:Al (1:2), ZnO was not supposed to be present in XRD patterns. Therefore, two hypotheses can be given.

- 1) The spinel phase was more loaded in Al and exhibited a stoichiometry higher than 1:2

but with similar peaks (for example pdf 01-077-0732 of $Zn_{0.3}Al_{2.4}O_4$ appendix 13), meaning that ZnO could be present.

- 2) Or that $ZnAl_2O_4$ was having the exact stoichiometry of 1:2 and amorphous Al oxides were present in small quantities. It was also possible that some Al was incorporated into ZnO as a dopant.

Once again, we would like to remind that XRD analysis and calculation on Diffrac.Eva are semi-quantitative.

Table 5-2: Characteristics of $Zn_1Al_2O-PAA2_z$

Temperature (°C)	S.S.A. / BET ($m^2 \cdot g^{-1}$)	Crystallite size / XRD (nm)		Metal loading (weight %)		Zn:Al (molar ratio)	TG / weight loss [200-600 °C] (%)
		ZnO	$ZnAl_2O_4$	Zn	Al		
As-prepared	223	A	A	--	--	--	30
400	333	--	--	25.2	26.5	1:2.4	8
600	137	--	13	--	--	--	2

(--: not determined, A: Amorphous)

The decrease in the molar ratio Zn:Al (and therefore an increase in the proportion of Al) resulted in a significant increase in the specific surface area for all materials. The hybrid as-prepared material ($Zn_1Al_2O-PAA2$) had an already very high specific surface area of $223 m^2 \cdot g^{-1}$. As before, calcination at 400 °C increased the specific surface area to $333 m^2 \cdot g^{-1}$ (confirmed by repeating the synthesis twice with a difference of only $10 m^2 \cdot g^{-1}$), which was a very high value unreported till now for $ZnAl_2O_4$ obtained by sol-gel method. Once again, at 600 °C a decrease in the specific surface area to $137 m^2 \cdot g^{-1}$ was observed.

Thermogravimetric analyses of the compounds $Zn_1Al_2O-PAA2_z$ (Figure 5-5), showed that the change in the molar ratio Zn:Al did not have a major impact on their thermal behaviour. The weight loss of the compound $Zn_1Al_2O-PAA2$ between 200 and 600 °C was about 30% (Table 5-2) slightly lower than that of $Zn_2Al_1O-PAA2$ (35%, Table 5-1). The TGA of calcined solids ($Zn_2Al_1O-PAA2_{400}$ and $Zn_2Al_1O-PAA2_{600}$) showed a slightly higher weight loss compared to $Zn_1Al_2O-PAA2_{400}$ and $Zn_1Al_2O-PAA2_{600}$. These suggested that the combustion of PAA2 did not occur exactly in the same way with high aluminium content.

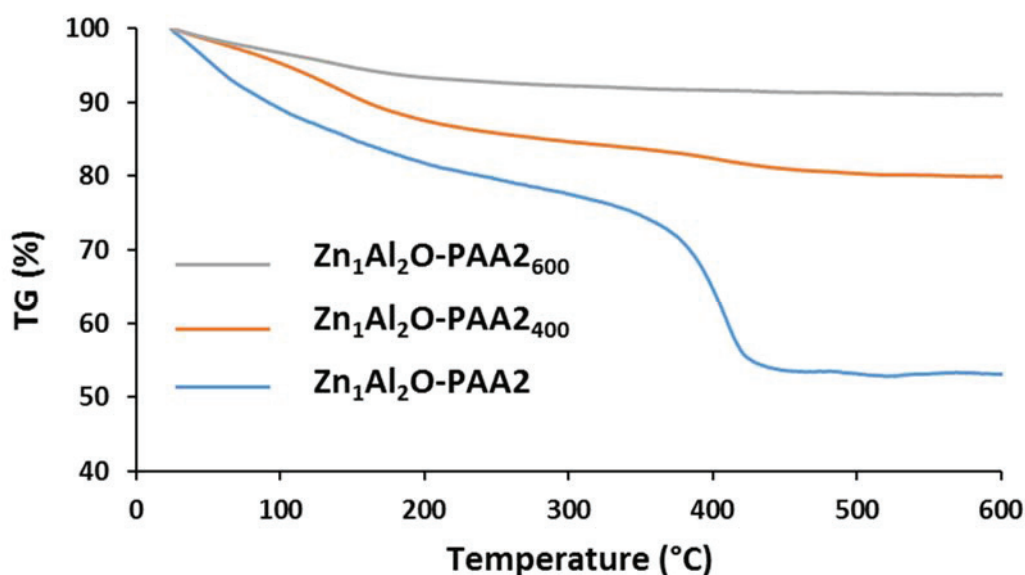
Figure 5-5: TGA curves of Zn₁Al₂O-PAA_{2z}

Figure 5-6 shows the TEM images of the material after synthesis and after calcination at 400 °C. The material after synthesis was essentially composed of aggregates without precise morphology and of sizes 100-200 nm (Figure 5-6 a & c). Calcination at 400 °C resulted in the appearance of two different types of nano-objects of different morphology: spherical nanoparticles and 2D nano-sheets (Figure 5-6 b & d). EDX measurements were performed for different spots of the material Zn₁Al₂O-PAA₂₄₀₀ (Figure 5-6 b & d) in order to correlate these morphologies to the two different phases present in XRD (ZnO, ZnAl₂O₄). The results summarized in Table 5-3 showed a higher abundance of Zn on 2D nano-sheets (zones 1, 11 and 12) with a molar ratio Zn:Al (1:1) on these spots, suggesting in that case a combination of ZnO and Al oxides as proposed after the XRD analysis. While a higher Al content was observed within spherical shapes (zones 2, 10 and 13) resulting in a higher stoichiometry for ZnAl₂O₄. It seemed that the two hypothesis proposed after XRD analysis were possible.

It could therefore be suggested that the 2D nano-sheets were more loaded with the ZnO phase as seen for ZnO-PAA₂ without adding aluminium (Chapter III, Figure 3-2) but contained as well some Al oxides. The nanoparticles could be attributed to the ZnAl₂O₄ phase.

In conclusion, the addition of aluminium in greater or lesser quantities during synthesis induced a loss of crystallinity of ZnO, an increase in the proportion of ZnO of 2D nano-sheet morphology combined with Al content which was accompanied by a significant increase in

the specific surface area. This addition also led at 600 °C to the appearance of the $ZnAl_2O_4$ phase regardless of the initial stoichiometry used.

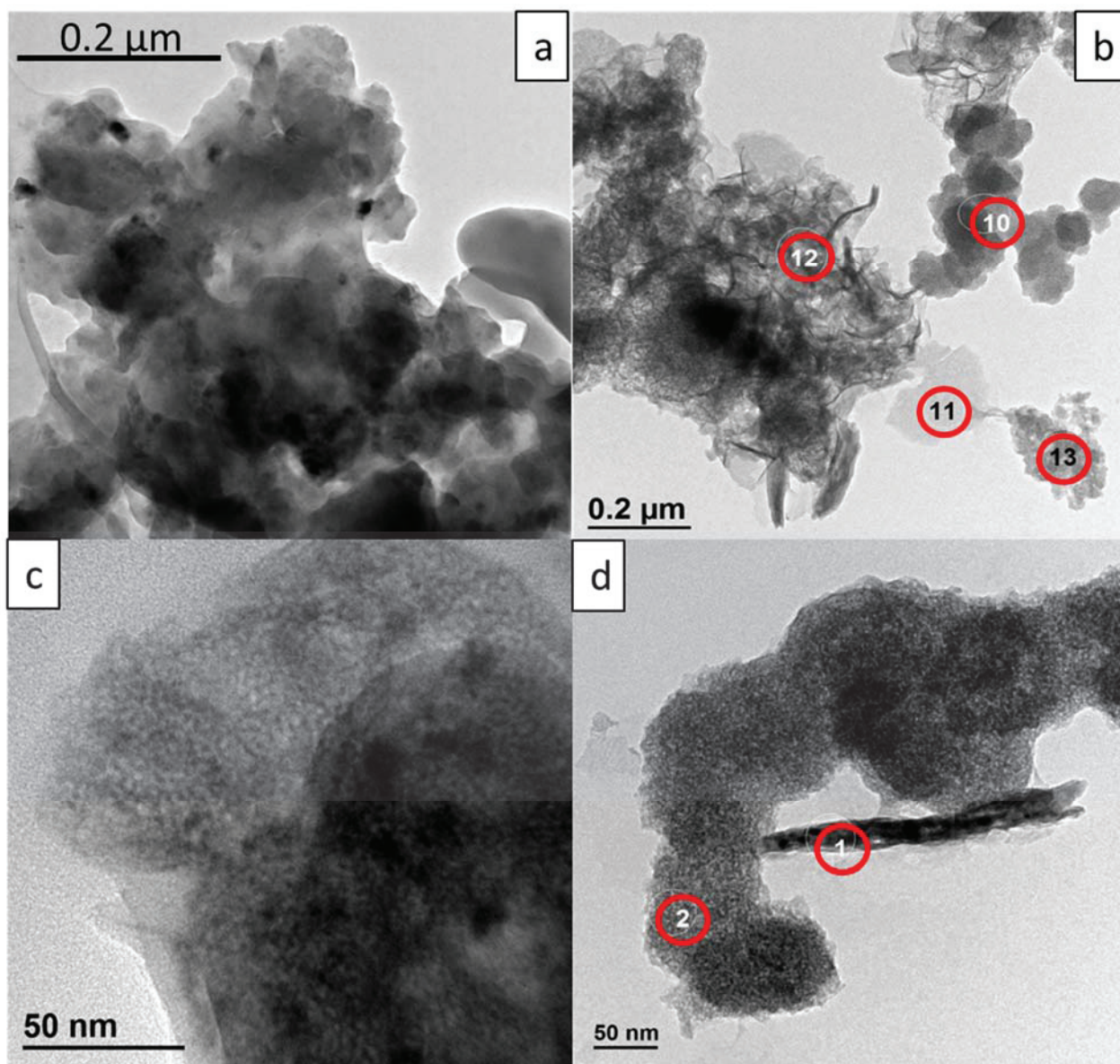


Figure 5-6: TEM images of a,c) Zn_1Al_2O -PAA2 and b,d) Zn_1Al_2O -PAA2₄₀₀

Table 5-3: EDX measurements of Zn_1Al_2 -PAA2₄₀₀

Area	Elements	Zn (molar %)	Al (molar %)	O (molar %)
1		19.3	25.3	55.4
2		5.9	31.4	62.7
10		8.9	35.8	55.2
11		21.4	23.0	55.6
12		15.8	22.4	61.8
13		7.2	31.1	58.7

The next parameter to be studied was the absence of the PAA2 polymer during synthesis since the 3D spherical self-assemblies were no longer formed.

1.3. Zn:Al (2:1) molar ratio without PAA2 ($Zn_2Al_1O_{-z}$)

As the objective was to see the effect of the absence of PAA2 on the final material, the sample was prepared under the same operating conditions as Zn:Al with PAA2 (section 1.1) using the old $AlMe_3$ bottle, except that the PAA2 solution was replaced by pure water. The physico-chemical characteristics of $Zn_2Al_1O_{-z}$ are summarized in Table 5-4. The ICP analysis of the material at 400 °C gave a formula of $Zn_{2.1}AlO_{5.1}$ very close to the stoichiometry obtained for Zn:Al with PAA2 but once again not corresponding to the theoretical one of 1:2.

Table 5-4: Characteristics of $Zn_2Al_1O_{-z}$

Calcination T° (°C)	S.S.A. / BET ($m^2.g^{-1}$)	Crystallite size / XRD (nm)		ICP (wt%)		Zn:Al (molar ratio)	TG/ weight loss [200-600 °C] (%)
		ZnO	$ZnAl_2O_4$	Zn	Al		
As synthesized	81	22	11	--	--	--	6
400	89	24	12	56.5	10.9	2.1:1	1
600	70	25	12	--	--	--	1

(--: not determined)

XRD patterns shown in Figure 5-7 showed that the absence of PAA2 had a significant effect on the crystallinity and nature of the final material. After synthesis, the solid was biphasic and consisted of 90% of well crystallized ZnO and 10% of $ZnAl_2O_4$ after calculation with Difffrac.Eva. The size of the crystallites calculated using the same peaks as previously gave an average size of 22 nm for ZnO and 11 nm for $ZnAl_2O_4$. Contrary to the system with PAA2, this one evolved very little according to the temperature since the particle sizes of ZnO and $ZnAl_2O_4$ remained unchanged and the proportion of $ZnAl_2O_4$ went from 10% to 17% (at 400 °C) and finally 23% (at 600 °C). Unlike the system with PAA2, the specific surface area was not significantly influenced by the calcination temperature, the average specific surface area being $80 m^2.g^{-1}$ for the 3 samples (Table 5-4). However, it followed the same trend as with PAA2 and a maximum of $90 m^2.g^{-1}$ was obtained after calcination at 400 °C.

In conclusion, the absence of PAA2 during synthesis in the presence of aluminium led to a more heterogeneous system with less $ZnAl_2O_4$ phase and low specific surface area. PAA2

could therefore act as a dispersing agent to homogenize the Zn/Al mixture at the molecular scale but also as a surfactant to increase the specific surface area.

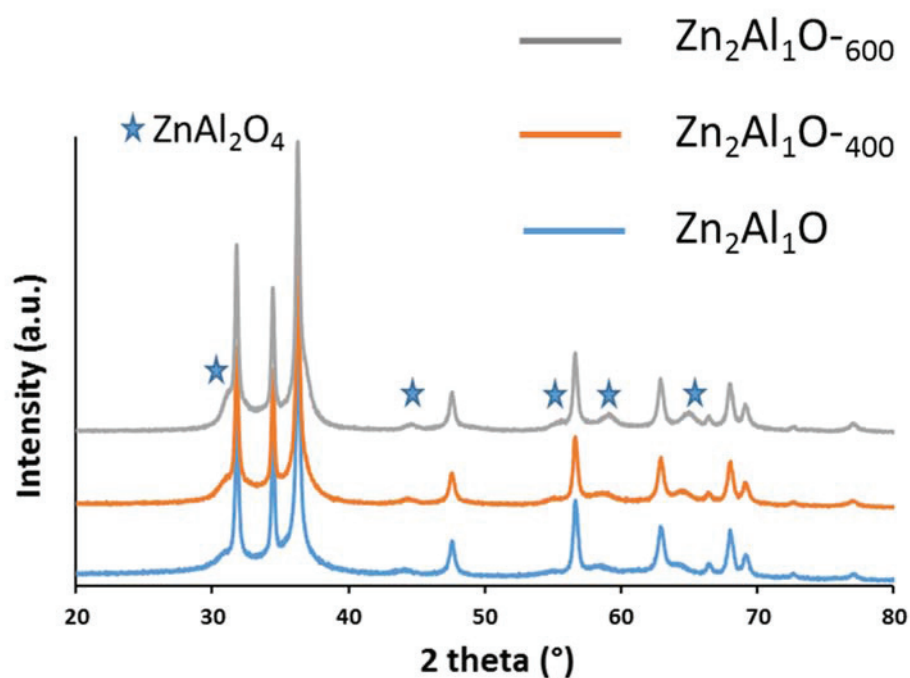


Figure 5-7: XRD diffraction patterns of $\text{Zn}_2\text{Al}_1\text{O}_z$

Our results could be compared with a study on the synthesis of ZnAl_2O_4 with and without surfactant⁸. In an article by Chaudary et al.⁸, ZnAl_2O_4 was obtained by a two-steps sol-gel process. A ZnAl precursor was obtained by dissolving aluminium isopropoxide and anhydrous zinc acetate in toluene and heating at reflux for 3 hours. The mixture was then evaporated under vacuum to give a white solid. This solid, considered as the mixed precursor ZnAl, was dissolved in a mixture of isopropanol and distilled water. The resulting gel was separated by centrifugation and washed with water and acetone. After drying, the powder was sintered at 500 °C for 2 hours. In order to study the surfactant effect during the hydrolysis step, a solution of cetyltrimethylammonium bromide (CTAB) or sodium lauryl sulfate (SLS) was added. The particle size decreased from 12 nm without the addition of surfactants to 6 nm with both types of surfactants. The specific surface area increased from 79 $\text{m}^2\cdot\text{g}^{-1}$ without surfactant to 130 $\text{m}^2\cdot\text{g}^{-1}$ and 82 $\text{m}^2\cdot\text{g}^{-1}$ with CTAB and SLS, respectively.

Thermogravimetric analysis of the as-prepared material showed that the only weight loss of 13 wt% corresponded mainly to the departure of the solvents with almost no loss after 200 °C

(Figure 5-8). The materials calcined at 400 and 600 °C showed no weight loss.

In conclusion, the absence of PAA2 led to the appearance of a ZnO + ZnAl₂O₄ biphasic system that evolved slightly, in terms of specific surface area and particle size, as a function of temperature. Surprisingly, this synthesis produced the ZnAl₂O₄ spinel phase at very low temperatures, whereas it was generally obtained at temperatures of 600 °C⁹. It was therefore interesting to see what this synthesis pathway gave when the starting stoichiometry is similar to that of ZnAl₂O₄.

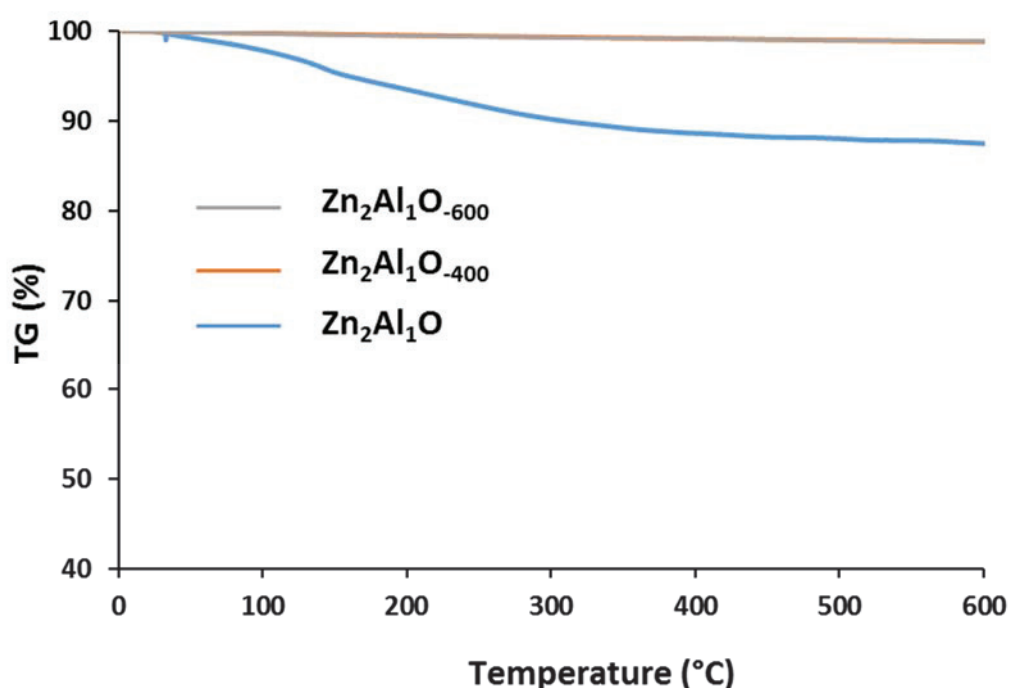


Figure 5-8: TGA curves of Zn₂Al₁O-z

1.4. Zn-Al (1:2) molar ratio without PAA2 (Zn₁Al₂O_{-z})

The sample illustrated in this section was elaborated with the new bottle of AlMe₃ as for Zn:Al (1:2) with PAA2 (section 1.2).

The physico-chemical characteristics of the different Zn₁Al₂O_{-z} materials are summarized in Table 5-5. The ICP analysis of the material at 400 °C gave a formula of ZnAl_{2.43}O_{6.9} very close to the initial stoichiometry suggesting a total precipitation of both metal without PAA2. It is also

similar to Zn₁Al₂O-PAA2₄₀₀ (Table 5-2) confirming that PAA2 was previously totally removed after calcination at 400 °C. Therefore, the two materials prepared with the new bottle of AlMe₃, in presence and absence of PAA2 showed an experimental molar ratio very similar to the theoretical one. This proved that the difference in stoichiometry is mainly attributed to the oxidation of the old bottle of AlMe₃ and not to the Al leaching under the operating conditions.

Table 5-5: Characteristics of Zn₁Al₂O-z

Calcination T° (°C)	S.S.A. / BET (m ² .g ⁻¹)	Crystallite size / XRD (nm)		ICP (weight %)		Zn:Al (molar ratio)	TG/ weight loss [200- 600 °C] (%)
		ZnO	ZnAl ₂ O ₄	Zn	Al		
As synthesized	274	26	--	--	--	--	12
400	260	22	6	27.3	27.1	1:2.4	5
600	169	35	6	--	--	--	2

(--: not determined).

XRD patterns in Figure 5-9 showed that the absence of PAA2 had again a significant effect on the crystallinity and nature of the final material. After synthesis, the solid was again biphasic ZnO + ZnAl₂O₄ but in this case the proportion of ZnAl₂O₄ raised to 47%, as estimated with Diffrac.Eva. The size of the ZnO crystallites calculated using the same peaks as previously gave an average size of 26 nm for ZnO. Contrary to the Zn₂Al₁O-z system, this one evolved much more according to the temperature since at 600 °C, the crystallite sizes of ZnO increased to 35 nm, while remaining unchanged for ZnAl₂O₄ at 6 nm. The proportion of ZnAl₂O₄ increased up to 82%, which is similar to Zn₁Al₂-PAA2-600. As it was suggested for Zn:Al (1:2) with PAA2, the ZnO phase could overlap with Al₂O₃, some Al could be incorporated into ZnO, or ZnAl₂O₄ could be more charged in Al.

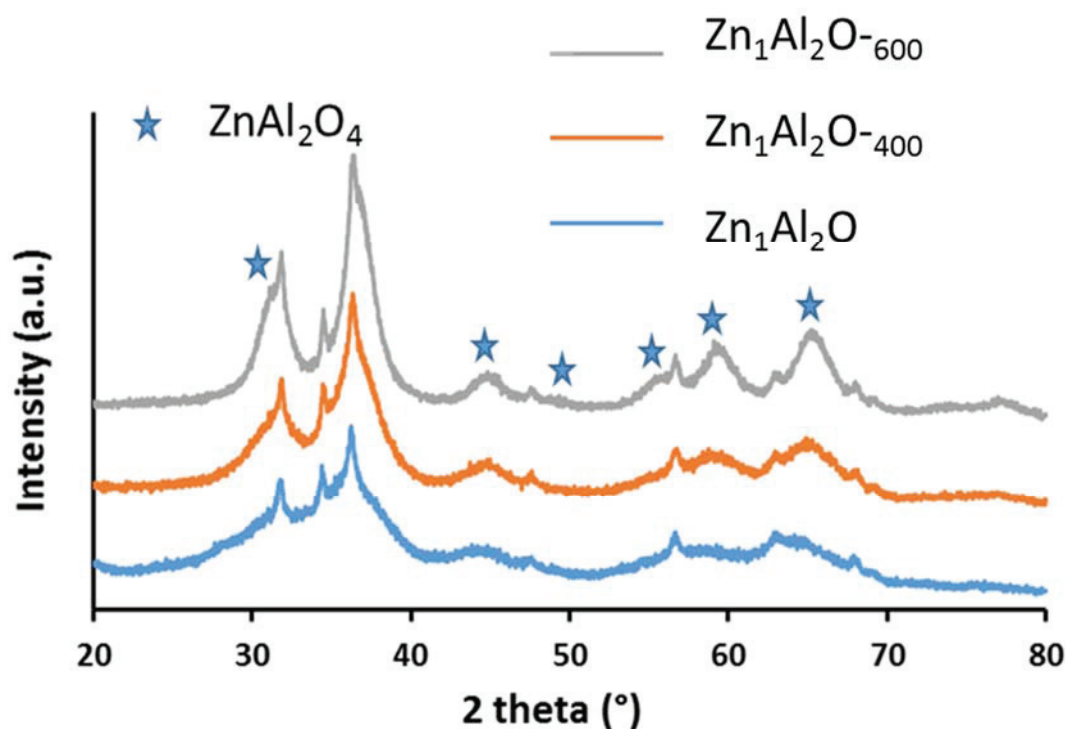
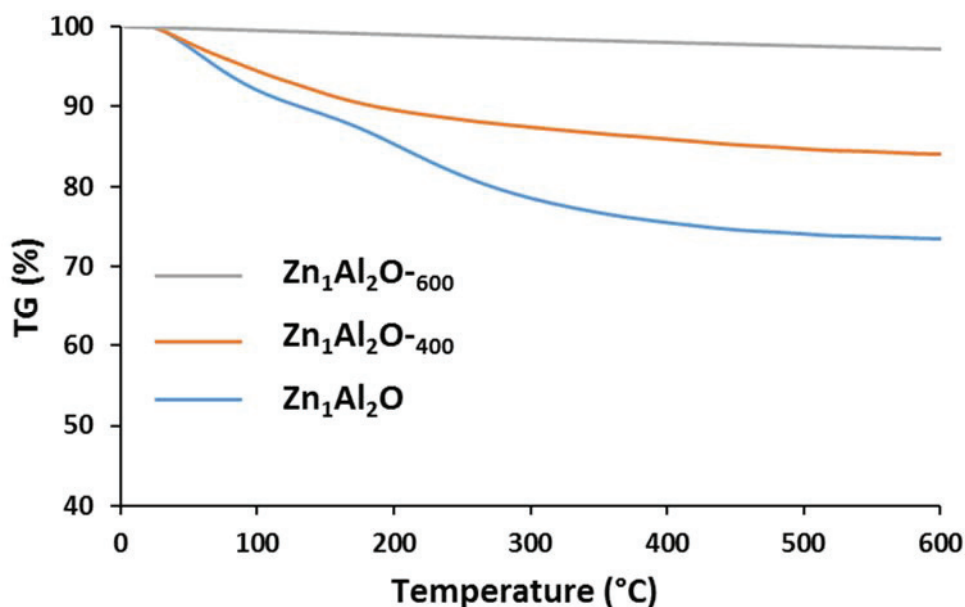


Figure 5-9: XRD diffraction patterns of $Zn_1Al_2O_z$

In terms of specific surface area, the as-prepared material had a higher specific surface area ($274 \text{ m}^2 \cdot \text{g}^{-1}$) than the one synthesized with PAA2 ($223 \text{ m}^2 \cdot \text{g}^{-1}$). As in the previous case without PAA2, it remained stable after calcination at $400 \text{ }^\circ\text{C}$ ($260 \text{ m}^2 \cdot \text{g}^{-1}$) then dropped to $169 \text{ m}^2 \cdot \text{g}^{-1}$ at $600 \text{ }^\circ\text{C}$.

Thermogravimetric analysis of the solid after synthesis showed a weight loss up to about $400 \text{ }^\circ\text{C}$, which suggested the possible presence of metal hydroxide in large quantities such as $Al(OH)_3$ or $AlO(OH)$. These amorphous phases would not be visible in XRD but could also explain the proportion of $ZnAl_2O_4$ obtained by XRD, not compatible with the stoichiometry obtained by ICP. For the solid calcined at $400 \text{ }^\circ\text{C}$, the weight loss of 16 wt% between 25 and $200 \text{ }^\circ\text{C}$ would confirm the loss of most metal hydroxides. In the paper of Kanari et al.⁹, zinc carbonate hydroxide started decomposing from $150 \text{ }^\circ\text{C}$ proving the decomposition of such compounds at low temperatures. For the one at $600 \text{ }^\circ\text{C}$ the weight loss was very low (3 wt%), in accordance with a system mainly composed of crystallized $ZnAl_2O_4$.

Figure 5-10: TGA curve of Zn₁Al₂O_{-z}

In conclusion, if we analyse the combined effect of the presence or absence of PAA2 with the aluminium content for the synthesis of supports under our operating conditions, we can draw some conclusions:

- The presence of PAA2 systematically led to a decrease in the crystallinity of the resulting compounds,
- The presence of PAA2 inhibited/delayed the appearance of the ZnAl₂O₄ phase regardless of the initial Zn/Al ratio,
- The presence of PAA2 generated greater structural homogeneity and the production of single-phase systems
- The presence of PAA2 had no impact on the stoichiometry of the material, which was the one initially set (no leaching effect),
- The presence of PAA2 significantly increases the specific surface areas of calcined materials at 400 °C, which then dropped,
- The presence of high quantity of aluminium was accompanied by a significant increase in the specific surface area and the obtaining of the ZnAl₂O₄ phase at low temperature.

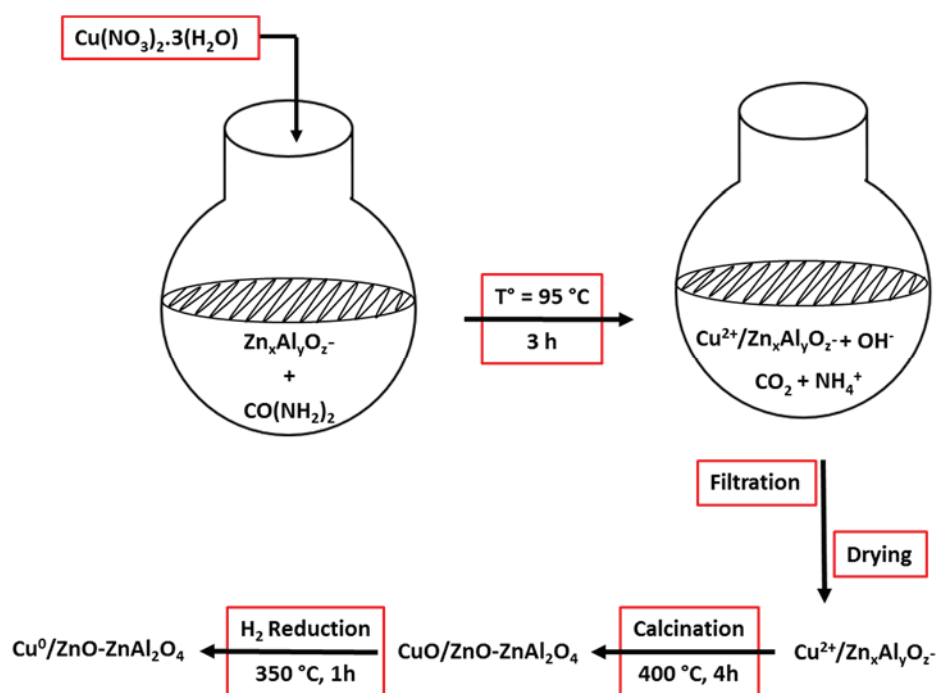
Following this study, we therefore had a range of mixed oxide supports ZnAl with two fixed and controlled Zn/Al ratios and a specific surface area ranging from 89 to 333 m².g⁻¹ at 400 °C,

the maximum temperature that the Cu/ZnAl catalyst will be subjected to. In the following section, copper depositions on all these supports were performed and the effects of nature, compositions and morphologies of the supports on the catalytic results were studied.

II. Synthesis of Cu/ZnAl by DPU: study of the Zn-Al effect

The first set of catalysts Cu/ZnAl was synthesised by the DPU method as described in Chapter II using Zn₂Al₁O-PAA2, Zn₂Al₁O-, Zn₁Al₂O-PAA2, Zn₁Al₂O-PAA₄₀₀ and Zn₁Al₂O- synthesized in the first section as supports.

As the highest glycerol conversion was obtained with Cu/ZnO-PAA2 at 20 wt% of copper and [Cu²⁺] = 20.8 mM, the first tests were performed with the same copper content on the new supports. The DPU and catalytic reaction conditions were the same as in the chapter IV (200 °C, 30 bar H₂ and 4.2% by weight of glycerol for 24 hours). Briefly, DPU process summarized in the scheme 5-1 consists on adding copper nitrate solution to a suspension of ZnAl as-prepared supports (with and without PAA2) in the presence of urea. The heating step (95 °C/3 hrs) was mandatory for the decomposition of urea, the filtration step helped to eliminate the non-precipitated ions and the heating treatments (calcination/400 °C and reduction/350 °C) led to the elaboration of the catalyst. As a reminder, after calcination, the catalyst lost all the polymer.



Scheme 5-1: Overview of DPU method on different Zn_xAl_yO_z- supports

II.1. Deposition of 20 wt% of copper on Zn₂Al₁O-PAA2 and Zn₂Al₁O materials by DPU

The properties of the catalyst obtained using Zn₂Al₁O-PAA2 and Zn₂Al₁O as supports are summarized in Table 5-6.

Table 5-6: Properties of Cu/Zn₂Al₁O-PAA2 and Cu/Zn₂Al₁O and their associated catalytic results after 24h

Catalysts	C.S. B. T. (nm)		C.S. A. T. (nm)		S.S.A. (m ² .g ⁻¹)		Conver- sion/ 24h (%)	Selectivity (%)	
	ZnO	Cu	ZnAl ₂ O ₄	Cu	B.T.	A.T.		1,2-PDO	EG
Cu/Zn ₂ Al ₁ O -PAA2	9	11	6	17	111	115	92	78	22
Cu/Zn ₂ Al ₁ O	30	17	6	13	90	219	44	81	19

B.T. : before test and A.T. : after test

The XRD diffractograms of the two catalysts with 20 wt% of copper (Figure 5-11) were similar to the supports without copper calcined at 400 °C, the only difference being due to the additional presence of copper peaks. As previously observed, the presence of PAA2 decreased the crystallinity of the compounds. The crystallite sizes of ZnO did not vary so much with or without copper and the Cu⁰ crystallite sizes were 11 and 17 nm for Cu/Zn₂Al₁O-PAA2 and Cu/Zn₂Al₁O, respectively, calculated by using the three peaks of copper at 43°, 51° and 74.5°. However, the specific surface area of the support with PAA2 dropped from 234 to 111 m².g⁻¹ for the catalyst (i.e. after copper deposition) while it remained the same for the two systems without PAA2 (89 and 90 m².g⁻¹). It therefore appeared that the Zn₂Al₁O-PAA2 support had not undergone the same structural evolution with and without copper. The decrease in surface area could be related to a strong interaction of the copper with the PAA2 during the deposition that influenced the surface of the support or the decomposition of the PAA2. Comparing to Cu/ZnO, the surface area was much higher (S.S.A of 25 – 40 m².g⁻¹ were obtained for all the Cu/ZnO using the commercial and the synthesized support as shown in chapter IV). **In conclusion, addition of aluminium led to increase of specific surface area of the catalysts as for the supports.**

With regard to the performance of these catalysts, the catalyst Cu/Zn₂Al₁O-PAA2 was found to be much more active than Cu/Zn₂Al₁O. Conversion increased from 44% to 92% when PAA2 was added to the support, with no effect on selectivity, both catalysts having an average selectivity of 80% to 1,2-PDO and 20% to ethylene glycol (EG) (Table 5-6). This difference in

performance might be due to the difference in Cu crystallite size. It was also accompanied by a difference in stability. Indeed, structural analyses by BET showed that the catalyst prepared from the support without PAA2 presented a huge increase in the specific surface area after catalysis, suggesting a significant transformation of the catalyst.

Figure 5-11 also shows the XRD data of the two catalysts after the catalytic reaction. As already observed in the last chapter, the catalyst with high conversion showed the appearance of new Zn-based carbonaceous phases [monoclinic aurichalcite $(\text{Cu,Zn})_5(\text{CO}_3)_2(\text{OH})_6$, PDF 00-038-0154 and monoclinic hydrozincite $\text{Zn}_5(\text{CO}_3)_2(\text{OH})_6$, PDF 00-019-1458] indicating C-C cleavage. The $\text{Cu/Zn}_2\text{Al}_1\text{O}$ catalyst was also transformed since only the ZnAl_2O_4 phase was visible. Both catalysts exhibited a ZnAl_2O_4 phase with an average crystallite size of 6 nm.

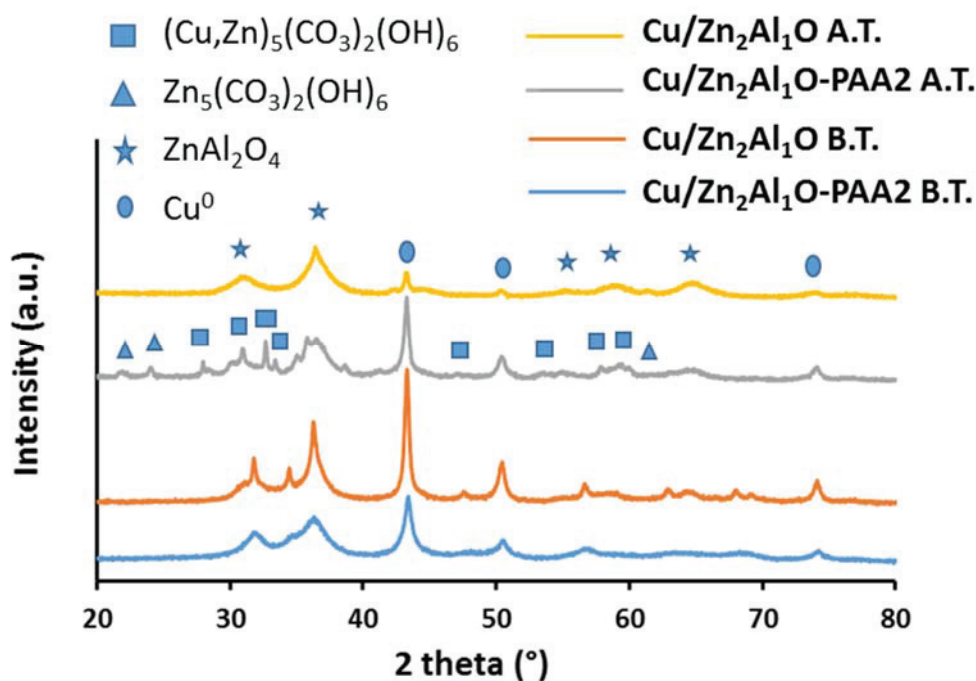


Figure 5-11: XRD diffraction patterns of $\text{Cu/Zn}_2\text{Al}_1\text{O}$ materials before and after catalysis. (B.T.: before test and A.T.: after test)

The metal contents of the catalysts were measured by ICP-AES and were compared to the ones of the support after calcination at 400 °C, to be as close as possible to the temperature at which the catalysts were prepared. The content in copper is presented as a fixed value (x) to highlight the difference in molar ratio of Zn:Al between the support and the catalyst.

The results, summarized in Table 5-7 showed that the major difference was due to the zinc content, which was 20 to 30% lower for the catalyst than for the support, regardless the

presence or absence of PAA2.

Table 5-7: Metal contents for Zn₂Al₁O supports and the resulting copper-based catalysts

Support	Support metal content* / ICP (wt%)		Formula Support	Catalysts metal content / ICP (%wt)			Formula Catalyst
	Zn	Al		Cu	Zn	Al	
Zn ₂ Al ₁ O-PAA2	55.8	11.8	Zn _{1.9} AlO _{4.7}	26.1	37.2	11.5	Cu _x Zn _{1.4} AlO _{3.7}
Zn ₂ Al ₁ O	56.5	10.9	Zn _{2.1} AlO _{5.1}	24.4	34.7	9.5	Cu _x Zn _{1.5} AlO _{5.6}
Reference tests	Solution Zn content / ICP (wt%)		Catalysts metal content / ICP (%wt)				
	Cu	Zn	Al				
DP with urea	12.4		22.9	39.3	12.0	Cu _x Zn _{1.4} AlO _{3.7}	
DP without urea	20.6		13.2	--	--		

(*: calculated for the support after calcination at 400 °C, --: not determined)

In order to verify if zinc was removed by filtration during the synthesis of the catalyst by DPU two references test were done. First, for a catalyst prepared in the presence of urea, a determination of zinc in the solution obtained after filtration was carried out by ICP-AES. The presence of 12.4 wt% of zinc proved a leaching phenomenon during catalyst synthesis by our DPU method. This phenomenon could be due to the pH (about 8 under our conditions) which could lead to the solubilization of part of the zinc. For this purpose, another catalyst synthesis was carried out without urea under the same conditions (3 hours of heating at 95 °C) to check the impact of the pH of the solution. The pH of the solution was 7 and the ICP results of the solution after filtration showed a zinc loss twice as high with 20.6 wt% of zinc content in the solution in the absence of urea. The ZnO solubility diagram in Figure 5-12¹⁰ has shown that ZnO solubility is low at pH between 9 and 12. Below pH 9 the solubility of ZnO increases, so urea could maintain a pH close to the area of low zinc solubility.

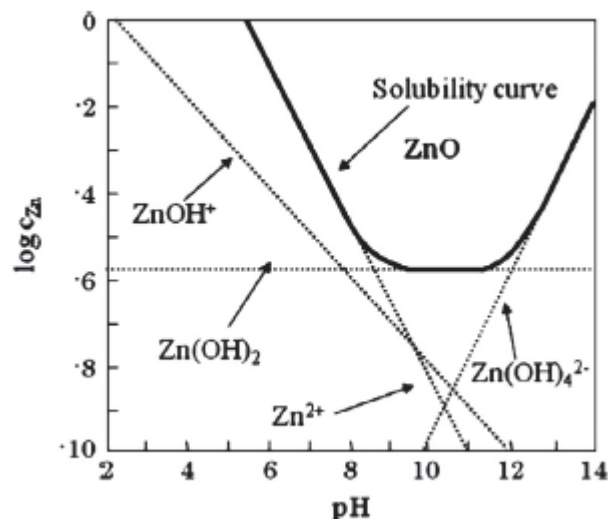


Figure 5-12: Solubility diagram of ZnO copied from reference 10

In conclusion, urea is necessary for copper precipitation but it is also necessary to prevent zinc leaching during the DPU process. However, we did not detect an impact of the presence of PAA2 on zinc retention and copper precipitation.

II.2. 20 wt% of copper on Zn_1Al_2O -PAA2 and Zn_1Al_2O materials by DPU

The deposition of copper was done on the second series of support Zn_1Al_2O under the same conditions of DPU. The calcined Zn_1Al_2O -PAA2₄₀₀ material was added to the list of supports. The properties of the catalysts are summarized in Table 5-8.

Table 5-8: Properties of Cu/Zn_1Al_2O -PAA2, Cu/Zn_1Al_2O -PAA2₄₀₀, and Cu/Zn_1Al_2O and their associated catalytic results after 24h

Catalyst	ZnAl ₂ O ₄ size (nm)		Cu ⁰ size (nm)		S.S.A. (m ² .g ⁻¹)		Conversion /24h (%)	Selectivity (%)	
	B.T.	A.T.	B.T.	A.T.	B.T.	A.T.		1,2-PDO	EG
Cu/Zn₁Al₂O-PAA2	7	8	9	26	167	110	51	92	7
Cu/Zn₁Al₂O-PAA2₄₀₀	--	14	8	19	185	239	64	88	12
Cu/Zn₁Al₂O	7	7	24	24	228	239	83	86	14

(B.T. : before test and A.T. : after test)

The XRD diffractograms of the three catalysts before reaction (Figure 5-13) were similar but slightly different from the initial supports without copper and calcined at 400 °C, the difference being the total disappearance of the peaks corresponding to ZnO. The average size of ZnAl_2O_4 was estimated at about 7 nm for $\text{Cu}/\text{Zn}_1\text{Al}_2\text{O}$ -PAA2 and $\text{Cu}/\text{Zn}_1\text{Al}_2\text{O}$, calculated with the peak at 65°, and the peaks at 31, 37 and 65°, respectively. For $\text{Cu}/\text{Zn}_1\text{Al}_2\text{O}$ -PAA2₄₀₀, the peaks overlapped too much to determine a relevant average size of ZnAl_2O_4 . The copper nanoparticles were well crystallized for all three samples and their size was calculated using the three peaks at 43, 51 and 74.5°. **The results showed a significant difference in copper size when using the substrate with PAA2, since an average size of 8, 9 and 24 nm was found for $\text{Cu}/\text{Zn}_1\text{Al}_2\text{O}$ -PAA2₄₀₀, $\text{Cu}/\text{Zn}_1\text{Al}_2\text{O}$ -PAA2 and $\text{Cu}/\text{Zn}_1\text{Al}_2\text{O}$, respectively. This was true even if PAA2 was removed at 400 °C before Cu deposition, suggesting a beneficial structural effect of PAA2 during support synthesis for copper dispersion.**

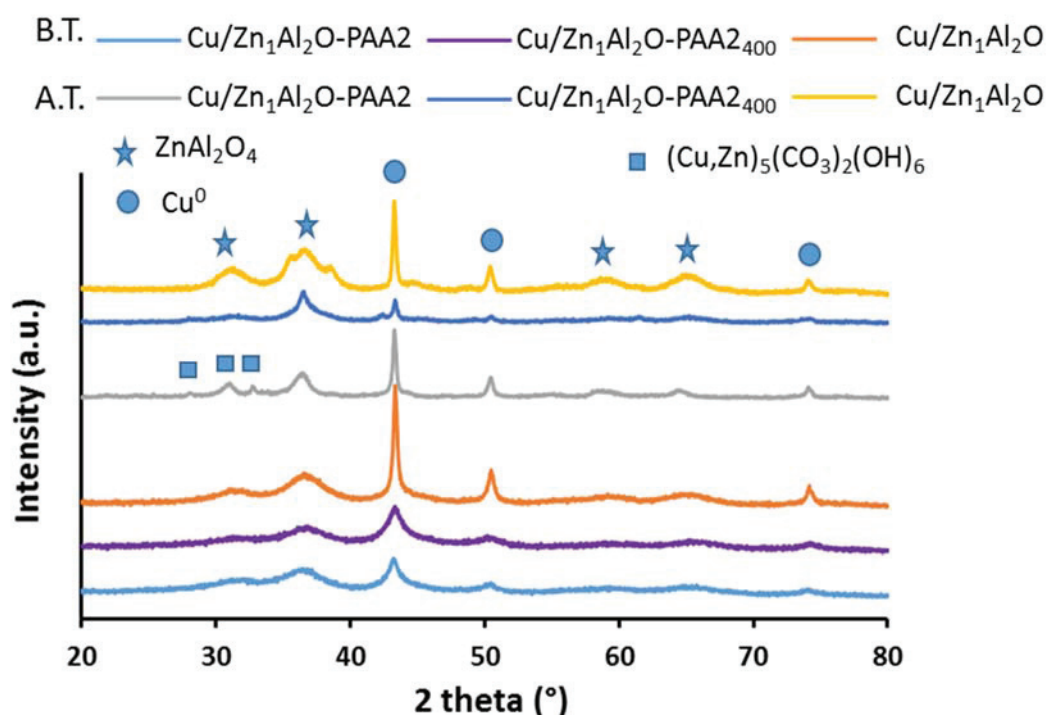


Figure 5-13: XRD diffraction patterns of $\text{Cu}/\text{Zn}_1\text{Al}_2\text{O}$ before and after catalysis (B.T.: before test and A.T.: after test)

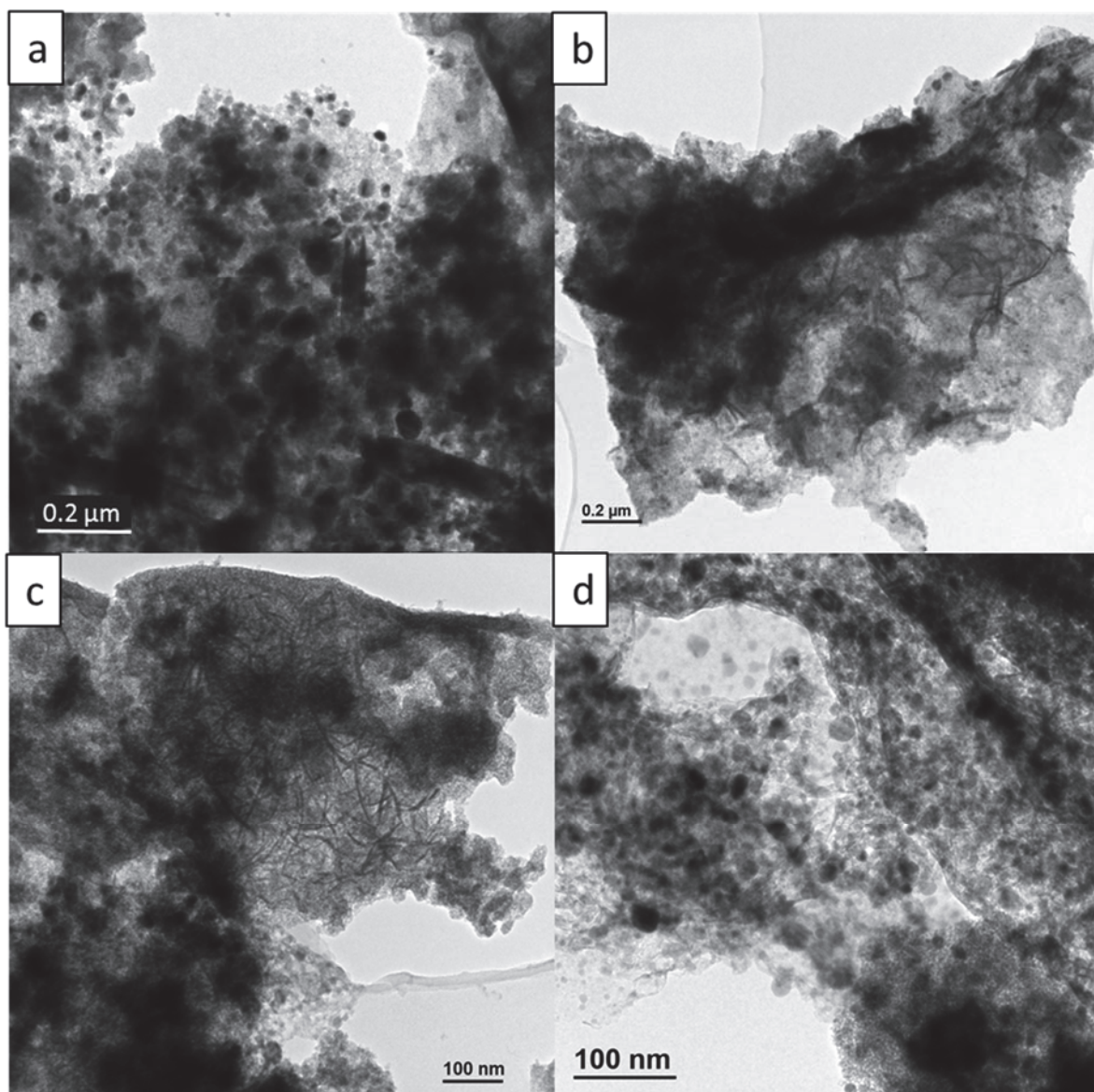


Figure 5-14: TEM images of :a,c) Cu/Zn₁Al₂O-PAA2, b,d) Cu/Zn₁Al₂O-PAA₂₄₀₀ before catalysis

The TEM images of the freshly reduced catalysts Cu/Zn₁Al₂O-PAA2 and Cu/Zn₁Al₂O-PAA₂₄₀₀ are shown in Figure 5-14. They showed similar morphologies and compositions with spherical nano-objects and 2D nano-sheets. These observations were in agreement with the XRD results, which showed that the presence of PAA2 was important during the synthesis of the support but became optional during copper deposition in terms of dispersion.

The metal contents of the supports and corresponding catalysts are summarized in Table 5-9. The values showed that only the Zn₁Al₂O-PAA2 support kept the same proportion of zinc after DPU. The use of the other two PAA2-free substrates for copper deposition resulted in zinc losses of up to 50%. In this aluminium-rich system, the presence of PAA2, when in contact

with copper, seemed to avoid a significant loss of zinc. It could be assumed that this system contained more amorphous zinc oxide or hydroxide soluble in basic conditions during urea decomposition or that PAA2 served as a buffer compound due to its carboxylic acid functions.

Table 5-9: Metal loading for supports and the resulting copper-based catalysts

	Support metal content*/ (ICP wt%)		Formula Support	Catalyst metal content/ (ICP wt%)			Formula Catalyst
	Zn	Al		Cu	Zn	Al	
Zn₁Al₂O-PAA2	25.5	25.9	ZnAl _{2.5} O _{7.8}	16.5	22.4	22.2	Cu _x ZnAl _{2.4} O _{7.1}
Zn₁Al₂O-PAA2₄₀₀	21.2	22.6	ZnAl _{2.6} O _{10.8}	24.4	10.6	24.1	Cu _x ZnAl _{5.5} O _{15.9}
Zn₁Al₂O	27.3	27.1	ZnAl _{2.4} O _{6.9}	22.7	17.4	22.4	Cu _x ZnAl _{3.1} O _{8.8}

(*: calculated for the support after calcination at 400 °C)

The specific surfaces of the aluminium-rich Zn₁Al₂ catalysts (Table 5-8) were significantly larger than those of the Zn₂Al₁ catalysts (Table 5-6) with values ranging from 170 to 230 m².g⁻¹, the maximum value being obtained without PAA2 as in the Zn₂Al₁ system.

In terms of reactivity, the catalyst without PAA2 proved to be the most efficient with a 24-hour conversion of 83% associated with a slightly lower selectivity towards 1,2-PDO (86%). However, it was difficult to extract from the previous data a major factor in these performances, except that the best catalyst seemed the most robust in terms of copper nanoparticles size (even if they are the biggest) and specific surface area (Table 5-8). However, XRD diffractograms showed the appearance of peaks at 34 and 37 ° attributed to ZnO that was not present in the catalyst before test, and that appeared due to the catalytic reaction conditions (Figure 5-12).

The other two catalysts showed lower performances and displayed weak modifications on the XRD diffractograms with the appearance of either weak proportion of carbonaceous phases [(Cu,Zn)₅(CO₃)₂(OH)₆ and Zn₅(CO₃)₂(OH)₆] (which were favourable for the Zn₂Al₁ system) or the sintering of Cu⁰ particles. The evolution of specific surface areas was more difficult to correlate with reactivity.

TEM images of catalysts with PAA2 after reaction (Figure 5-15) showed similar morphologies and the increase in copper crystallite size measured by XRD could not be observed on these

images. However, the crystalline phase of ZnAl_2O_4 was visible in Figure 5-14 c and d and had an average particle size similar to that of the crystallites calculated by XRD of 6 nm for both catalysts.

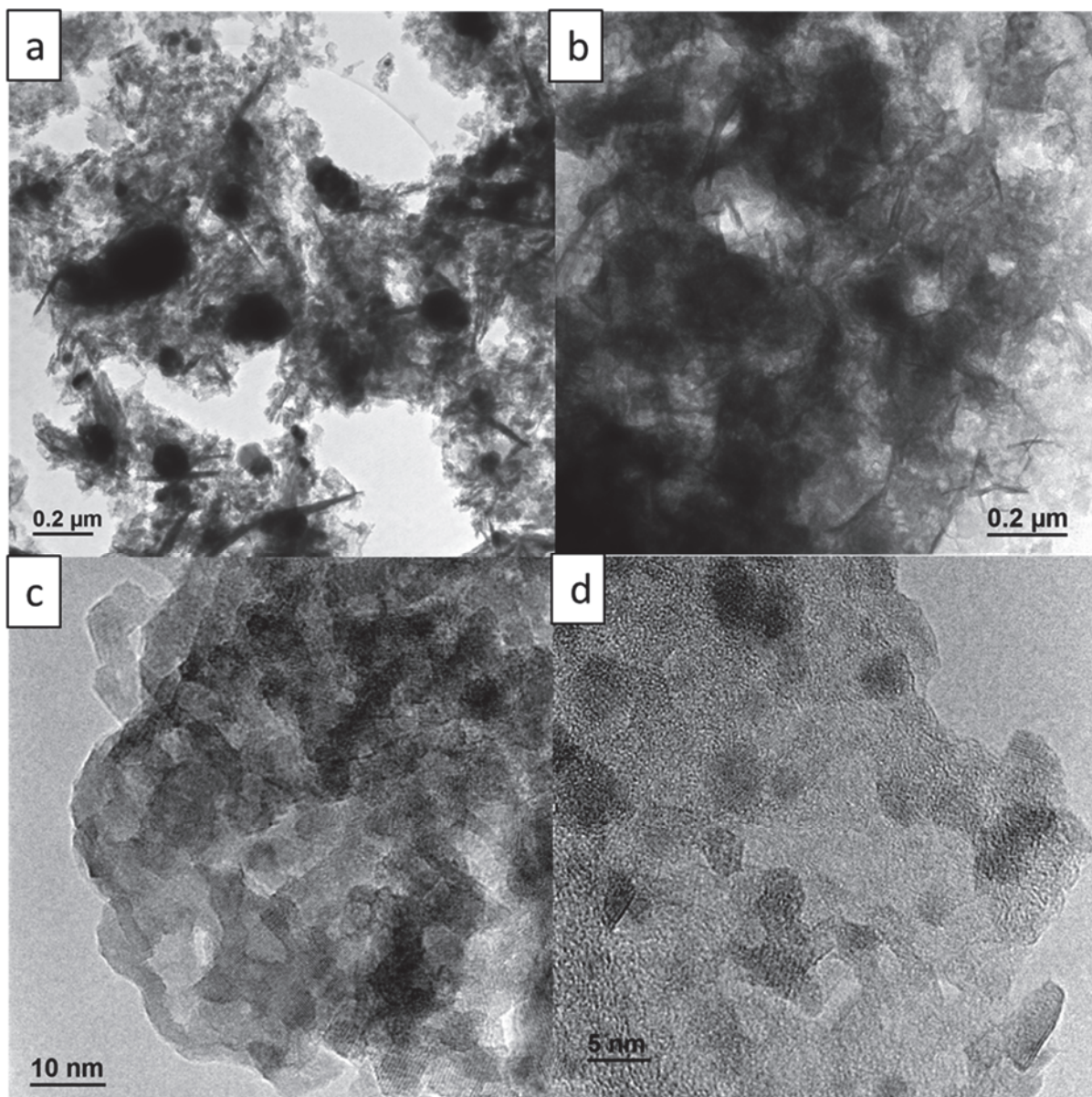


Figure 5-15: TEM images of: a,c) $\text{Cu}/\text{Zn}_1\text{Al}_2\text{O-PAA}_2$, b,d) $\text{Cu}/\text{Zn}_1\text{Al}_2\text{O-PAA}_{2400}$ after catalysis

In conclusion, the development of copper catalysts by DPU through the use of our various ZnAl mixed supports has shown that:

- Zinc content tended to decrease mainly by leaching during the DPU process but in less extent with the presence of urea

- Presence of PAA2 reduced zinc loss and was more effective when the amount of zinc was low. This could be explained by the fact that PAA2 can buffer the environment by avoiding pH hits during urea decomposition and thus the passage of zinc-based species in solution.

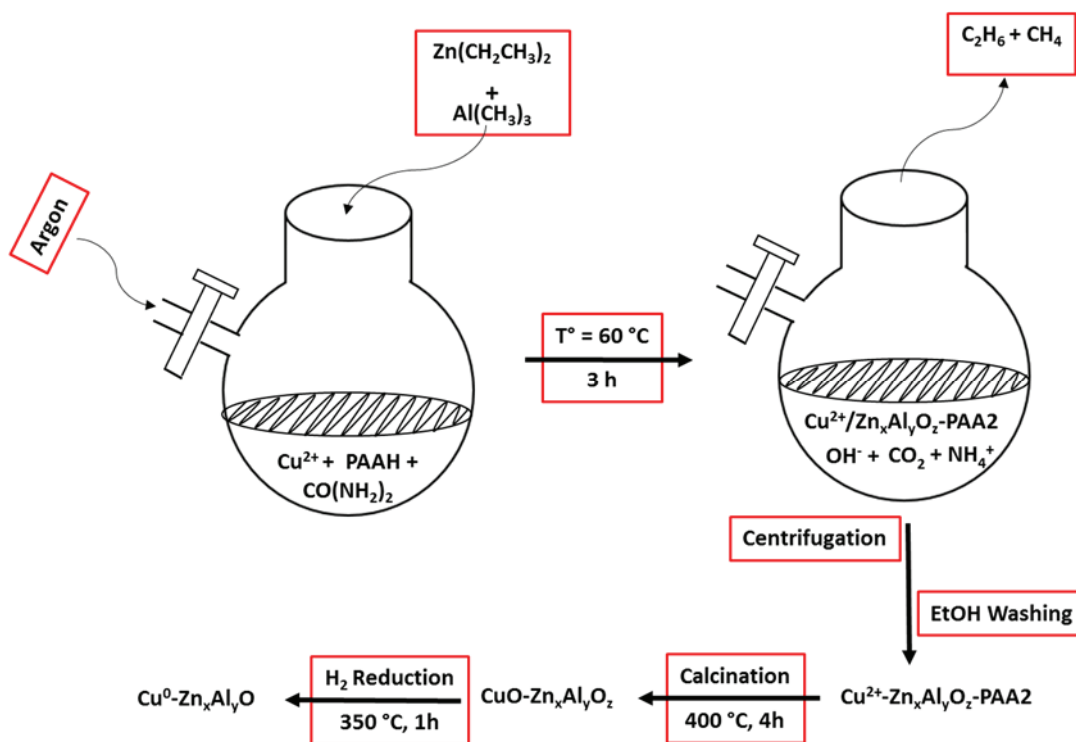
This loss of zinc during the DPU process led, during our study, to a variability in the characteristics of our catalysts, which we tried to avoid by setting up a "one pot" synthesis route by adding copper in the PAA2 solution when elaborating the ZnO and the ZnAlO.

III. Synthesis of $\text{Cu-Zn}_x\text{Al}_y\text{O}_z$ by a "one pot method": Study of the synthesis parameters

This new one-pot method was divided into two routes: a "one-pot-one step" and a "one pot-two step" in relation to the synthesis strategies; further steps of calcination and reduction were still needed to get the final Cu-ZnAl catalyst.

As mentioned at the beginning of the chapter, the old bottle of AlMe_3 used to elaborate ZnAl oxides, was also used for the elaboration of the catalysts by the "one pot" method.

III.1. Synthesis of $\text{Cu-Zn}_x\text{Al}_y\text{O}_z$ by a "one pot - one step" route



Scheme 5-2: Overview of the one pot – one step method

As for Cu-ZnO, all the precursors were added in the same flask and the method was called “one pot - one step”. Scheme 5-2 shows a brief sum up of the steps, this one pot consists on mixing the copper precursor with the PAA2 solution and urea at room temperature, heating at 60 °C before adding the mixture of ZnEt₂ and AlMe₃ stored in a schlenk flask. After 3 hours, the slurry was centrifuged, washed with 90 mL of EtOH and after drying overnight, the powder underwent thermal treatment to elaborate the catalyst.

In the case of this sample, the molar ratio Zn:Al targeted was 1:2 due to the high activity reported with this molar ratio in Cu-Zn-Al for the hydrogenolysis of glycerol¹. The ICP analysis of the catalyst after reduction, gave metal content of:

Cu= 31.1 wt%, Al = 10.1 wt%, and Zn= 34.6 wt% resulting in a formula Cu_xZn_{1.4}Al₁O_{4.1}. As for the ZnAl oxides, the catalyst has a lower content in Al compared to the theoretical one due to the oxidized bottle of AlMe₃.

Table 5-10: Properties of “one pot - one step” Cu-Zn_xAl_yO_z

Catalyst	S.S.A. BET (m ² .g ⁻¹)	ZnO size (nm)	Cu ^o size (nm)
After synthesis	28	A	--
After calcination	54	17	CuO
After reduction	25	17	13
After reaction	114	--	16

(A: amorphous, --: not determined).

The materials were characterized by BET and XRD after each step and the results are shown in Table 5-10. The specific surface area of the catalyst after synthesis had a low value reminding the one obtained for Cu-ZnO prepared by one pot – one step method (Chapter IV, section III.1). Calcining the sample led to an increase of the surface area from 28 to 54 m².g⁻¹. However, after reduction the specific surface area was low, similar to that obtained with Cu-ZnO-PAA2 (24 m².g⁻¹) and much lower than Cu/Zn_xAl_yO_z obtained by DPU. The increase in the surface area after calcination seemed to be related to the ZnO and not to the crystallization of Al because it was followed by a decrease after reduction.

XRD diffractograms (Figure 5-16) fitted well with the BET data showing an amorphous phase of ZnO after synthesis reminding the ZnO-PAA2 obtained in the chapter III resulting in such low specific surface area. As expected, the calcination step did not allow the crystallization of Al species but it resulted in well crystallized phase of monoclinic CuO (PDF number 00-045-

0937) (unassigned on the figure but characterized by the main peaks at 35° and 39°) with an average crystallite size of 16 nm. After reduction, the catalyst was essentially composed of the ZnO phase and Cu⁰. This latter one had average sizes of about 13 nm calculated with the three peaks at 43, 51 and 74.5°. The size of ZnO was not changing after each step while ZnAl₂O₄ was mostly amorphous, the crystallite size could not be determined. Comparing to the catalyst obtained by DPU method in presence of PAA2 (Table 5-6) and with same molar ratio of Zn:Al (1.4:1), Cu⁰ crystallites were in the same range (11 nm).

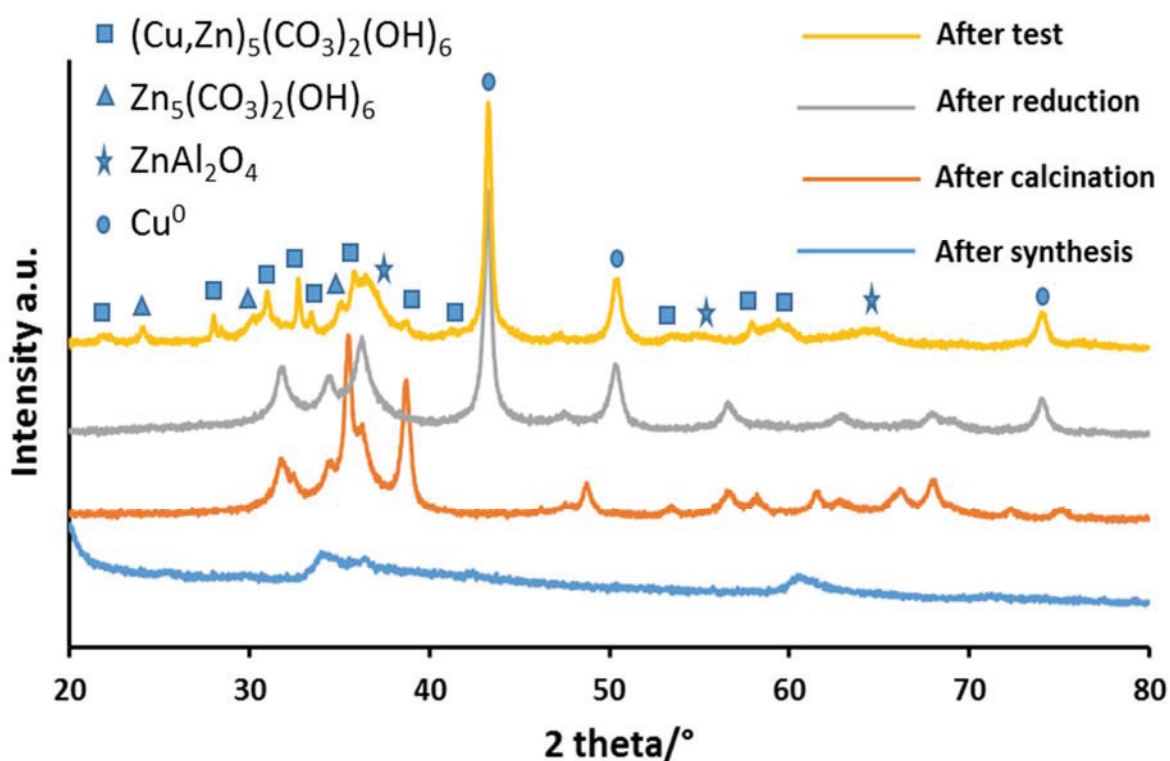


Figure 5-16: XRD of Cu_x-Zn_{1.4}Al_{1.0}O_{4.1} prepared by the "one pot - one step" method

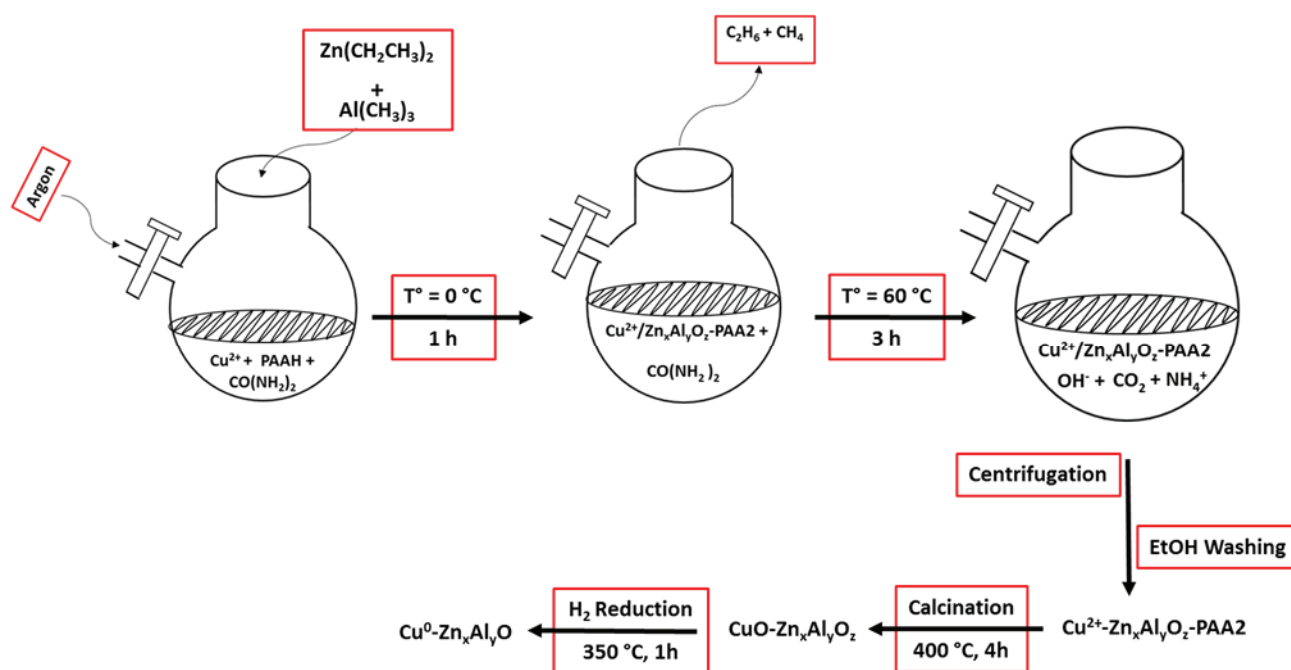
The catalytic results will be presented in the following III.3. section, with the catalyst obtained by the "one pot–two steps" route in order to compare the effect of the synthesis method on the behaviour of the catalyst.

III.2. Synthesis of Cu-Zn_xAl_yO_z by a "one pot -two steps" route

As for Cu-ZnO (Chapter IV, section III.2), the "one pot" method was modified into a two steps approach. The main difference was that the synthesis was conducted at two temperatures. As before, the copper precursor solution is mixed with PAA2 solution and urea at room temperature but the Zn and Al precursors are added at 0 °C instead of 60 °C. Scheme 5-3 shows a brief sum up of the syntheses steps, the centrifugation, 90 mL EtOH washing step and the

thermal treatments for the elaboration of the final catalyst. As it was explained in the fourth chapter, the idea from the “one pot – two steps” route was to allow the precipitation of $Zn_xAl_yO_z$ -PAA2 before increasing the temperature. Once the heating began, urea started decomposing and led to an increase in the pH.

The “one pot – two steps” route in this chapter was studied in depth and the scheme below shows the first attempt for the elaboration of Cu-Zn-Al via this approach englobing all the steps and / or the additives (PAA2, urea). In the upcoming section (III.4.), some parameters will be changed.



Scheme 5-3: Overview of the one pot – two steps method

Once again, the catalyst was prepared with the old bottle of $AlMe_3$ as for the catalyst elaborated by the “one pot – one step” approach.

Table 5-11 summarizes the properties of the materials after each step and those of the catalyst regenerated and recycled.

Table 5-11: Properties of “one pot - two steps” route for Cu-Zn_xAl_yO_z

Catalyst	S.S.A. BET (m ² .g ⁻¹)	ZnO size (nm)	Cu size (nm)
After synthesis	62	35	--
After calcination	64	--	CuO
After reduction	97	--	13
After reaction	143	--	18
Recycled (2 nd run)	149	--	18
After 2 nd run	150	8	20
After 3 rd run	155	10	21

The ICP analysis of the catalyst after reduction, gave metal content of: Cu= 25.1 wt%, Al = 16.5 wt%, and Zn = 28.8 wt% resulting in a formula Cu_x-Zn₁Al_{1.4}O_{4.2}. As expected from the old bottle, the stoichiometry did not reflect the expected one.

Nevertheless, the separation of the synthesis into two steps resulted in higher surface area after each step compared to the catalyst prepared by the “one pot – one step” route. The surface area of the catalyst after synthesis (62 m².g⁻¹) was in the range of ZnO-PAA2 elaborated at 0 °C presented in chapter III, section I.4.1. Calcining the sample did not show an increase in the specific surface area which was not a common behavior nor for ZnO neither for ZnAl₂O₄. However, the reduction step resulted in an increase till 97 m².g⁻¹, showing a value in the same range as the Cu/ZnAl catalysts prepared by DPU with molar ratio Zn:Al (2:1) shown in Table 5-6.

Comparing the S.S.A value of the reduced catalyst obtained by the “one pot – one step” route (25 m².g⁻¹) and “one pot – two steps” route (97 m².g⁻¹) demonstrated again the importance of the synthesis temperature even in the presence of aluminium.

XRD in Figure 5-17 shows a crystallized phase of hexagonal ZnO for the material after synthesis with an average crystallite size of 35 nm calculated with the peaks at 36°, 42° and 62°. A peak corresponding to ZnAl₂O₄ was seen at 35° but the crystallite size could not be calculated due to the wide diffraction of the peak. After calcination, the catalyst had a similar structure as the catalyst prepared by the “one pot – one step” route however the CuO phase was less intense despite the similar crystallite size of 21 nm. Once again ZnAl₂O₄ was not present after calcination and that was also expected since no increase in surface area occurred after calcination. ZnO was less crystallised than the catalyst prepared by the “one pot – one step”

route and the crystallite size could not be calculated.

After reduction, the catalyst was a combination of the three phases with similar percentage for ZnO (24%) and ZnAl₂O₄ (29%). Even that ZnAl₂O₄ was highly present compared to the catalyst prepared in one step, the peaks were too large and the crystallite size could not be calculated. Cu⁰ calculated with the three peaks at 43, 51 and 74.5° showed an average value of 13 nm similar to the “one step” route.

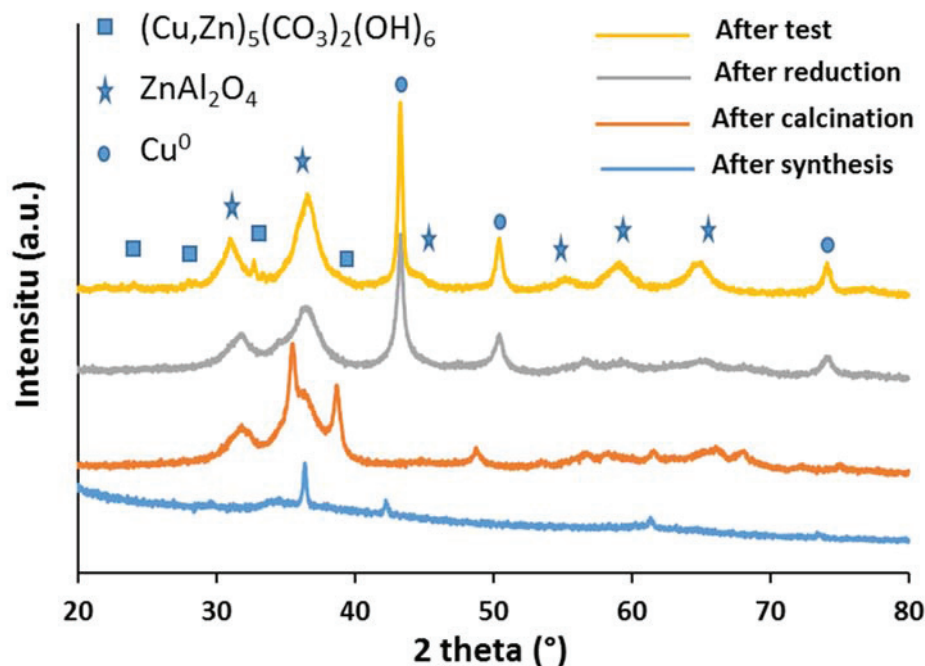
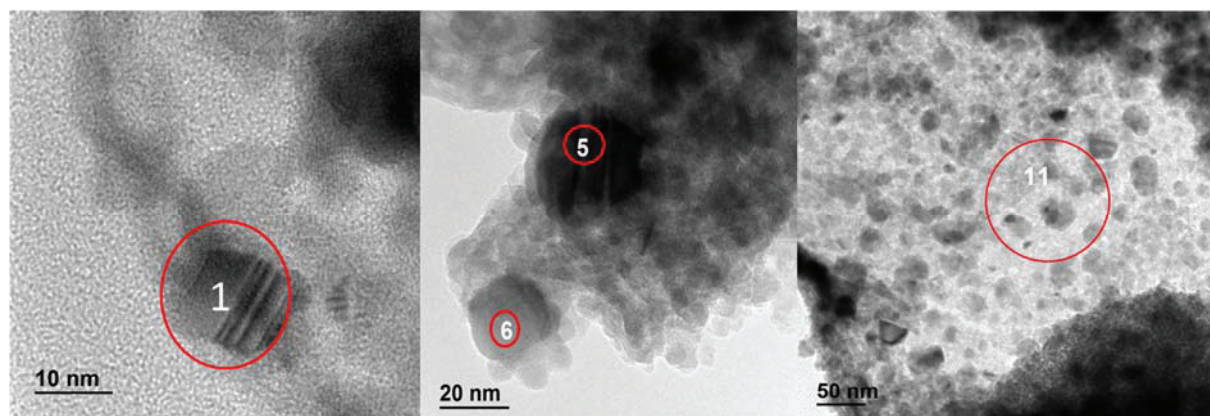


Figure 5-17: XRD diffraction patterns of “one pot - two steps” Cu_x-Zn₁Al_{1.4}O_{4.2} (after test corresponds to after the 1st run)

The TEM images of the material are shown in Figure 5-18 and the associated EDX measurements in Table 5-12. The images showed highly dispersed particles with mesospheric shapes. The EDX spot 6 of Figure 5-18 suggested the presence of a large copper particle. The molar ratio obtained by ICP (Zn:Al, 1:1.4) could be associated with the spots 1 and 11. Moreover, the area number 1 was representative of the ZnAl₂O₄ with the oriented fringes. Area 5 showed higher content in Al compared to Zn, suggesting again the possibility of elaborating Al oxides or Zn_xAl_yO_z with high Al content, as seen for ZnAl oxides for a molar ratio Zn:Al (1:2) (section I.2).

Figure 5-18: TEM images of $\text{Cu}_x\text{-Zn}_1\text{Al}_{1.4}\text{O}_{4.2}$ one pot two steps before catalysisTable 5-12: EDX measurements of $\text{Cu}_x\text{-Zn}_1\text{Al}_{1.4}\text{O}_{4.2}$ one pot two steps before catalysis.

Area	Elements	Zn (molar %)	Al (molar %)	Cu (molar %)
	1	20.7	34.5	54.9
	5	5.8	32	62.2
	6	0	4.2	97.0
	11	19.5	41.8	38.7

III.3. Catalytic results over $\text{Cu-Zn}_x\text{Al}_y\text{O}_z$ prepared by “one pot” routes

The catalytic behaviours of the two catalysts elaborated by “one pot” routes are shown in the Table 5-13.

Table 5-13: Catalytic results obtained with $\text{Cu-Zn}_x\text{Al}_y\text{O}_z$ catalysts prepared by “one pot” routes

Catalyst	Run	Conversion 24h (%)	Selectivity (%)	
			1,2-PDO	EG
One step	1 st run	83	78	21
Two steps	1 st run	96	83	17
Two steps	2 nd run	93	83	17
Two steps	3 rd run	90	84	16

The catalyst obtained by the “one step” approach showed a lower conversion (83%) compared to the one elaborated by the “two steps” approach (96%) but with selectivity toward 1,2-PDO in the same range of ca. 80%.

The catalyst obtained by the “one step” route with a molar ratio Zn:Al (1.4:1) and 31.1 wt% of

Cu could be compared to the Cu/Zn₂Al₁-PAA2 prepared by DPU shown in Table 5-6 resulting in similar properties : 26 wt% of copper, Zn:Al molar ratio (1.4:1). The conversion obtained with the later catalyst (92%) was higher than the one obtained by the one pot process (83%). The main difference between the two catalysts was the copper weight percentage which was higher in the case of the catalyst prepared by the “one pot” method. The higher copper percentage could be responsible for the decrease in conversion for the one pot catalyst due to the surface saturation phenomenon as seen in chapter IV with different catalysts.

The “two steps” catalyst showed higher conversion (96%) compared to the “one step” route. If we compared the properties of the two catalysts, the “two steps” catalyst had a higher amount of Al with a molar ratio Zn:Al (1.1.4), lower amount of Cu (25% vs. 31%), higher surface area (97 m².g⁻¹ after reduction) and similar Cu⁰ crystallite size (13 nm). The catalysts obtained by DPU could not be compared to the “two steps” catalyst because none of them had the same Zn:Al molar ratio. But in term of behaviour, the higher Al content in the “one pot” method seemed to be more favourable compared to the DPU where the conversion decreased at a higher content of Al (Table 5-8). Moreover, it seemed that having a Cu loading above 30% was detrimental for the activity.

A three-run recyclability test was performed with the catalyst developed using the “two-steps” route. The catalyst properties and the conversion shown in Table 5-13 proved that the recyclability test worked very well. There was no copper leaching during the reaction and the conversion and selectivity were not influenced by recyclability. For the sake of clarity, before each test, the catalyst was regenerated by calcination and reduced because, as with Cu-ZnO, when no regeneration was performed, the conversion decreased from 96% to 43%.

XRD showed a more robust system for the “two steps” catalyst (Figure 5-16) than the “one step” catalyst (Figure 5-15). The specific surface areas remained similar, however there was a slight increase in Cu crystallite size.

Figure 5-19 shows TEM images of the catalyst after test. Comparing to the catalyst before test, no agglomeration was detected. EDX measurements (Table 5-14) showed less content of copper in the catalyst after test compared to the one before test indicating on the same kind of spots (fringes in the area 1 of Figure 5-17 and those in area 4 of Figure 5-18). At the same time, the Zn content seemed to be high compared to the molar ratio Zn:Al (1:1.4) obtained by ICP. Nevertheless, spot 2 showed an approximate value corresponding to the molar content

of each metal proving that the catalyst after test was a combination from the freshly reduced catalyst and the new phases obtained due to the catalytic conditions.

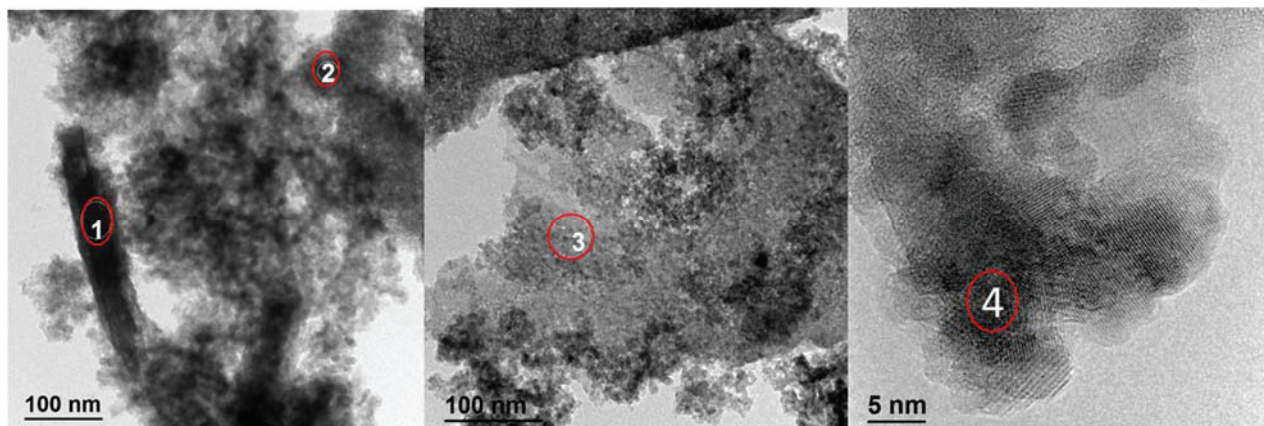


Figure 5-19: TEM images of $\text{Cu}_x\text{-Zn}_1\text{Al}_{1.4}\text{O}_{4.2}$ one pot two steps after catalysis

Table 5-14: EDX measurements of $\text{Cu}_x\text{-Zn}_1\text{Al}_{1.4}\text{O}_{4.2}$ one pot two steps after catalysis.

Area	Elements	Zn (molar %)	Al (molar %)	Cu (molar %)
1		74.8	18.2	7.0
2		15.6	27.1	57.3
3		42.8	49.5	7.7
4		17.1	78.4	4.5

The recyclability of our catalyst is worth noting because in the literature most Cu/ZnAl catalysts lost in conversion¹¹ or selectivity after each cycle¹.

III.4. Effect of synthesis parameters on $\text{Cu-Zn}_x\text{Al}_y\text{O}_z$ by “one pot-two steps” route:

As mentioned previously, synthesis parameters have a significant impact on catalyst properties leading to a change in glycerol conversion. In this section, we have studied different synthesis parameters such as the molar ratio Zn:Al, the presence of urea, the Cu wt%, the temperature and the presence of PAA2.

As seen in the upper part, the catalyst prepared by the “one pot – two steps” route showed a higher conversion than the one prepared by “one pot – one step”. For this reason, the synthesis of following batches were done only through the “two steps” route.

Table 5-15 shows the properties and the associated catalytic results of Cu-ZnAl catalysts,

classified by increasing amount of copper percentage and labelled as CZA-XUHP where:

- CZA: Cu-ZnO-ZnAl₂O₄,
- X is the theoretical weight percentage of copper,
- U means the use of urea,
- H heated at 60 °C for 3 hours
- and P means the use of PAA2.

So for example, the catalyst labelled CZA-5UHP was a catalyst loaded with 5 wt% of copper, made with urea and PAA2 and heated at 60 °C while a catalyst labelled CZA-20H was a catalyst loaded with 20 wt% of copper elaborated without urea and without PAA2 but heated at 60 °C for 3 hours.

Table 5-15: Effect of synthesis parameters on CZA catalysts prepared by “one pot-two steps” route

CZA catalysts	Cu content / ICP (wt%)	S.S.A. / BET (m ² .g ⁻¹)	Cu ⁰ size (nm)	Formula	Conversion /24 (%)	Selectivity (%)	
						1,2-PDO	EG
5UHP	4.35	143	13	Zn _{2.2} Al ₁ O _{5.0}	34	97	2.6
5HP	5.21	123	15	Zn _{2.0} Al ₁ O _{4.7}	50	91	8.5
10UHP	9.7	154	12	Zn _{2.1} Al ₁ O _{4.5}	44	85	16
10HP	12.31	141	13	Zn _{1.9} Al ₁ O _{4.1}	66	89	12
20UHP	19.2	76	17	Zn _{2.1} Al ₁ O _{4.9}	66	83	16
20HP	19.8	70	14	Zn _{1.9} Al ₁ O _{4.3}	98	88	11
20UP	14.3	79	13	Zn _{1.4} Al ₁ O _{4.9}	14	99	0.5
20P	15.6	70	11	Zn _{1.2} Al ₁ O _{4.2}	79	90	10
20H	19.2	64	30	Zn _{2.1} Al ₁ O _{4.9}	46	91	9
20HP	15.2	135	15	ZnAl _{1.1} O _{3.3}	83	83	17
20UHP	17.8	185	16	ZnAl _{3.7} O _{11.5}	80	86	14

By analyzing the data in Table 5-15 and for the same Zn/Al ratio of 2:1, several conclusions can be drawn:

- **High specific surfaces of the catalysts were obtained by either using urea (above 76 m².g⁻¹) or a low copper content (above 140 m².g⁻¹).**
- **The metallic copper contents measured by ICP were generally very close to the theoretical target percentages (5, 10 and 20 wt%) suggesting that complete copper deposition could be done even without urea but only when heating at 60**

- °C for 3 hours. Without this heating, a copper default was observed (CZA-20UP and CZA-20P), which could be explained by a partial precipitation of the copper.
- In addition, unlike the DPU process, all Zn/Al ratios were very close to 2 except, again, if no heating to 60 °C was performed. In conclusion, the step of heating to 60 °C for 3 hours was mandatory to have a control on the stoichiometry of Cu:Zn:Al. Heating was also mandatory if urea was used, otherwise its non-decomposition led to deactivation of the catalyst by probable poisoning of its surface (14% conversion for the CZA-20UP catalyst).

Figure 5-20 shows the XRD diffractograms of CZA-5HP, CZA-5UHP, CZA-20HP and CZA-20UHP as examples. As before, peaks associated with ZnAl_2O_4 and Cu are labelled on the figure, the peaks without labels correspond to ZnO. For all the catalysts, the Cu^0 crystallite sizes are included in Table 5-15 and they are within the range 12-17 nm, with an average of 15 nm, calculated with the three peaks at 43, 51 and 74.5°. Moreover, small crystallites of ZnO (7 nm) were observed (calculated with the peaks at 57, 63 and 69°) along with very small crystallites of ZnAl_2O_4 (size undetermined by Diffrac.Eva). CZA-20H was the exception with 30 nm for Cu^0 and 19 nm for ZnO. **Therefore, another important factor to mention is the use of PAA2 by comparing CZA-20HP with CZA-20H, the conversion decreased to 46% without PAA2 due to the sintering of the copper particles during the synthesis.** Keeping the polymer during the synthesis helps the elaboration of the homogeneous mesospheres of ZnO- ZnAl_2O_4 leading to a better dispersion of Cu^0 more active in catalysis.

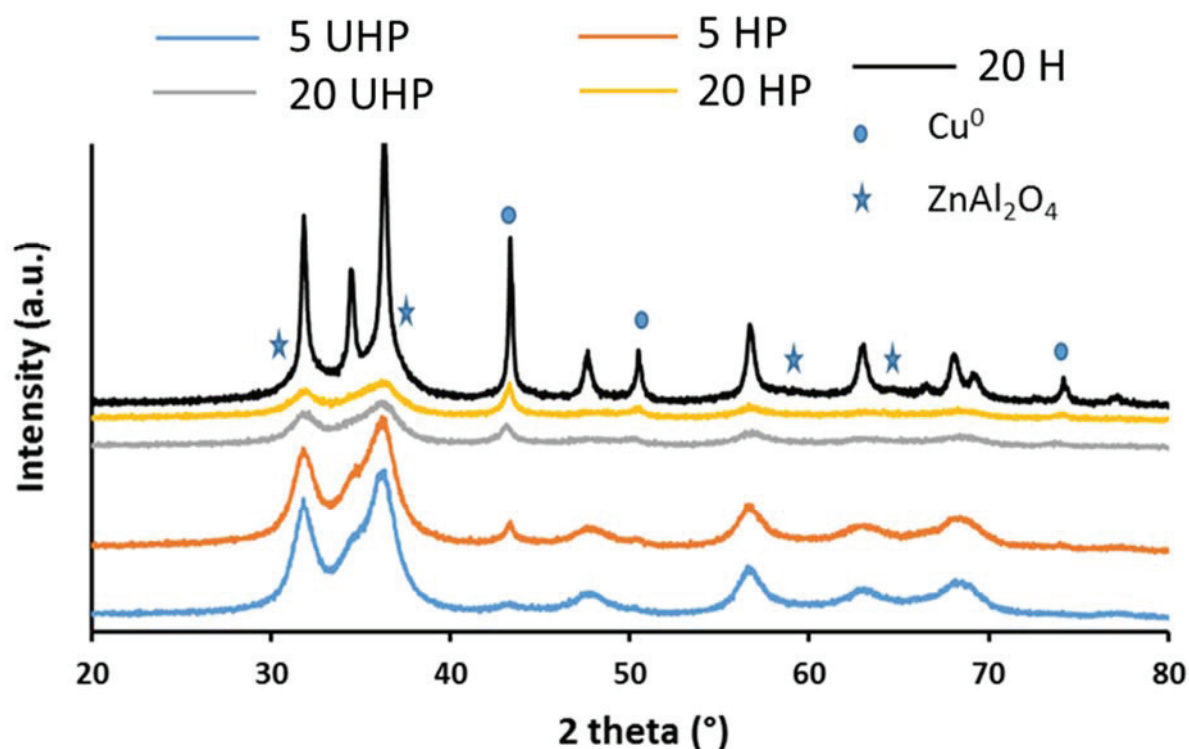


Figure 5-20: XRD diffractograms of CZA-20H and CZA [XUHP, XHP/ (X= 5 and 20)] before catalysis

The best performance (98 % of conversion) was obtained for the CZA-20HP catalyst elaborated with 20 wt% of copper, with PAA2 and heating at 60 °C and more importantly without urea.

When we compared the catalysts synthesised with (UHP) or without (HP) urea, with 5%, 10% or 20% of Cu, no urea exhibited higher conversion. For each Cu loading (5, 10, 20), the specific surface area and Cu^0 crystallite sizes were similar for the UHP and HP catalysts. In order to understand the effect of urea on the properties of the catalysts, XRD and SEM were carried out with CZA-20UHP (66% conversion) and CZA-20HP (98% conversion). XRD diffractograms of the catalysts after tests in Figure 5-21 showed similar structure for both catalysts with differences in the percentage of the phases calculated by Diffrac.Eva software. It could be seen that the CZA-20HP exhibited a higher stability compared to CZA-20UHP as ZnO phase was not transformed into hydrozincite or copper zinc hydroxide. Table 5-16 resumes the properties of the 2 catalysts before and after test.

Table 5-16: CZA-20UHP and CZA-20HP (Zn:Al ; 2:1) summarized properties before and after test.

CZA Catalyst	S.S.A. BET ($\text{m}^2.\text{g}^{-1}$)		CuO size (nm)		ZnO size (nm)	
	B.T.	A.T.	B.T.	A.T.	B.T.	A.T.
20UHP	76	147	17	15	12	--
20HP	70	138	14	14	8	95

SEM images for the catalysts before and after test are shown in Figure 5-22. The catalysts before test did not have the same morphology with irregular spheres for CZA-20UHP and rod-like assemblies for CZA-20HP. After catalysis, the difference in the morphology of the catalysts was more pronounced. Figure 5-22 d presenting CZA-20HP after catalysis shows particular needles of ZnO and ZnAl_2O_4 where copper particles can be easily dispersed. This was reflected by the total conversion of glycerol with CZA-20HP with a selectivity toward 1,2-PDO of 88% and 11% for EG compared to 66% conversion with CZA-20UHP and a same range of selectivity.

Therefore, the use of urea had a deleterious effect on the conversion rates of copper-based catalysts, regardless of the copper content. This could be explained by a decrease of the acidity of the catalyst or the precipitation mechanism of the metals. Since the reactants were so active and the formation of the material was occurring at the first step of the synthesis (at 0 °C), the presence of urea at that stage was leading to structural changes and might be responsible for differences in the precipitation phenomenon and the crystal growth leading to a difference in the catalysts activity.

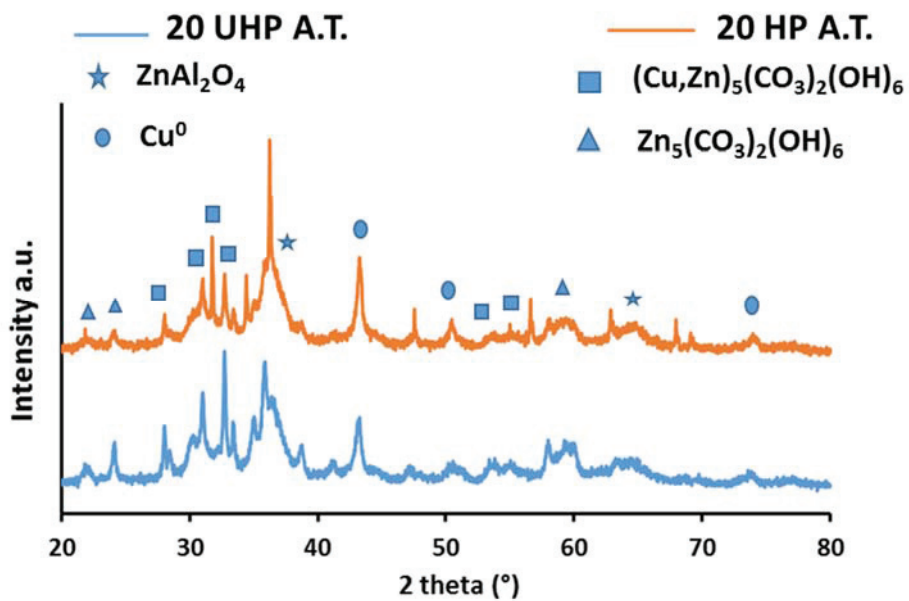


Figure 5-21: XRD diffractograms of CZA-20UHP and CZA-20HP (Zn:Al ; 2:1) after catalysis (A.T.: after test)

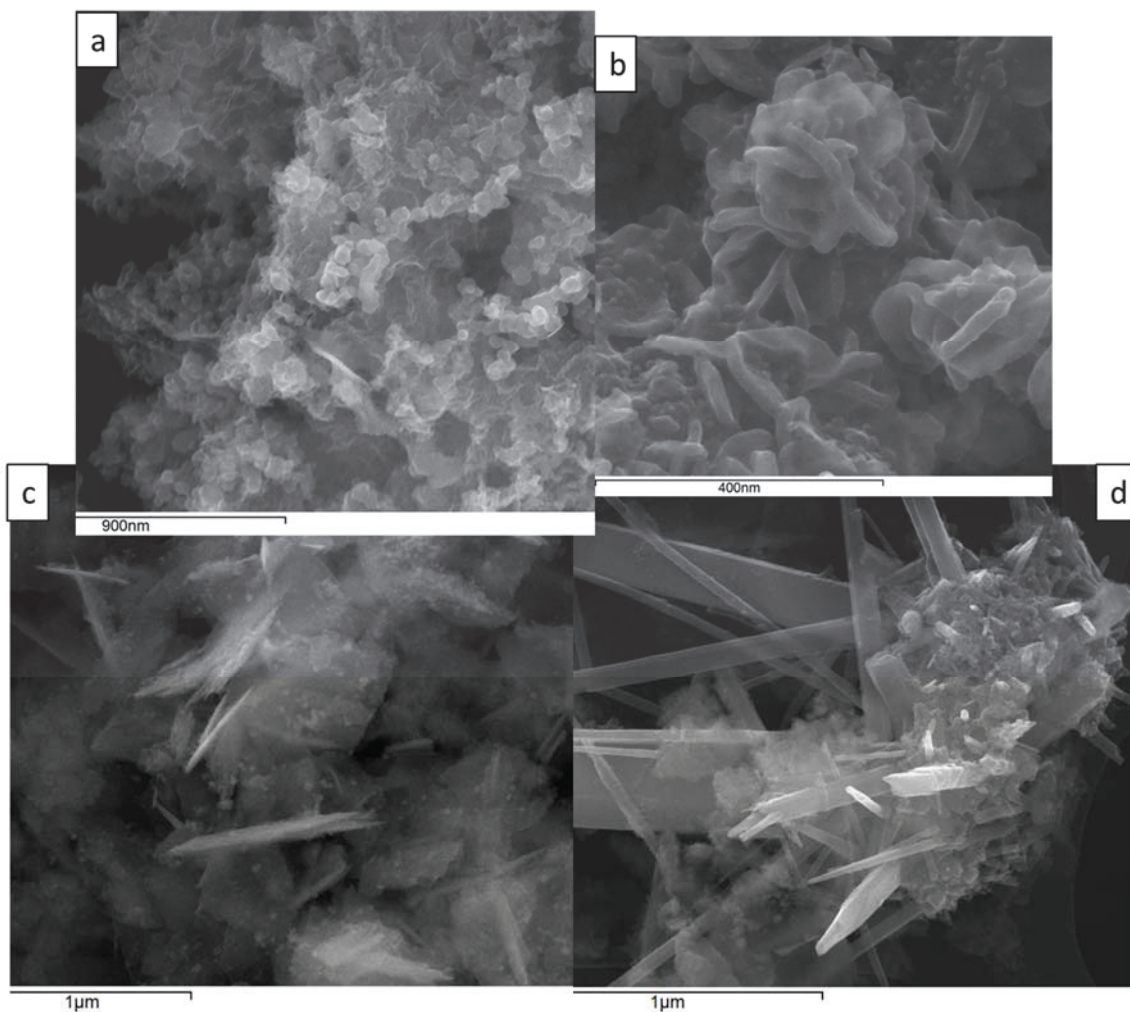


Figure 5-22: SEM images of a,c) CZA-20UHP and b,d) CZA-20HP (Zn:Al ; 2:1) before (a, b) and after (c, d) catalysis

For the same copper content of 20 wt%, we have also studied the increase of aluminium content for Zn/Al ratio of 1:1 and 1:4 (two last entries; Table 5-15) and found that increasing Al content led to an increase of the specific surface area without changing the size of the Cu^o NPs (ca. 15 nm). Nevertheless, the higher specific surface area did not affect the performance, where the two catalysts had similar results and were amongst the best of our study (above 80% of conversion and selectivity).

Having a higher content of Al, at similar wt% of copper (20UHP Zn:Al 2:1 and 20UHP last entry with Zn:Al 1:4), led to an increase of the activity of the catalyst from a conversion of 66% to 80%, respectively, and this could be related to three main factors:

- Increase in the specific surface area of the catalyst ¹²,
- Stabilization of ZnO caused by Al at higher loading ¹³
- And increase in the acidity (bronsted and Lewis) of the catalyst ¹⁴. However due to lack of time, the acidity of these catalysts were not characterised.

Comparing to the literature, the results were acceptable, as we mentioned in the introduction of this chapter the Zn:Al molar ratio with the highest conversion was changing from a study to another. For example, in the paper of Tan et al.¹, the highest conversion of 86% with selectivity toward 1,2-PDO (92%) and 2% for EG was obtained with Cu/ZnO/ZnAl₂O₄ catalyst (with a molar ratio of Cu:Zn:Al equal to 1:3:6 resulting in Zn:Al 1:2). The conditions of the catalytic test were, 80 wt% of glycerol in 20 mL of water, under 40 bar H₂ at 180 °C and with a catalyst weight: glycerol/Cu ratio of 200 after 10 hours of reaction.

On the other hand, a study of kim et al ¹⁵ showed that Cu:Zn:Al molar ratio 2:2:1 was showing the highest conversion with 5 wt% of catalyst and 20 wt% of glycerol, under 17 bar H₂ at 200 °C and after 20 hours of reaction, the conversion for this system was 73% with 76% selectivity for 1,2-PDO and 7.6% selectivity for EG.

IV. Conclusions

This chapter showed many interesting results that allowed understanding the behaviour of the catalysts. In term of Zn-Al synthesis, the effect of adding PAA2 during the synthesis led to a remarkable specific surface area ($333 \text{ m}^2.\text{g}^{-1}$) of ZnO-ZnAl₂O₄ calcined at 400 °C and obtained with (Zn:Al) molar ratio (1:2).

The deposition precipitation method was not easy to reproduce. Many parameters should be finely controlled and studied before. Using Cu/Zn₂Al₁-PAA2 prepared by DPU, the conversion of glycerol was 92% into 1,2-PDO (with 500 mg of catalyst, 4.2 wt% of glycerol in 100 mL of water, under 30 bar H₂ at 200 °C and after 24 hours) with 78% of selectivity toward 1,2-PDO. In addition, the effect of the support was easily confirmed in this section where the molar ratio of Zn:Al had an impact on the conversion. It was proved that each catalyst has its own characteristics and these characteristics were influencing the conversion of glycerol. However, it was hard to decorrelate the influence of each parameter separately.

The conversion obtained with the catalyst elaborated by the “one pot – one step” approach was 83% with 78% selectivity toward 1,2-PDO versus 96% conversion and 83% selectivity toward 1,2-PDO with the catalyst elaborated by the “one pot – two step approach”.

On the other hand, the “one pot method” was showing a define trend for each studied parameter. Once again, separating the method into two steps allowed the elaboration of well-defined catalysts with high specific surface area of $185 \text{ m}^2.\text{g}^{-1}$ even after calcination/reduction.

The study of the effect of urea during the “one pot” synthesis showed that removing urea (at the same Zn:Al molar ratio and copper weight percentage), allowed an increase of the conversion.

A very good catalyst was obtained in presence of PAA2 without heating and gave competitive results comparing to the same system obtained with heating in term of conversion (79%) and selectivity (90%) resulting in more ecological and time saving process. This result proved the importance of having PAA2 in the “one pot” method as well. Changing the molar ratio of Zn:Al had also an impact on the conversion. Taking in consideration the cited results, the most active catalyst was obtained for a molar ratio Zn:Al of 2:1 but as mentioned above it depended on many parameters and the lack in experiments for other molar ratio prevented us of generalizing this result. Anyway, the conversion obtained with this catalyst (loaded at 20 wt%

of copper) was 98% with a selectivity of 88% toward 1,2-PDO.

Furthermore, comparing the catalytic activity of the Cu-Zn-Al systems and Cu-ZnO obtained in the fourth chapter, the effect of adding Al to the catalyst was approved and the conversions were much higher in the case of the former system, under the same synthesis and catalytic conditions.

V. References

1. Tan, H. *et al.* One-pot synthesis Of Cu/ZnO/ZnAl₂O₄ catalysts and their catalytic performance in glycerol hydrogenolysis. *Catal. Sci. Technol.* **3**, 3360-3371 (2013).
2. Zhiming, Z. *et al.* Kinetics of hydrogenolysis of glycerol to propylene glycol over Cu-ZnO-Al₂O₃ catalysts. *Chin. J. Chem. Eng.* **18**, 384–390 (2010).
3. Saikia, P. & Goswamee, R. L. The effect of strength of bases and temperature on the synthesis of Zn-Al layered double hydroxides by a non-aqueous ‘soft chemical’ sol-gel method and formation of high surface area mesoporous ZnAl₂O₄ Spinel. *ChemistrySelect* **3**, 7619–7626 (2018).
4. Miroliaee, A., Hoshdari, S., Mohammadi Chahaki, M. & Abdouss, M. High surface area ZnAl₂O₄/reduced graphene oxide nanocomposites with enhanced photocatalytic performance. *Mater. Werkst.* **50**, 140–154 (2019).
5. Du, X., Li, L., Zhang, W., Chen, W. & Cui, Y. Morphology and structure features of ZnAl₂O₄ spinel nanoparticles prepared by matrix-isolation-assisted calcination. *Mater. Res. Bull.* **61**, 64–69 (2015).
6. Da Silva, A. A., de Souza Gonçalves, A. & Davolos, M. R. Characterization of nanosized ZnAl₂O₄ spinel synthesized by the sol-gel method. *J. Sol-Gel Sci. Technol.* **49**, 101–105 (2009).
7. Belyaev, A. V. *et al.* Sol-gel synthesis and characterization of ZnAl₂O₄ powders for transparent ceramics. *Ceram. Int.* **45**, 4835–4839 (2019).
8. Chaudhary, A., Mohammad, A. & Mobin, S. M. Facile synthesis of phase pure ZnAl₂O₄ nanoparticles for effective photocatalytic degradation of organic dyes. *Mater. Sci. Eng. B* **227**, 136–144 (2018).
9. Kanari, N., Mishra, D. & Dupré, B. Thermal decomposition of zinc carbonate hydroxide. *Thermochimica Acta.* **410**, 93–100 (2004).
10. Liu, Y. & Gao, W. Growth process, crystal size and alignment of ZnO nanorods synthesized under neutral and acid conditions. *J. Alloys Compd.* **629**, 84–91 (2015).
11. Mondal, S., Janardhan, R., Meena, M. L. & Biswas, P. Highly active Cu-Zn-Mg-Al-O catalyst derived from layered double hydroxides (LDHs) precursor for selective hydrogenolysis of glycerol to 1,2-propanediol. *J. Environ. Chem. Eng.* **5**, 5695–5706 (2017).
12. Zhang, C. *et al.* Preparation and CO₂ hydrogenation catalytic properties of alumina microsphere supported Cu-based catalyst by deposition-precipitation method. *J. CO₂ Util.* **17**, 263–272 (2017).
13. Mota, N., Guil-Lopez, R., Pawelec, B. G., Fierro, J. L. G. & Navarro, R. M. Highly active Cu/ZnO–Al catalyst for methanol synthesis: effect of aging on its structure and activity. *RSC Adv.* **8**, 20619–20629 (2018).
14. Wang, S. & Liu, H. Selective hydrogenolysis of glycerol to propylene glycol on Cu–ZnO catalysts. *Catal. Lett.* **117**, 62–67 (2007).
15. Kim, D. W. *et al.* Hydrogenolysis of glycerol to propylene glycol on nanosized Cu–Zn–Al catalysts prepared using microwave process. *J. Nanosci. Nanotechnol.* **15**, 656–659 (2015).

General Conclusion

In conclusion, our work opens up promising results in terms of hybrid ZnO materials as support for copper-based catalyst for the hydrogenolysis of glycerol.

We showed that if only the synthesis of ZnO-PAA2 and ZnO-PAA5 resulted in 3D self-assembled mesospherical morphology, batches were also accompanied by 2D ZnO-based nano-sheets. Therefore, studies of synthesis parameters were exclusively done for ZnO-PAA2 and ZnO-PAA5 systems and demonstrated that precise synthetic conditions were required to give materials with high specific surface area and small crystallites. In the case of ZnO-PAA2, nanohybrids mesospherical particles with an average of specific surface area of $90 \text{ m}^2 \cdot \text{g}^{-1}$ (BET) and aggregate size between 100- 200 nm (TEM) were obtained at low temperature (0-10 °C) with a PAA2 weight concentration between 0.5-0.63 wt% and washed with 90 mL of ethanol. For ZnO-PAA5, a high specific surface area ($120 \text{ m}^2 \cdot \text{g}^{-1}$) and smaller aggregates around 40 nm were elaborated at 40 °C with a PAA5 weight percentage of 0.63% and washed as well with 90 mL of ethanol. The increase of specific surface areas was generally associated with appearance of 2D nanosheets in addition to the 3D self-assembled mesospheres. The calcination and thermal behavior of the ZnO-PAA2 and ZnO-PAA5 materials were, unfortunately, studied before elaborating the material with the highest surface areas. Nevertheless, starting from a material with a surface of $20\text{-}30 \text{ m}^2 \cdot \text{g}^{-1}$, the calcination temperature at 350 °C resulted in an increase of the specific surface. For ZnO-PAA2, the mesospherical morphology was intact till 325 °C calcination temperature but the higher surface area was obtained for ZnO calcined at 350 °C with S.S.A = $51 \text{ m}^2 \cdot \text{g}^{-1}$ and smaller aggregate size 10-20 nm while ZnO-PAA5 showed higher thermal sensitivity and the mesospheres transformed into ZnO with undefined shapes after calcining at 300 °C.

Before using these diverse ZnO-PAAX as supports for the elaboration of copper catalysts, an optimization of the DPU method was done while using commercial ZnO as support. The effect of the weight percentage of copper and the concentration of Cu^{2+} in the solution showed an optimum at 20.8 mM for 10 wt% of copper. At higher copper percentage, it seemed that the low surface area of the commercial ZnO (around $13 \text{ m}^2 \cdot \text{g}^{-1}$) resulted in saturation of ZnO supports leading to a decrease in the glycerol conversion. The most active catalyst elaborated with the commercial ZnO resulted in 25% conversion and 90% selectivity toward 1,2-PDO after

24 hours of reaction in a batch reactor at 200 °C, under 30 bar of H₂, with 4.2 wt% of glycerol and 500 mg of catalyst in 100 mL of water.

In a second time, all the ZnO-PAAX systems elaborated in the third chapter were tested under the same catalytic conditions. Results have shown that the conversion increased when the commercial ZnO support was substituted by the ZnO-PAAX one. In addition, it was possible to load the catalyst with higher copper content (37.9 wt%) since the specific surface area of the ZnO-PAAX was higher (135 m².g⁻¹), without decreasing conversion neither sintering the copper particles.

Nevertheless, most of the catalysts (with the two types of supports), at high conversion (> 20%) have shown structural modifications of the catalysts. In the case of the commercial ZnO, the catalysts showed sintering of copper particles and a phase change of the ZnO toward a carbonaceous phase or hydrozincite. In the case of the ZnO-PAAX supports, the catalysts were mostly having the phase change but the sintering problem was not as important as with the commercial ZnO. The highest conversions obtained for the three systems were 25, 70 and 70% for commercial ZnO, ZnO-PAA2 and ZnO-PAA5, respectively, with similar selectivities around 90% toward 1,2-PDO. ZnO-PAA100 resulted in a total deactivation of the catalyst with less than 1% conversion.

The calcination of ZnO-PAA2 support before adding copper resulted in average to a lower conversion compared to the catalysts elaborated with the hybrid and uncalcined support (highest conversion obtained with the calcined support was 55% vs 70% for the uncalcined one). For ZnO-PAA5, the conversion decreased drastically from 70% to 27% with the calcined support. This results proved that the precipitation of copper onto the support, in presence of the PAAH polymer, allowed a better interaction of copper with the ZnO support resulting in highly dispersed material. Nevertheless, all the catalysts were highly selective toward 1,2-PDO with an average of 85-99% depending on the conversion and the major by-product was ethylene glycol (EG) with selectivities between 2-14%.

Even if the catalysts elaborated with the ZnO-PAAX supports seemed to be more active than the one elaborated with the commercial ZnO, catalysts showed some problems of reproducibility when up-scaling was done. The increase of the catalyst's weight led to an increase in the glycerol conversion to 60% with 90% selectivity toward 1,2-PDO with 1 g of catalyst after 24 hours. Recyclability tests have shown that the conversion and the selectivity

of these catalysts were recovered when they were regenerated. Regarding the low cost of our systems, this result may be interesting for an application on large scale.

Due to the reproducibility problems, a “one pot method” was developed in order to have a better control on the properties of the catalyst. In term of conversion, this route did not show any improvement but it allowed the elaboration of a robust catalyst highly resistant towards the catalytic conditions compared to all the series of other catalysts (with commercial ZnO and hybrid ZnO) with no change of phase after catalysis.

Based on the literature, the activity of Cu/ZnO systems could be enhanced by adding a promoter such as aluminium. We studied its addition to the catalyst under different synthesis conditions. As for ZnO, we started by elaborating the ZnAlO_x-PAA2 hybrid support (only PAA2 was used) oxide with two different molar ratio of Zn/Al (1:2 or 2:1) and deposited copper NPs by DPU method. We studied the effect of the polymer by elaborating ZnAl oxides with and without PAA2 at 0 °C and with 90 mL of ethanol washing at the end of the syntheses. In terms of materials, the as-synthesized ZnAl oxide with 1:2 molar ratio elaborated in presence of PAA2 showed the highest surface area of 222 m².g⁻¹. Calcining the material at 400 °C resulted in an increase in the specific surface area up to 333 m².g⁻¹ followed by a decrease to 137 m².g⁻¹ at 600 °C. An interesting point was that the Zn-Al systems elaborated with/without PAA2 had the same behavior. As already observed in the literature, this led then to an increase of the specific surface area of the resulting catalysts and also, depending of the Zn/Al ratio, to the appearance of the spinel phase of ZnAl₂O₄. Both seemed to play a major role in enhancing the properties of copper-based catalysts.

The DPU method was used to elaborate the catalysts by following the same conditions as before and we compared then different catalytic systems. We demonstrated the remarkable properties of these supports, in term of high specific surface area, small particles (3-12 nm for ZnAl₂O₄, 8-35 nm for ZnO) and good thermal behavior. The conversion of the glycerol increased to 96% with the catalyst elaborated with Zn:Al molar ratio 1:2 with a selectivity toward 1,2-PDO of 83%. Nevertheless, a leaching of zinc occurred during the DPU process resulting in a lower content of Zn in the catalyst compared to the one in the support. The change in the phase after catalysis was also seen for these new Cu/Zn-Al catalysts.

Therefore, a “one pot” method was applied to elaborate Cu/Zn-Al catalysts. Its optimization was made by study any synthetic parameters such as the presence of urea, of PAA2 and the heating step. The results showed that PAA2 is mandatory to obtain highly dispersed systems

with interesting properties by a better control of the pH of the solution. While, in the opposite, the presence of urea in this synthesis method did not seem to be beneficial and resulted in a decrease in the conversion. The heating step seemed also to be important and the most active catalyst was the one prepared with 20 wt% of copper, without urea, in the presence of PAA2 with a molar ratio Zn:Al of (2:1). It resulted in an almost total conversion (98%) of glycerol with 88% selectivity towards 1,2-PDO.

To enclose this part, a three run recyclability test was done with the catalyst elaborated with Zn:Al showing a molar ratio 1:1 (obtained by DPU) and it resulted in the conservation of the conversion (90-93%) and the selectivity (83-84%). After each regeneration the catalyst seemed to recover the properties of the freshly reduced catalyst.

Perspectives

The study opens up perspectives towards different subjects. In term of ZnO and ZnAl₂O₄, the interesting properties of these materials can be applied as we saw in the literature in varied domain of applications as in nanotechnological applications, optoelectronics, photocatalysis... Since our previous study on ZnO was done in order to enhance the luminescent properties of the material, the new hybrid system elaborated at low temperatures resulting in homogeneous dispersed materials may be more interesting for such application.

In the case of ZnAl₂O₄, the spinel phase is known to have a high mechanical resistance and high chemical and thermal stability making this material a nice candidate for applications in optical coatings, host matrix or in ceramics syntheses. Since we were interesting in its catalytic behavior, no mechanical characterizations were done. Nevertheless, the thermal stability was proved by TGA and the resistance of the material toward the catalytic conditions allow to consider it as promising system for these applications.

Moving to the catalysts, the Cu/ZnO is highly studied for the hydrogenation of CO₂ into methanol. In a first step, and with the collaboration of some researchers in our institute (Laurent Piccolo and the PhD student Thomas Len), we tested the ZnO as support for Pd and compared it to the commercial Pd/ZnO catalyst under the following reaction conditions (250 °C, 50 mL.min⁻¹ H₂/CO₂/Ar (30/10/10) for 60 hours). In a second time, the test was done with

the Cu/ZnO prepared at 5 wt% of copper elaborated by DPU on ZnO-PAA2 uncalcined synthesized at 0 °C. The catalytic results are summarized in the table below.

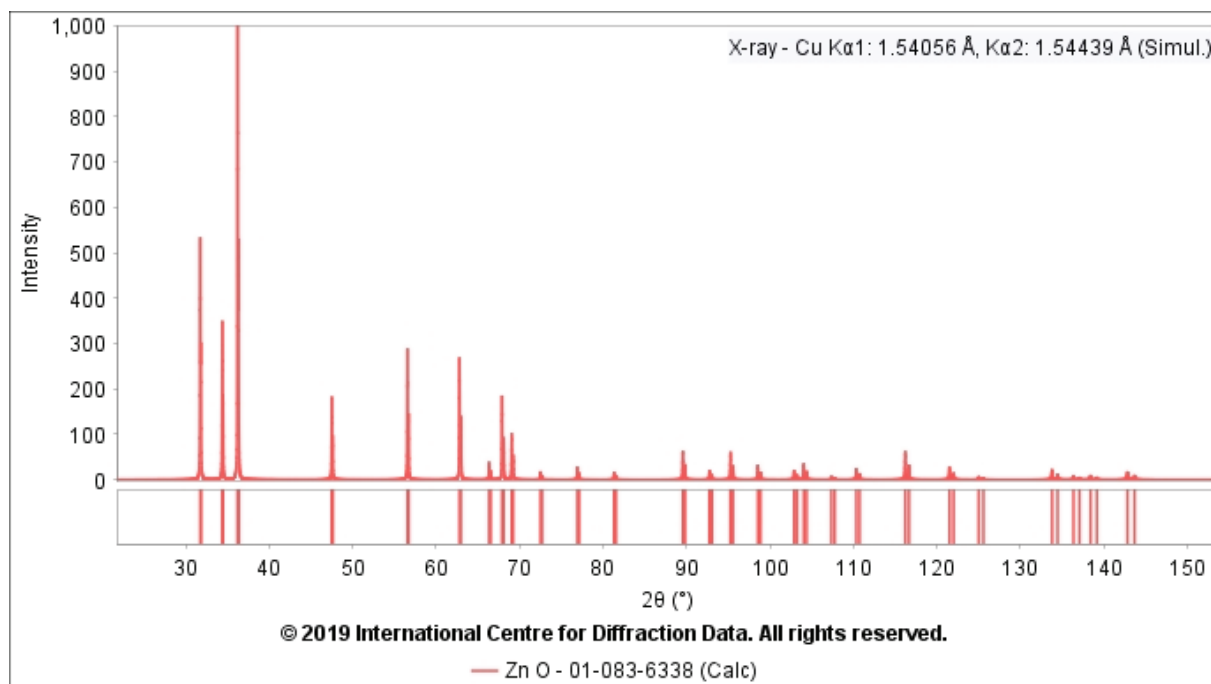
Catalyst	Selectivity CO (%)	Selectivity MeOH (%)	Conversion (%)
Industrial catalyst	53.4	46.6	19.43
0.3 wt% Pd / ZnO	47.2	43.3	1.06
5 wt% Cu / ZnO	54.5	45.5	5.48

The Cu/Zn-Al showing the highest conversion for glycerol hydrogenolysis (prepared by “one pot-two steps” route with PAA2 and at a Zn/Al molar ratio of 2:1 without urea) is under test. Due to the higher selectivity of copper catalysts toward C-O bond cleavage, the catalysts can be tested in more sophisticated biomass reactions such as the hydrogenolysis of sugar alcohols (e.g. sorbitol, xylitol). Other studies were done in this field but most of them used mono or bimetallic systems based on noble metal. The challenge is to have high conversion with noble metal-free catalysts.

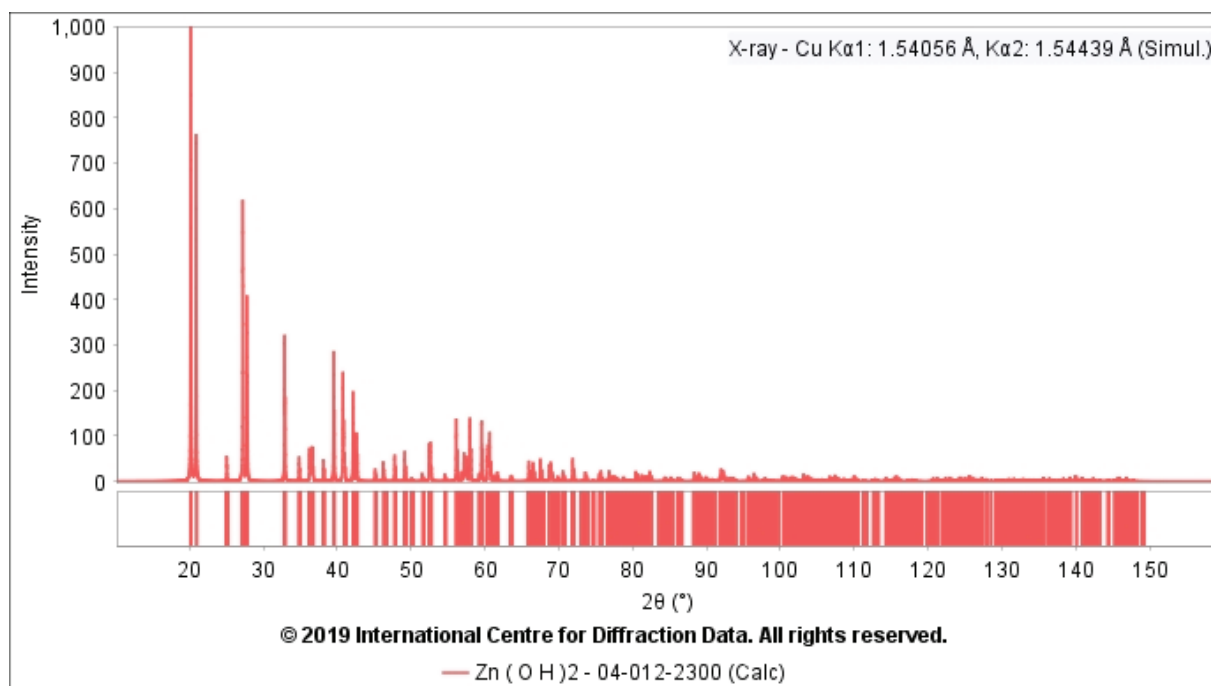
A step further would be the development of other noble metal-free systems using the synthesis methods developed in this thesis. As we already synthesized Cu/ZnO, the next catalysts can be other mono or bimetallic catalysts such as Ni/ZnO or Ni-Cu/ZnO and Cu-Al/ZnO.

Last but not least, an interesting test can be done by substituting the thermal treatment, applied to elaborate the active catalyst, for NaBH₄ as a reducing agent for example in order to keep the PAAX inside the catalysts and study their effect on the conversion of glycerol.

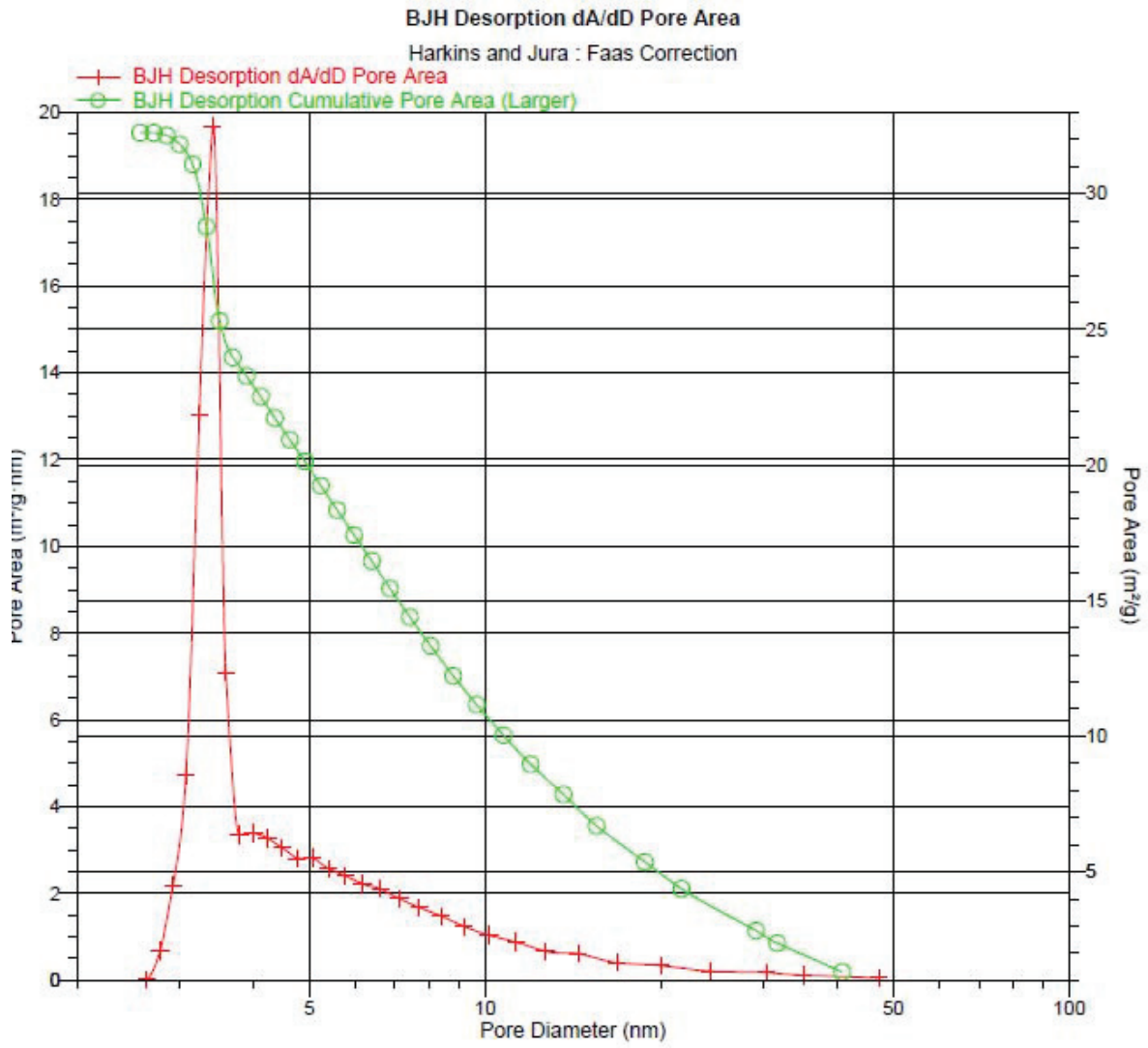
Appendix 1



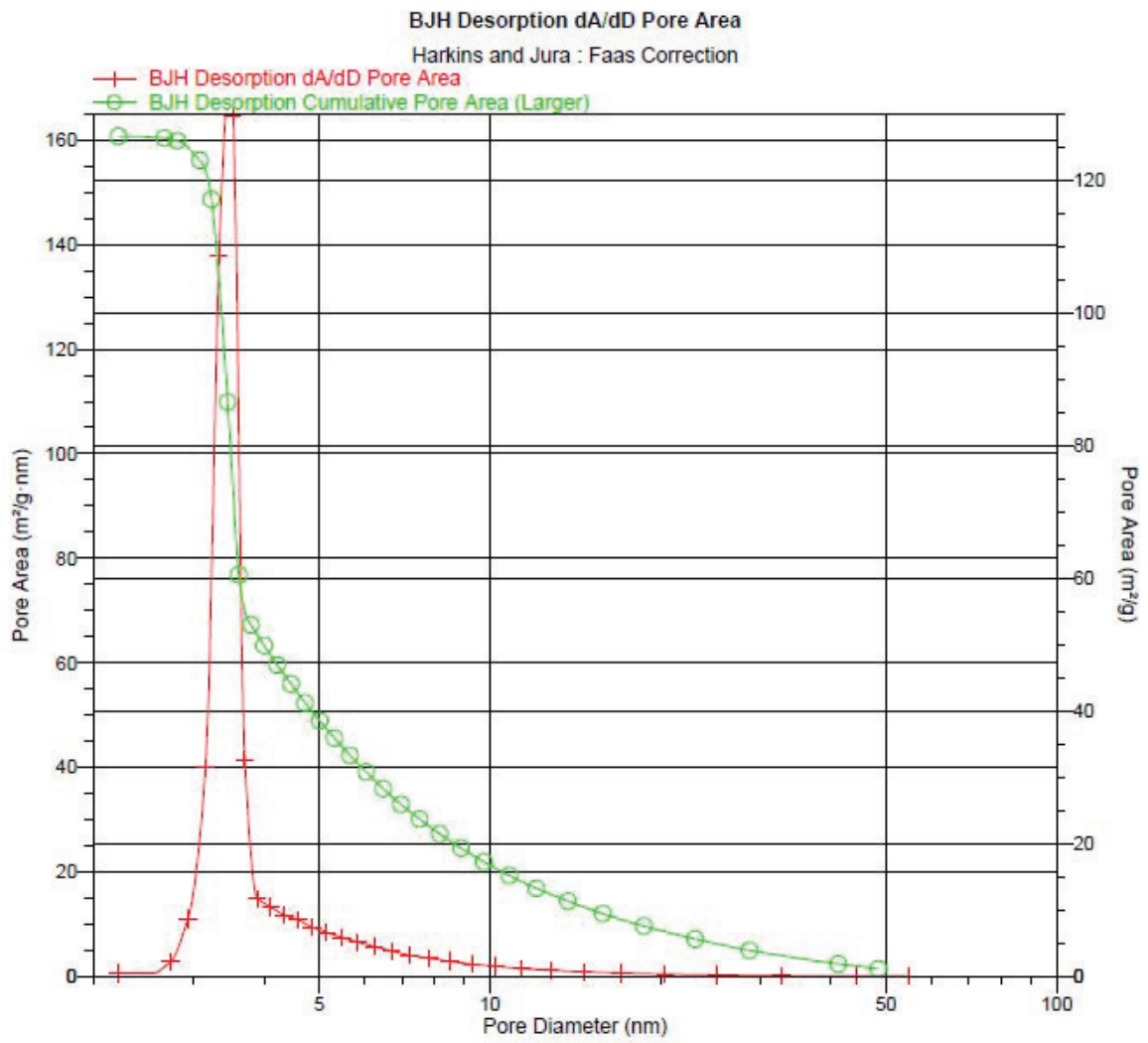
Appendix 2



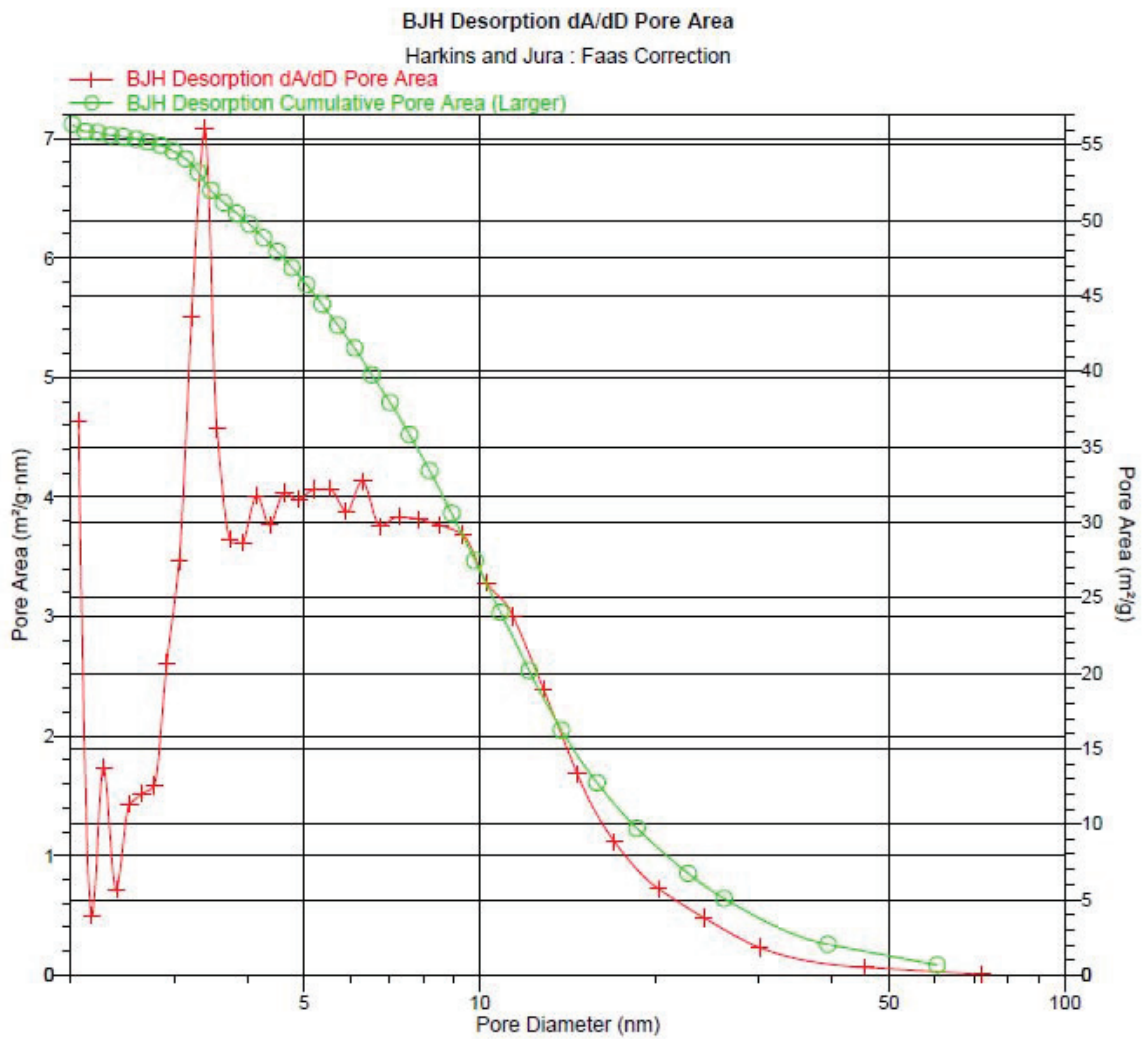
Appendix 3 ZnO-PAA2



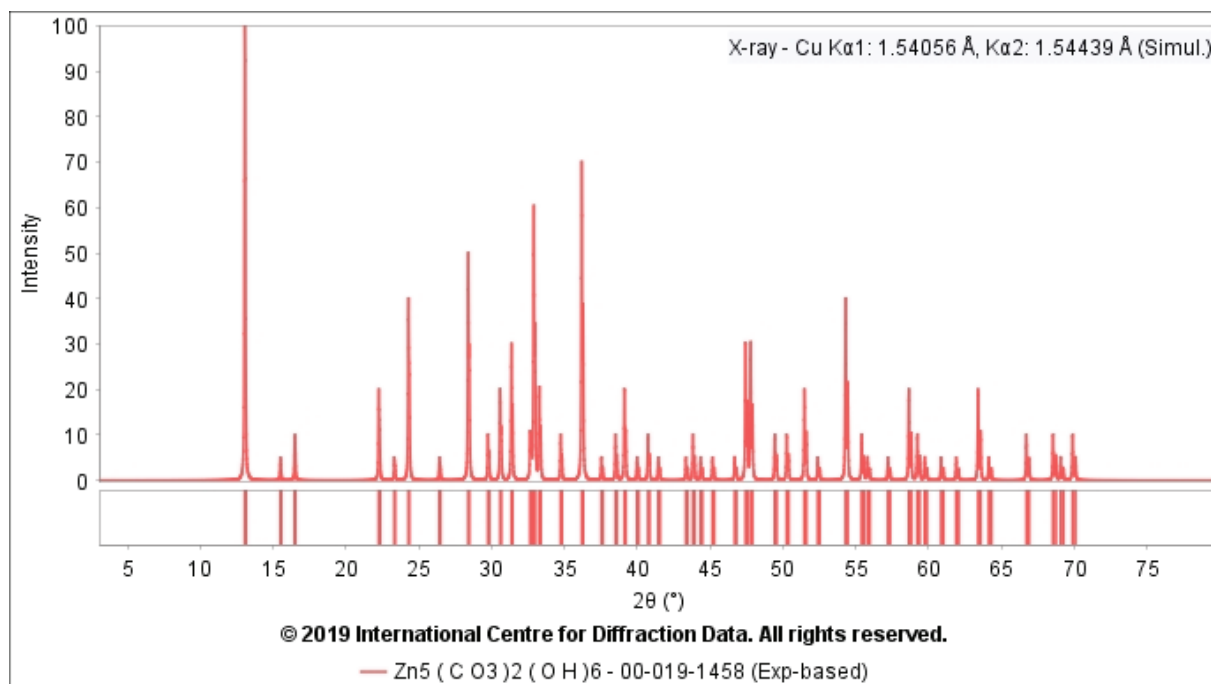
Appendix 4 ZnO-PAA5



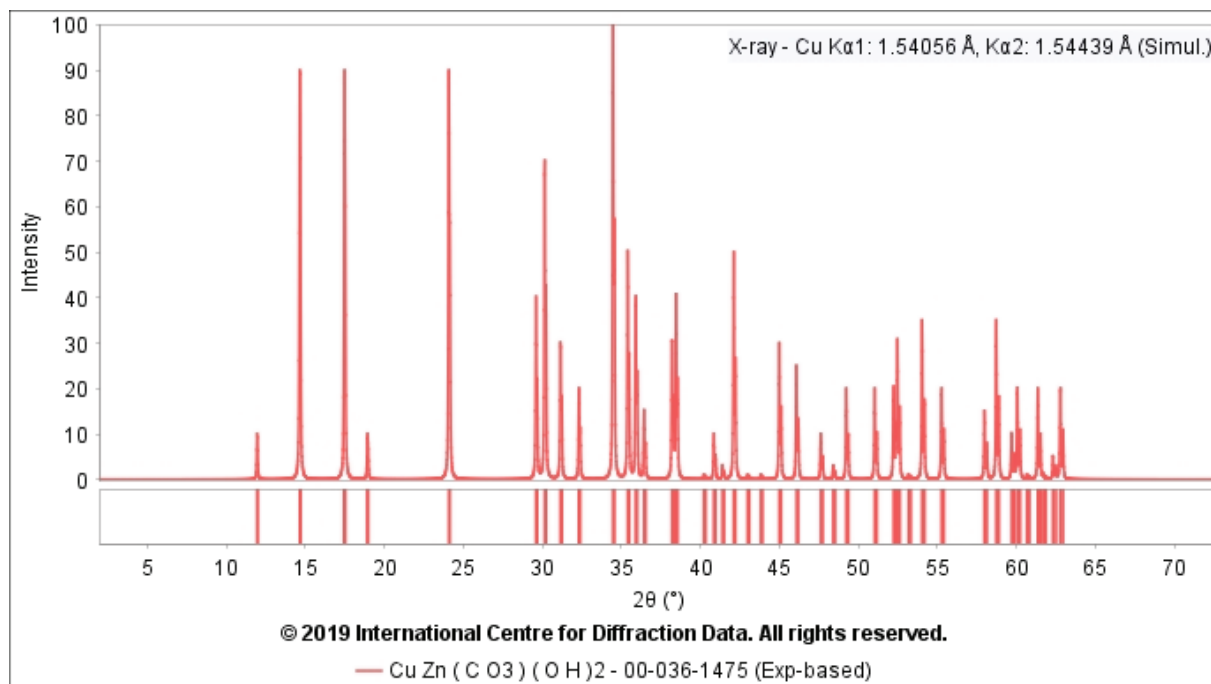
Appendix 5 ZnO-PAA100



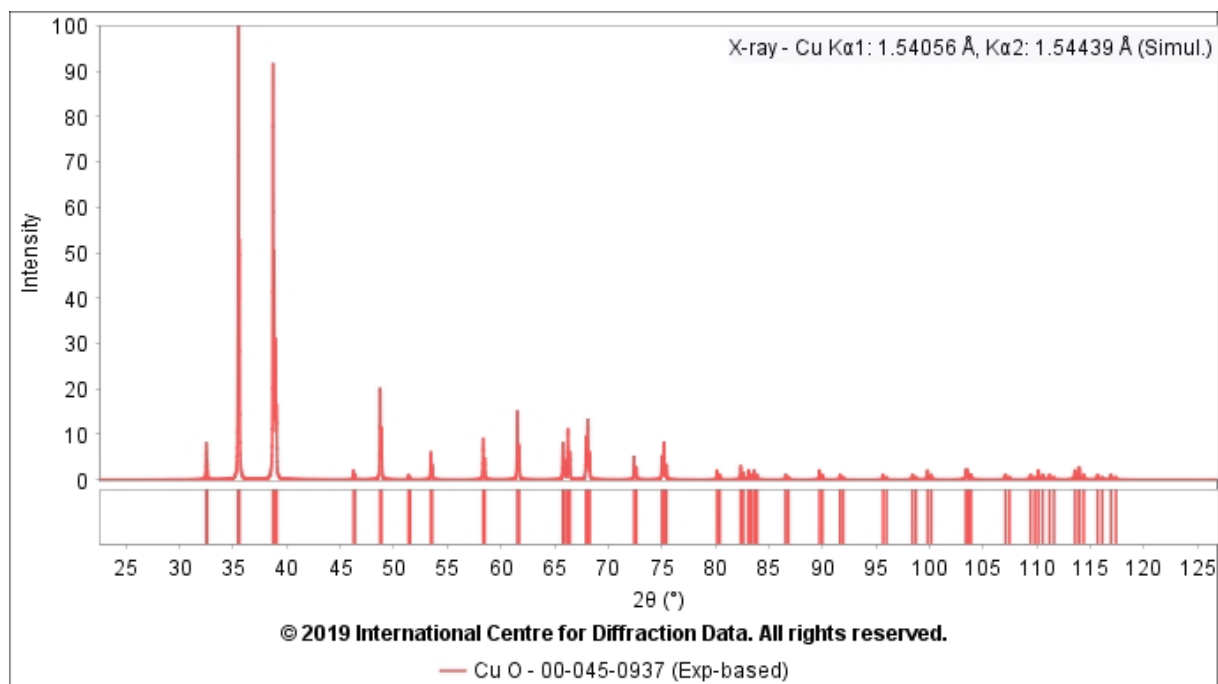
Appendix 6



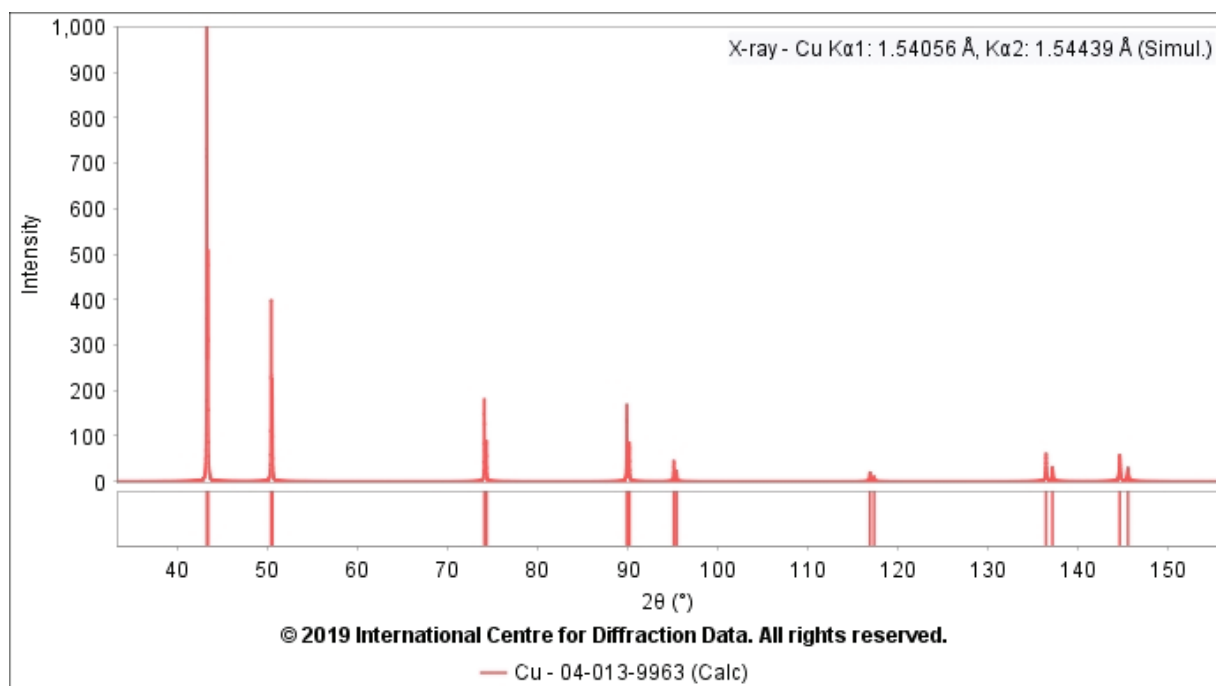
Appendix 7



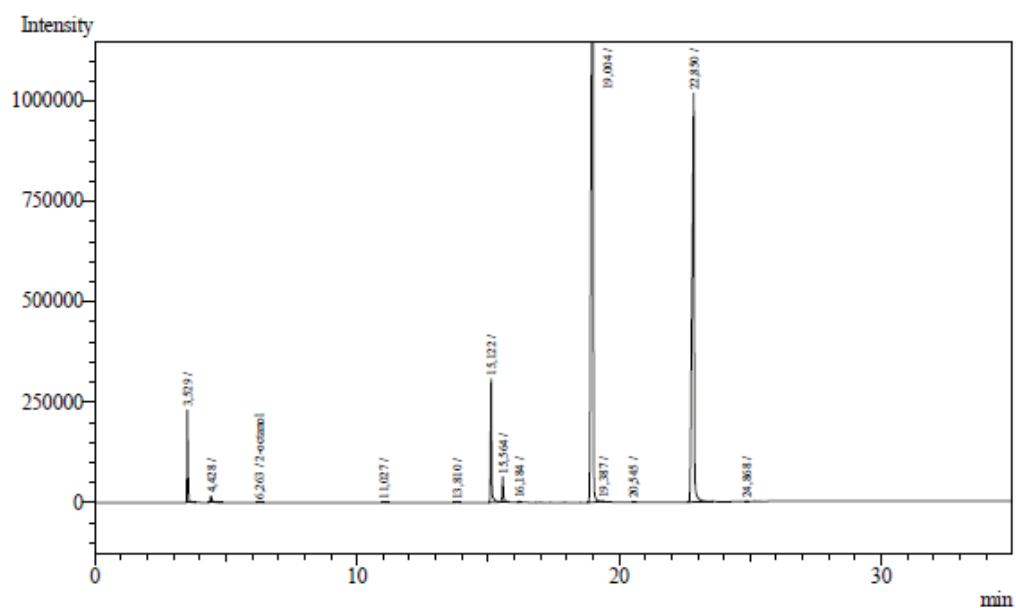
Appendix 8



Appendix 9

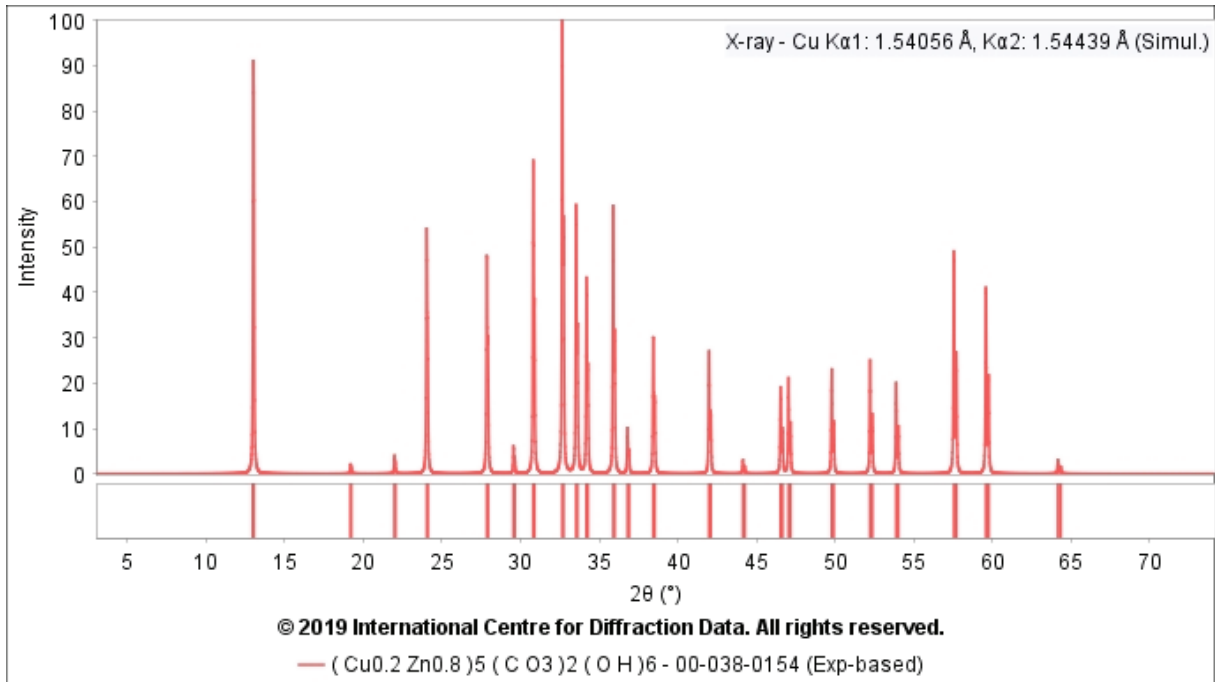


Appendix 10

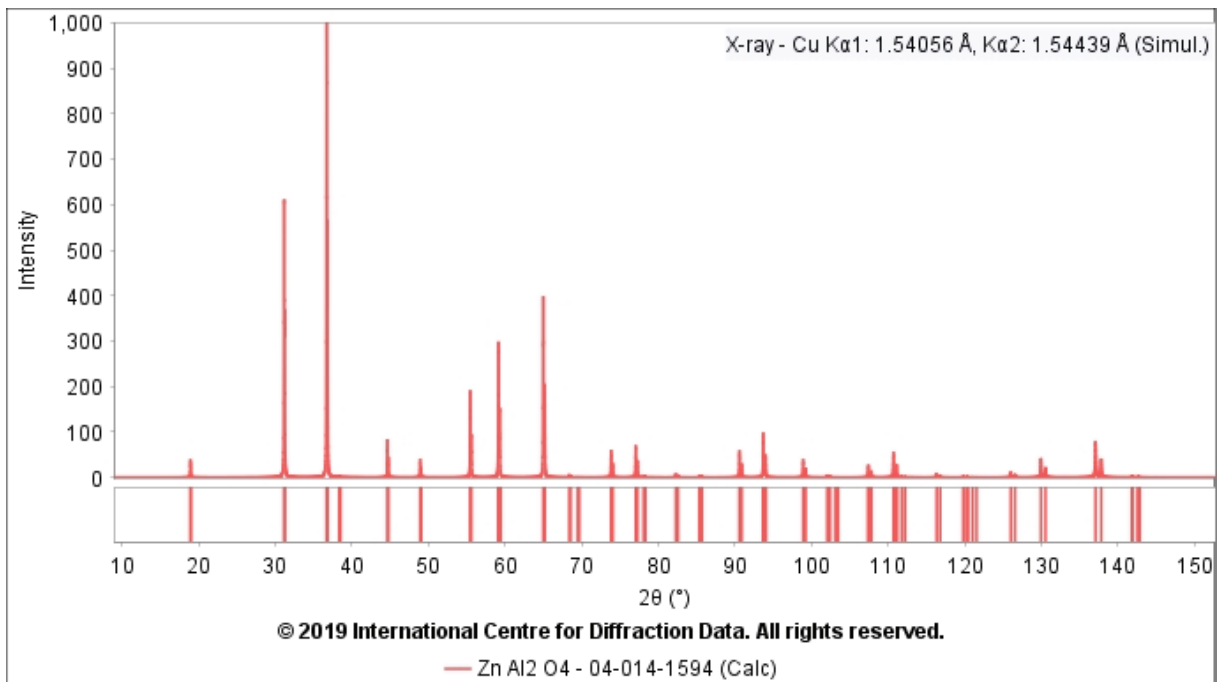


Peak#	Ret. Time	Area	Height	Conc.	Unit	Mark	ID#	Compd Name
1	3,529	580323	230580	0,000				
2	4,428	76618	16379	0,000				
3	6,263	3871	797	0,000	ppm		4	2-octanol
4	11,027	3453	1221	0,000				
5	13,810	3913	469	0,000				
6	15,122	885940	307410	0,000				
7	15,564	188853	62164	0,000				
8	16,184	6378	2444	0,000				
9	19,004	9994634	2027080	0,000				
10	19,387	5681	2253	0,000				
11	20,545	5090	1941	0,000				
12	22,850	5942707	1017167	0,000				
13	24,868	3652	1288	0,000				
Total		17701113	3671193					

Appendix 11



Appendix 12



Appendix 13

